TABLE OF CONTENTS

NASA Contractor Report 3023

Workbook for Estimating Effects of Accidental Explosions in Propellant Ground Handling and Transport Systems

W. E. Baker, J. J. Kulesz, R. E. Ricker,
P. S. Westine, V. B. Parr, L. M. Vargas,
and P. K. Moseley

CONTRACT NAS3-20497
AUGUST 1978

NASA

NASA Contractor Report 3023

Workbook for Estimating Effects of Accidental Explosions in Propellant Ground Handling and Transport Systems

W. E. Baker, J. J. Kulesz, R. E. Ricker,
P. S. Westine, V. B. Parr, L. M. Vargas,
and P. K. Moseley

Southwest Research Institute
San Antonio, Texas

Prepared for
Lewis Research Center
under Contract NAS3-20497

National Aeronautics
and Space Administration

**Scientific and Technical
Information Office**

1978

BLANK PAGE

FOREWORD

Many staff members at Southwest Research Institute, in addition to the authors, contributed substantially to the work reported here. The authors gratefully acknowledge the special contributions of the following:

- Mr. T. R. Jackson, for assistance in debugging and running the complex TUTTI computer program for calculating two-dimensional blast wave properties.

- Ms. Deborah J. Stowitts, for organizing and editing the report.

We also gratefully acknowledge the help of Dr. Del Lehto, Naval Surface Weapons Center, White Oak Laboratory, for providing the TUTTI code documentation, and consulting on its use.

The technical support and guidance of our project manager at the NASA Lewis Research Center, Mr. Paul M. Ordin, contributed materially to the success of this work. In particular, he provided excellent technical guidance throughout the contract, and also provided several excellent accident reports as input data for fragment characteristics in Chapter IV.

BLANK PAGE

TABLE OF CONTENTS

SUMMARY

This workbook is a supplement to an earlier NASA publication, NASA CR-134906, which is intended to provide the designer and safety engineer with rapid methods for predicting damage and hazards from explosions of liquid propellant and compressed gas vessels used in ground storage, transport and handling. As in the earlier workbook, information is presented in the form of graphs and tables to allow easy calculation, using only desk or handheld calculators. When complex methods have been used to develop simple prediction aids, they are fully described in appendices.

Topics covered in various chapters are:

(1) Estimates of explosive yield
(2) Characteristics of pressure waves
(3) Effects of Pressure waves
(4) Characteristics of fragments
(5) Effects of fragments and related topics

A short concluding chapter gives a general discussion and some recommendations for further work.

Microfiche copies of the companion workbook, NASA CR-134906, are attached for the convenience of the reader.

INTRODUCTION

General Discussion

This workbook is a companion to an earlier NASA workbook [Baker, et al (1975)], NASA CR-134906, which was prepared to aid designers and safety engineers in predicting damage and hazards from accidental explosions involving liquid propellants and compressed gases in flight hardware. This book, in contrast, is devoted to blast and fragment hazards for the same classes of accidental explosion sources in propellant ground handling and transport systems. Prediction methods which were thoroughly covered in the earlier workbook and which apply without change will not be repeated here. Instead, explosion hazards peculiar to ground storage and transport systems, or ranges of input parameters specific to these systems, will be emphasized. For completeness, the reader should use the earlier workbook in conjunction with this one.

A microfiche supplement of the workbook is attached to the back cover for the convenience of the reader.

Nature of the Hazards

The general nature of the hazards from accidental explosions in propellant and industrial gases ground handling systems is similar in many respects to the hazards which occur in such explosions in flight vehicles. These accidents cause damage by air blast loading, fragment or appurtenance impact, radiation from fireballs, or fire from ignition of combustible materials following an explosion. Damage can occur to buildings and other facilities, vehicles, and flora and fauna--including humans. Depending on the severity, type and location of an explosion accident, the damage can range from minor to extensive.

The sequences of events or causes of accidental explosions in ground handling systems for liquid propellants and compressed gases can be quite similar to those which can occur in flight vehicles, or can differ markedly. Failure by material fatigue on overstress can occur in either case. But, many of the possible causes of flight vehicle explosions such as loss of thrust during launch, guidance system failure, or rupture of a bulkhead separating a fuel from an oxidizer, are inapplicable for ground handling systems. Conversely, transportation accidents followed by explosions are causes which are absent in flight vehicle accidents.

Ground handling systems usually have less serious weight constraints than do flight vehicles. This difference dictates some of the differences in the nature of the hazards. Ground sys-

tems can employ relatively massive, ductile materials in pressure vessel and piping construction. On failure, such vessels generate relatively few fragments compared to similar failures in flight-weight vessels. A failure of a long cylindrical vessel near one end can often result in most of the vessel remaining intact, and "rocketing" as the internal compressed fluid is ejected from the rupture. This mode of failure has never been observed in flight-weight pressure vessels or tankage, which have less ductility and instead break into a relatively large number of fragments. Pressure vessels used in ground systems are often of much larger capacity than flight systems. The total stored energy in compressed gases or total chemical energy in stored fuels and oxidants can then be much greater than for many flight systems.

Unfortunately, many more accidental explosions have occurred involving fuels and compressed fluids in ground handling than in flight vehicles. There is a considerable body of accident report literature [see, for example, Strehlow & Baker (1975, 1976)] which highlight the probable types of accident. These are (not necessarily in order of probability):

1) Simple pressure vessel failure because of fatigue or flaw growth.

2) Vessel failure induced by impact during a transportation accident.

3) Vessel failure by overpressure because of overheating. This often follows a derailment accident with railroad tank cars.

4) Vessel and pipeline failure by overpressure, corrosion or erosion.

5) Fuel leakage followed by a vapor cloud explosion.

Blast and some type of fragment or massive body impact usually result from the first four types of accident; the last type causes primarily a pressure wave and fireball; while the first four may or may not cause fireball or fire depending on the fluid and circumstances in the accident.

Assessment of the magnitudes and the effects of the blast and fragments for ground system explosions is the topic of this workbook.

Means for Assessment of Risk

The term "risk assessment" implies not only the estimation of effects of some potentially dangerous operation or situation,

but also the estimation of the probability that the event will occur and cause some level of damage. We do not address here the overall problem of risk assessment, but instead cover only the prediction of the effects. Throughout, we assume that some postulated explosive accident can and has happened. This workbook therefore covers only the more deterministic aspects of explosions and their effects, but can serve as inputs to the probabilistic models used in complete risk assessment studies.

Scope and Significance of Material Presented

From the material presented in this workbook, one should be able to make predictions of blast and fragment characteristics and effects for a wide range of possible explosion accidents in ground systems. The body of the workbook gives the prediction methods in the form of graphs, equations, or tables. All detailed development and some computer programs are given in appendices. Given a number of accident scenarios, the material should allow prediction of:

1) Explosive energy yield or energy release.

2) Characteristics of blast pressure waves generated by spherical and non-spherical explosions.

3) Effects of pressure waves on certain classes of targets or for blast loading conditions not covered in Baker, et al (1975).

4) Characteristics of fragments generated by ground equipment explosions. This includes massive vessel parts which "rocket."

5) Effects of fragment impact not covered in Baker, et al (1975), including effects of fragment revetments on blast waves.

The scope of the material presented here is deliberately limited to avoid duplication with the previous workbook [Baker, et al (1975)]. As noted earlier, it should be used in conjunction with that reference. (Microfiche)

Significant advances presented here are:

1) Prediction of blast wave characteristics for non-spherical sources.

2) Some additional methods for rapid prediction of structural damage from blast waves and massive fragment impact.

3) Extensions of methods of predicting such fragment characteristics as initial velocity, maximum range, and impact conditions.

4) Development of method for predicting trajectories and impact conditions for "rocketing" vessels.

5) Inclusion of predictions for effects of barricades on blast waves.

Intended Purpose and Limits of Use

The purpose of the workbook is to provide safety engineers with methods for rapid estimation of blast and fragment hazards from accidental explosions in ground support and transport equipment. It should require only a desk or pocket calculator, or slide rule to perform any of the needed calculations. There are, of course, a number of limits to the calculations and their applicability which the user should observe. Because almost all of the data we will use are graphical, these limits will often be self-evident from the extreme values on the graphs. In general, one should not extend or extrapolate these graphs, but should instead merely report that prediction is not possible if input parameters fall outside the range of the plot.

Factors of safety are included in the prediction methods in various ways. When curves are based on experiments, error bands are usually given. Use of average curves through the data will give most probable values for such loading parameters as blast overpressure and impulse; use of the upper limits of the error band will assure conservatism by encompassing all of the extreme values in the measured data rather than the most probable. Most of the fragment data must be presented statistically. The user is often given a choice of several regression lines through the data. Choice of such a line with a very high probability of, say, predicting that all fragments less than a certain mass will fall to earth within a given distance, will assure a high factor of safety in estimating exclusion distances for possible fragment damage. In estimating effects of blast and fragments, factors of safety are included by estimating different degrees of damage given blast envelopment or fragment impact. For structures, estimates can be made for lower limits to damage (threshold of no damage at all) through quite severe structural damage to buildings, vehicles, etc. For estimation methods which are based on sparse data or analysis, we have large bands of uncertainty--the user should apply upper limits of these bands, if in doubt.

Applications to Areas Other Than Aerospace Propellant and High Pressure Gas Handling Facilities

This workbook can be as easily applied to many types of industrial explosive accidents as to those limited to aerospace propellants and high pressure gases. There have been many gas pressure vessel failures, road and rail tanker accidents with fuels such as LPG (liquified petroleum gas) followed by explosion and fire, and piping failures in chemical plants followed by vapor cloud explosions. For all such accidents, the methods presented here can be applied to estimation of blast and fragment hazards.

Additional Areas of Research

The methods given here are based on the best test data, analysis methods, and accident reports available to us. But, in many of these areas, the data base is quite sketchy and the governing physical processes are as yet poorly understood. We feel that additional work is needed in the following areas:

1) A better understanding and better methods of prediction of conditions under which vapor cloud explosions will occur, and the blast wave properties for such explosions.

2) A more thorough study of non-spherical accidental explosion effects.

3) Extension of the pressure-impulse (P-I) damage concept to typical blast waves for accidental explosions. In particular, the pronounced negative phase characteristics of such explosions should be considered.

4) Better definition of impact effects for large, massive fragments or objects.

5) Establishment of a more comprehensive and accurate system or method for reporting of explosion accidents. In particular, good industrial accident reporting could greatly increase the data base for comparison with these prediction methods or for judging explosion severity.

REFERENCES

Baker, W. E., Kulesz, J. J., Ricker, R. E., Bessey, R. L., Westine, P. S., Parr, V. B. and Oldham, G. A. (1975) "Workbook for Predicting Pressure Wave and Fragment Effects of Exploding Propellant Tanks and Gas Storage Vessels," NASA CR-134906, Contract NAS3-19231, Nov. 1975 (reprinted Sept. 1977).

Strehlow, R. A. and Baker, W. E. (1975), "The Characterization and Evaluation of Accidental Explosions," NASA CR-134779, Grant NSC 3008, June 1975.

Strehlow, R. A. and Baker, W. E. (1976)"The Characterization and Evaluation of Accidental Explosions" Progress in Energy and Combustion Science, 2, 1, pp. 27-60.

CHAPTER I

ESTIMATES OF EXPLOSIVE YIELD

1-1 General

Methods for estimating explosive yields, i.e., total energies which can be released in an explosive accident, are discussed in some depth by Baker, et al (1975) for the common mixtures of fuels and oxidizers employed in liquid-fueled rockets. Methods are given in that reference for estimating explosive yields for a variety of classes of explosive accident and propellant mixtures. No new data or methods have been developed since, and one should simply use that reference to estimate explosive yields for liquid propellant mixtures.

Baker, et al, (1975) also give a formula for estimating explosive yields for bursts of compressed gas vessels. Considerable analytic and experimental work on this topic has been done recently, and we will use this work as a basis for improving estimation of blast yields for this source.

A significant number of explosive accidents have occurred after failure of pressure vessels containing flash-evaporating liquids under high pressure, either at ambient temperature or heated. Methods have been developed to estimate blast yields for such explosions and these will be presented here.

An important class of accidental explosions in ground systems is the unconfined vapor cloud explosion. A quantity of fuel is released to the atmosphere as a vapor or aerosol, the fuel mixes with the air, and the resulting fuel-air mixture is then ignited by some ignition source. An explosion may or may not result, depending on a number of variables. We will survey knowledge on this class of accidental explosion, and recommend some ways of obtaining rough estimates of blast yield.

1-2 Compressed Gas Bursts

In Baker, et al (1975), the formula for total energy release originally proposed by Brode (1959) was used to predict explosive yield for compressed gas vessel bursts. This formula is

$$E = \left(\frac{p_1 - p_a}{\gamma_1 - 1} \right) V_1 \qquad (1\text{-}1)$$

where E is blast yield (energy), p_1 is initial absolute pressure in the vessel, p_a is outside atmosphere absolute pressure, and γ_1 is the ratio of specific heats for the gas in the vessel. A number of other formulas have been proposed, and these are

discussed in some detail and analyzed by Adamczyk and Strehlow (1977). They include an estimate based on isentropic expansion from initial burst pressure to atmospheric pressure [Baker (1973), Brinkley (1969)],

$$E = \frac{p_1 V_1}{\gamma_1 - 1}\left[1 - \left(\frac{p_a}{p_1}\right)^{\frac{\gamma_1 - 1}{\gamma_1}}\right] \qquad (1\text{-}2)$$

and, as a lower limit, the energy released by constant pressure addition of energy to the explosion source region [Adamczyk and Strehlow (1977)],

$$E \approx p_a\ (V_f - V_1) \qquad (1\text{-}3)$$

where V_f is the final volume occupied by the gas which was originally in the vessel. These three equations are given in descending order of total blast energy, with eq. (1-3) representing the energy release for a process which is so slow that no blast wave is formed.

Adamczyk and Strehlow (1977) show that the blast yield must lie between eqs. (1-2) and (1-3). However, eq. (1-1) gives only slightly higher values than does (1-2), and is simpler. So, realizing that its use results in an overestimate of blast yield, we retain it for this workbook. The reader can use eq. (1-2), however, for a somewhat more accurate estimate which is <u>still</u> an overestimate, and hence is conservative.

The equations given here for blast yield are all based on the assumption that all of the energy which can drive a blast wave does so, depending only on the energy release rate. For real vessels, some energy must be absorbed by the vessel as it fractures, both in the fracturing process itself and in accelerating the vessel pieces or fragments to their maximum velocity. For failure of a compressed gas vessel, the energy absorbed in the fracture process is negligible because the vessel is already stressed to failure. But, the energy absorbed in accelerating vessel fragments can be significant. In experiments such as those of Esparza and Baker (1977a) and Boyer, et al (1958) with pressurized glass spheres and Pittman (1972), (1975) with metal pressure vessels, the fragments were observed with high speed cameras or other velocity measuring systems. In accidental vessel bursts, the velocities of fragments can be estimated by methods to be presented in Chapter IV. Knowing mean fragment velocity U and total mass M of the vessel, one can then compute the kinetic energy of the vessel fragments

$$E_k = M\ U^2/2 \qquad (1\text{-}4)$$

To obtain an estimate of effective blast yield for gas vessel bursts, we then use either eq. (1-1) or (1-2) and subtract fragment kinetic energy, i.e.,

$$E_e = E - E_k \tag{1-5}$$

1-3 Flash-Evaporating Liquid Bursts

Many fluids are stored in vessels under sufficient pressure that they remain essentially liquid at the vapor pressure corresponding to the storage temperature for the particular liquid. Examples are the fuels propane or butane which are normally stored at "room" temperature, methane (LNG) and hydrogen (LH_2) which must be stored at cryogenic temperatures, and refrigerants such as ammonia or the Freons which are also stored at room temperature. If a vessel containing such fluids fails, the resulting sudden pressure release can cause expansion of vapor in ullage space and partial flash evaporation of the liquid, and drive a blast wave into the surrounding air.

Because the properties of flash-evaporating fluids differ markedly from perfect gases, the methods for estimating blast yield for gas vessel bursts are inapplicable. Instead, one must know the complete thermodynamic properties of the fluid in the vessel as functions of state variables such as pressure, specific volume, temperature, and entropy.

For any expansion process from state 1 to state 2, the specific work done is defined (see any basic thermodynamics text) as

$$e = u_1 - u_2 = \int_1^2 p\, dv \tag{1-6}$$

where u is internal energy, and v is specific volume. We assume that an isentropic expansion process occurs after vessel burst. This process is shown schematically in a p-v diagram in Fig. 1-1, and in a T-s (temperature-entropy) diagram in Fig. 1-2. The particular initial state 1 shown in these two figures lies in the superheated vapor region, and so does the final state 2 after isentropic expansion to ambient pressure p_a. The cross-hatched area in Fig. 1-1 is the integral of eq. (1-6), and therefore represents the specific energy e. Also shown in the two figures are the saturated liquid and saturated vapor lines, which bound the wet vapor region. Whenever the expansion process occurs near or in the wet vapor region, as is always true for flash-evaporating fluids, the functional relationship between pressure and specific volume is quite complex and the integral in eq. (1-6) cannot be obtained analytically. But fortunately, there are tables of thermodynamic properties available for many fluids, and the in-

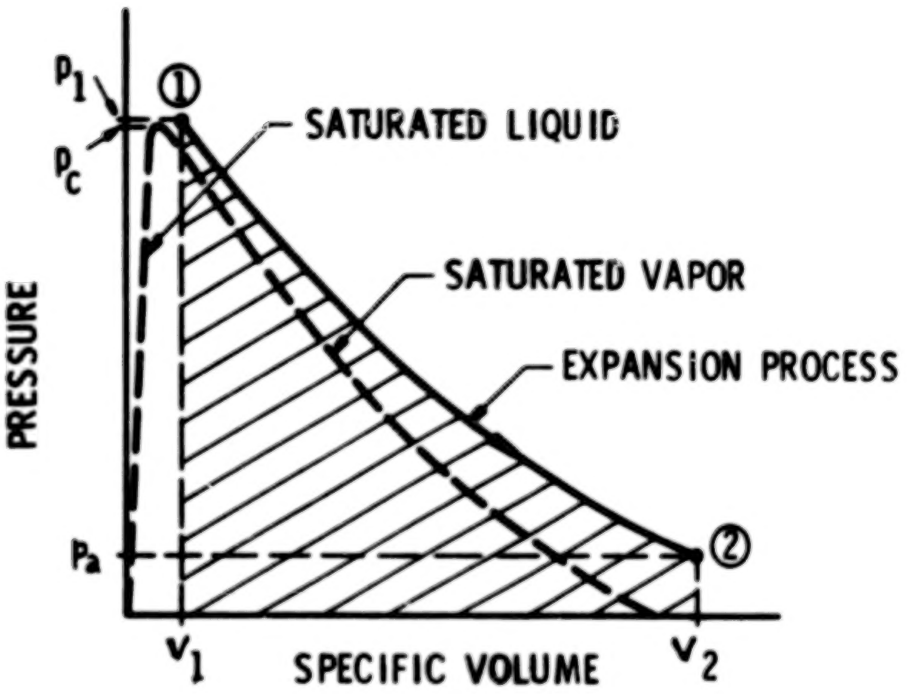

FIGURE 1-1. P-V DIAGRAM OF EXPANSION

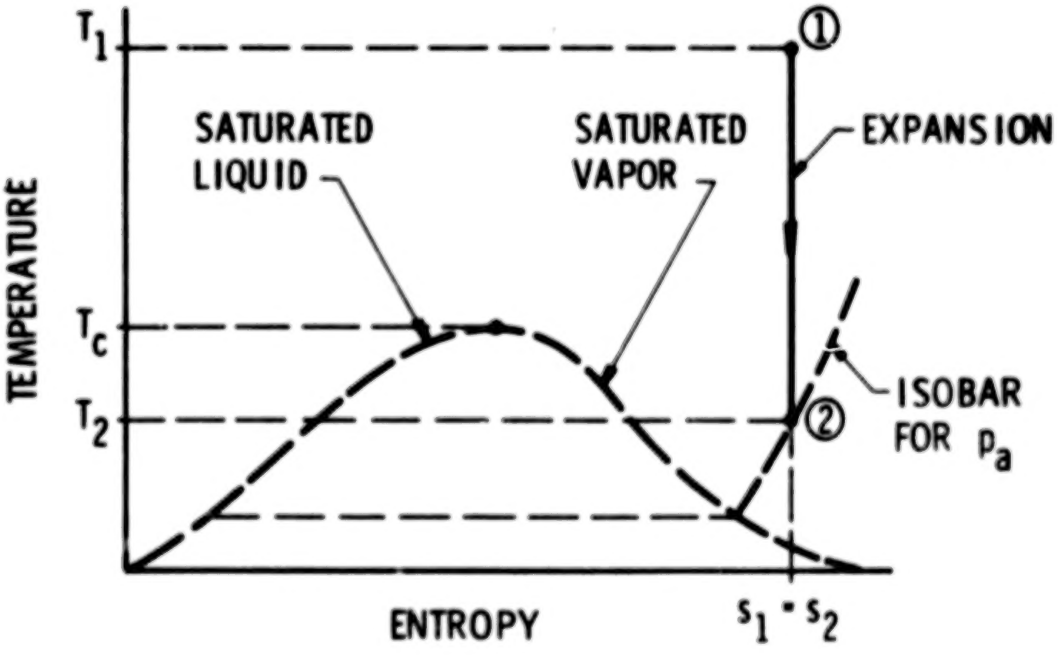

FIGURE 1-2. T-s DIAGRAM OF EXPANSION

ternal energy u or enthalpy h defined as

$$h = u + pv \tag{1-7}$$

are tabulated for the entire wet vapor region and the superheat region, as functions of pressure and specific volume, or temperature and entropy. When an initial or a final state falls within the wet vapor region, an important parameter is the quality of the vapor, defined as

$$x = \frac{v-v_f}{v_g-v_f} = \frac{s-s_f}{s_g-s_f} = \frac{u-u_f}{u_g-u_f} = \frac{h-h_f}{h_g-h_f} \tag{1-8}$$

where subscript f refers to fluid (saturated liquid) and subscript g refers to gas (saturated vapor). Also, within the wet vapor region, a given pressure uniquely defines a corresponding temperature, and vice versa.

In bursts of vessels containing flash-evaporating fluids, three combinations of state variables are possible at states 1 and 2. These are:

Case 1) Superheated vapor at state 1 and at state 2 (as for the process shown in Figs. 1-1 and 1-2)

Case 2) Superheated vapor at state 1 and wet vapor at state 2

Case 3) Wet vapor (including both saturated liquid and saturated vapor) at state 1, and wet vapor at state 2.

The process of estimating e and total blast yield E is basically the same, but, depending on where state 1 lies, the procedure for entering the thermodynamic tables differs somewhat. The basic procedure is as follows:

Step 1) Estimate the initial state variables, including p_1, v_1, s_1, u_1, or h_1

Step 2) Assume isentropic expansion to atmospheric pressure p_a, i.e., $s_2 = s_1$. Determine v_2, u_2, or h_2.

Step 3) Calculate specific work e from eq. (1-6)

Step 4) Calculate total blast yield E by multiplying e by mass m of fluid initially present in the vessel.

In Step 4, we use the basic definition of specific volume to obtain

the mass m of fluid from the known vessel volume V_1,

$$v_1 = V_1/m \tag{1-9}$$

and compute E from

$$E = m(u_2 - u_1) \tag{1-10}$$

Let us describe the differences in the three cases enumerated above. In Cases 1 and 2, the initial state conditions must be obtained from superheat tables for the fluid, usually entering with knowledge of the pressure and temperature together. In Case 1, superheat tables are also used for $p_2 = p_a$, $s_2 = s_1$, to obtain the final state conditions; while in Case 2, the saturated vapor tables must be used with the definition of final quality x_2, determined from final entropy s_2, being the most important factor. In case 3, all values are found in the saturated vapor table, with initial quality x_1 usually being determined from a real or fictitious initial specific volume. This case is probably the most common for flash-evaporating fluid vessel bursts. The fictitious initial specific volume for a vessel which is partially filled is obtained simply from eq. (1-9) by using m as the mass of liquid in the vessel of volume V_1.

Some tables of thermodynamic properties for fluids which can be used to estimate blast yields by the process just described are the ASHRAE Handbook of Fundamentals for refrigerants, Keenan, et al (1969) for steam, Din (1962) for a number of fluids including fuels such as propane and ethylene, and Goodwin (1974) and Goodwin, et al (1976) for methane and ethane. In many instances, these tables do not include internal energy u directly, but instead include h, p and v. One then has to use eq. (1-7) to calculate u. Also, most of tables are given in English units, so calculations are usually made in these units. SI units are shown, and a conversion table is provided.

Several example calculations of blast energy for Freon 12 refrigerant, using tables from the ASHRAE handbook, follow:

Isentropic expansion of Freon-12 liquid at $p_1/p_a = 20.3$ and room temperature $\theta = 76°F$. Since no properties for compressed (subcooled) liquid Freon-12 seem to be available, properties for state 1 will be assumed as those of a saturated liquid. Furthermore, since this is an estimate of the change in internal energy caused by the expansion of the pressurized refrigerant, interpolation of table values will be minimized.

For p_1 = 290 psi ≃ 296 psia

specific volume $v_1 = 0.01465\ ft^3/lb_m$

enthalpy $h_1 = 48.065\ Btu/lb_m$

entropy $s_1 = 0.09115^9\ Btu/lb_m\,°F$

and internal energy $u_1 = h_1 - p_1v_1$,

therefore $u_1 = 47.27\ Btu/lb_m$.

At state 2 after expansion ($s_1 = s_2$) to p_2 ~ 14.22 psia, the quality of vapor x_2 is

$$x_2 = \frac{s_1 - s_f}{s_g - s_f} = 0.508$$

Therefore,

$$v_2 = v_f + x\ v_{fg} = 1.328\ ft^3/lb_m$$

$$h_2 = h_f + x\ h_{fg} = 39.759\ Btu/lb_m$$

and

$$u_2 = h_2 - p_2v_2 = 36.263\ Btu/lb_m$$

Thus,

$$e = u_1 - u_2 = 11.0\ Btu/lb_m$$

Converting this to an energy per unit volume,

$$\frac{e}{v_1} = 247.6\ Btu/ft^3$$

For a vessel with initial volume $V_1 = 31.24\ in^3$, the estimated energy available due to an isentropic expansion was

$$E = \frac{e}{v_1} V_1 = 247.6 \text{ Btu/ft}^3 \times 9336 \text{ in-lb}_f/\text{Btu} \times \frac{1}{1728} \text{ ft}^3/\text{in}^3 \times 31.24 \text{ in}^3$$

or

$$E = 11{,}200 \text{ Joules}$$

If the fragment velocity is measured, then the kinetic energy of the fragments would be subtracted to obtain the energy available for driving a blast wave, using eq. (1-5).

For an isentropic expansion of Freon-12 vapor at $p_1/p_a = 3.45$ and $\theta_1 = 78°F$,

$$v_1 = 0.90 \text{ ft}^3/\text{lb}_m$$

$$h_1 = 88.42 \text{ Btu/lb}_m$$

$$s_1 = 0.17984 \text{ Btu/lb}_m - °F$$

and

$$u_1 = h_1 - p_1 v = 80.2 \text{ Btu/lb}_m$$

At $P_2 \sim 14.0$ psia

$$s_2 = s_1 > s_g \text{ (still in superheated region)}$$

$$v_2 = 2.83 \text{ ft}^3/\text{lb}_m$$

$$h_2 = 78.42 \text{ Btu/lb}_m$$

and

$$u_2 = 71.09 \text{ Btu/lb}_m$$

Therefore,

$$e = 9.11 \text{ Btu/lb}_m$$

and

$$\frac{e}{v_1} = 3.337 V_1$$

For a vessel with $V_1 = 37.59 \text{ in}^3$

$$E = 3.337 \text{ BTU/ft}^3 \times 9336 \text{ in-lb}_f/\text{BTU} \times \frac{1}{1728} \text{ ft}^3/\text{in}^3 \times 37.59 \text{ in}^3$$

$$E = 678 \text{ in-lb}_f$$

or

$$E = 76.5 \text{ Joules}$$

1-4 Vapor Cloud Explosions

A number of very damaging explosions have occurred after release of fuels as gases or aerosols. Strehlow and Baker (1975) have listed some of the more significant accidental explosions of this nature. Probably the most damaging vapor cloud explosion to date occurred in a chemical plant at Flixborough [Tucker (1975), Parker, et al (1974)] in 1974, with 28 fatalities and well over $100 million in damage including almost complete destruction of the plant. The fuel which was released in this explosion was the hydrocarbon cyclohexane, an ingredient used in the manufacture of nylon.

The history of vapor cloud explosions shows that almost any liquid or gaseous fuel can cause such explosions, given appropriate time for mixing with the air, appropriate ratios of fuel to air, and an ignition or explosion source. In Strehlow and Baker (1975), fuels noted as causing serious explosions were propane, ethylene, propylene, butane, liquid hydrocarbon residues, and hot cyclohexane. For some fuels, true detonations can occur, i.e., rapid chemical reactions progressing at rates greater than sound velocity in the fuel-air cloud. For the vast majority of accidental vapor cloud explosions, it is unlikely that detonations have or will occur because this most violent type of reaction requires fuel-air mixtures within the rather narrow detonable limits plus a strong ignition source, or a very large cloud in which a less violent burning or deflagration can build to a detonation.

Also, this transition usually requires some confinement. But detonating fuel-air mixtures are used as weapons [Robinson (1973)], and gaseous fuels mixed with oxygen are used as large blast sources for simulation of nuclear weapons blast [Choromokos (1972)].

Assessment of damage and correlation of the damage with blast yield has been attempted for some large vapor cloud explosions [Tucker (1974), Strehlow and Baker (1975)]. Generally, these estimates show that accidental vapor cloud explosions are almost invariably much less damaging than the planned vapor detonations mentioned above. Blast yields seem to have been, at most, 20% of values estimated on the basis of total heats of combustion of the fuels involved. This is probably so because not all (perhaps very little) of the fuel-air cloud has a mixture ratio lying within the detonable range, because no strong ignition sources capable of starting detonations were present, and because only a deflagration rather than a detonation occurred. This is of small comfort to the victims of vapor cloud explosions, but does indicate that the full potential for damage is probably never realized in an accident. In a way, this conclusion parallels the results of Project PYRO tests for explosions of liquid propellants, which are summarized by Baker, et al (1975). In those experiments, blast yields were seldom greater than a few percent of the maximum potential yield for large-scale experiments.

Because of the great variability in vapor cloud explosions and the uncertainties noted above, estimation of the blast yield of vapor cloud explosions can only be very approximate. We suggest the following procedure:

1) Assume a stoichiometric mixture of the fuel in air and calculate the total heat of combustion, E_c.

2) Multiply the heat of combustion by some blast effectiveness factor less than one to obtain estimated blast yield E. The effectiveness factor can be based on past accident data and should at present be considered as a very crude estimate. Accident data to date indicate that it should probably never be greater than 20%.

Fuels which are gaseous at normal ambient conditions, but have vapor densities* greater than one, seem the most potentially dangerous candidates for vapor cloud explosions because they remain near the ground surface as they mix with air. Table 3-1 gives a partial listing of some such common fuels, together with detonable limits (when known), flammable limits expressed as volume percents in air, and values of E_c from Zabetakis (1965). This table also contains properties for the two most common fuels shipped or stored as cryogenics, hydrogen and methane.

*Vapor density is defined as the ratio of the density of the vapor to that of air at standard temperature and pressure.

Fuels which are gaseous but have low vapor densities (< 1) under normal ambient conditions seem potentially much less susceptible to vapor cloud explosions, because they rise rapidly as they mix with air. The two most common such fuels are methane (natural gas) with a vapor density of 0.55 and hydrogen, with a vapor density of 0.07. But both of these fuels are very energetic, and have wide flammability limits, so they cannot be completely excluded as potential sources for vapor cloud explosions.

By listing or mentioning only a limited number of fuels, we, of course, do not mean to exclude only liquid or gaseous fuel as a potential source for vapor cloud explosions. At present, we also cannot give good guidelines for estimating the effectiveness factor for converting maximum chemical energy release to blast yield.

BLANK PAGE

BLANK PAGE

TABLE 1-1. SOME FUELS WITH HIGH POTENTIAL FOR VAPOR CLOUD EXPLOSIONS

Fuel	Molecular Wt, M	Vapor Density	Boiling Point, °F	Detonability Limits Lower, %	Detonability Limits Upper, %	Flammability Limits Lower, %	Flammability Limits Upper, %	E_c, kcal/mol
Acetylene	26.04	0.91	gas	10	25	2.5	100	301.5
Ethylene oxide	44.05	1.736	51	6	24	3.0	100	281.1
Ethylene	28.05	0.97	gas	7	21	2.7	36	316.2
Propane	44.09	1.52	gas	--	--	2.1	9.5	488.5
1,3-Butadiene	54.09	1.9	gas	--	--	2	12	576.3
Monomethyl-amine	31.06	1.105	gas	--	--	4.2	20.8	--
Propylene	42.08	1.5	gas	--	--	2	11	460.4
Vinyl chloride	62.50	2.2	7	--	--	3.6	33	--
Butane	58.12	2.01	gas	--	--	1.8	8.4	635.4
Ethane	30.07	1.044	gas	--	--	3.0	12.4	341.3
1-Butene	56.10	1.995	gas	--	--	1.6	10	607.7
Propadiene	40.06	1.38	gas	--	--	2.6	--	--
Hydrogen	2.016	0.07 1.11	gas at B.P (-400.3)	20	65	4.0	75	241
Methane	16.043	0.55 1.52	gas at B.P (-115.8)	6	14	5.0	15	801

REFERENCES, CHAPTER I

Adamczyk, A. A. and Strehlow, R. A., (1977) "Terminal Energy Distribution of Blast Waves From Bursting Spheres", NASA CR 2903, Grant NSG 3008, September 1977.

ASHRAE Handbook of Fundamentals, (1972) American Society of Heating, Refrigerating and Air Conditioning Engineers, Inc. New York, N.Y., 1972.

Baker, W. E. (1973) Explosions In Air, University of Texas Press, Austin, Texas, 1973.

Baker, W. E., Kulesz, J. J., Ricker, R. E., Bessey, R. L., Westine, P. S., Parr, V. B. and Oldham, G. A., (1975) "Workbook for Predicting Pressure Wave and Fragment Effects of Exploding Propellant Tanks and Gas Storage Vessels," NASA CR-134906, Contract NAS3-19231, Nov 1975 (reprinted September 1977).

Boyer, D. W., Brode, H. L., Glass, I. I. and Hall, J. G., (1958) Blast From a Pressurized Sphere, UTIA Report No. 48, Institute of Aerophysics, University of Toronto, 1958.

Brinkley, S. R., (1969) "Determination of Explosive Yields," AIChE Loss Prevention 3, 1969, pp 79-82.

Brode, H. L., (1959) "Blast Wave From a Spherical Charge," Physics of Fluids 2, 1959, p 217.

Choromokos, J., (1972) "Detonable Gas Explosions - SLEDGE," Proceedings 3rd International Symposium on Military Applications of Blast Similators, Schwetzingen, Germany, September 1972, pp B4-1 through B4-10.

Esparza, E. D. and Baker, W. E., (1977a) "Measurement of Blast Waves From Bursting Pressurized Frangible Spheres," NASA CR-2843, Grant NSG 3008, May 1977.

Goodwin, R. D., (1974) "The Thermophysical Properties of Methane, from 90 to 500K of Pressures to 700 Bar," NBS Technical Note 653, U.S. Department of Commerce, National Bureau of Standards, April 1974.

Goodwin, R. D., Roder, H. M. and Straty, G. C., (1976) "Thermophysical Properties of Ethane, From 90 to 600K at Pressures to 700 Bar," NBS Technical Note 684, National Bureau of Standards, August 1976.

Parker, R. J., Pope, J. A., Davidson, J. F. and Simpson, W. J., (1974) "The Flixborough Disaster, Report of the Court of Inquiry," Her Majesty's Stationary Office, London, June 1974.

Pittman, J. F., (1976) "Blast and Fragments From Superpressure Vessel Rupture," Report No. NSWC/WOL/TR 75-87, Naval Surface Weapons Center, White Oak, Silver Spring, Md, February 1976.

Pittman, J. F., (1972) " Blast and Fragment Hazards From Bursting High Pressure Tanks," NOLTR72-102, U.S. Naval Ordnance Laboratory, Silver Spring, Md, May 1972.

Robinson, C. A., Jr., (1973)"Special Report: Fuel Air Explosives, Services Ready Joint Development Plan," Aviation Week and Space Technology, February 19, 1973, pp 42-46.

Strehlow, R. A. and Baker, W. E., (1975) "The Characterization and Evaluation of Accidental Explosions," NASA CR-134779, Grant NSG 3008, June 1975.

Tucker, D. M., (1975) "The Explosion and Fire at Nypro (UK) Ltd., Flixborough, on 1 June 1974," Building Research Establishment, Fire Research Station, Borehamwood, Hertfordshire, England, 1975.

Zabetakis, M. G., (1965) "Flammability Characteristics of Combustible Cases and Vapors," Bulletin 627, Bureau of Mines, U. S. Department of the Interior, 1965.

CHAPTER II

CHARACTERISTICS OF PRESSURE WAVES

2-1 General

The characteristics of blast waves from liquid propellant explosions and spherical gas vessel bursts, and their similarities and differences compared to waves from condensed high explosives such as TNT, are discussed at some length by Baker, et al (1975). Much of the data presented in that reference can be used with no change to predict blast wave properties for explosions in ground systems. Here, we supplement that reference with discussions of later theoretical predictions and experimental results, and give some additional curves for prediction of blast properties based on the more recent work. The theory we will present includes some two-dimensional blast propagation effects for bursting pressure vessels, while the new test data include measurements of blast waves from bursting, frangible spheres containing high pressure gases and a flash-evaporating fluid.

2-2 Two-Dimensional Blast Wave Characteristics

Gases are often stored in tanks under high pressure. When a pressure vessel bursts, a shock wave propagates away from it. To estimate the damage and injury from such an explosion, one must know the side-on overpressure P_s and the side-on specific impulse I_s.

In Baker et al (1975), a method is given for calculating side-on overpressure and specific impulse, P_s and I_s, from a pressure vessel burst. The flowfield is assumed to be spherical, and the effects of the container upon the blast wave are ignored. This treatment is reasonably good for lightweight vessels, e.g., spacecraft tanks. However, for heavy vessels, one must account more accurately for the effects of the vessel itself.

The following is a method for predicting P_s and I_s from a spherical pressure vessel burst of a type common in failure of ground-based vessels, with the vessel breaking in half and the two pieces being propelled in opposite directions. The situation is shown in Figure 2-1. The analysis is based on the computer program TUTTI and is discussed in Appendix A.

Briefly, to find the overpressure at a given distance from the center of the vessel, one calculates a "starting overpressure" and locates this pressure on a curve on a graph of dimensionless overpressure versus dimensionless distance, $\bar{P}_s$ vs $\bar{R}$. The nearest $\bar{P}_s$ vs $\bar{R}$ curve is used to find P_s at the given distance. The specific impulse is calculated as in Baker, et al (1975).

The "starting overpressure" is calculated as follows: The terms

$$\frac{P_1}{P_a}$$

and

$$\frac{\gamma_1 (MW)_a T_1}{\gamma_a (MW)_1 T_a}$$

are computed, where p_1 is pressure, γ is the ratio of specific heats, (MW) is molecular weight, and T is absolute temperature. The subscript 1 refers to conditions inside the vessel before it bursts, and a refers to conditions in the surrounding atmosphere. The point

$$\left(\frac{P_1}{P_a} , \frac{\gamma_1 (MW)_a T_1}{\gamma_a (MW)_1 T_a} \right)$$

is located on one of the graphs in Figures 2-2, 2-3, or 2-4, depending on γ_1. $\bar{P}s_o$ is read for the point. The "starting overpressure" is $\bar{P}_A = 0.21\ \bar{P}s_o$. Figure 2-5 is a graph of $\bar{P}_s$ vs $\bar{R}$, where

$$\bar{P}_s = \frac{P_s}{P_a}$$

and

$$\bar{R} = \frac{r p_a^{1/3}}{E^{1/3}}$$

[r is the distance along the plane of symmetry from the center of the tank, and the energy in the tank is given by eq. (1-1)]. On Figure 2-5, the intersection of the constant $\bar{P}_s$ line (where $\bar{P}_s = \bar{P}_A$) and Curve A is found. This is the starting point. The nearest curve or curves give the $\bar{P}_s$ vs $\bar{R}$ behavior. For the distance of interest, calculate $\bar{R}$. $\bar{P}_s$ is then read from the appropriate curve.

$\bar{I}_s$ is read from Figure 2-6 or 2-7, whichever is more convenient.

$$\bar{I} = \frac{I_s A_a}{p_a^{2/3} E^{1/3}}$$

where A_a is the speed of sound in the surrounding atmosphere.

$$I_s = \bar{I} \frac{p_a^{2/3} E^{1/3}}{A_a}$$

P_s and I_s are accurate to about ±15%. The curves should <u>not</u> be extrapolated.

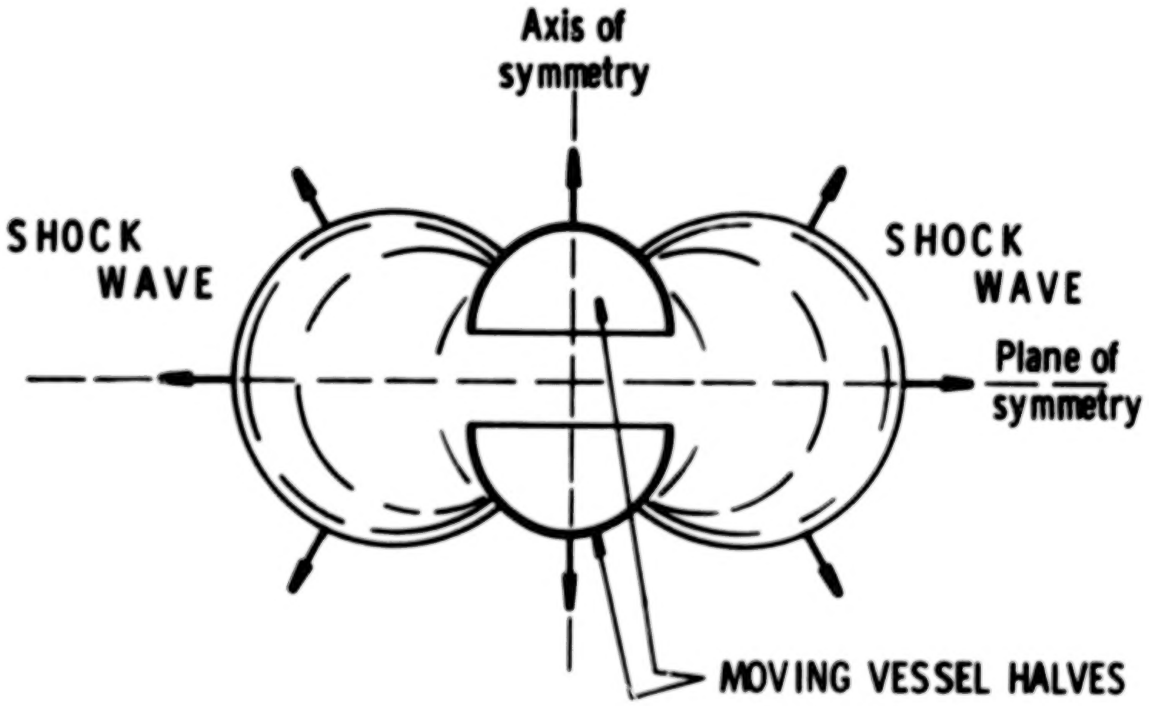

FIGURE 2-1. BURST OF A SPHERICAL PRESSURE VESSEL

The computer analysis on which these curves are based does not extend far enough in time to allow prediction of negative phase characteristics or second shock characteristics.

Example: A spherical vessel containing air ($\gamma_1 = 1.4$) at a pressure of $10^8 P_a$ (987.2 atm) and a temperature of 300°F bursts at sea level. The inner vessel radius is 0.19m. Find P_s and I_s at a distance r of 1.14m along the plane of symmetry from the center of the vessel.

Solution:

$$\frac{P_1}{P_a} = 987.2$$

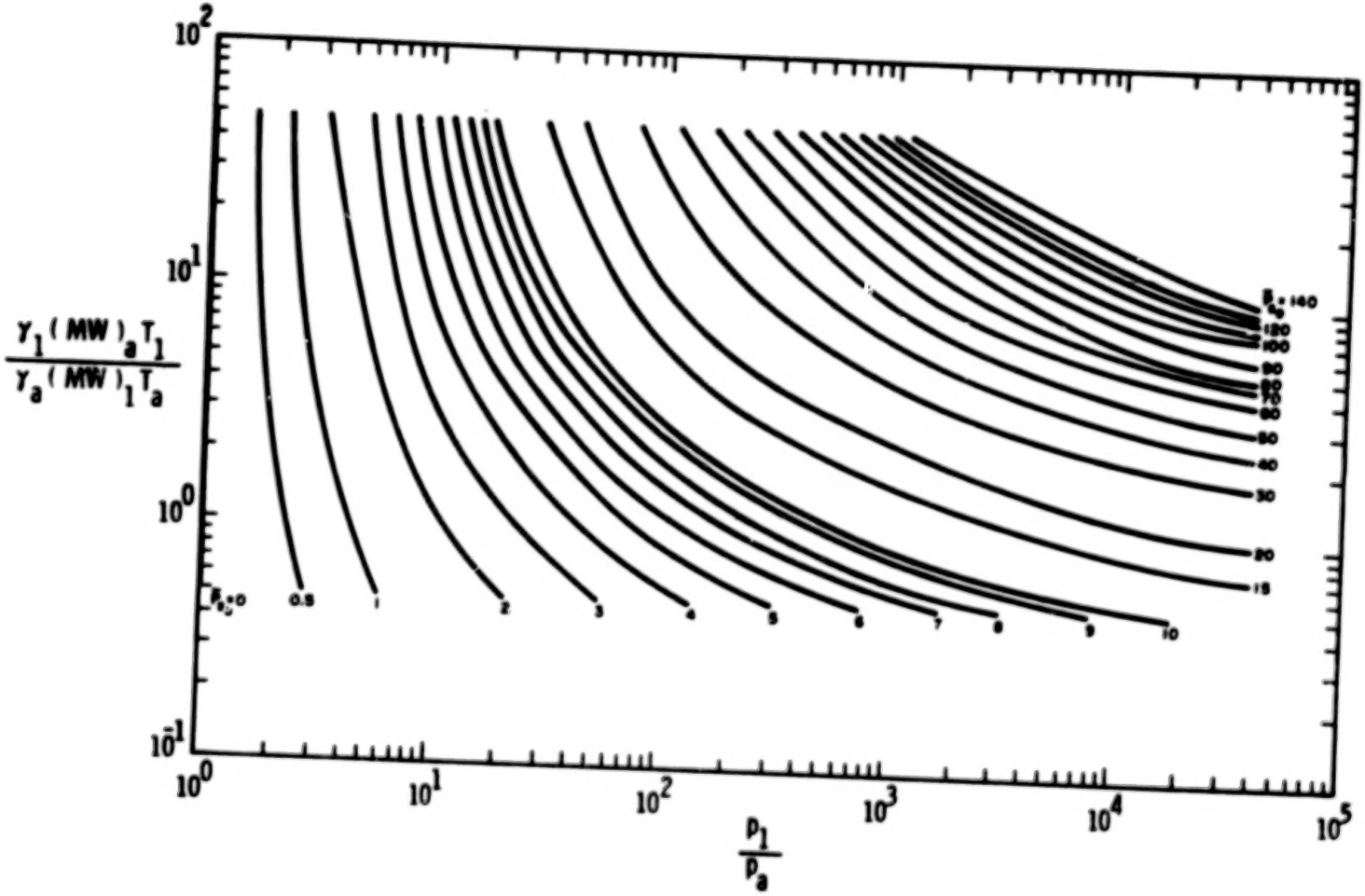

FIGURE 2-2. SCALED STARTING CONDITIONS FOR VARIOUS $\bar{P}_{s_o}$, $\gamma_1 = 1.4$

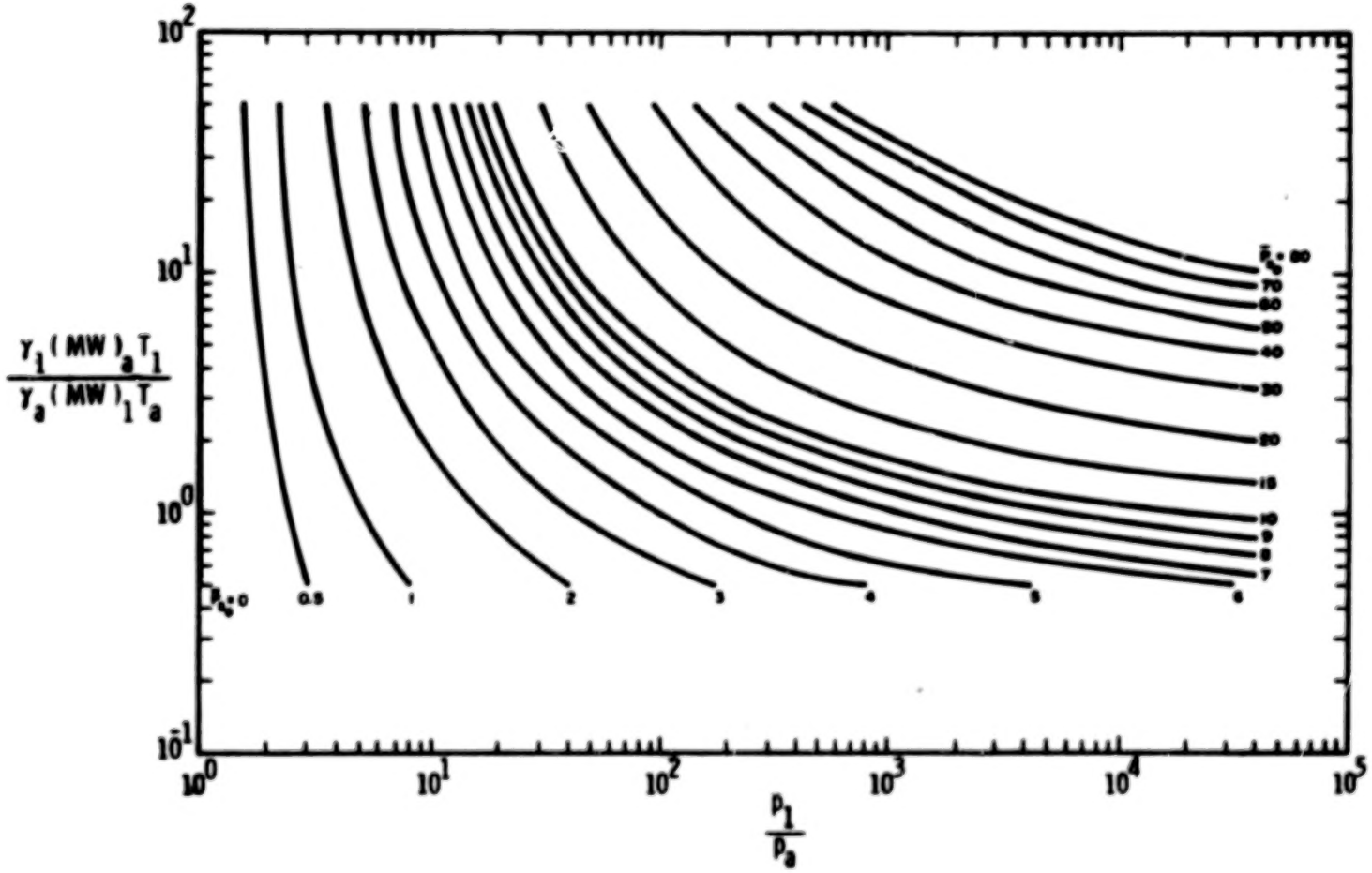

FIGURE 2-3. SCALED STARTING CONDITIONS FOR VARIOUS $\bar{P}_{s_o}$, γ_1 = 1.667

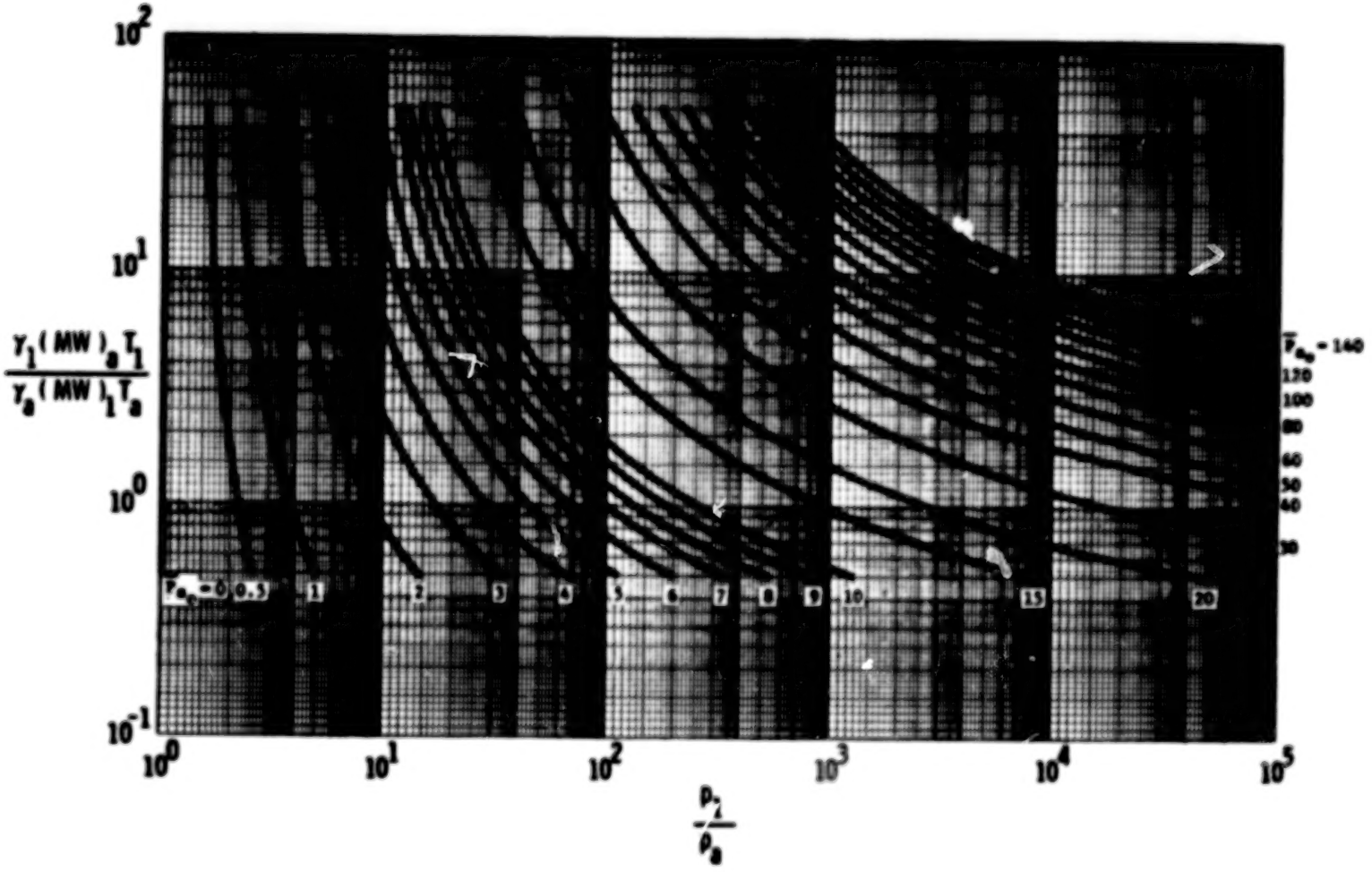

FIGURE 2-4. SCALED STARTING CONDITIONS FOR VARIOUS $\bar{P}_{s_o}$, $\gamma_1 = 1.2$

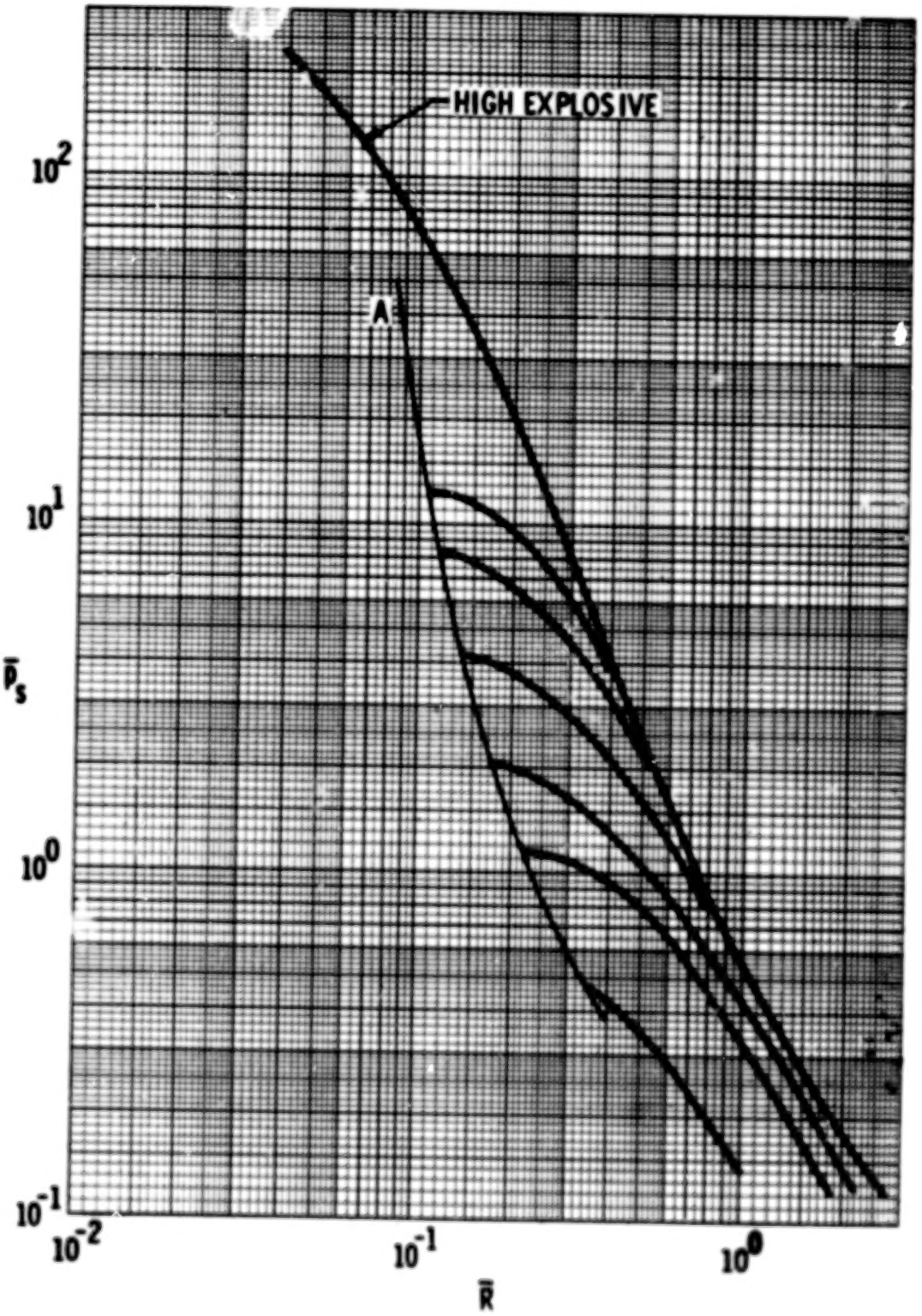

FIGURE 2-5. $\bar{P}_s$ VS. $\bar{R}$ FOR OVERPRESSURE CALCULATIONS. DISTANCE ALONG PLANE OF SYMMETRY

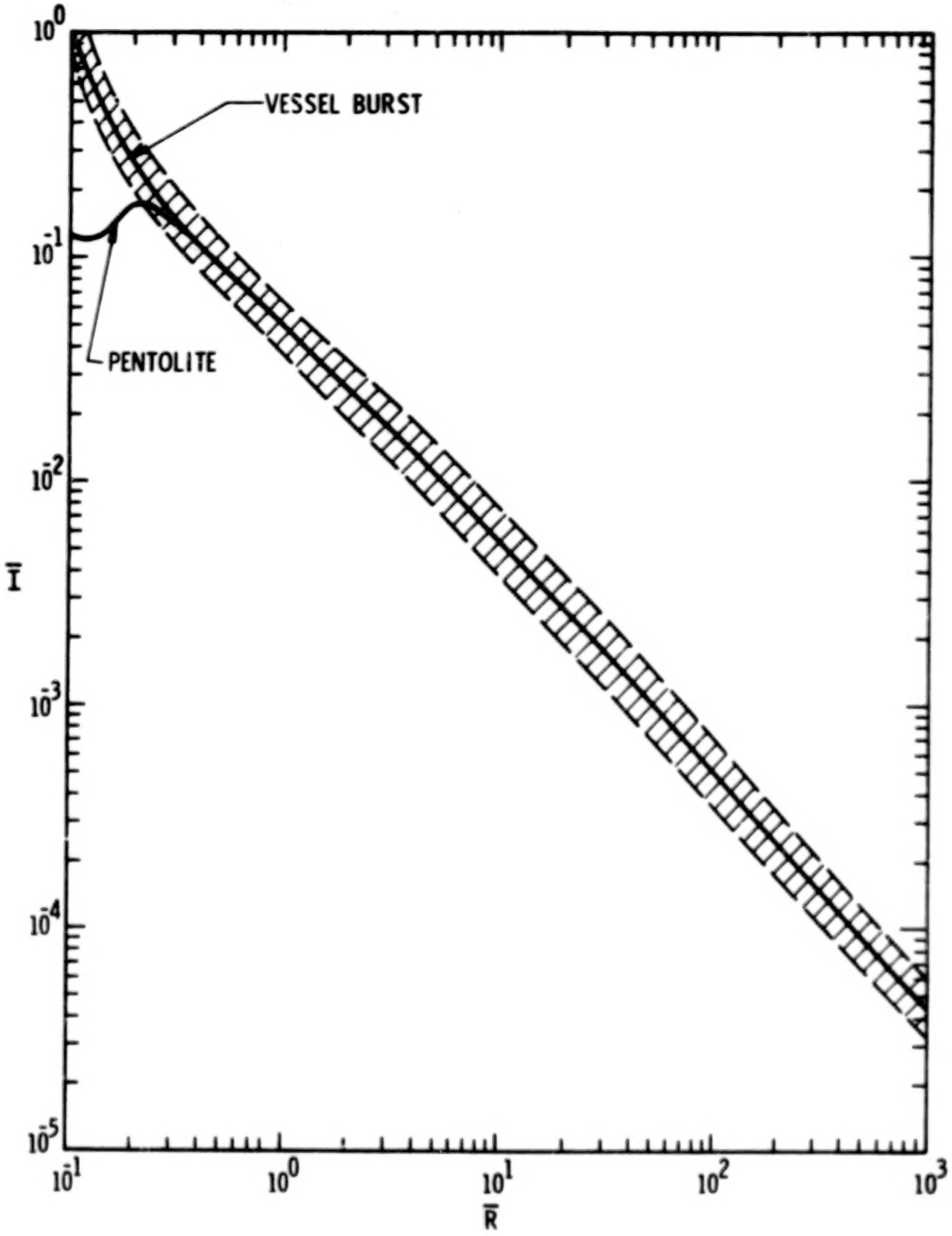

FIGURE 2-6. $\bar{I}$ VS $\bar{R}$ FOR PENTOLITE AND GAS VESSEL BURSTS

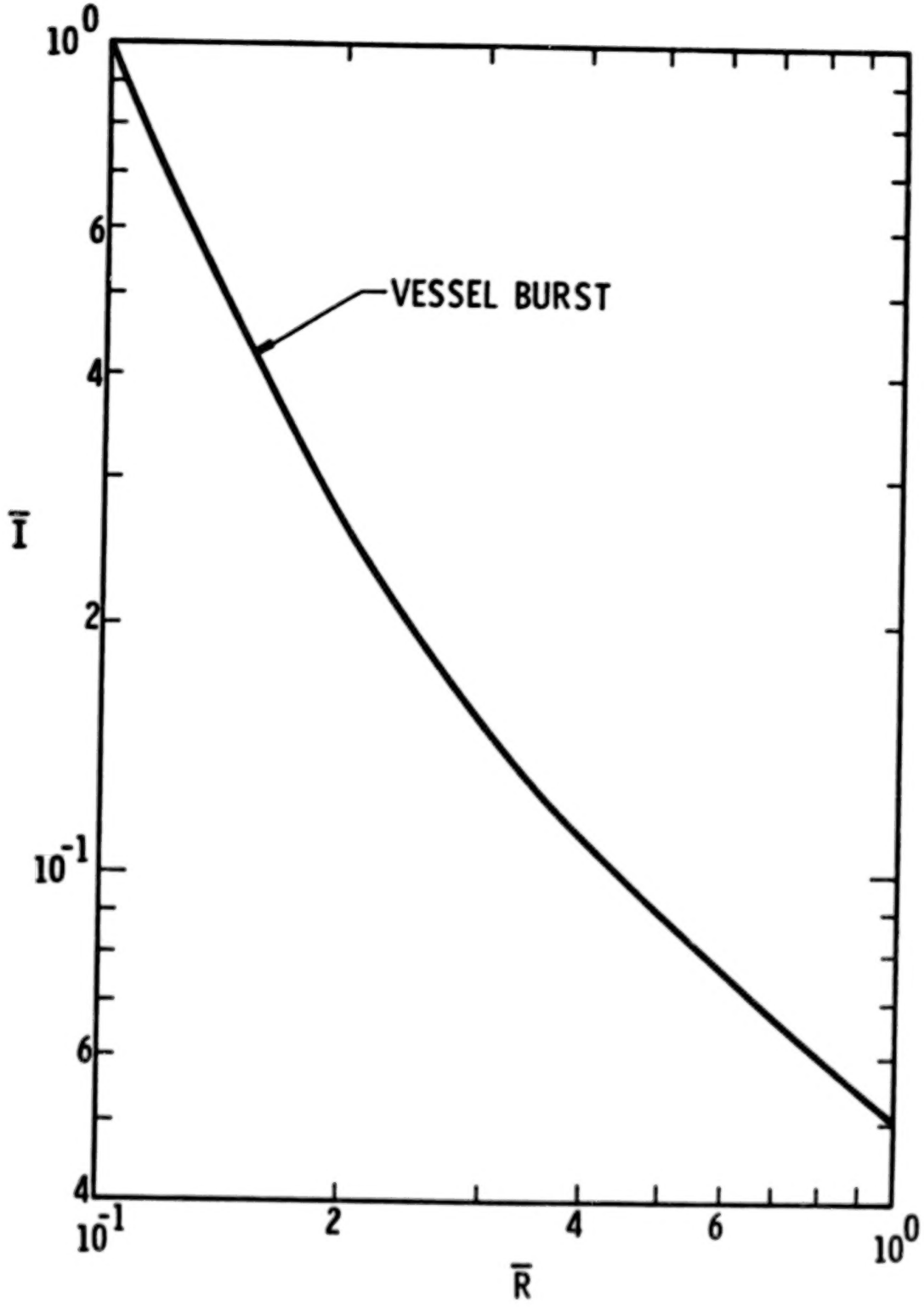

FIGURE 2-7. $\bar{I}$ VS $\bar{R}$ FOR GAS VESSEL BURSTS, SMALL $\bar{R}$

$$\frac{\gamma_1 (MW)_a T_1}{\gamma_a (MW)_1 T_a} = 1$$

Locating this point on Figure 2-2, $\bar{P}_{so} = 11$.

$$\bar{P}_A = 0.21\ \bar{P}_{so} = 0.21(11) = 2.3$$

Next, find the point on Figure 2-5 where Curve A crosses

$$\bar{P}_s = \bar{P}_A = 2.3.$$

This is near the third curve from the bottom of the page. This gives the $\bar{P}_s$ vs $\bar{R}$ behavior.

$$E = V_1 \frac{P_1 - P_a}{\gamma_1 - 1} = \frac{4\pi}{3} (0.19)^3 \frac{10^8 - 1.013X10^5}{1.4-1} = 7.8 \times 10^6\ J$$

$$\bar{R} = \frac{r\ p_a^{1/3}}{E^{1/3}} = \frac{1.14m(1.013X10^5 Pa)^{1/3}}{(7.18X10^6)^{1/3}} = 0.27$$

For this value of $\bar{R}$, $\bar{P}_s = 1.8$. $P_s = \bar{P}_s\ p_a = (1.8)\ (1.013 \times 10^5 Pa)$

$$= 1.8X10^5 Pa$$

From Figure 2-7, $\bar{I}_s = 0.16$. Then $I_s = \bar{I} \frac{p_a^{2/3} E^{1/3}}{A_a} =$

$$\frac{0.16(1.013X10^5)^{2/3}(7.18X10^6)^{1/3}}{344\ m/s} = 1.9 \times 10^3\ Pa \cdot s$$

2-3 Blast Waves from Bursting Frangible Spheres

Two recent experimental studies form the basis for some additional prediction curves for blast wave properties near bursting pressure spheres. Esparza and Baker, (1977a) and (1977b), report measurements of blasts from bursting frangible pressure spheres containing air and argon (1977a), and the refrigerant Freon 12 as both a compressed liquid and a compressed vapor (1977b).

These measurements, which include side-on pressure-time data over a range of scaled distances, show that compressed gas and vapor sphere explosions can generate waves which are distinctly different from the more familiar waves from condensed explosives.

A typical pressure-time trace is shown in Fig. 2-8. The distinctive characteristics are the pronounced negative phase compared to the first positive phase, and the strong second shock wave. By contrast, waves from condensed explosives show much smaller negative phases and seldom have a discernible second shock.

To report these blast wave properties, we must define more parameters than the usual ones. We have chosen the following ones (see Fig. 2-8).

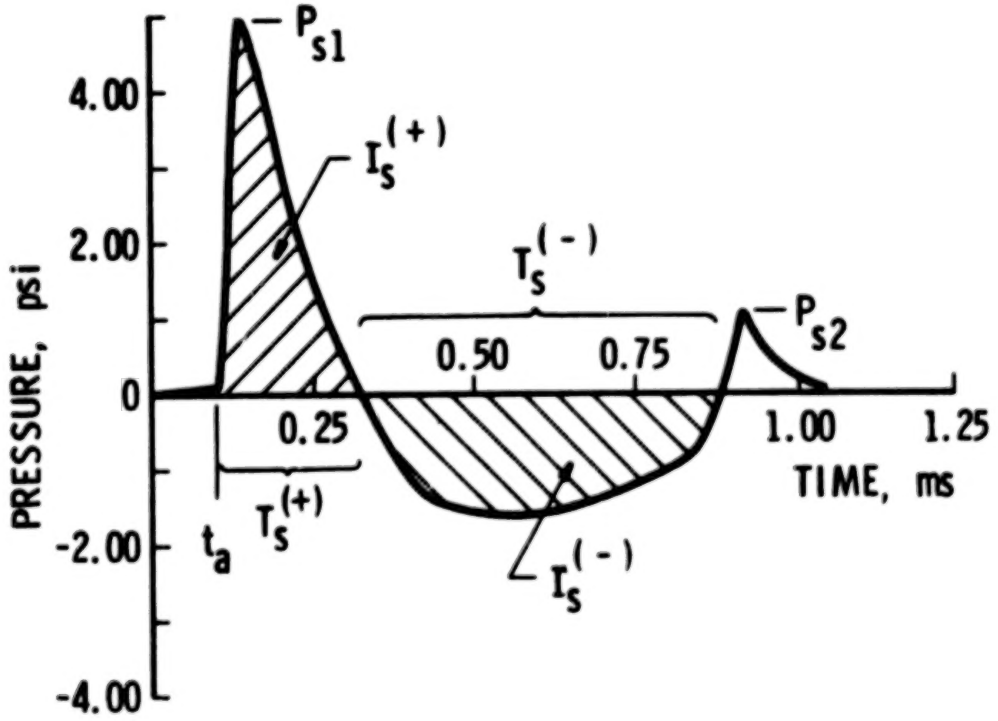

FIGURE 2-8. TYPICAL BLAST PRESSURE HISTORY FOR FRANGIBLE GAS SPHERE BURST

P_{s1} first shock side-on overpressure

$I_s^{(+)}$ positive phase impulse for first shock

$T_s^{(+)}$ duration of positive impulse for first shock

$I_s^{(-)}$ negative phase impulse for first shock

$T_s^{(-)}$ duration of negative phase for first shock

P_{s2} second shock side-on overpressure.

Prediction curves for scaled values of these parameters are given here. As in section 2-2, the scaling is given by:

$$\begin{aligned} \bar{P} &= P/p_a \\ \bar{I} &= I\, A_a\, p_a^{2/3}/E^{1/3} \\ \bar{T} &= T\, A_a\, p_a^{1/3}/E^{1/3} \\ \bar{R} &= R\, p_a^{1/3}/E^{1/3} \end{aligned} \tag{2-1}$$

and blast yield E is defined by

$$E = E' - E_k \tag{2-2}$$

where

$$E' = \frac{V_1(p_1 - p_a)}{(\gamma_1 - 1)} \tag{2-3}$$

for perfect gases and

$$E' = \frac{V_1}{v_1}\ (u_1 - u_2) \tag{2-4}$$

for wet vapors or gases near the thermodynamic "vapor dome."*

Figures 2-9 through 2-16 are derived from Esparza and Baker (1977a) for compressed gases. Blast wave characteristics were found to be only weakly dependent on specific heat ratio γ_1 for gas in the vessels and on initial pressure ratio (p_1/p_a). The latter parameter was varied over the range $9.9 \leq (p_1/p_a) \leq 42.0$ in the tests. Because of the weak dependence on these two parameters, all data are combined for various initial pressure ratios and ratios of specific heat. The figures show the range of all test data within the cross-hatched areas, and a "best fit" solid curve through the data. We suggest that the best fit curve be used for estimation, but one can use the upper limit curves to indicate uncertainties in the data.

Figures 2-17 through 2-22 are curves for compressed vapor for Freon-12 refrigerant, similar to the previous figures for compressed gases, from Esparza and Baker (1977b). That reference

*Chapter 1 gives methods for calculating the internal energy change $(u_1 - u_2)$.

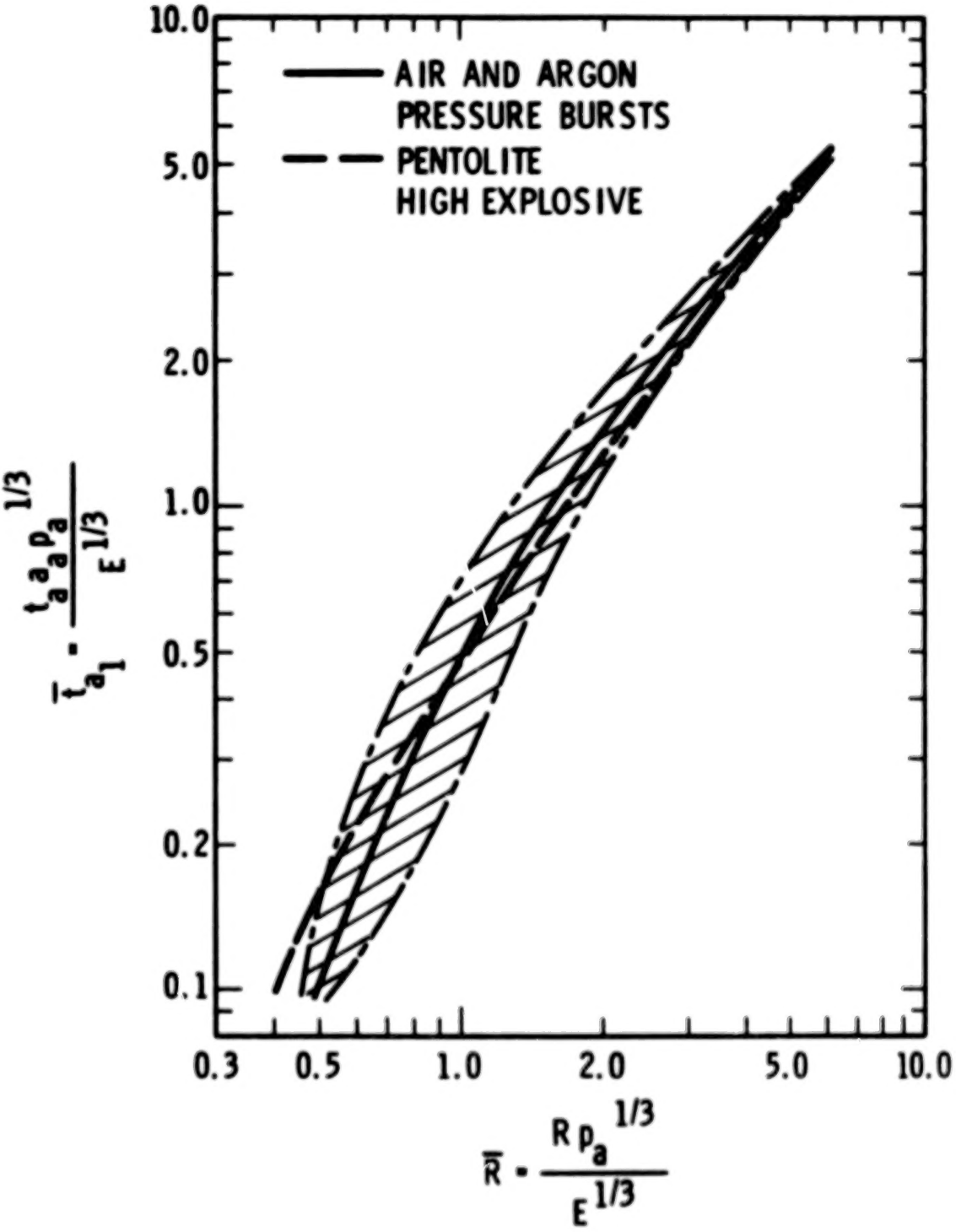

FIGURE 2-9. SCALED TIME OF ARRIVAL OF FIRST SHOCK WAVE FROM BURSTING GAS SPHERES

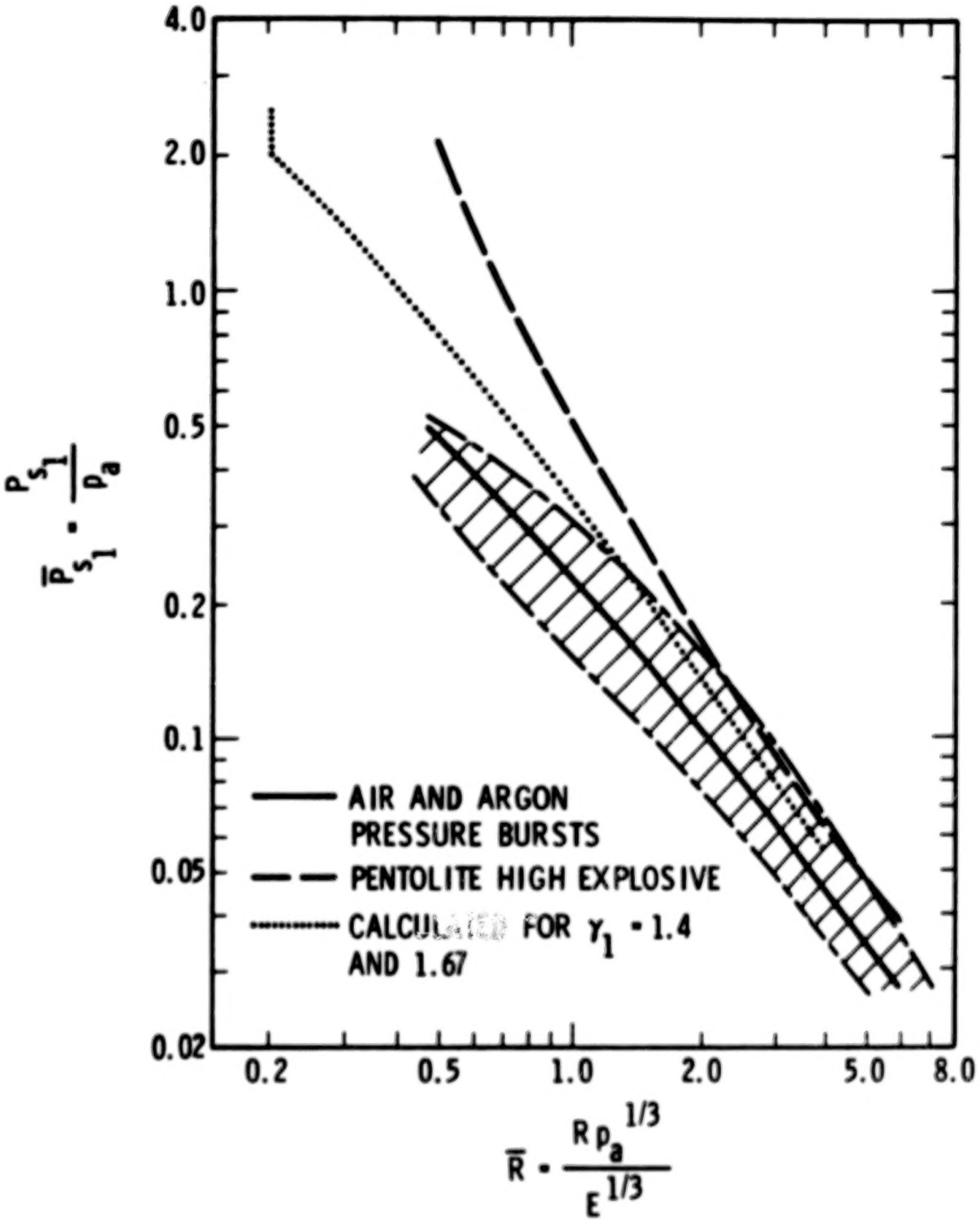

FIGURE 2-10. SCALED SIDE-ON PEAK OVERPRESSURE FOR FIRST SHOCK FROM BURSTING GAS SPHERES

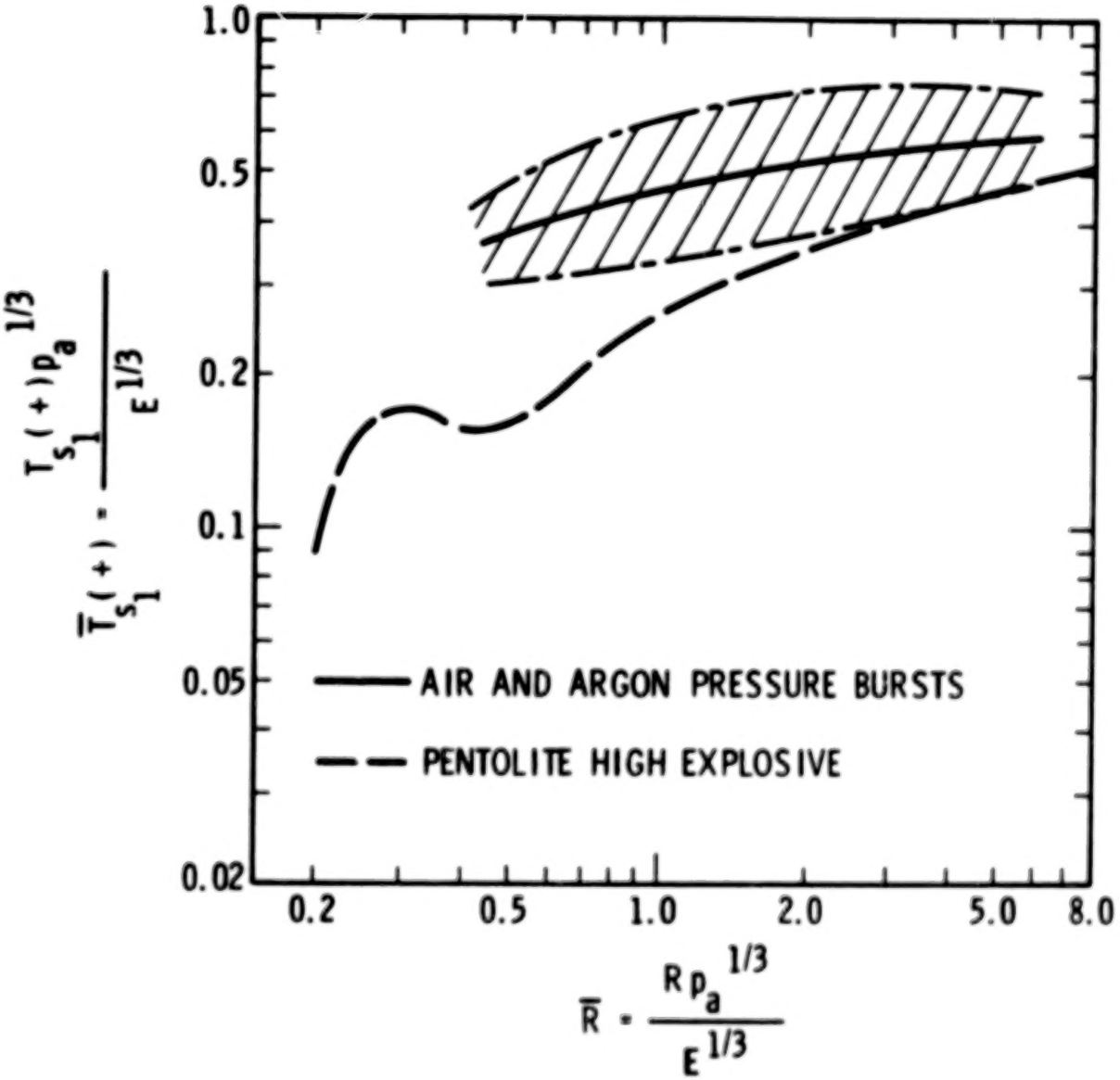

FIGURE 2-11. SCALED DURATION OF FIRST POSITIVE PHASE OF BLAST WAVE FROM BURSTING GAS SPHERES

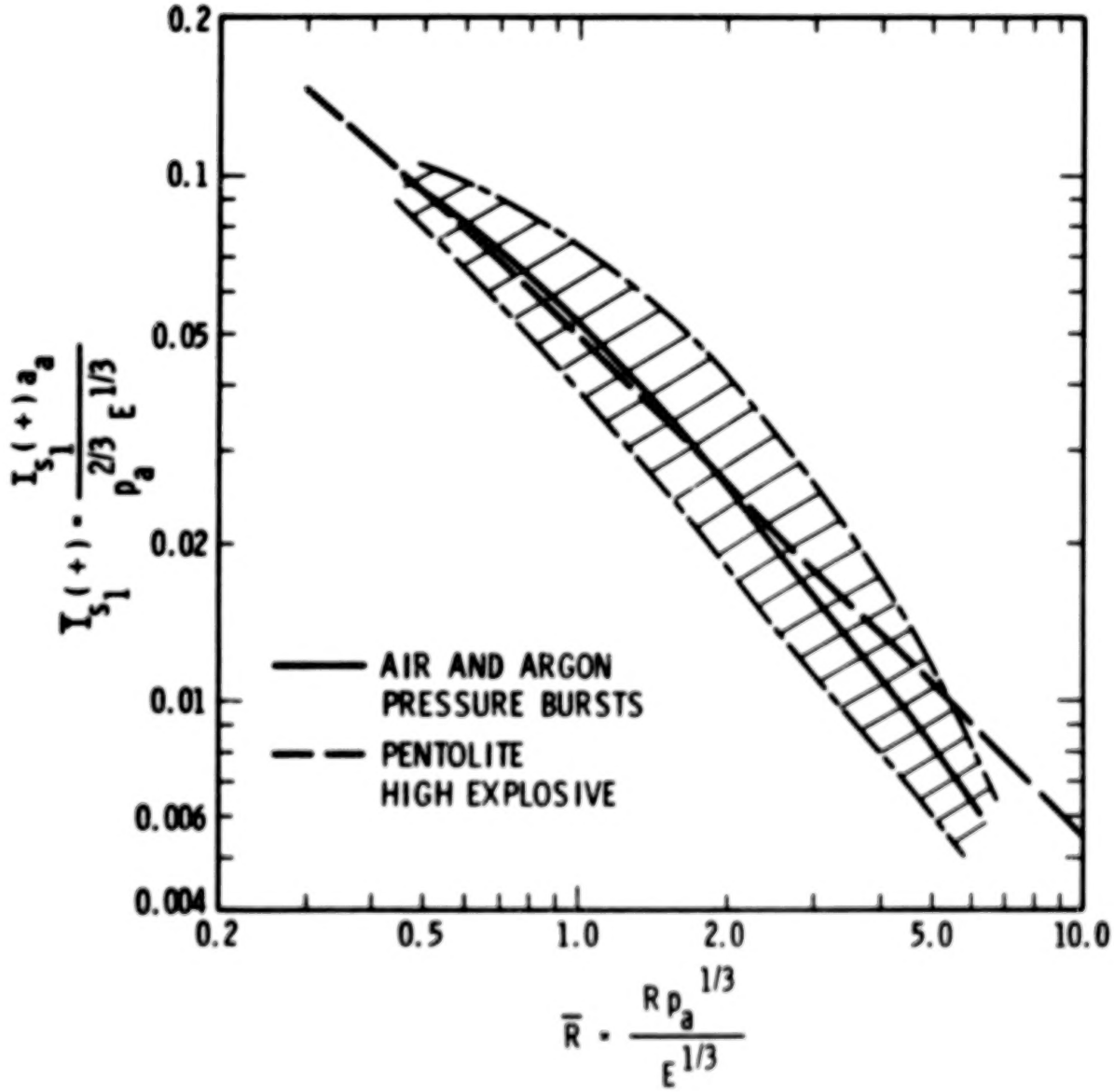

FIGURE 2-12. SCALED SIDE-ON POSITIVE IMPULSE FROM BURSTING GAS SPHERES

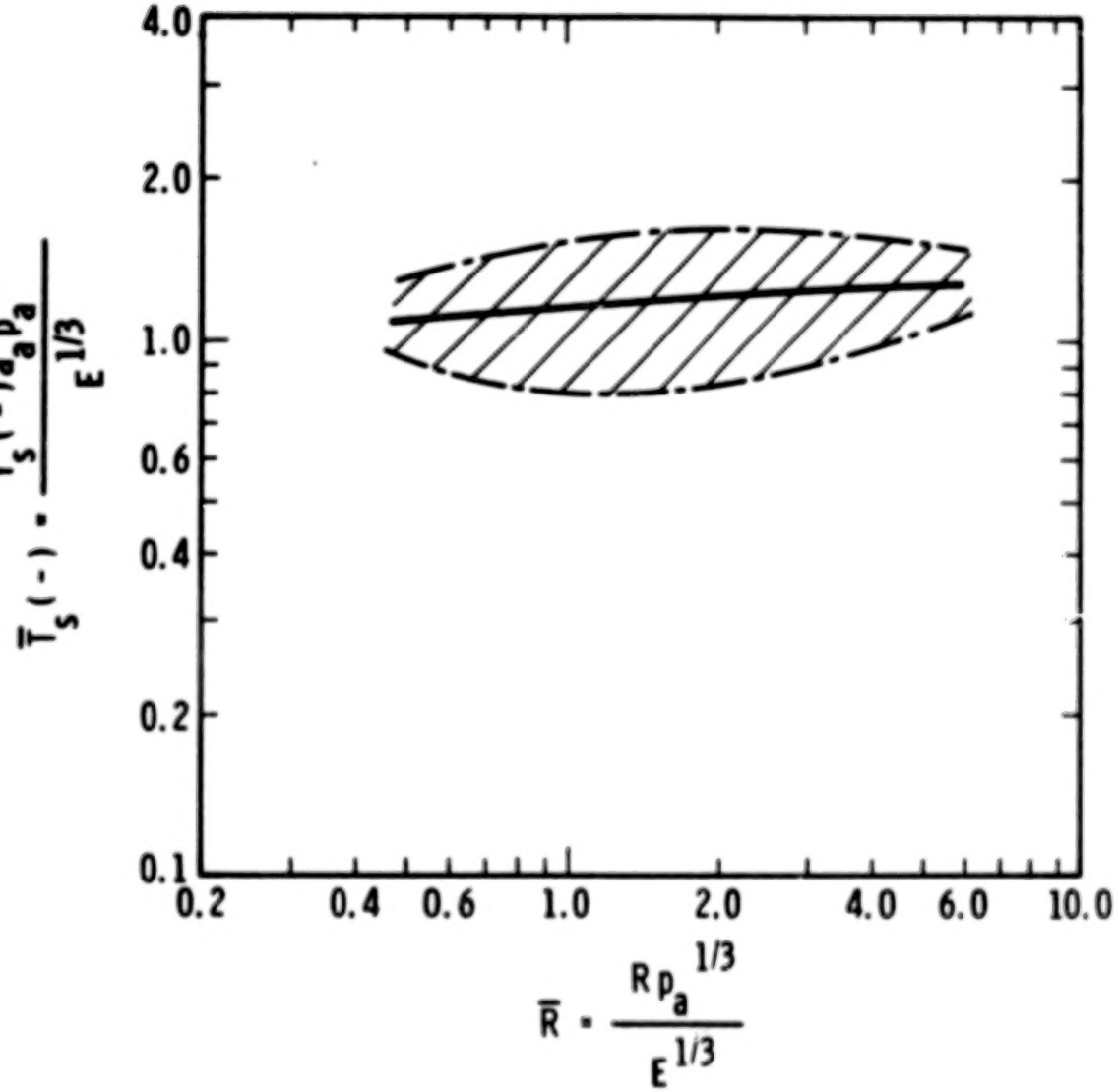

FIGURE 2-13. SCALED DURATION OF NEGATIVE PHASE OF BLAST WAVE FROM BURSTING GAS SPHERE

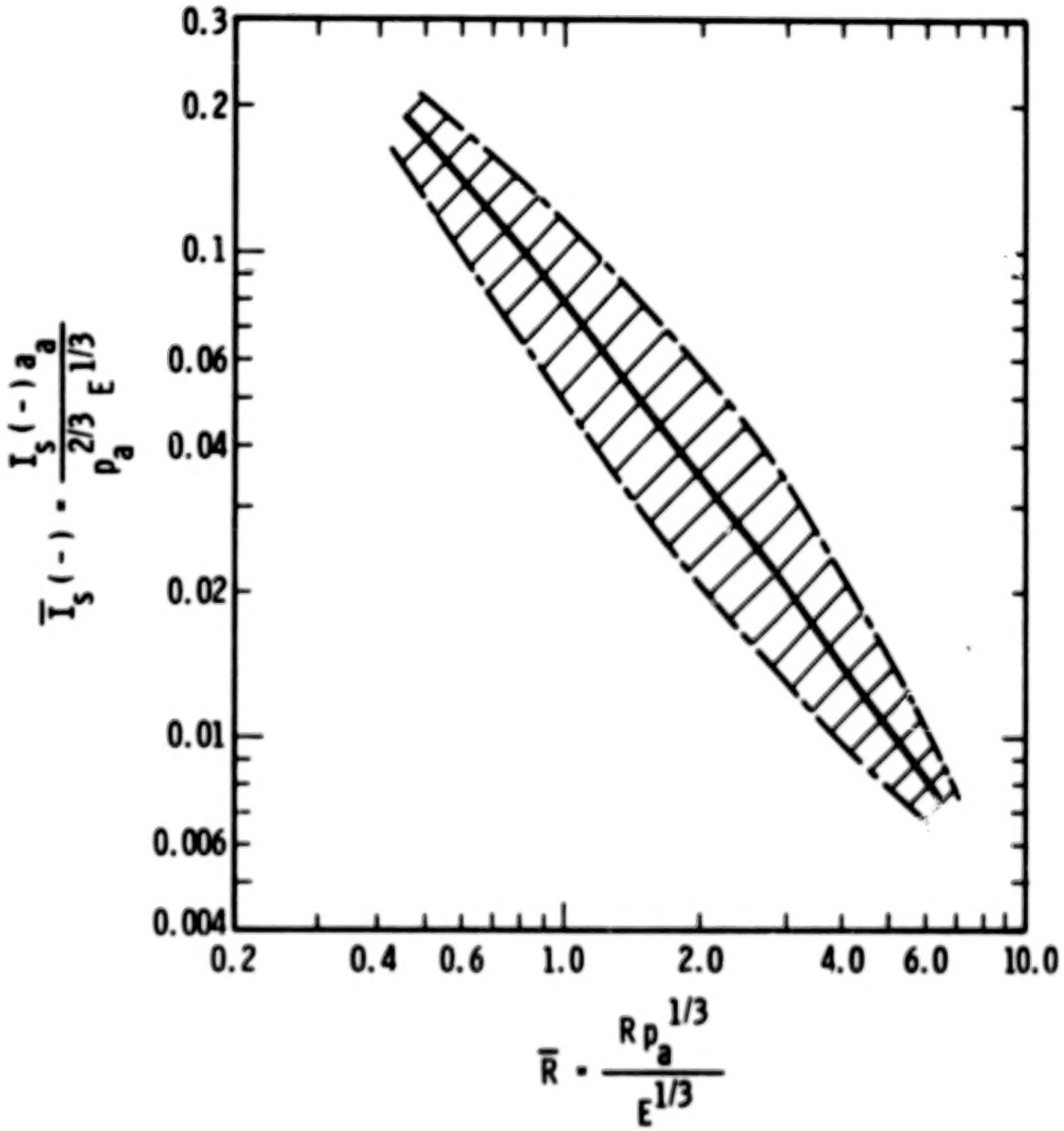

FIGURE 2-14. SCALED SIDE-ON NEGATIVE IMPULSE FROM BURSTING GAS SPHERES

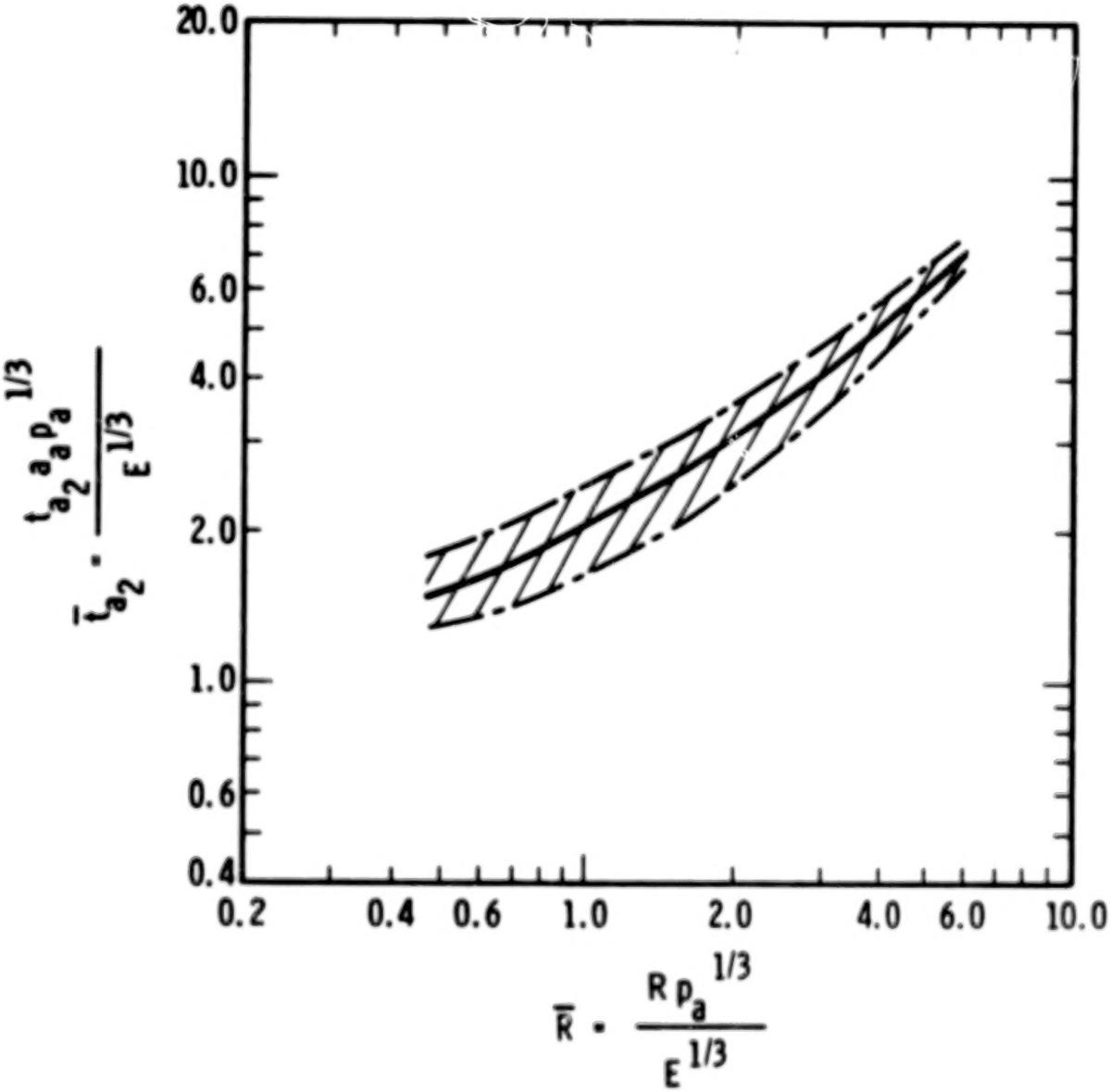

FIGURE 2-15. SCALED TIME OF ARRIVAL OF SECOND SHOCK WAVE FROM BURSTING GAS SPHERES

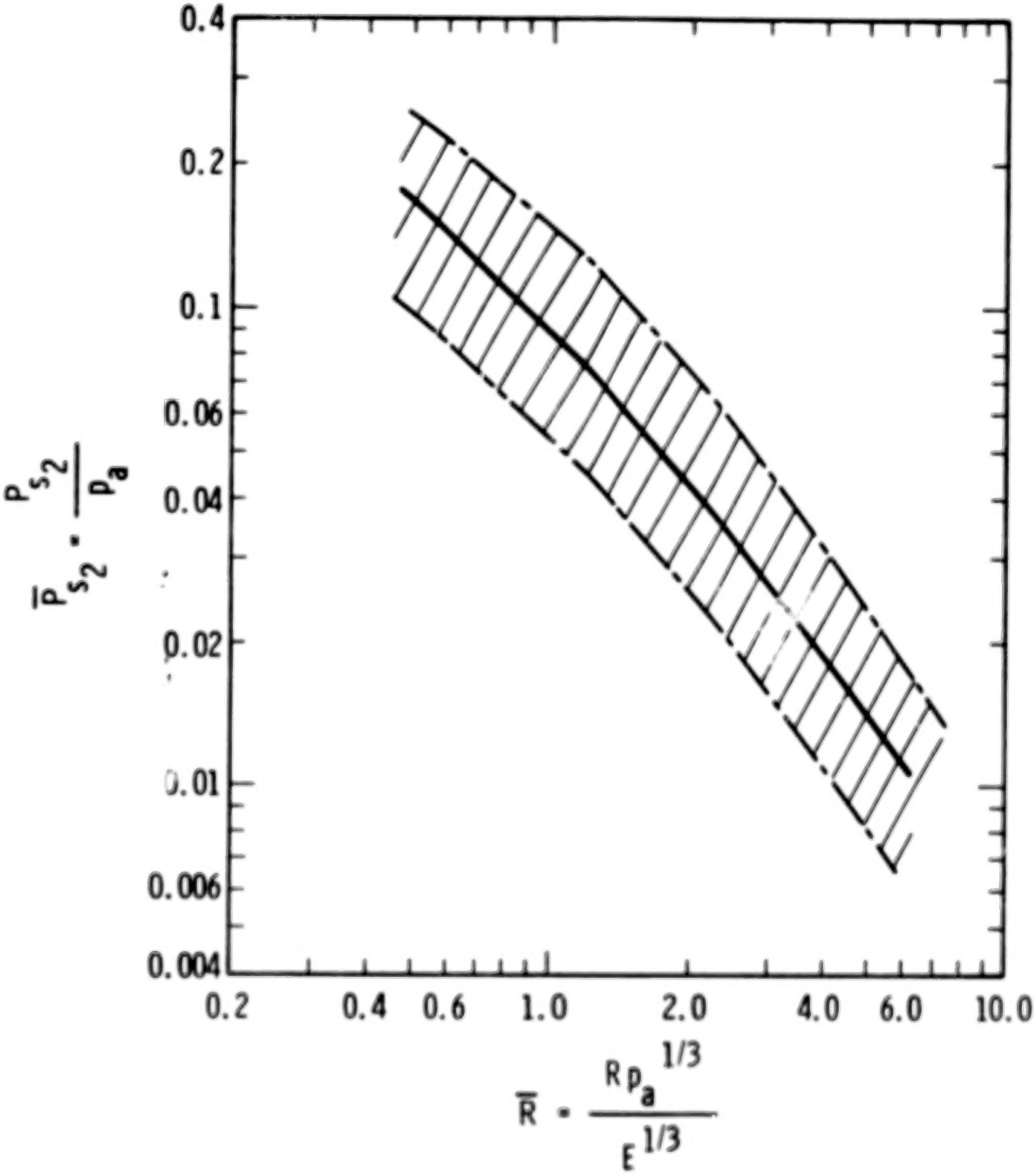

FIGURE 2-16. SCALED SIDE-ON PEAK OVERPRESSURE OF SECOND SHOCK FOR BURSTING GAS SPHERES

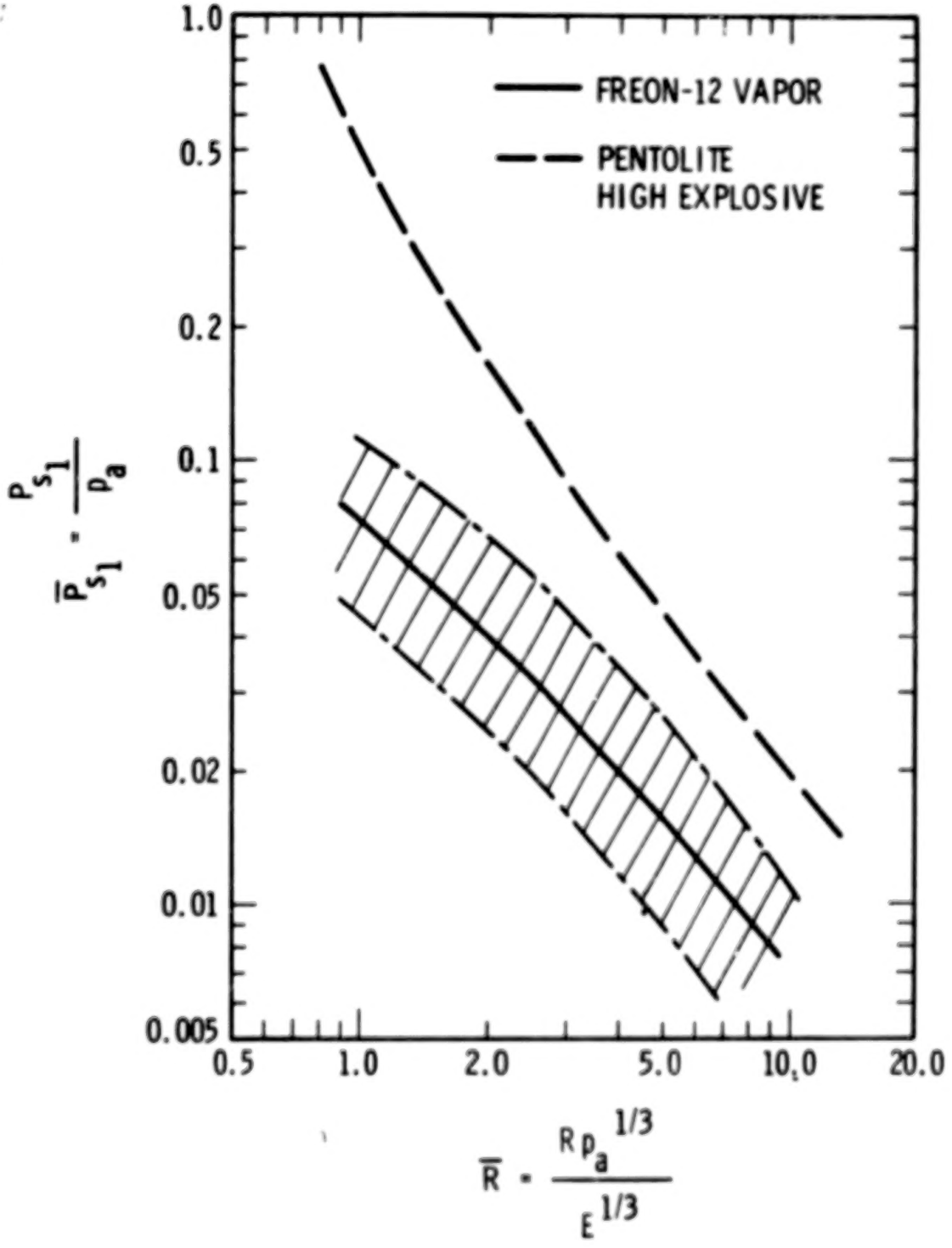

FIGURE 2-17. SCALED SIDE-ON PEAK OVERPRESSURE FOR BURSTING FREON-12 VAPOR SPHERE AT ROOM TEMPERATURE

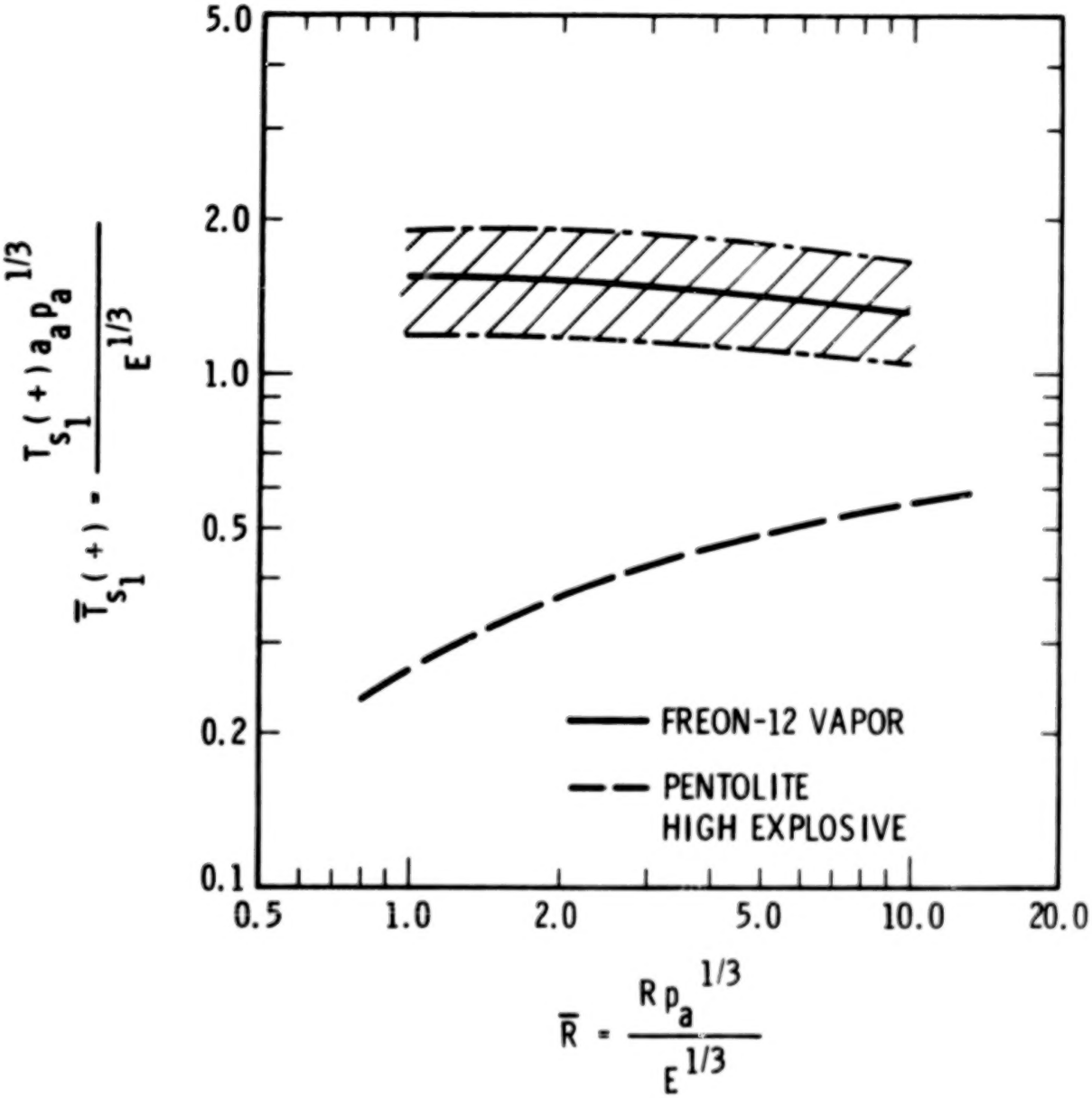

FIGURE 2-18. SCALED DURATION OF POSITIVE PHASE OF BLAST WAVE FROM BURSTING FREON-12 VAPOR SPHERE

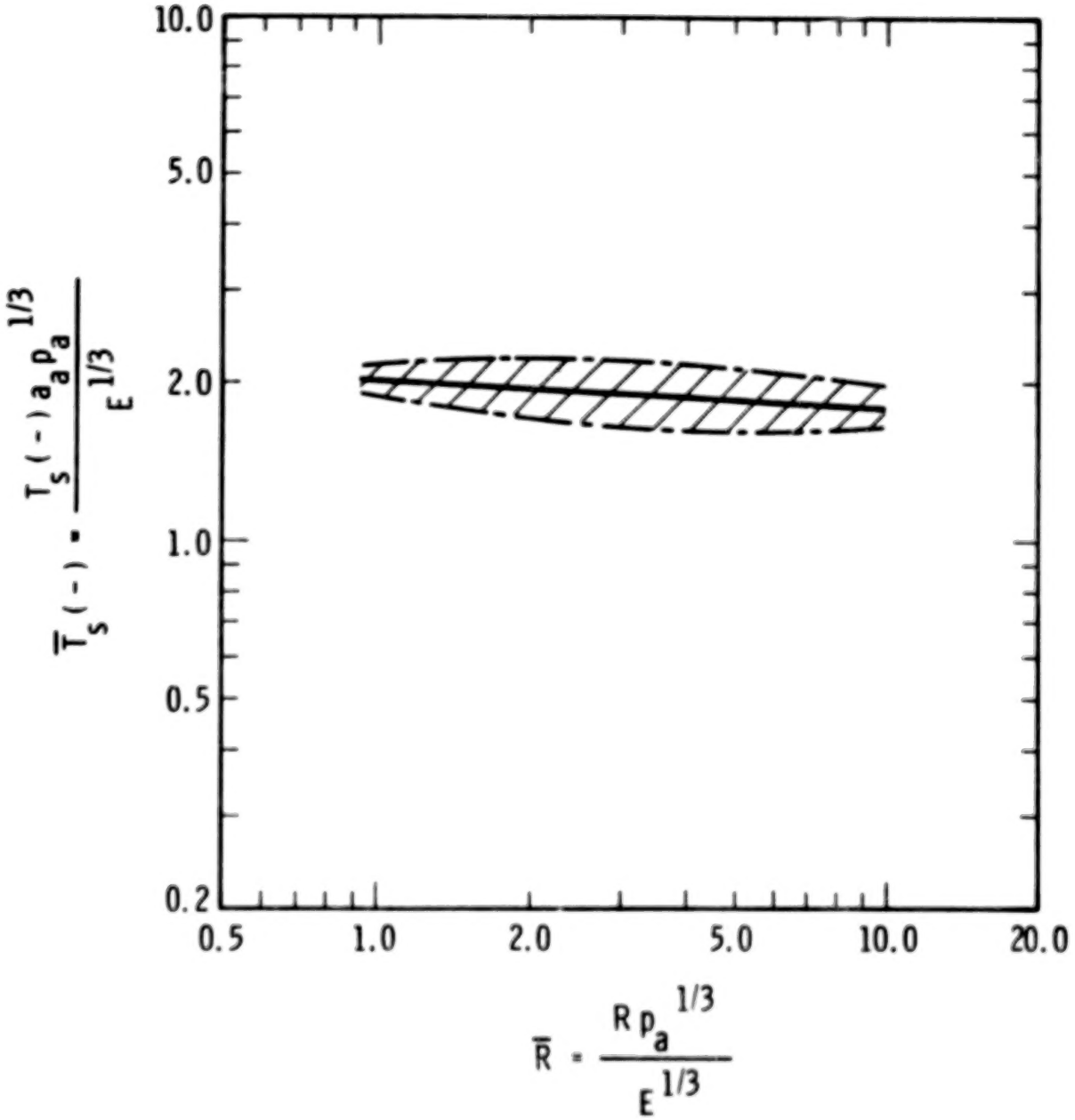

FIGURE 2-19. SCALED DURATION OF NEGATIVE PHASE OF BLAST WAVE FROM BURSTING FREON-12 VAPOR SPHERE

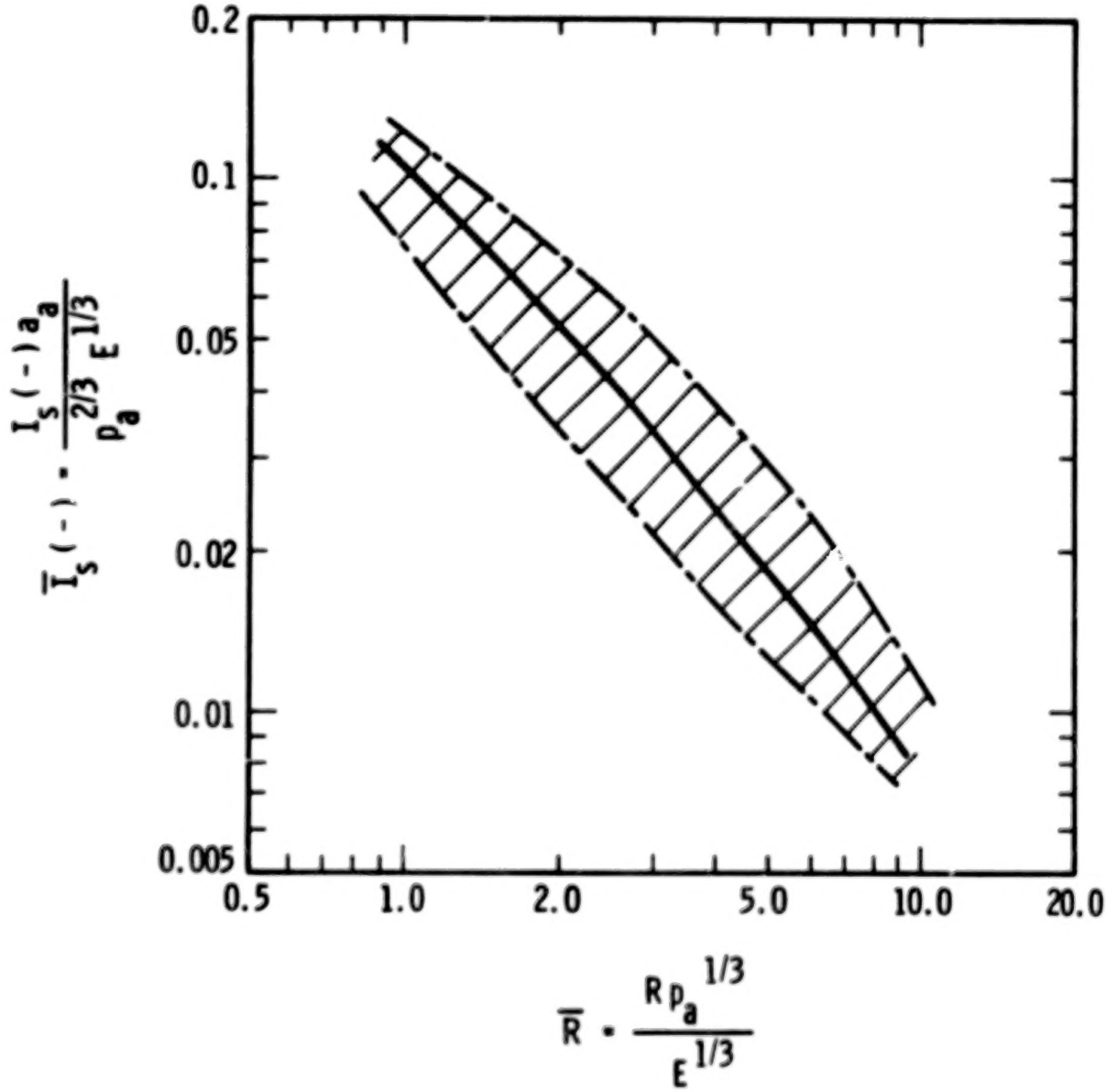

FIGURE 2-20. SCALED SIDE-ON NEGATIVE IMPULSE FROM BURSTING FREON-12 VAPOR SPHERE

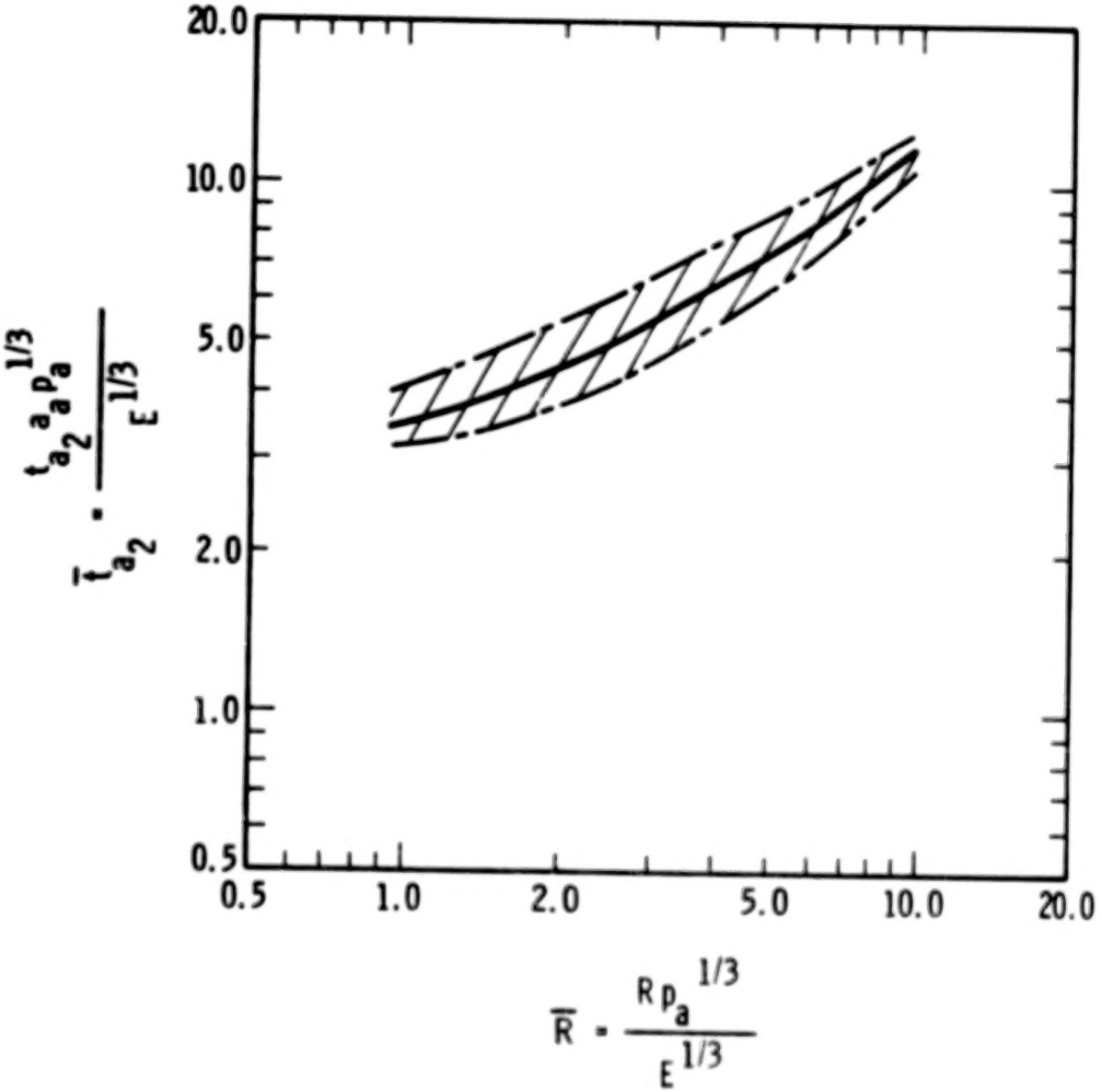

FIGURE 2-21. SCALED TIME OF ARRIVAL OF SECOND SHOCK WAVE FROM BURSTING FREON-12 VAPOR SPHERE

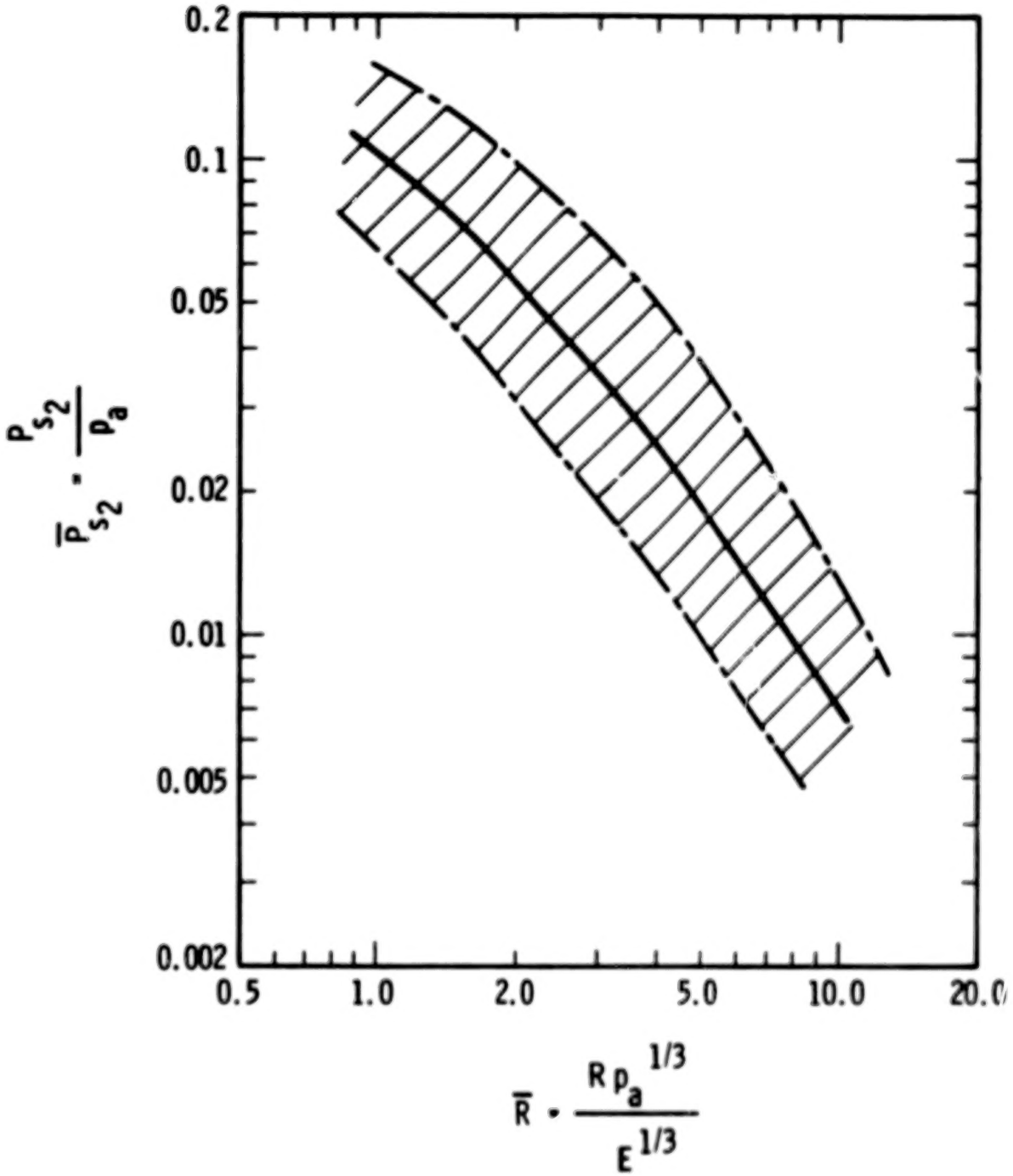

FIGURE 2-22. SCALED SIDE-ON PEAK OVERPRESSURE OF SECOND SHOCK WAVE FROM BURSTING FREON-12 VAPOR SPHERE

shows that blast waves from sudden release of compressed liquid Freon-12 were almost always so weak that they were essentially sound waves, and therefore had negligible damaging potential. No data were taken for the intermediate cases of wet vapor, which should have intermediate explosion properties between saturated liquid and saturated vapor.

Some data exist for blast waves generated by bursts of heated, ductile pressure vessels containing steam as a flash-evaporating fluid [Baker, et al (1978)] which show that such bursts can indeed be quite energetic blast sources. Strong vessels containing varying amounts of water which were heated to steam and burst at pressures of about 32 MPa generated strong blast waves, with specific source energies as great as 2.31×10^8 J/m^3 on a volume basis or 4.04×10^5 J/kg of fluid on a mass basis. The latter figure, when compared to the specific energy for TNT of 4.19×10^6 J/kg, gives a "TNT equivalent" of 0.097 kg TNT/kg H_2O. But, the data are too sparse to generate prediction curves.

REFERENCES, CHAPTER II

Baker, W. E., Kulesz, J. J., Ricker, R. E., Bessey, R. L., Westine, P. S., Parr, V. B. and Oldham, G. A., (1975) "Workbook For Predicting Pressure Wave and Fragment Effects of Exploding Propellant Tanks and Gas Storage Vessels," NASA CR-134906, Contract NAS3-19231, November 1975 (reprinted September 1977).

Baker, W. E., Esparza, E. D., Hokanson, J. C., Funnell, J. E., Moseley, P. K. and Deffenbaugh, D. M., "Initial Feasibility Study of Water Vessels for Arresting Lava Flow," AMSAA Contractor Report to be published.

Esparza, E. D. and Baker, W. E., (1977a) "Measurements of Blast Waves From Bursting Pressurized Frangible Spheres," NASA CR-2843, Grant NSG 3008, May 1977.

Esparza, E. D. and Baker, W. E., (1977b) "Measurements of Blast Waves From Bursting Frangible Spheres Pressurized with Flash-Evaporating Vapor or Liquid," NASA CR-2811, National Aeronautics and Space Administration, Washington, D. C., November 1977.

CHAPTER III

EFFECTS OF PRESSURE WAVES

3-1 General

It should be clear from the discussions in earlier chapters that the pressure (blast) waves from accidental explosions in groun systems can differ significantly from "classical" blast waves from condensed explosives. But, the basic methods presented by Baker, et al (1975) for predicting effects of pressure waves are independent of the exact character of the explosion source, and are primarily related to blast wave properties such as peak side-on overpressure P_s and positive impulse i_s, or peak reflected over-pressure P_r and the corresponding reflected impulse i_r.

Because of the correlation of the blast effects prediction methods in Baker, et al (1975) with blast wave properties, all of the graphs and equations in Chapter III of that reference are equally applicable for the ground burst accidents which are the topic of this workbook. Topics covered in Baker, et al (1975) are:

1) Thresholds for glass breakage.

2) Empirical blast damage estimates for residential buildings.

3) Toppling or overturning of vehicles and other objects.

4) Damage thresholds for beam structural elements.

5) Damage predictions for brittle and ductile rectangular plate elements.

6) Damage thresholds for rectangular membranes.

7) Blast injury estimates for humans.

We will not duplicate any of those prediction methods here, but will instead give supplementary prediction curves based on further damage prediction analyses by our staff.

3-2 Additional Beam Response Predictions

Methods were given in Baker, et al (1975) for prediction of damage thresholds for beams with various boundary conditions. The techniques used to obtain that set of prediction curves were based on assumed rigid-plastic beam behavior, and energy balance methods. Other prediction curves can be obtained by assuming elastic-plastic beam behavior, or purely elastic behavior. The curves are given here, and the procedures used in developing them are given in

Appendix B.

Figure 3-1 is a nondimensionalized pressure-impulse (P-i) diagram for determining the maximum strain and deflection in beams loaded by a blast wave. The blast wave is characterized by its peak applied pressure P and impulse i. These pressures and impulses are either side-on or reflected ones dependent upon the orientation of the building relative to the enveloping wave. In this graphical solution, we assume that the loading is uniform over the entire span of length ℓ. The beam has a loaded width b, a mass density ρ, a cross-sectional area A, a total depth H, an elastic modulus E, a yield point σ_y, a second moment of area I, and a plastic (not elastic) section modulus Z.

Different boundary conditions can be evaluated by inserting the appropriate nondimensional numbers, i.e., the appropriate Ψ coefficients from the table in Figure 3-1. Simply-supported, clamped-clamped, clamped-pinned, and cantilever beams are all included in this graphical solution. No strain energy is absorbed in extensional or shear behavior. This solution is entirely a bending one. Any self-consistent set of units can be used because this solution is nondimensional.

As an illustration of how Figure 3-1 may be applied, consider a 12H5 as a joist in a flat roof.* The joist will have 4-ft centers and be a simply-supported beam with a 20-ft span. The weight of the concrete and insulation being supported by this joist is assumed to equal 30.2 lb/ft^2. The joist is made of steel with a weight density of 0.283 lb/in^3, an elastic modulus of 30×10^6 psi, and a yield stress of 33,000 psi. The AISC handbook gives a weight per length of 7.1 lb/ft, a maximum moment based on a 30,000-psi yield of 222 in-kips, and a depth of 12.0 inches. These properties indicate that the second moment of area equals $Mh/2\sigma$, or 44.4 in^4, and that the elastic section modulus is $2I/h$, or 7.4 in^3. We will assume that the plastic section modulus Z equals the elastic section modulus in a beam with this shape. In a simply-supported beam, the Ψ_p number equals 10.0, Ψ_i equals 0.913, and Ψ_ε equals 1.25.

Next the nondimensional quantities

$$\frac{Pb\ell^2}{\Psi_p \sigma_y Z}$$

and

*English units are used in this and some subsequent examples because all of the handbook properties of structural steel members are given in these units, and they are the common units used by structural designers.

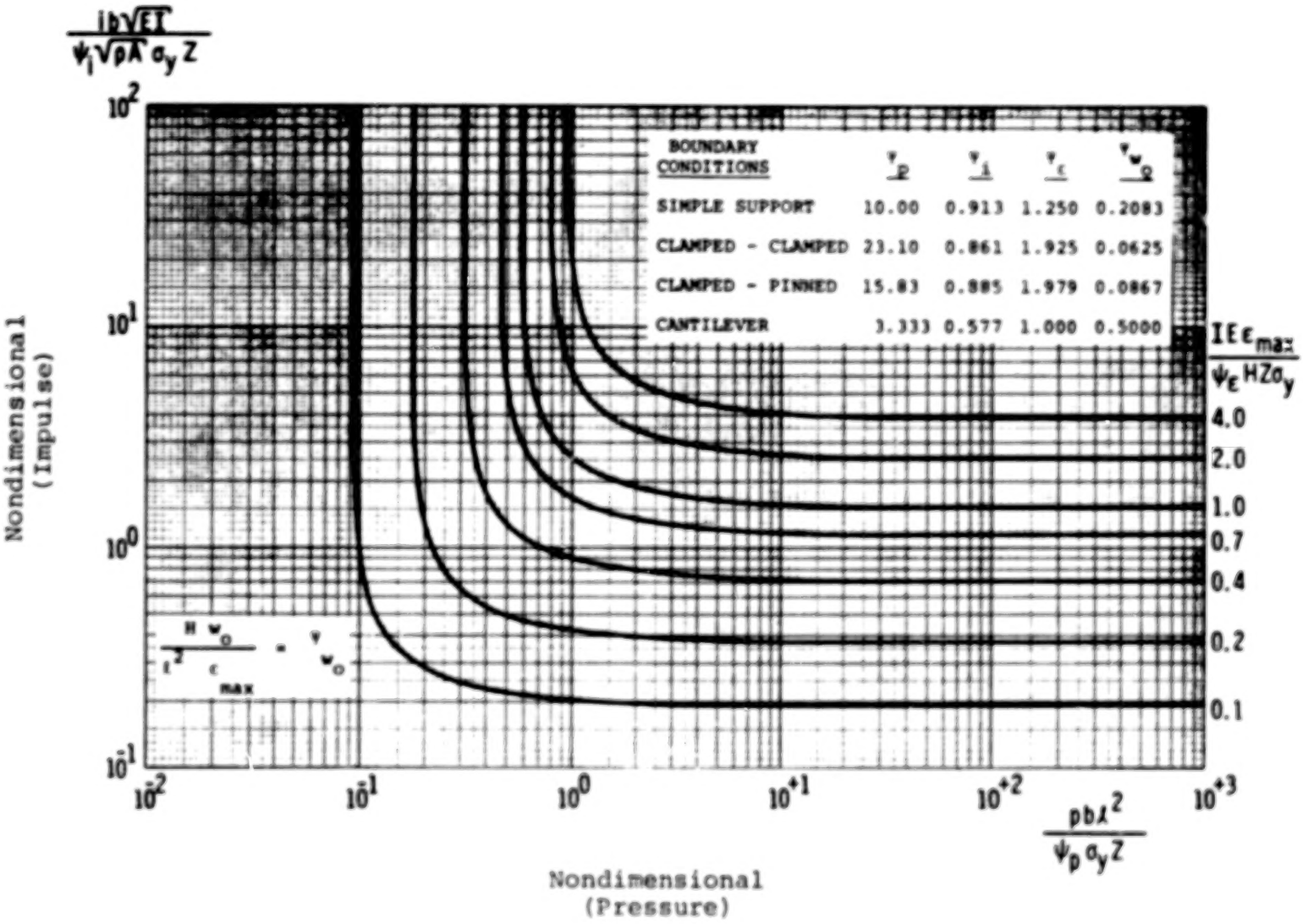

FIGURE 3-1. ELASTIC-PLASTIC SOLUTION FOR BLAST LOADED BEAMS

$$\frac{ib\sqrt{EI}}{\Psi_i \sqrt{\rho A}\ \sigma_y Z}$$

must be computed for some given input pressure and impulse. Let us assume that these values are P = 1.42 psi and i = 0.0145 psi-sec. Substituting P = 1.42 psi, b = 48 in., ℓ = 240 in., Ψ_p = 10.0, σ_y = 33,000 psi, and Z = 7.4 in^3 gives a scaled pressure of 1.61 for the quantity

$$\frac{Pb\ell^2}{\Psi_p \sigma_y Z}.$$

Before the quantity

$$\frac{ib\sqrt{EI}}{\Psi_i \sqrt{\rho A}\ \sigma_y Z}$$

can be determined, multiplying and dividing by $\sqrt{g}$, the square root of the acceleration of gravity, simplifies computations by forming the quantity

$$\frac{ib\ \sqrt{EI}\ \sqrt{g}}{\Psi\ \sqrt{\rho g A}\ \sigma_y Z}$$

The quantity (ρgA) is the weight per unit length for both the beam and the roof that it supports. Because of the 2.0-ft centers, the quantity (ρgA) equals [(30.2 x 4) + 7.1] 1/12, or 10.66 lb/in. Substituting i = 0.0145 psi-sec, b = 48 in., E = 30 x 10^6, I = 44.4, g = 386 in/sec, Ψ_i = 0.913, ρgA = 10.66, σ_y = 33,000 psi, and Z = 7.4 gives a scaled impulse of 0.685 for the quantity

$$\frac{ib\ \sqrt{EI}\ \sqrt{g}}{\Psi_i\ \sqrt{\rho g A}\ \sigma_y Z}.$$

Now Figure 3-1 can be entered to determine the scaled strain for this loading. The scaled strain

$$\frac{IE\ \epsilon_{max}}{\Psi_c\ HZ\sigma}$$

equals 0.33. The strain ϵ_{max} is found to equal 907 $\mu\epsilon$ after substituting 44.4 for I, 30 x 10^{+6} for E, 33,000 for σ_y, 7.4 for Z, 12 for H, and 1.25 for Ψ_c. This strain is elastic and corresponds to a stress of about 27,200 psi.

Figure 3-2 is a corresponding bending beam solution for elastic response only. The major added benefit derived from Figure 3-2 is that it can be used to estimate the shear forces at the supports. For a Bernoulli-Euler beam, a plastically responding beam has no shear force at the instant of maximum deformation, as

$$\frac{dM}{dx} = 0.$$

Obviously, a maximum shear is reached earlier in the response which is not handled by an energy solution. An energy solution only handles end states; it never yields a transient solution. For an elastic solution, a maximum shear force V is reached when the beam is in its maximum elastically deformed position. Provided the response is elastic, Figure 3-2 essentially yields the same solution as an elastically responding beam from the more generalized Figure 3-1 solution.

We will illustrate the use of Figure 3-2 with the same 12H5 roof joint exposed to the same 1.42 psi and 0.0145 psi-sec pressure-impulse blast loading as in the previous example. The elastic scaled pressure and impulse quantities which must be calculated are

$$\frac{PbH\ell^2}{\alpha_p EI} \text{ and } \frac{ibH}{\alpha_i \sqrt{\rho EIA}} .$$

Once again multiply and divide the scaled impulse by $g^{1/2}$ to form

$$\frac{ibH\sqrt{g}}{\alpha_i \sqrt{(\rho gA)EI}}$$

which takes advantage of the weight per unit length quantity (ρgA). Substituting as before, $P = 1.42$ psi, $b = 48$ in., $H = 12$ in., $\ell = 240$ in., $\alpha_p = 8.00$, $E = 30 \times 10^{+6}$ psi, and $I = 44.4$ in^4 gives 4.42×10^{-3} for the scaled pressure quantity

$$\frac{PbH\ell^2}{\alpha_p EI} .$$

Substituting $i = 0.0145$ psi-sec, $b = 48$ in., $H = 12$ in., $g = 386$ in/sec^2, $\alpha_i = 1.461$, $(\rho gA) = 10.66$ lb/in, $E = 30 \times 10^{+6}$, and $I = 44.4$ in^4 gives 9.43×10^{-4} for the scaled impulse quantity

$$\frac{ibHg^{1/2}}{\alpha_i \sqrt{\rho Ag\ EI}} .$$

BLANK PAGE

BLANK PAGE

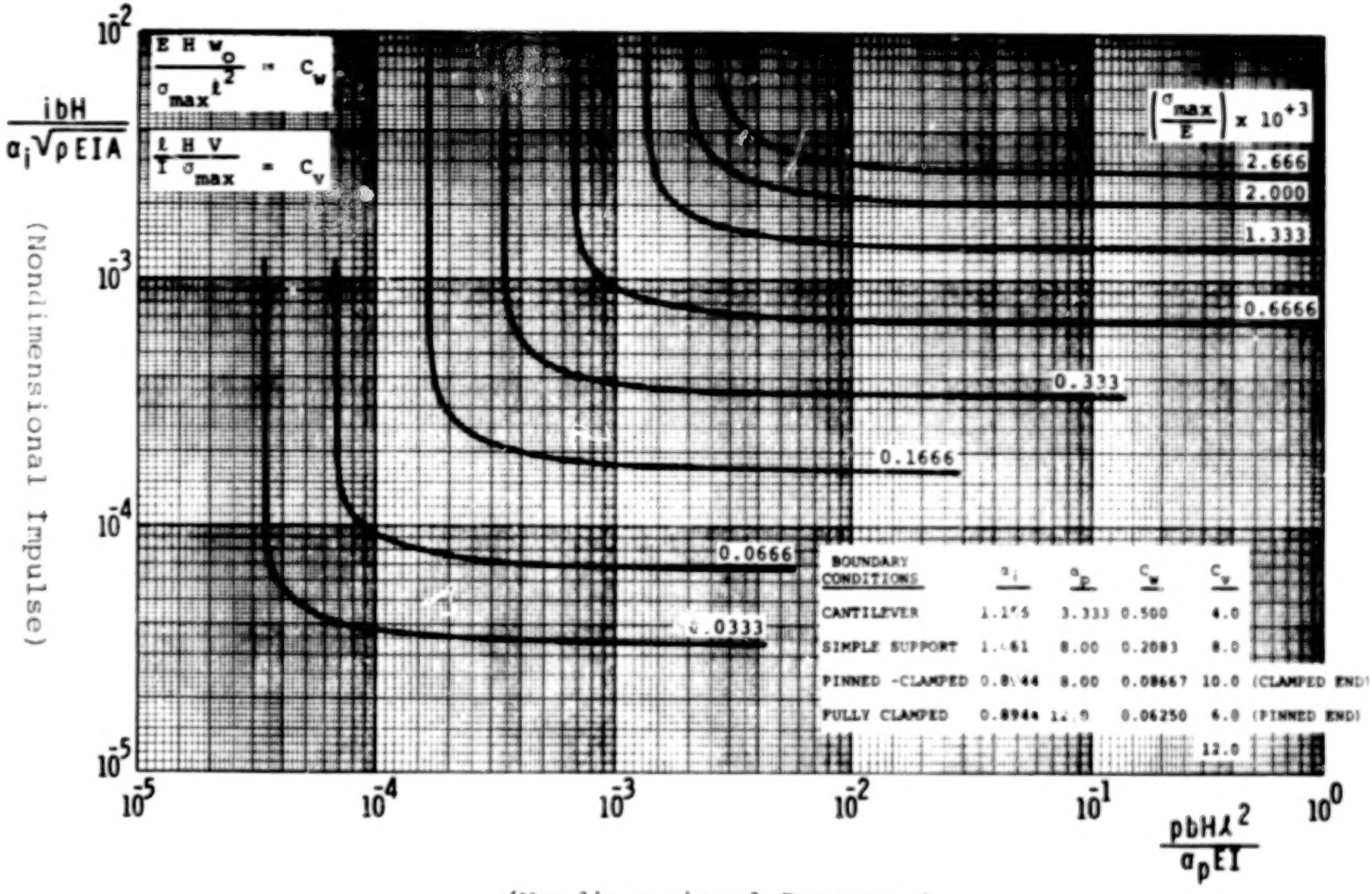

FIGURE 3-2. STRESSES, SHEARS, AND DEFLECTIONS IN BLAST LOADED ELASTIC BEAMS

The coefficients differ in Figures 3-1 and 3-2; however, the appropriate values are provided in tabular inserts. Entering Figure 3-2 for this specific combination of scaled pressure and scaled impulse gives a scaled stress

$$\left(\frac{\sigma_{max}}{E} \times 10^{+3}\right)$$

of approximately 1.0 after extrapolating. After substituting for E, this calculation indicates that the maximum stress caused by the air blast wave is approximately 30,000 psi. This answer is identical, within the limits of graphical accuracy, to the 27,200 psi stress found using Figure 3-1. In addition, the shear force at the support caused by this dynamic load can also be determined. The equations in the upper left hand corner of Figure 3-2 permit the maximum elastic deformation w_o and the shear force at the supports to be determined after σ_{max} has been computed. The coefficients C_w and C_v, also found in the table accompanying Figure 3-2, depend upon the boundary conditions. For a simply-supported beam, $C_v = 8.0$. Substituting $C_v = 8.0$, $\sigma_{max} = 30{,}000$ psi, $I = 44.4$ in^4, $\ell = 240$ in., and $H = 12$ in. gives 3,700 lbs for the maximum elastic shear force caused by the blast load.

Whenever a member undergoes large deformations relative to its thickness, the principal mode of energy dissipation is extensional rather than bending. Figure 3-3 presents an elastic-plastic, one-dimensional, extensional solution. An extensional solution assumes that the ends are constrained from moving together so that in-plane forces can be developed. The results presented in Figure 3-3 are very similar to the previously presented bending solution in that contours of constant scaled strain are presented on a plot of scaled applied impulse and pressure. All loads are assumed to be uniformly distributed over the member being loaded. After the strain has been determined, the maximum deformation, the slope at the boundaries, and the magnitude of the anchoring force can all be determined using Figure 3-3.

The symbols in Figure 3-3 are very similar to those used previously. The one new symbol is A, the cross-sectional area of the member. Other symbols include the applied reflected or side-on overpressure P, the applied reflected or side-on impulse i, the loaded width b, the total span ℓ, the mass density ρ, the elastic modulus E, the yield point σ_y, the maximum strain ε_{max}, the maximum deformation w_o, and the maximum slope

$$\left(\frac{dy}{dx}\right)_{max} .$$

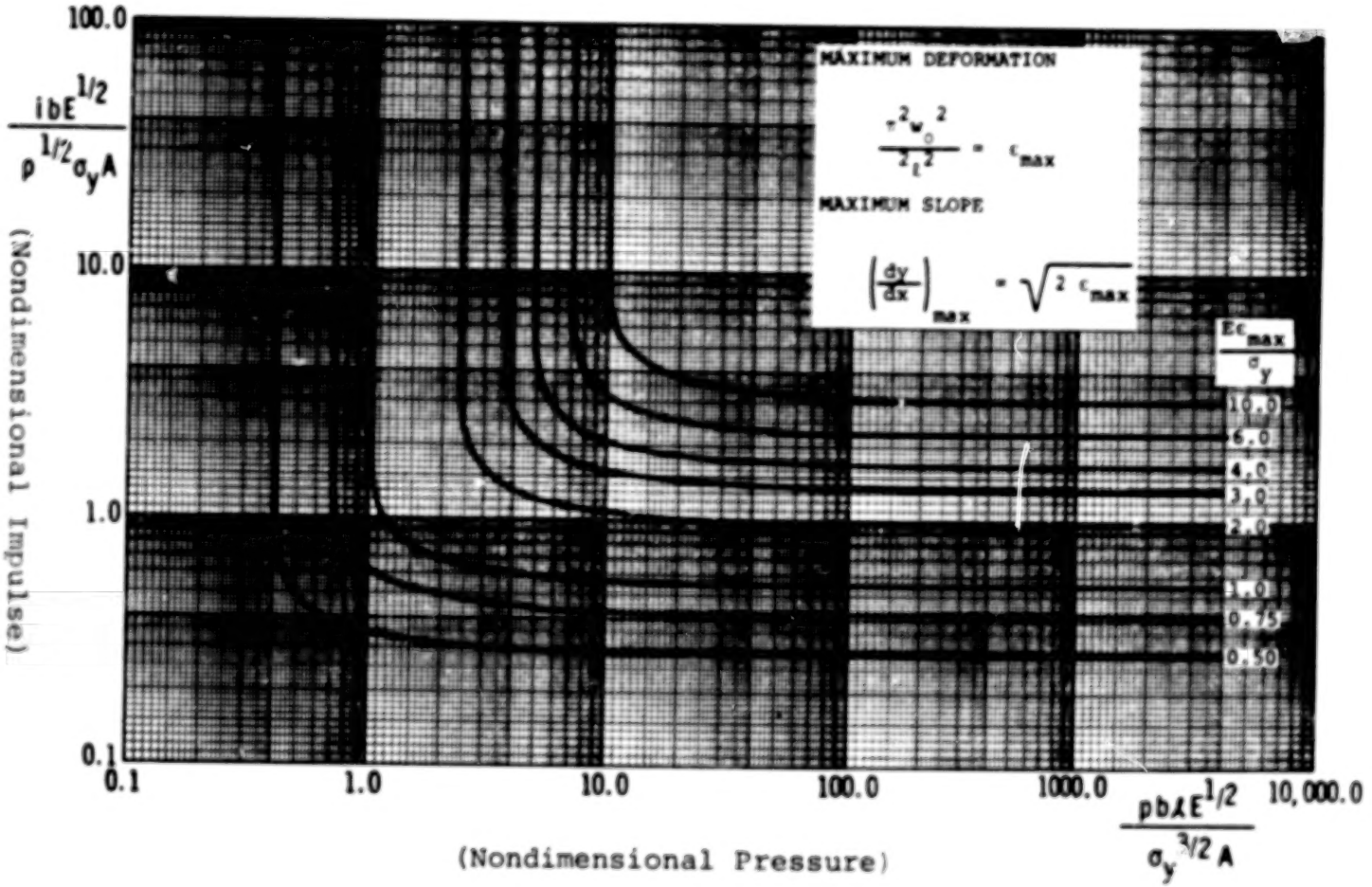

FIGURE 3-3. ELASTIC-PLASTIC STRING SOLUTION

Any self-consistent set of units can be used, as all scaled quantities are nondimensional.

We will illustrate the use of Figure 3-3 by evaluating wall siding. Let us assume normally reflected pressure of 3.0 psi, and a normally reflected impulse of 30.0 psi-ms. Most siding is corrugated so one direction is much stiffer than its orthogonal counterpart. This observation means we can use a strip theory for estimating the response. If we have a steel siding with a yield point of 33,000 psi, a cross-sectional area per inch of width of 0.0625 in^2/in, a weight per inch width and per inch length of 0.0236 lb/in^2, and a span of 156 in., then the scaled pressure can be presented in the format

$$\frac{P\ell E^{1/2}}{\sigma_y^{3/2}(A/b)}$$

which equals

$$\frac{(3.00)(156)(30 \times 10^{+6})^{1/2}}{(33{,}000)^{3/2}(0.0625)} , \text{ or } 6.84.$$

The scaled impulse should be multiplied and divided to $g^{1/2}$ to form

$$\frac{iE^{1/2}g^{1/2}}{\left(\rho g\frac{A}{b}\right)^{1/2}\sigma_y\left(\frac{A}{b}\right)^{1/2}} ,$$

which equals

$$\frac{(0.030)(30 \times 10^{+6})^{1/2}(386)^{1/2}}{(0.0236)^{1/2}(33{,}000)(0.0625)^{1/2}} , \text{ or } 2.55.$$

Entering Figure 3-3 for these values of scaled pressure and impulse gives a scaled strain

$$\frac{E\varepsilon_{max}}{\sigma_y}$$

of approximately 4.0. Because

$$\frac{\sigma_y}{E}$$

is the yield strain, this calculation predicts a maximum strain of 4.0 times the yield strain. The maximum in-plane stress at the support will equal 33,000 psi because the member has yielded. This stress will act at an angle of

$$\sqrt{2(4)\ \frac{33{,}000}{30 \times 10^{+6}}}$$

or 0.0938 radians, according to the formula for the maximum slope in Figure 3-3. Because the in-plane stress and line of action are known, fasteners for attaching this wall could be selected and appropriately spaced.

3-3 Buckling of Axially-Loaded Members

Figure 3-4 shows a scaled pressure-impulse diagram for buckling of an axially loaded elastic column. Different boundary conditions and whether or not side-sway can occur is accounted for in the α_p and α_i coefficients associated with pressure and impulse. The solid line in Figure 3-4 is the threshold separating unstable column response from stable. If the nondimensionalized loads imparted to a column establish a point which is to the left and/or below the threshold line, then the column should remain stable. On the other hand, should these nondimensionalized loads establish a point above and to the right of the threshold, large permanent, unstable deformation should be expected. In developing this solution, energy procedures were once again applied. The major new parameter is the mass (not weight) of the overlying floor M. We assume that the mass of the column is insignificant relative to the mass of the rigid floor above. The parameters ℓ, E, I, σ_y, and H all pertain to the total span, modulus of elasticity, second moment of area, yield point, and total depth of the column itself. The parameter A is the loaded area of the roof or floor over the column. All influence of dead weight effects is ignored in this solution; they are assumed to be insignificant relative to the dynamic loads from the applied blast wave.

As an illustrative example, consider a W10 x 49 with a 150-in. span acting as a clamped-clamped column that might undergo side-sway. The second moment of area equals 93.0 in^4, and the depth is 10.0 in. about the minor axis of this column. We will assume a 33,000 psi yield strength, a 288 by 240 in. loaded area over each column, and an 0.2285 lb/in^2 weight per unit area for the overlying roof. The side-on pressure applied to the roof is 1.42 psi, and the side-on impulse is 0.0145 psi-sec. From the table inserted into Figure 3-4, we learn that the α_i coefficient equals 1.41, and the α_p coefficient equals 9.87 for a clamped-clamped column undergoing side-sway. Substituting these values into the scaled pressure parameter

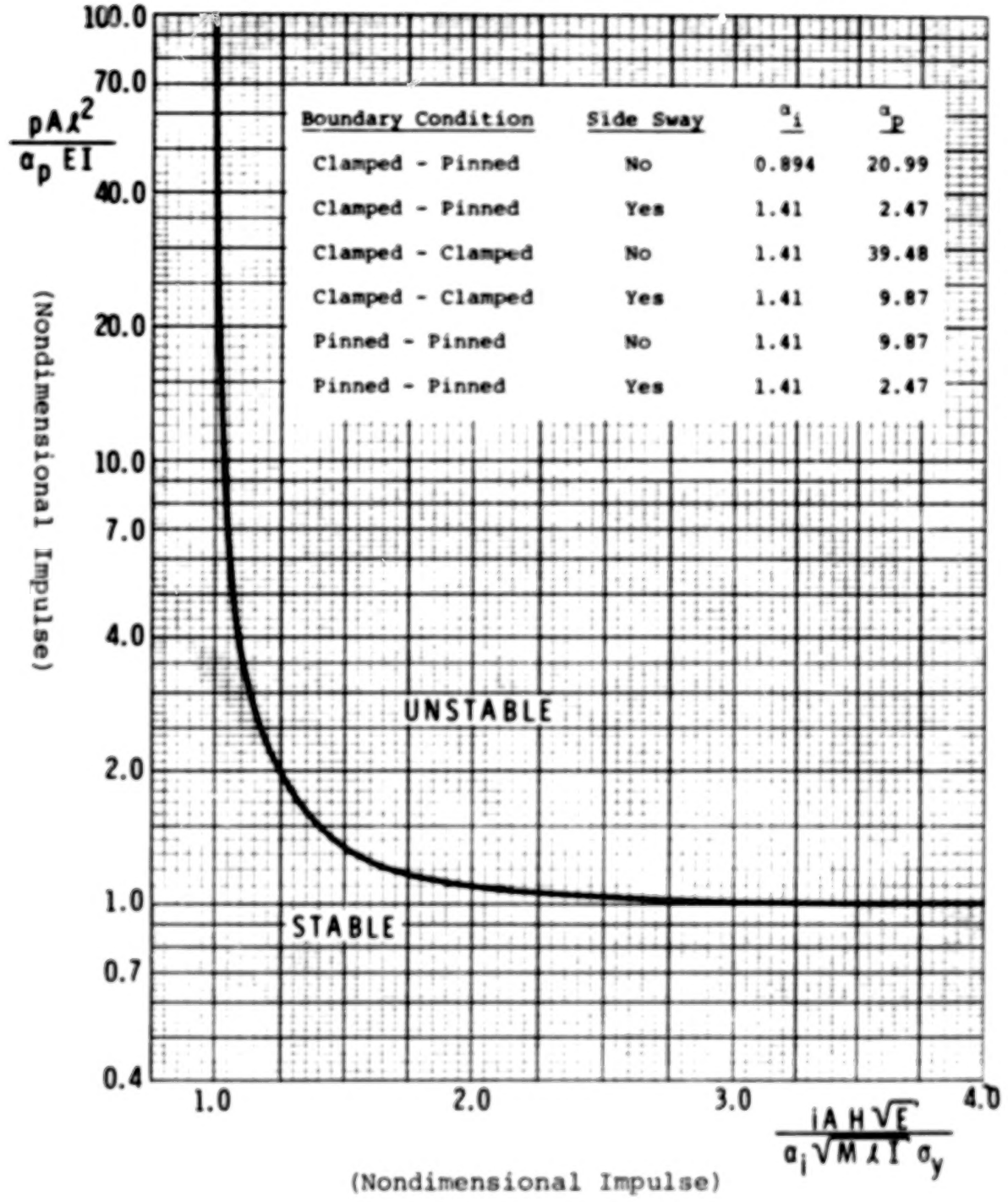

FIGURE 3-4. BUCKLING FOR DYNAMIC AXIAL LOADS

$$\frac{PAl^2}{\alpha_p EI}$$

gives

$$\frac{(1.42)(288 \times 240)(150)^2}{(9.87)(30 \times 10^{+6})(93.0)},$$

or 0.0802. The scaled impulse parameter

$$\frac{iAH\sqrt{E}}{\alpha_i \sqrt{MI}\,\sigma_y}$$

gives

$$\frac{(0.0145)(288 \times 240)(10)(30 \times 10^{+6})^{1/2}}{1.41\sqrt{\frac{0.02285 \times 288 \times 240}{386}}\,(150)(93)\,(33{,}000)},$$

or 1.56. Because this combination of loads plots below the scaled pressure asymptote of 1.0, the column should be stable.

REFERENCES, CHAPTER III

AISC Handbook, (1961) "Steel Construction," American Institute of Steel Construction, 5th Edition, New York, New York, 1961.

Baker, W. E., Kulesz, J. J., Ricker, R. E., Bessey, R. L., Westine, P. S., Parr, V. B. and Oldham, G. A., (1975) "Workbook for Predicting Pressure Wave and Fragment Effects of Exploding Propellant Tanks and Gas Storage Vessels," NASA CR-134906, Contract NASA-19231 November 1975 (reprinted September 1977).

CHAPTER IV

CHARACTERISTICS OF FRAGMENTS

4-1 General

In Baker, et al (1975), there was extensive coverage of such characteristics of fragments from flight-weight vehicles as initial velocities, size and mass distributions, fragment trajectories, and the distances or ranges the fragments travelled. The data and prediction methods given in that reference were based on accident reports and tests with liquid propellant explosions and lightweight gas vessel bursts, development and exercise of a variety of special-purpose computer programs, and statistical analysis of test and accident data.

Accidental explosions in ground systems tend to produce very different types of fragments or missiles than do similar explosions in flight-weight systems. The most striking difference lies in the number of fragments generated, with the number usually being much less for the ground systems than for flight systems. This difference is primarily a function of the differences in storage or pressure vessel materials and construction. Relatively thick-walled vessels, made of ductile steels, dominate in ground storage and transport systems. These vessels often split, or fragment into only two pieces, after failure. Accidental explosions which generate more than a dozen vessel fragments are quite uncommon. For storage or transport vessels containing flash-evaporating liquids such as propane (LPG), a common failure mode is an asymmetric burst of a long cylindrical vessel, with the major part remaining intact and "rocketing" as the fluid exhausts and flashes. Accident reports of such failures show that the vessel can travel great distances, and of course cause a major hazard where they impact.

In this chapter, we present the results of studies on the characteristics of fragments from ground vessel explosions, and highlight the differences from fragmentation of flight-weight vehicles. As before, a survey and statistical analysis of accident data is included; several new computer programs were developed and exercised; and prediction curves on methods generated for various characteristics of the relatively large and massive fragments generated in accidental explosions in ground systems are presented.

4-2 Analytical Predictions of Fragment Velocity Distributions

Estimates of Initial Velocities of Fragments from Bursting Spheres and Cylinders

Equal Fragments

The method developed by Taylor and Price (1971) and modified by Baker, et al (1975) for calculating velocities of fragments from bursting spherical and cylindrical pressure vessels was used to provide velocities of various fragments which could be plotted in some form of prediction curve. The model analyses for reducing and analyzing the data and the results of these analyses are explained in Appendix C. The development of the necessary equations, the numerical iteration method used to simultaneously solve the differential equations and the computer programs can be found in Appendix IV A and Appendix IV C of Baker, et al (1975) (see microfiche). The only assumptions included here are those needed to determine fragment velocities.

The basic assumptions are:

1) The vessel with gas under pressure bursts into equal fragments. If there are only two fragments, and the vessel is cylindrical, the vessel bursts perpendicular to its axis of symmetry. If there are more than two fragments, and the vessel is cylindrical, strip fragments (end caps are ignored) are formed and expand radially about the axis of symmetry (see Figure 4-1).

2) The cylindrical containment vessel has hemispherical end caps. (These are ignored when the vessel bursts into multiple fragments.)

3) The thickness of the containment vessel is uniform.

4) Vessels have a length-to-diameter (L/D) ratio of 10.0 for cylinders or 1.0 for spheres.

5) Contained gases are either hydrogen (H_2), air, argon (Ar), helium (He) or carbon dioxide (CO_2).

Figure 4-2 contains plots of the velocity term versus the pressure term for two fragments, ten fragments and one hundred fragments from spherical or cylindrical vessels. Three separate regions have been bounded to account for scatter: (1) cylindrical vessels bursting into multiple fragments; (2) spherical vessels bursting in half or multiple fragments and (3) cylindrical vessels bursting into two fragments. Estimates of the initial velocities of cylinders and spheres can be extracted from the nondimensional terms read directly from the appropriate bounded regions on the graph. The two nondimensional

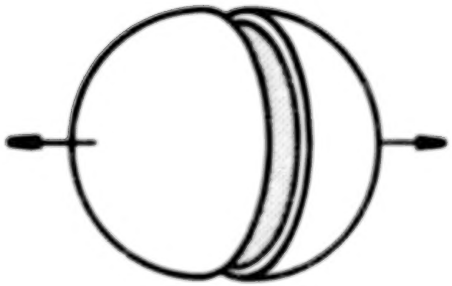

(a) Spheres bursting into two equal fragments

(b) Cylinder bursting into two equal fragments

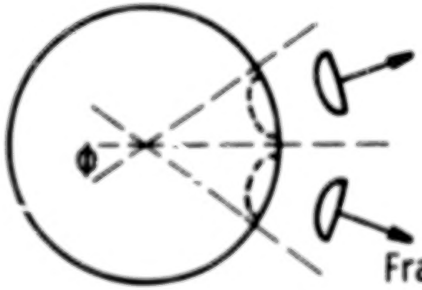

(c) Sphere bursting into n equal fragments

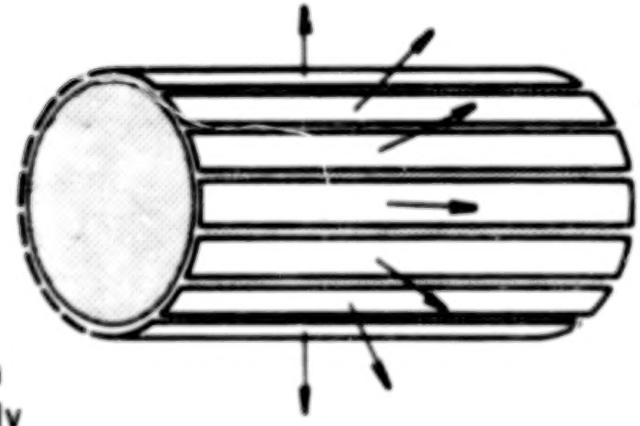

(d) Cylinder bursting into n equal strip fragments

FIGURE 4-1. ASSUMED FRAGMENTATION PATTERNS

terms in Figure 4-2 are:

1) Nondimensional pressure term

$$= \frac{(P-p_a)V_o}{M_c \gamma R_m T_o} = \frac{(P-p_a)V_o}{M_c\, a^2_{gas}} =$$

$$\frac{\text{(pressure - atm. pressure) (Volume)}}{\text{(Mass of container) (sound speed of the gas)}^2}$$

2) Nondimensional velocity term

$$= \frac{u}{K\sqrt{\gamma R_m T_o}} = \frac{u}{K a_{gas}} = \frac{\text{(velocity)}}{\text{(constant) (sound speed of the gas)}}$$

where K equals 1.0 for equal fragments.

The technique for predicting initial fragment velocities for spherical or cylindrical pressure vessels bursting into equal fragments requires knowledge of the internal pressure P, internal volume V_o, mass of the container M_c, ratio of specific heats γ, ideal gas constant adjusted for the gas R_m, and the temperature of the gas T_o, at burst. Table 4-1 contains the corresponding γ's and R_m's for the gases for which this analysis is appropriate.

In summary, in order to estimate the initial velocity of fragments from pressurized spheres and cylinders which burst into <u>equal</u> fragments, one should use the following procedures:

Step 1. Calculate the nondimensional pressure term $\frac{(P-p_o)V_o}{M_c \gamma R_m T_o}$

Step 2. Locate the corresponding value of the nondimensional velocity term $\frac{u}{K\sqrt{\gamma R_m T_o}}$ and solve for velocity u (Note: K = 1.0 for equal fragments)

Note: Axes of Figure 4-2 are nondimensional terms and merely require that one use a self-consistent set of units.

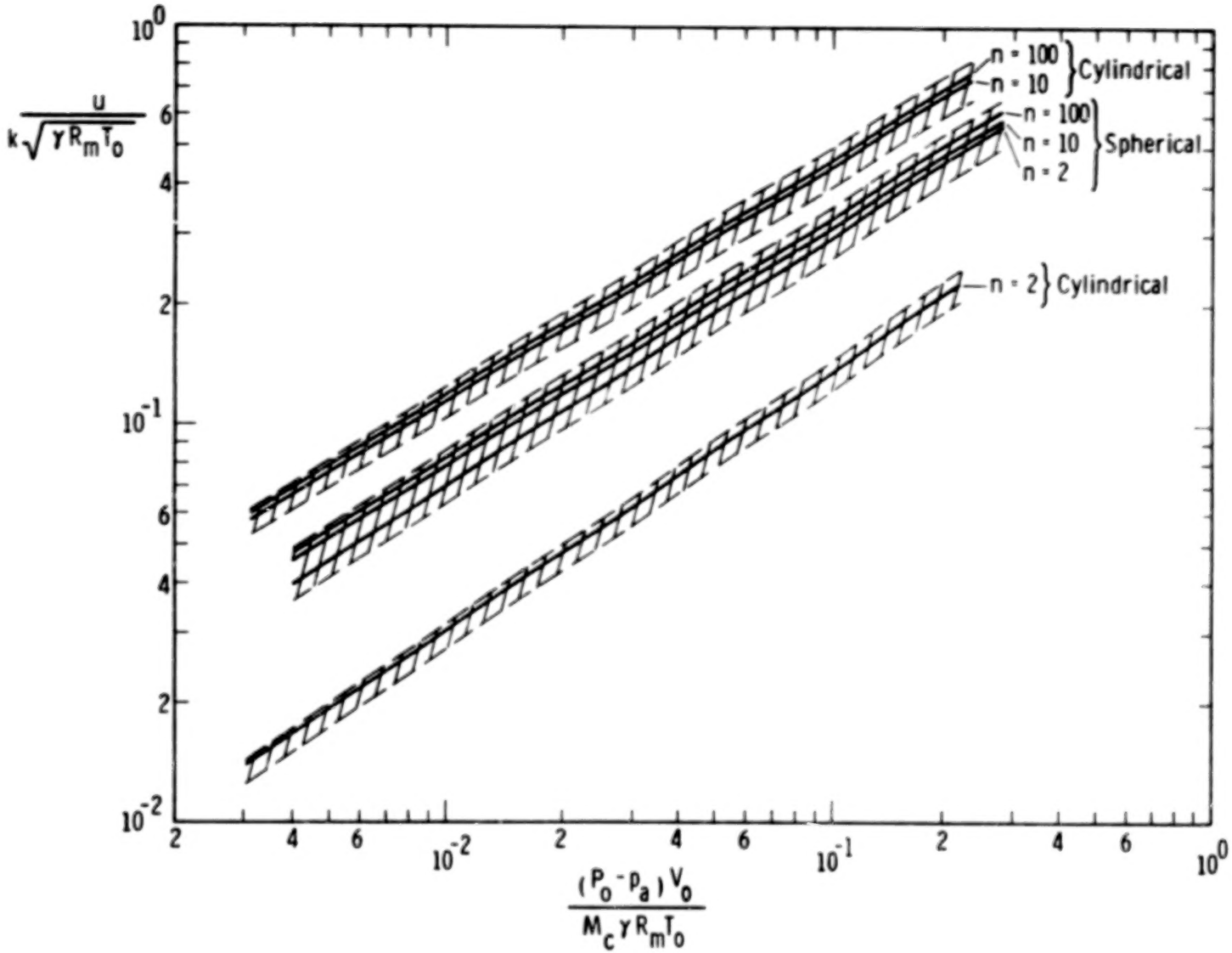

FIGURE 4-2. SCALED FRAGMENT VELOCITY VS. SCALED PRESSURE

TABLE 4-1. SUMMARY OF RATIOS OF SPECIFIC HEAT AND IDEAL GAS CONSTANTS FOR DIFFERENT GASES

Gas	Ratio of Specific Heats γ	Ideal Gas Constant R_m $\left(\frac{m^2}{sec^2 \cdot °K}\right)$	Ideal Gas Constant R_m $\left(\frac{in^2}{sec^2 \cdot °R}\right)$
Hydrogen	1.4	4124	3.551×10^6
Air	1.4	287.0	2.471×10^5
Argon	1.67	208.1	1.792×10^5
Helium	1.67	2078	1.789×10^6
Carbon Dioxide	1.225	188.9	1.627×10^5

Example 1:

Determine the initial velocity of a fragment from a pressurized sphere containing hydrogen gas which bursts in half. The following properties may be assumed:

$P = 10 \times 10^6$ Pa(1464.7 psi)

$V_o = 0.03 m^3$ (1830 in^3)

$M_c = 17.13$Kg (37.76 lbs)

$T_o = 300°K$

From Table 4-1 $\gamma = 1.4$

$$R_m = 4124 \frac{m^2}{sec^2 \cdot °K} \left(3.551 \times 10^6 \frac{in^2}{sec^2 \cdot °R}\right)$$

Step 1. Nondimensional pressure term =

$$\frac{(P-p_o)V_o}{M_c \gamma R_m T_o} = \frac{(10 \times 10^6)\ (0.03)}{(17.13)\ (1.4)\ (4124)\ (300)} = 0.01011$$

Step 2. Since the sphere bursts in half, K = 1.0. From Figure 4-2 $\frac{u}{K\sqrt{\gamma R_m T_o}} = .071$ and solving for u results in an initial velocity of 93.44 m/sec (306.6 ft/sec).

Program SPHERE [See Chapter IV, Baker, et al (1975) (microfiche)] results show the initial velocity to be 94.92 m/sec (311.4 ft/sec).

$$\text{Percent Error} = \frac{94.92-93.44}{94.92} \times 100 = 1.6\%$$

Example 2:

Determine the initial velocity of a fragment from a pressurized cylindrical vessel containing argon which bursts into 50 equal fragments. Assume the following properties:

$P = 1.5 \times 10^6$ Pa(217.7 psi)

$V_o = 0.03 m^3$ (1830 in^3)

$M_c = 3.21$Kg (7.07 lbs)

$T_o = 700°K$

From Table 4-1 $\gamma = 1.67$

$$R_m = 208.1 \frac{m^2}{sec^2 \cdot °K} \left(1.792 \times 10^5 \frac{in^2}{sec^2 \cdot °R}\right)$$

Step 1. Nondimensional pressure term =

$$\frac{(P-p_o)V_o}{M_c \gamma R_m T_o} = \frac{(1.4X10^6)\ (0.03)}{(3.21)\ (1.67)\ (208.1)\ (700)} = 0.0538$$

Step 2. Since the cylinder bursts into 50 equal fragments, K = 1.0. From Figure 4-2, $\frac{u}{K\sqrt{\gamma R_m T_o}} = 0.3$ and solving for u results in an initial velocity of 148 m/sec (485 ft/sec).

Program SPHERE results show the initial velocity to be 149.2 m/s (489.4 ft/sec).

$$\text{Percent error} = \frac{149.2-148}{149.2} \times 100 = 0.80\%$$

Cylinders with Length-to-Diameter Ratio of 10.0 Bursting into two Unequal Fragments

The Taylor and Price (1971) method modified by Baker, et al (1975) for calculating velocities of fragments from bursting spherical and cylindrical gas vessels has been expanded to provide initial velocities of unequal fragments from cylindrical vessels. The development of the necessary equations and the subsequent computer program UNQL are explained in depth in Appendix D. The assumptions essential to the velocity calculations follow:

1) The vessel with gas under pressure breaks into two unequal fragments along a plane perpendicular to the cylindrical axis, and the two container fragments are driven in opposite directions (see Figure 4-3).

2) The containment vessel is cylindrical and has hemispherical end caps.

3) The thickness of the containment vessel is uniform.

4) Vessels have a length-to-diameter (L/D) ratio of 10.0.

5) Contained gases are either hydrogen (H_2), air, argon (Ar), helium (He) or carbon dioxide (CO_2).

The technique for predicting initial fragment velocities for fragments from a cylinder (L/D = 10.0) which breaks into two unequal fragments perpendicular to its axis of symmetry is identical to that for equal fragments except for the value of the constant K. The value of K depends on the ratio of the fragment mass to the total mass of the cylinder as shown in Figure 4-4. To estimate the initial velocity of a fragment from a pressurized cylinder (L/D = 10.0) which bursts into unequal fragments, one should use the following procedures:

Step 1. Calculate the nondimensional pressure term = $\dfrac{(P-p_o)V_o}{M_c \gamma R_m T_o}$

Step 2. Locate the corresponding value of the nondimensional velocity term $\dfrac{u}{K\sqrt{\gamma R_m T_o}}$ in the region bounded for

n = 2 (cylindrical vessels).

Step 3. Determine the value of K from Figure 4-4.

Step 4. Solve for velocity u.

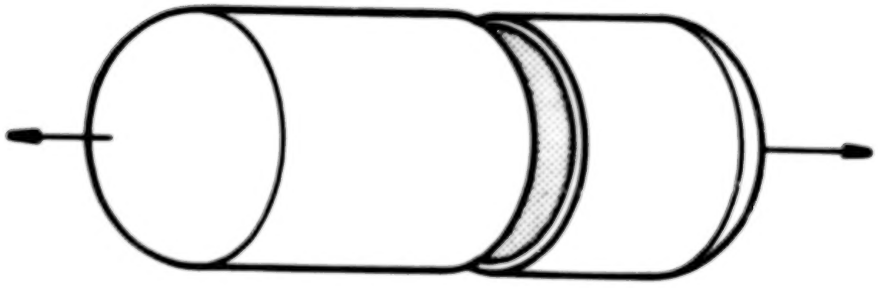

FIGURE 4-3. ASSUMED BREAKUP INTO TWO UNEQUAL FRAGMENTS

Note: Axes of Figure 4-2 are nondimensional terms and merely require that one use a self-consistent set of units.

Example 1:

Determine the initial velocity of a fragment from a pressurized cylindrical vessel containing carbon dioxide which bursts into two unequal fragments. Assume the following properties:

$P = 69 \times 10^6$ Pa (10,010 psi)

$V_o = 30.0 m^3$ (1.83×10^6 in^3)

$M_c = 1.92 \times 10^5$ kg (4.23×10^5 lbs)

$T_o = 500°K$

From Table 4-1, $\gamma = 1.225$

$$R_m = 188.9 \frac{m^2}{sec^2 \cdot °K} \left(1.627 \times 10^5 \frac{in^2}{sec^2 \cdot °R}\right)$$

Fraction of the total mass for fragment under consideration = 0.75.

Step 1. Nondimensional pressure term =

$$\frac{(P-p_o)V_o}{M_c \gamma R_m T_o} = \frac{(68.9 \times 10^6)\ (30.0)}{(1.92 \times 10^5)\ (1.225)\ (188.9)\ (500)} = 0.093$$

Step 2. The corresponding value of $\frac{u}{K\sqrt{\gamma R_m T_o}} = 0.13$.

Step 3. From Figure 4-4, K = 0.61.

Step 4. Solving for u gives an initial velocity of 27 m/s (88 ft/sec).

Program UNQL results (Appendix D) show the initial velocity to be 26.5 m/s (86.9 ft/sec).

Percent error = $\frac{27-26.5}{26.5} \times 100 = 1.9\%$

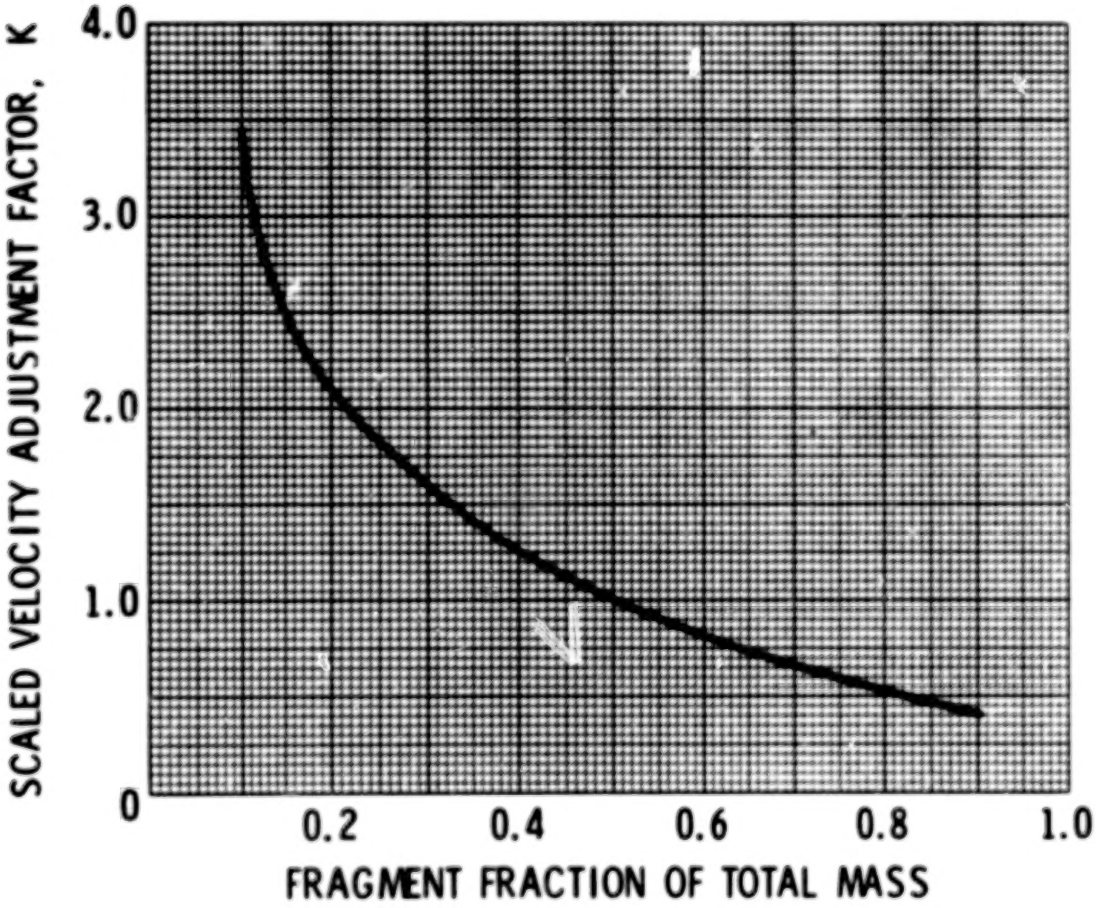

FIGURE 4-4. ADJUSTMENT FACTOR FOR UNEQUAL MASS FRAGMENTS

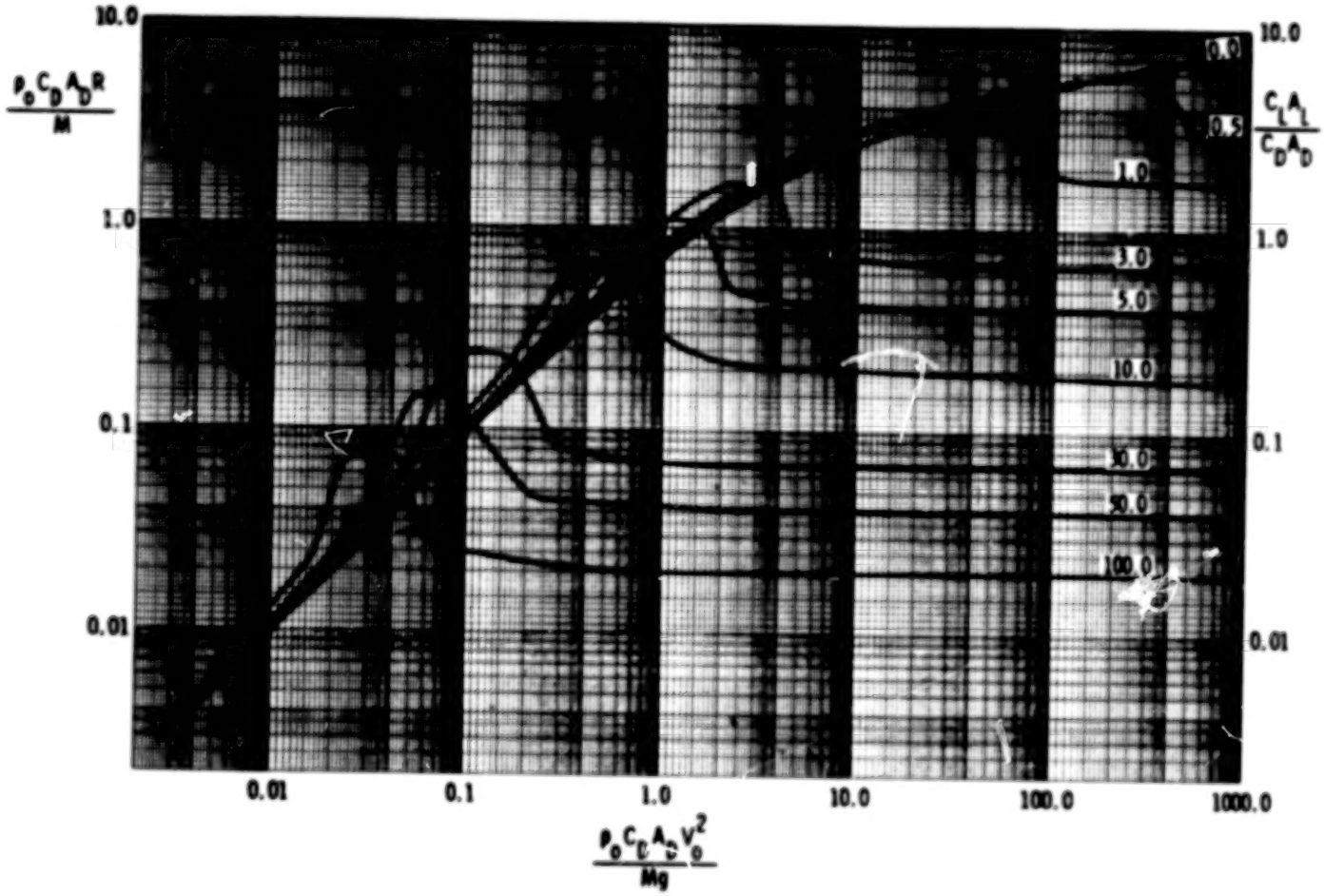

FIGURE 4-5. SCALED CURVES FOR FRAGMENT RANGE PREDICTION

4-3 Analytic Predictions of Fragment Trajectories, Ranges and Impact Conditions

Predicting Ranges of Free-Flying Fragments

The range of a flying fragment from a bursting container is dependent on the lift and drag forces acting on the fragment. Two types of fragment cases were studied in this analysis: (1) fragments whose geometry is such that both the lift and drag forces act on them during flight, i.e., disc-shaped fragments and long, thin fragments; and (2) fragments whose geometry is such that only the drag forces act and there is no lift. A method of predicting the distance traveled by a fragment was developed and computerized (Code FRISB) by Baker, et al (197[illegible], and this section expands on their efforts.

A set of generalized curves (Figure 4-5) was developed for use in estimating the maximum fragment range. These curves were developed by performing a model analysis to generate dimensionless parameters which describe the general problem (Appendix E), next using the computer code FRISB to determine ranges for selected cases, and then plotting the results to form the curves. It should be noted that, in generating these curves, several initial trajectory angles were used in the analysis to obtain the maximum range for the respective fragments. For ease in understanding the use of these curves, the example which follows is presented. The procedure for determining fragment range is:

Step 1. Calculate the lift/drag ratio = $\frac{C_L A_L}{C_D A_D}$ for the fragment.

Step 2. Calculate the velocity term = $\frac{\rho_o C_D A_D V^2}{Mg}$ for the fragment.

Step 3. Select the curve on the graph for the appropriate lift/drag ratio; locate the velocity term on the horizontal axis; find the corresponding range term, $\frac{\rho_o C_D A_D R}{M}$ and determine the range, R.

Note that, for lift to drag ratios $\frac{C_L A_L}{C_D A_D}$ that are not on the curve, a linear interpolation procedure can be used to determine the range from the curve. Interpolation in the steep areas of the curve can cause considerable error and it is recommended that, for these cases, the computer code FRISB be exercised.

FRISB example: Assume ρ_o = density of air = 1.293 $\frac{kg}{m^3}$

g = gravity constant = 9.807 m/s^2

Example 1, for lifting fragments:

Determine the maximum range of a long rectangular fragment assuming the following properties: V_i = 100 m/s (328 ft/sec), Mass = 30.827 kg (67.96 lb_m), Projected area = 0.03018m^2 (0.3249 ft^2), Cylinder length = 1.58m (5.18 ft), Thickness of fragment = 0.0191m (0.0627 ft), Planform or lift area = 0.20623m^2 (2.2198 ft^2), Drag coefficient = 2.05, lift coefficient = 0.3, and the initial trajectory of the fragment at t = 0 was α_i = 20°.

Step 1. Determine the lift/drag ratio for the fragment =

$$\frac{C_L A_L}{C_D A_D} = \frac{(0.3)\ (0.20623)}{(2.05)\ (0.03018)} = 1.0$$

Step 2. Determine the value of the velocity term =

$$\frac{\rho_o C_D A_D V^2}{Mg} = \frac{(1.293)\ (2.05)\ (0.03018)\ (100)^2}{(30.827)\ (9.807)} = 2.65$$

Step 3. From Figure 4-5 $\frac{\rho_o C_D A_D R}{M}$ = 1.65 and solving for R results in a range of 635.8 meters (2086 ft).

Program FRISB results show the maximum range to be 633.43m (2078 ft).

Percent error = $\frac{635.8-633.43}{633.43}$ X 100 = 0.37%

Predicting Ranges of Rocketing Fragments

In an accident involving propellant (propane, butane, etc.) storage systems, large fragments (greater than one-fourth of the vessel), which travel long distances, are sometimes generated. These large fragments are typically sections of the tank which break free intact and initially contain some entrapped propellant. These large fragments exhibit a rocketing behavior (see Appendix E) which results from the changing of all or part of the liquid propellant into a gas when the external pressure is released during the fracturing of the vessel (flash evaporation). The gas escapes from the opening in the vessel in a manner similar to gas exiting a rocket motor and propels the somewhat stabilized fragment to great distances.

The physics of this process is explained in greater detail in Appendix F. This appendix also contains a computer program for predicting the range and impact velocity of the rocketing

TABLE OF CONTENTS

fragment. As explained in the model analysis in Appendix G, this phenomenon is not readily adaptable to consolidated prediction curves and requires some further development effort in this area. Therefore, for the present, in order to predict the distance traveled by "thrusting" fragments, one must either run the computer program in Appendix F or acquire the values from Table 4-2, (see Appendix G, p. 7) if the storage tanks and fragments being examined have characteristics similar to the vessels and fragments contained in the table. Table 4-2 was generated for comparison to some accident reports. Calculated values for fragment ranges were in good agreement with actual values, considering limitations in available information. In general, rocketing fragments from accidents of this type have low launch angles (5-10 degrees). To determine range, or impact velocity, of rocketing fragments (see Table 4-2 and/or Appendix F), one needs to know the pressure of the fluid at rupture, the volume of the container, the volume partially enclosed by the fragment, the volume of the liquid before rupture, the volume of the vapor before rupture, the exit area for the propellant contained in the fragment, the mass of the fragment, and the launch angle of the fragment.

4-4 Statistical Analysis of Fragments

Statistical Analysis of Accidental Explosions

Introduction

Data were gathered on twenty-five events. A detailed description of these events, in terms of the explosive source and the containment vessel, is given in Table H-1 in Appendix H. Table H-2 in Appendix H gives available fragment information (mass, range, trajectory elevation and shape) for each event.

Due to the limited amount of data on most of the events, it was desirable to group the data from like events in order to yield an adequate base for meaningful statistical analysis. From Tables H-1 and H-2, the six groups of like events shown in Table 4-3 were obtained. Statistical analyses were performed on data from each of the groups to yield (as the data permitted) estimates of fragment range distribution, fragment mass distribution and fragment mean velocity as a function of the ratio of explosion energy to vessel weight. Other relationships were also investigated and the results are given in the following paragraphs.

Fragment Range Distribution

As shown in Appendix H-2, the fragment range for each of the groups of events follows a log normal distribution. That is, the logarithms of the fragment ranges follow a normal or

TABLE 4-2. PREDICTED RANGES FOR ROCKETING FRAGMENTS

EXAMPLE NUMBER	SOURCE OF ACTUAL DATA	INITIAL PRESSURE (P_o)	VOLUME OF CONTAINER (m^3)	VOLUME OF FRAGMENT ENCLOSURE (m^3)	VOLUME OF LIQUID BEFORE RUPTURE (m^3)	VOLUME OF VAPOR BEFORE RUPTURE (m^3)	EXIT AREA (m^2)	MASS OF FRAGMENT (kg)	LAUNCH ANGLE (degrees)	CALCULATED IMPACT VELOCITY (m/s)	CALCULATED RANGE (m)	ACTUAL RANGE (m)	PERCENT DIFFERENCE IN RANGE (%)	BEST ESTIMATE FOR LAUNCH ANGLE (degrees)
1	NTSB-HAR-76-4 4/29/75	701,197	38.02	28.23	33.10	4.916	3.75	3885	5	194	426	314	36	5
2	NTSB-HAR-73-4 9/21/72	1,034,214	37.85	30.32	27.29	10.56	3.41	5083	5	189	471	398	18	5
3	NTSB-HAR-73-4 9/21/72	1,034,214	37.85	1.28	27.29	10.56	3.41	652	5	94	154	165	-6.7	5
4a	Propane Tank Explosion in San Antonio	1,378,951	1.8927	0.5513	1.586	0.3067	2.336	171	5	159	450	123	266	5-10
4b	Propane Tank Explosion in San Antorio	1,378,951	1.8927	0.5513	1.586	0.3067	2.336	171	10	154	846	123	-588	5-10
4c	Propane Tank Explosion in San Antonio	1,378,951	1.8927	0.2002	1.586	0.3067	0.6567	171	5	72	90	123	-27	5-10
4d	Propane Tank Explosion in San Antonio	1,378,951	1.8927	0.2002	1.586	0.3067	0.6567	171	10	71	[illegible]	123	66	5-10

TABLE 4-3. GROUPS OF LIKE EVENTS TAKEN FROM TABLES H-1 and H-2

Event Group Number	Event	Explosion Source		Vessel		
		Material	Energy Range, J	Shape	Mass, kg	Number of Fragments
1	1,2,3,18	Propane, anhydrous ammonia	1.487×10^5 to 5.95×10^5	RR Tank Car	25,542 to 83,900	14
2	6,7,8,9,10, 13,14,15,19	LPG	3814 to 3921.3	RR Tank Car	25,464	28
3	17	Air	5.198×10^{11}	Cylinder Pipe and Spheres	145,842	35
4	20,24	LPG, Propylene	549.6	Semi Trailer (cylindrical)	6,343 to 7,840	31
5	21,22,23	Argon	2.438×10^9 to 1.133×10^{10}	Sphere	46.26 to 187.33	14
6	25	Propane	24.78	Cylinder	511.7	11

Gaussian distribution. Figure 4-6 presents the fragment range distributions for groups 1 and 2, and Figure 4-7 presents the fragment range distributions for groups 3, 4, 5 and 6.

Figures 4-6 and 4-7 can be used to estimate the percentage of fragments which will have a range, R_i, equal to or less than a particular range.

For example, if we wished to estimate the percentage of fragments which would have a range equal to or less than 600 m for an explosion involving a rail tank car filled with propane (group 1), we would refer to Figure 4-6, and on the range axis (abscissa) at 600 m go upward to the intersection of the group 1 line. Then, at the intersection point read the percentage value from the ordinate, which is 96%. Conversely, if we wanted to know what range 90% of the fragments would not exceed, we would enter the chart on the 90% line, go over to the intersection of the group 1 line and read downward to the range axis the value of 380 m.

Fragment Mass Distribution

Pertinent fragment mass information was available on three event groups (2, 3 and 6). As shown in Appendix H-3, the fragment mass for each of the three groups follows a log normal distribution. Figure 4-8 presents the fragment mass distributions for groups 2 and 3, and Figure 4-9 presents the fragment mass distribution for group 6.

These charts can be used in the same manner as Figures 4-6 and 4-7 are used for fragment range.

Mean Fragment Mass as a Function of Normalized Yield

In events 21, 22 and 23, spherical containers were pressurized until rupture. The spheres were constructed of steel with an approximate ultimate stress (σ_u) of 834 MPa. The spheres were the same volume for all three events. The wall thickness of the spheres was the same within events, but was different across events.

Pertinent data and calculated parameters for each of the spheres are given in Table 4-4, where $\bar{W}$ is the geometric mean fragment mass for each event, W(T) is the sphere weight for each event, $\bar{P}$ is the average burst pressure for each event, and E_o is the energy of detonation of 1 gram of TNT or 4190J.

Figure 4-10 is a plot of the normalized yield ($\bar{P}V/E_o$) versus mean fragment mass ($\bar{W}$) for the three events. One could estimate the mean (geometric) fragment mass for any decided ratio of $\bar{P}V/E_o$ from 693 to 2347.

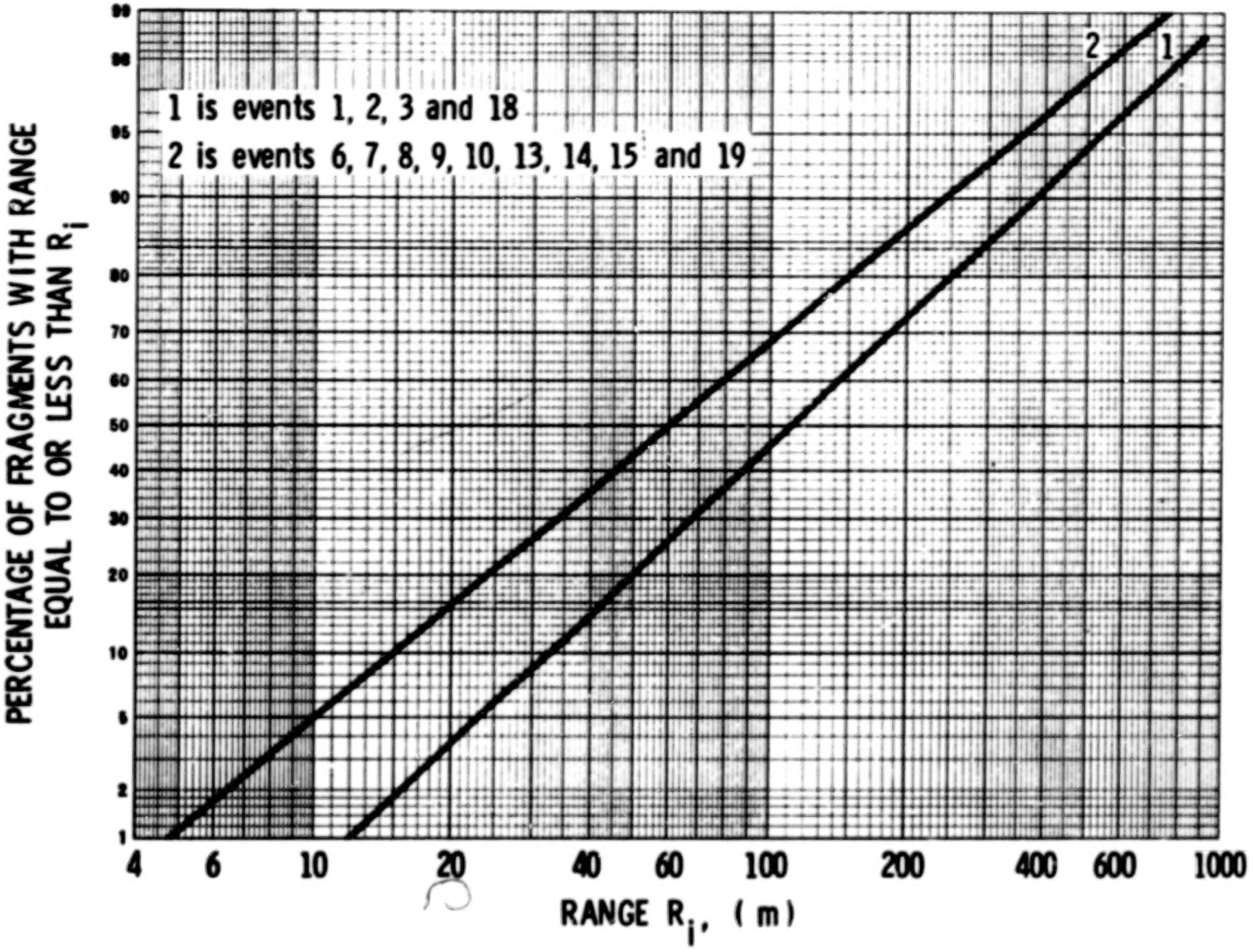

FIGURE 4-6. FRAGMENT RANGE DISTRIBUTION FOR EVENT GROUPS 1 AND 2.

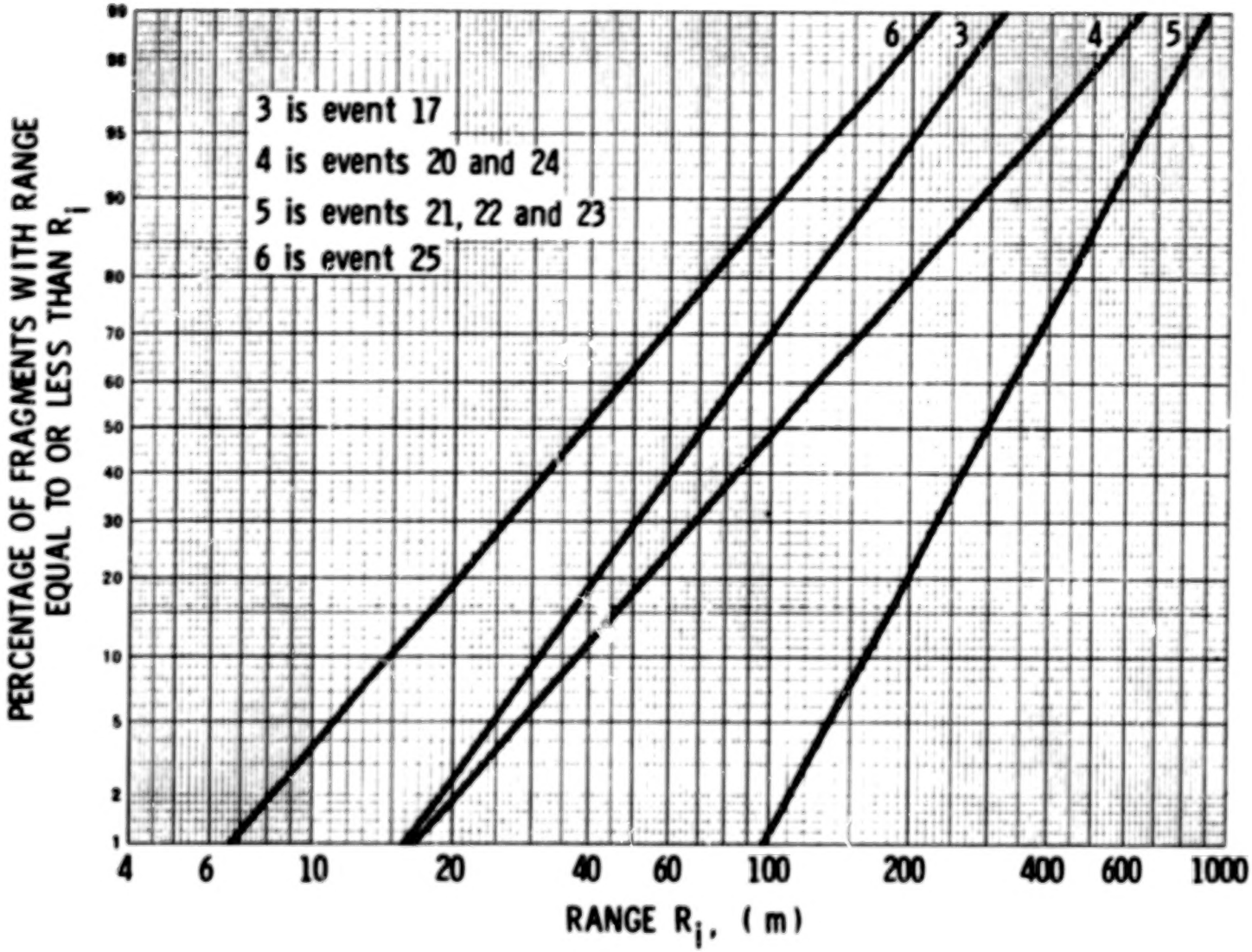

FIGURE 4-7. FRAGMENT RANGE DISTRIBUTION FOR EVENT GROUPS 3, 4, 5 AND 6

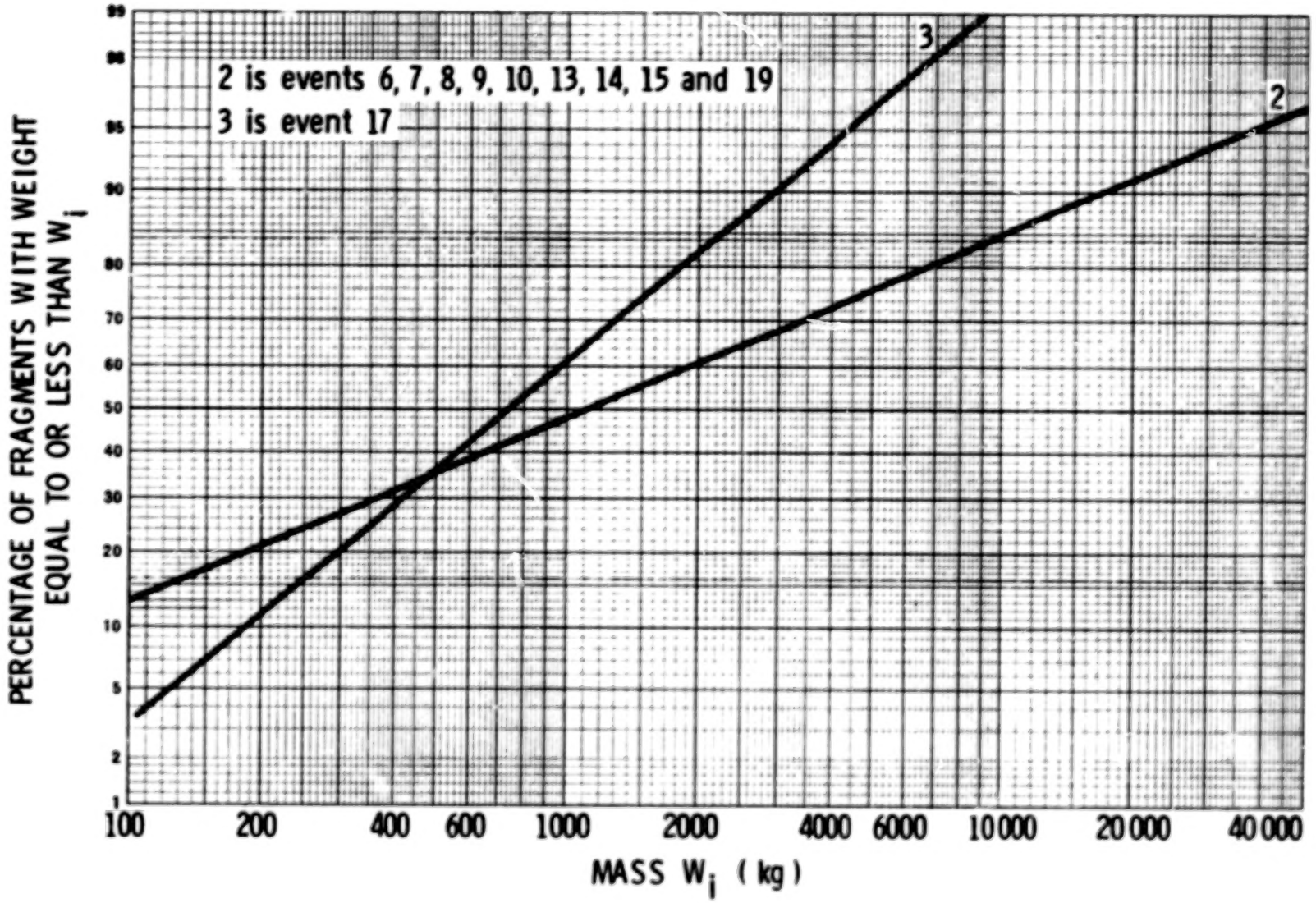

FIGURE 4-8. FRAGMENT MASS DISTRIBUTION FOR EVENT GROUPS 2 AND 3

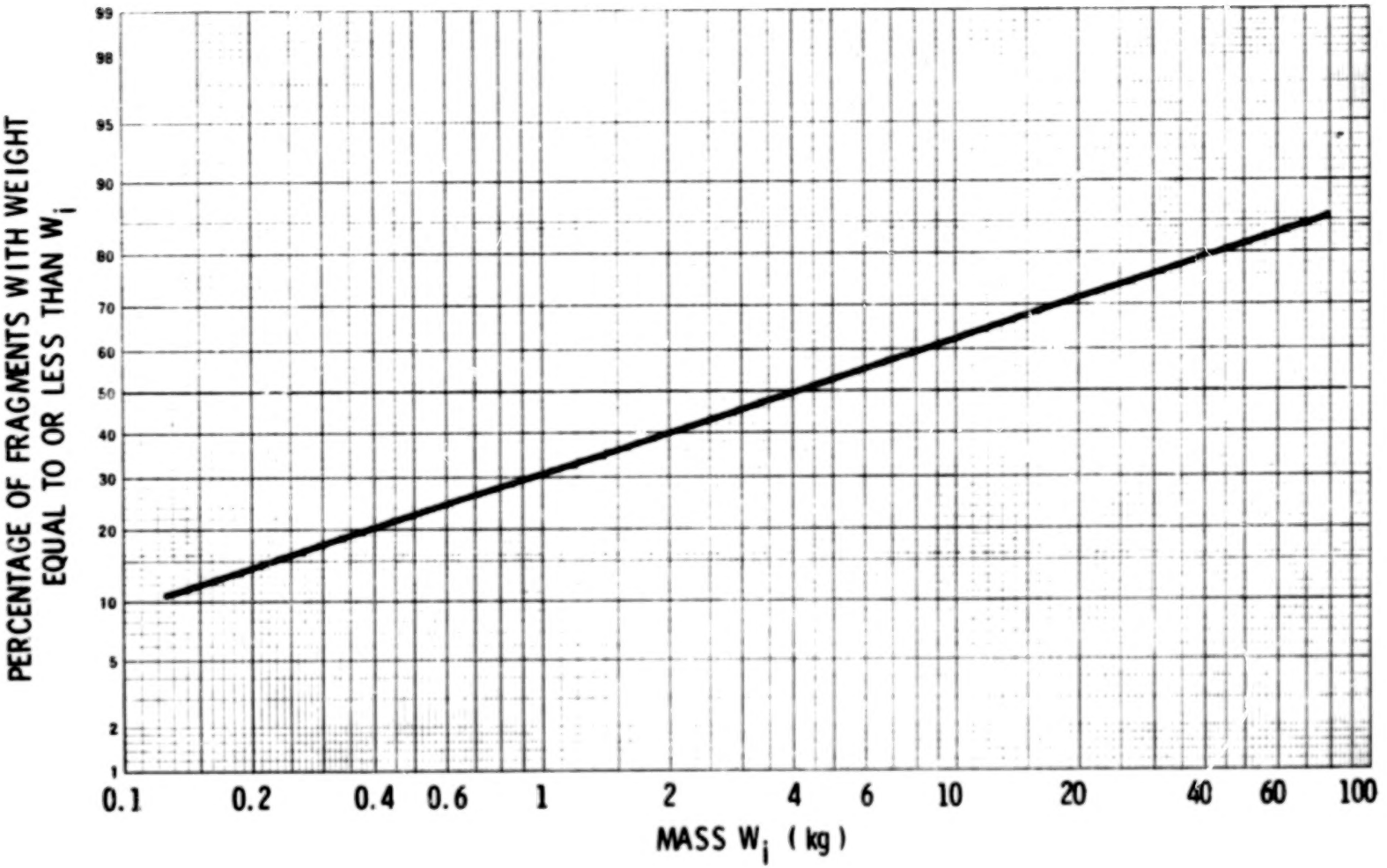

FIGURE 4-9. FRAGMENT MASS DISTRIBUTION FOR EVENT GROUP 6 (EVENT 25)

The correlation coefficient, r, for the regression equation shown on Figure 4-10 was 0.9999, which indicates a high degree of correlation between $\overline{PV}/E_o$ and $\overline{W}$.

Correlation Between Fragment Range and Fragment Mass Within Event Groups

Only three event groups (2, 3 and 6) contained sufficient fragment range and mass data for correlation analysis. Various curve fitting techniques were employed to determine if a predictable relationship existed between fragment range and mass as indicated by the data on the three events. Appendix H-4 contains a description of the techniques and the results.

Figure 4-11 depicts the relationship of the fragment range to fragment mass for Group 2. The correlation coefficient is 0.79.

Figure 4-12 shows the relationship of the fragment range to fragment mass for Group 6. The correlation coefficient is 0.68.

Correlation of Fragment Range to the Ratio of Mean Fragment Weight to Vessel Weight for Cylindrical Tanks

Five events contained sufficient information for this type of analysis. Data for each of the events are contained in Appendix H-5. Figure 4-13 is a plot of the mean (arithmetic) fragment weight versus the ratio of mean fragment weight to the vessel weight for the events.

From Figure 4-13, one could estimate the mean fragment range for any decided ratio of mean fragment weight to vessel weight for the types of tanks in the events.

Correlation of Fragment Velocity to the Ratio of Energy to Vessel Weight

Only in event group 5 were there reports of mean velocity for fragments. Figure 4-14 is a plot of the relationship between the mean fragment velocity and the ratio of the energy to vessel weight. The velocities were chosen as the maximum velocity reported within an event for events 21, 22 and 23 (see Table 4-4). The correlation coefficient for the regression equation is 0.93.

One could use Figure 4-14 to predict the average velocity for fragments from bursting steel spheres over a range of an energy to vessel weight ratio of 4.5×10^7 to 6.05×10^7. However, the analytic predictions for fragment velocity presented earlier in this chapter are more useful because they cover a much wider range of bursting vessel conditions.

TABLE 4-4. PARAMETERS OF BURSTING SPHERES

Event	Shot No.	Fragment Mass, Kg	Fragment Average Velocity, (m/s)	Burst Pressure, P, Pa	Volume, V (m^3)	Vessel Weight WT. (kg)	Energy, J	Average(1) Fragment Weight, $\bar{W}$, kg	(2) $\frac{\bar{P}V}{E_o}$
21	1	22.49 23.77	96.9	1.044×10^8	.0283	46.26	2.438×10^9	23.14	693.43
	2	22.36 23.90	98.6	1.030×10^8	.0283	46.46			
	6	23.18 23.18		1.006×10^8	.0283	46.26			
22	3	69.18 66.90	107.59	2.372×10^8	.0283	136.08	6.078×10^9	55.69	1541.6
	7	48.99 42.41	83.52	2.193×10^8	.0283	136.08			
23	4	117.03 70.03	65.84	3.475×10^8	.0283	187.33	1.133×10^{10}	89.75	2347.1
	5	122.91 64.41	71.63	3.475×10^8	.0283	187.33			

(1) Geometric mean fragment mass

(2) $\bar{P}$ = Average burst pressure

E_o = Energy of detonation of 1 g TNT

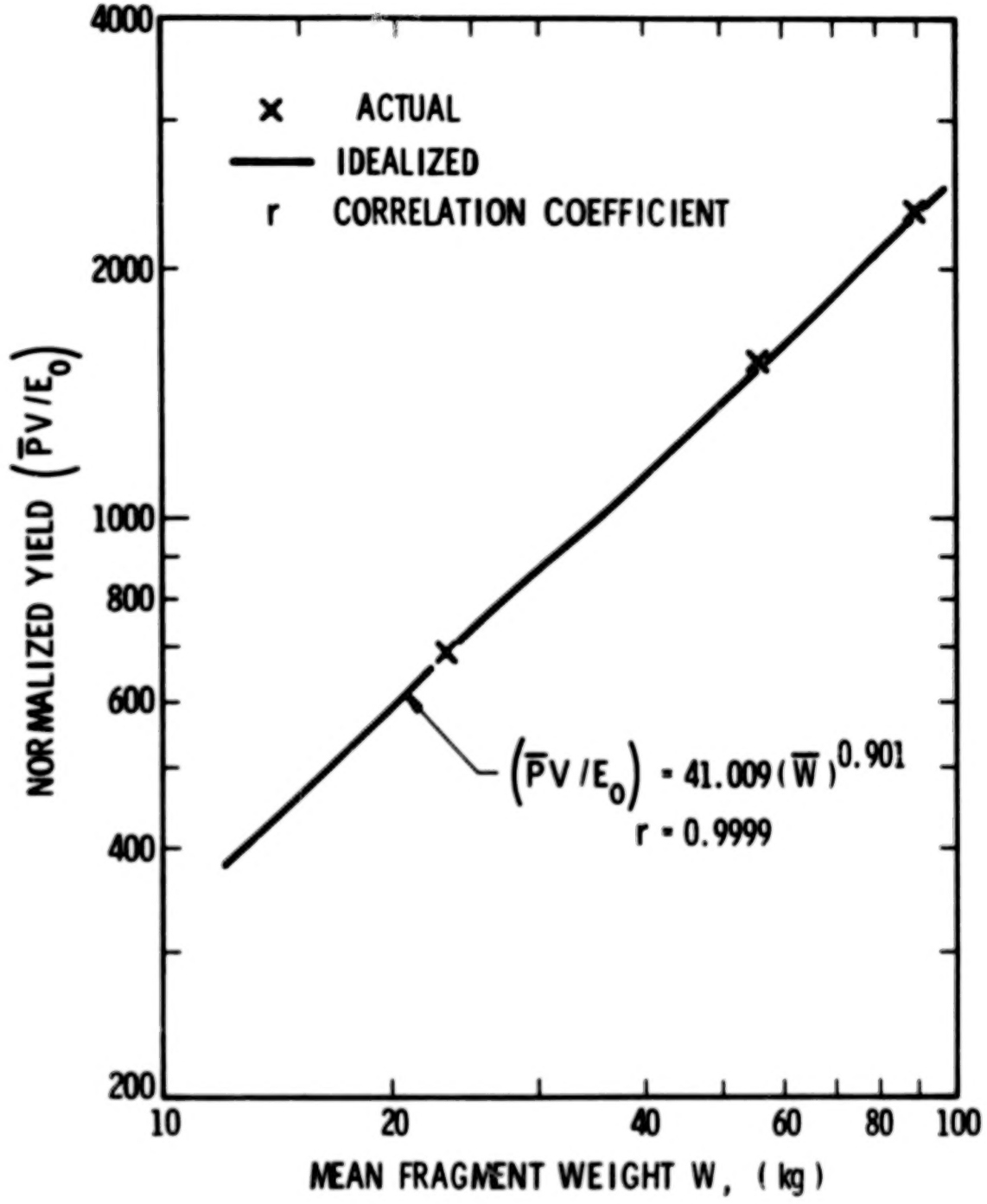

FIGURE 4-10. NORMALIZED YIELD VERSUS MEAN FRAGMENT WEIGHT FOR BURSTING SPHERES

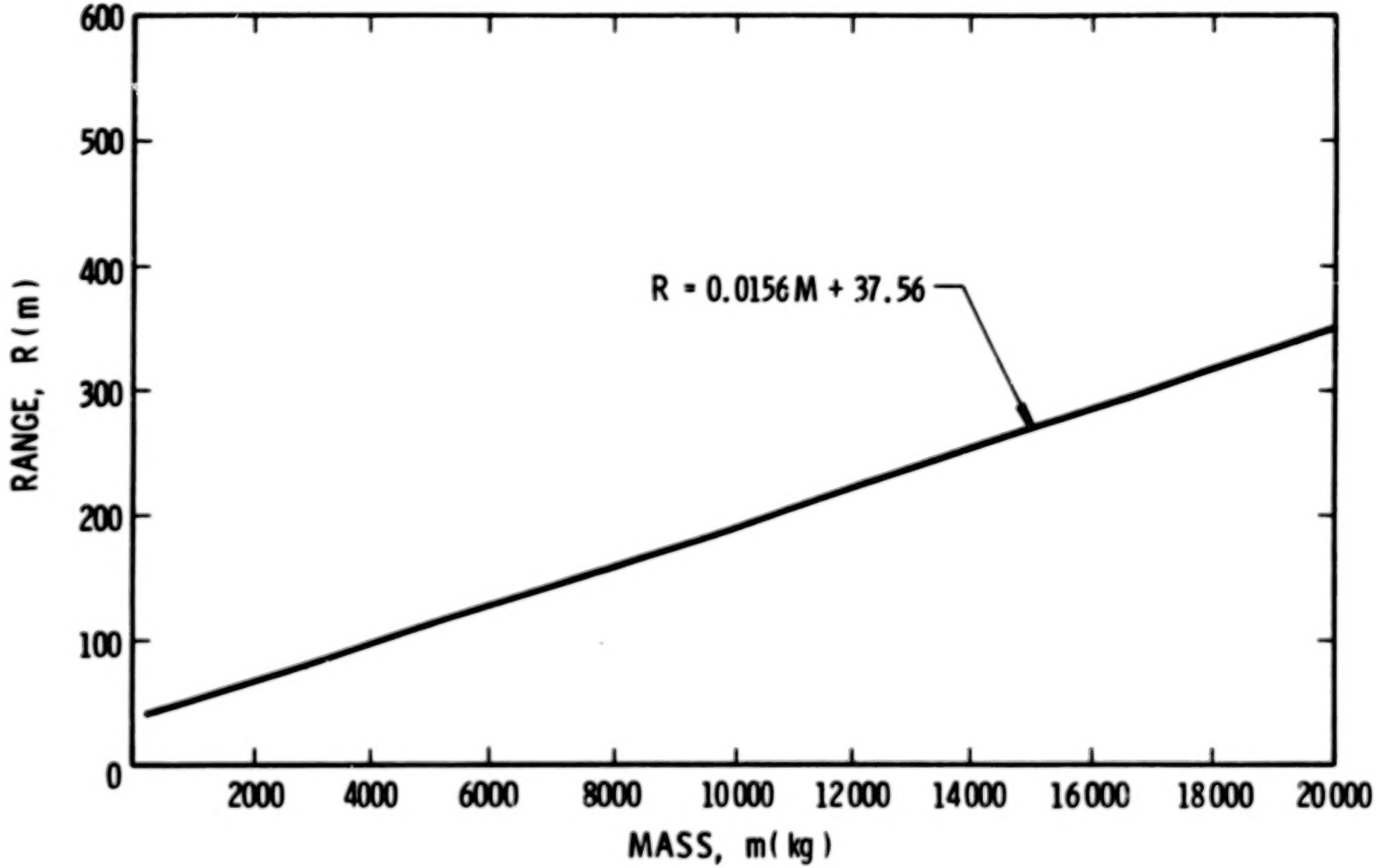

FIGURE 4-11. FRAGMENT RANGE VERSUS FRAGMENT MASS FOR EVENT GROUP 2

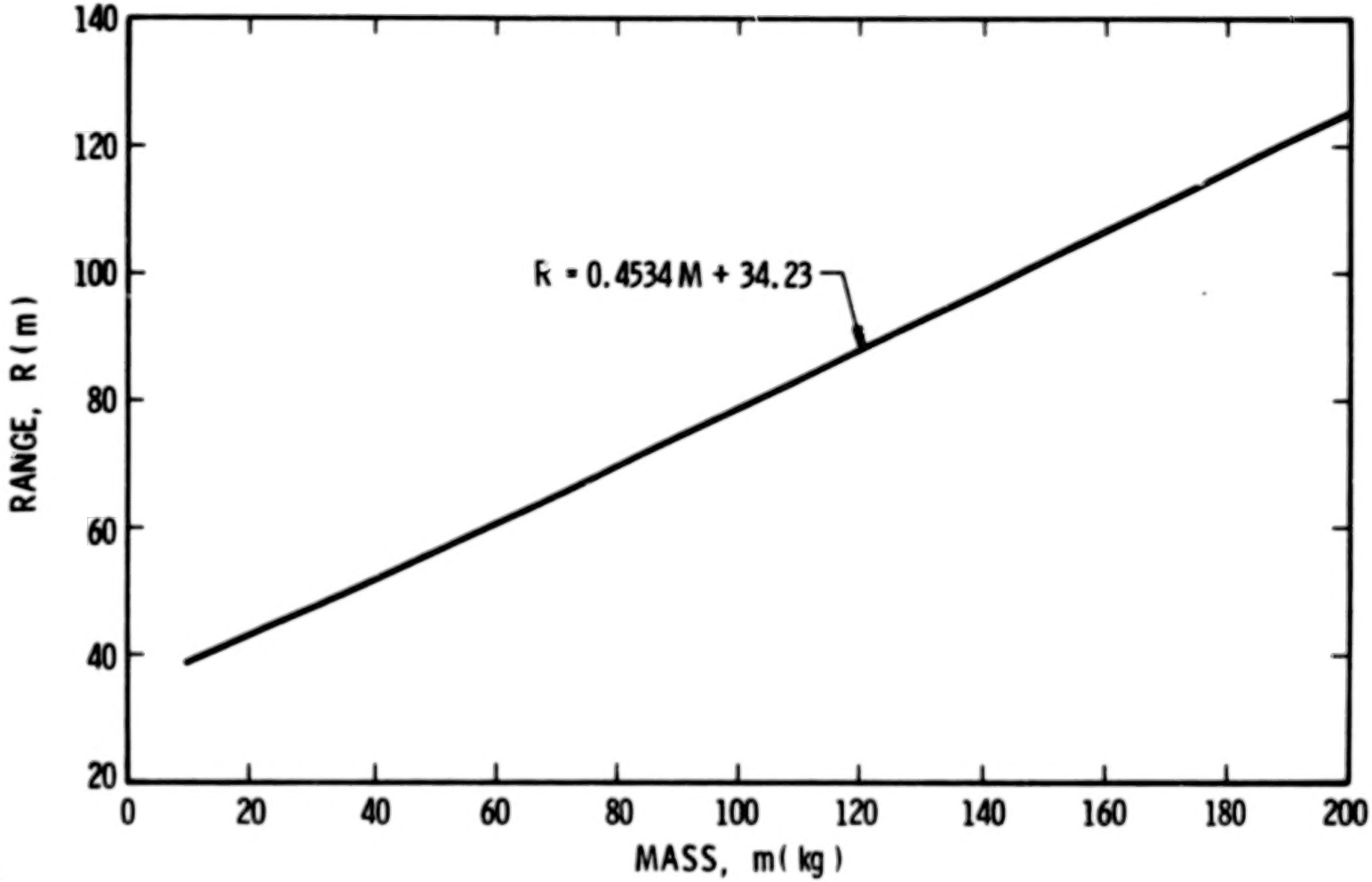

FIGURE 4-12. FRAGMENT RANGE VERSUS FRAGMENT MASS FOR EVENT GROUP 6

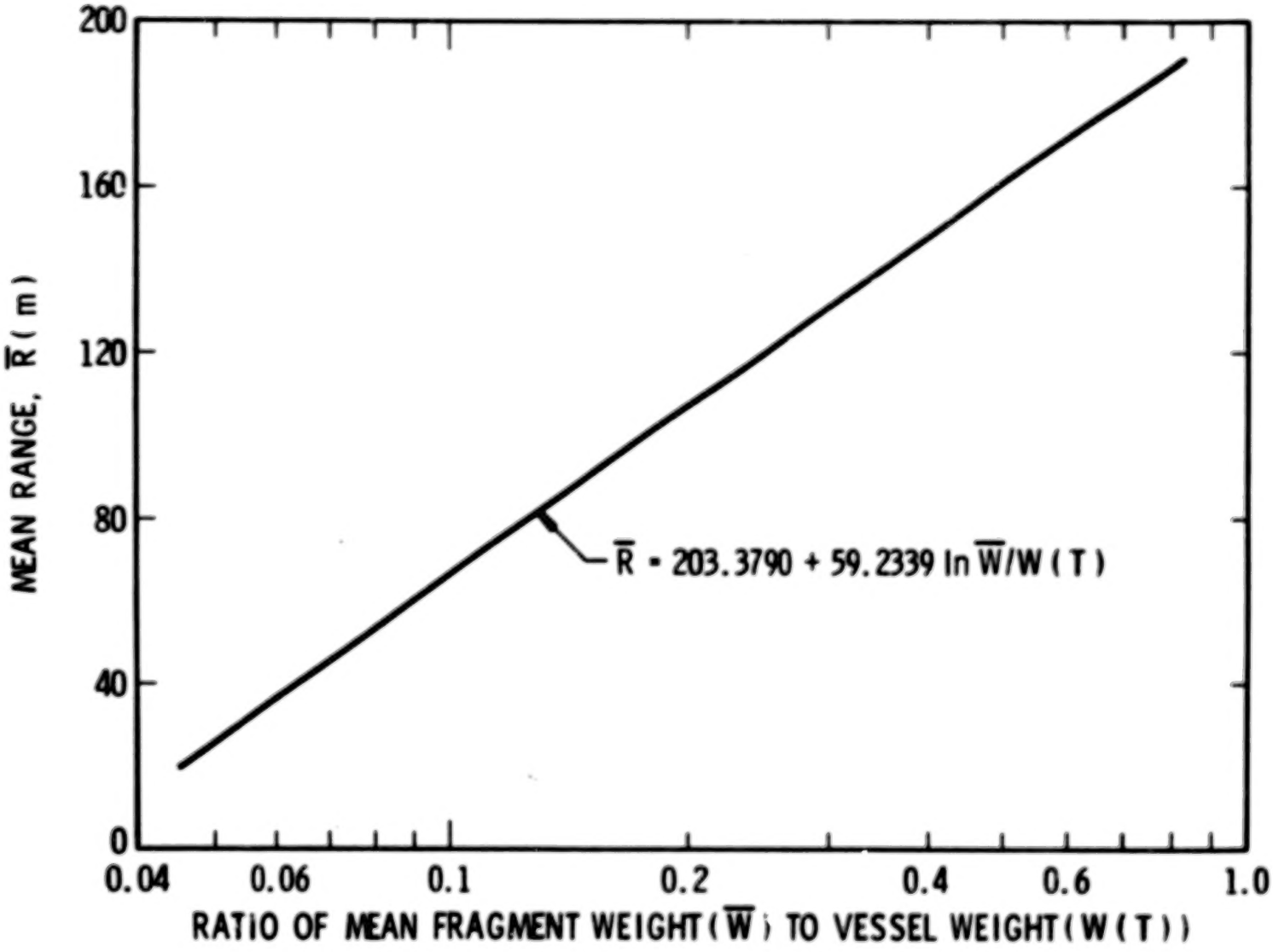

FIGURE 4-13. RANGE VERSUS THE RATIO OF MEAN FRAGMENT WEIGHT TO TANK WEIGHT FOR CYLINDRICAL VESSELS

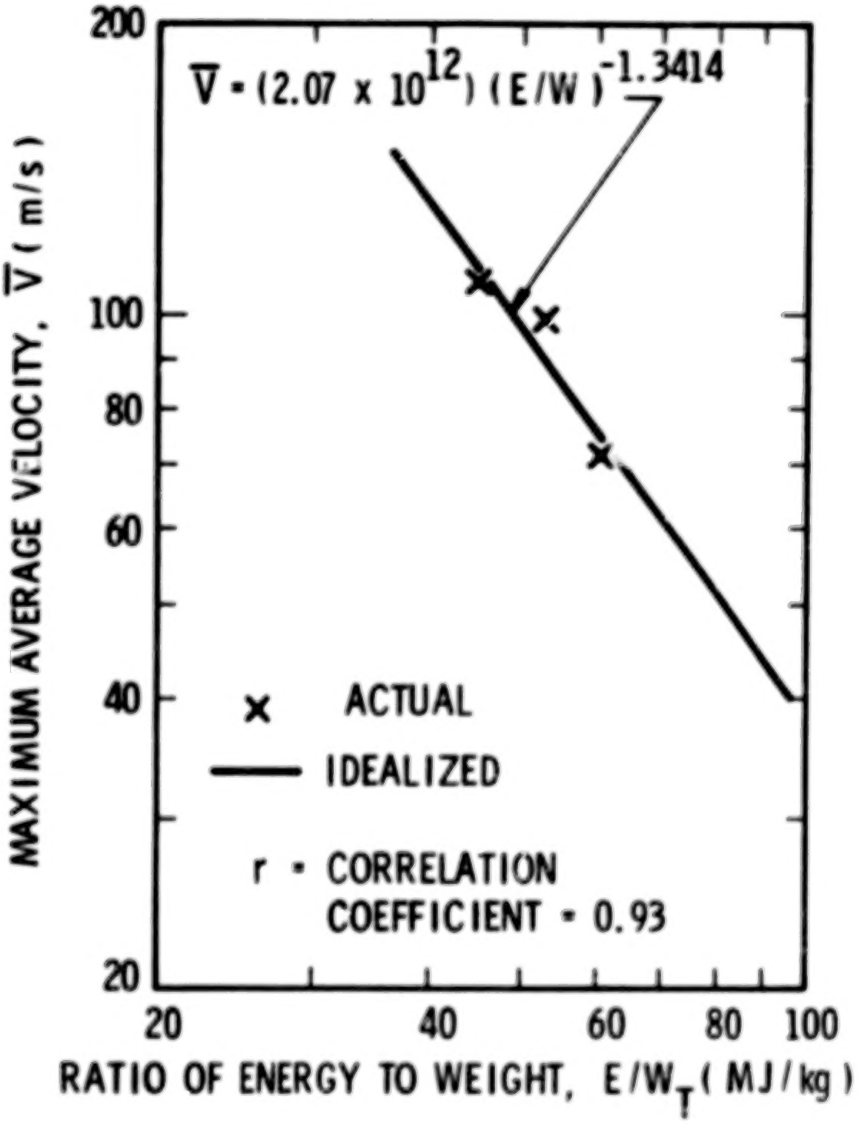

FIGURE 4-14. MAXIMUM MEAN VELOCITY VERSUS RATIO OF ENERGY TO VESSEL WEIGHT FOR BURSTING SPHERES

LIST OF REFERENCES

1. Baker, W. E., Kulesz, J. J., Ricker, R. E., Bessey, R. L., Westine, P. S., Parr, V. B. and Oldham, G. A.(1975) "Workbook for Predicting Pressure Wave and Fragment Effects of Exploding Propellant Tanks and Gas Storage Vessels", NASA CR-134906, Contract NASA-19231, November 1975 (reprinted September 1977).

2. Taylor, D. B. and Price, C. F. (1971), "Velocities of Fragments From Bursting Gas Reservoirs", ASME Transactions, Journal of Engineering for Industry, November 1971.

CHAPTER V

EFFECTS OF FRAGMENTS AND RELATED TOPICS

5-1 General

In Chapter V of Baker, et al (1975), some methods were given for prediction of effects of impact of typical fragments from accidental explosions involving flight-weight hardware. For the even more massive fragments typical of explosions in ground systems, the voluminous literature on terminal effects of military fragments and projectiles is of very little use. But, since the earlier workbook was prepared, some data and prediction methods have been developed related to impact effects of tornado-borne missiles. Generally, this class of missile lies within the range of masses and velocities shown in Chapter IV for fragments from explosions in ground systems. Wooden poles and planks, pipes, pieces of steel reinforcing bar, and more massive bodies such as compact cars and entire storage tanks have been picked up and hurled at damaging velocities by tornadoes. Much of this work is summarized in Peterson (1976), and has its impetus in tornado-proof design requirements for nuclear plants.

Similarly, new nuclear plants must now be designed to be proof against other accidents including crash of aircraft on the containment structures, and external vapor-cloud explosions. Some preliminary design methods have evolved for massive, non-penetrating missile impacts to meet the aircraft crash design requirements. Typical of recent literature references to this problem are Drittler and Gruner (1976 a and b) Hammel (1976), and Degen, et al (1976). But in spite of these recent additions to the literature, we feel that impact effects of quite massive, but crushable, missiles are not well enough known to be reduced to design graphs in this workbook.

In Baker, et al (1975), methods were given to predict velocities of fragments and objects located near accidental explosions (appurtenances). In preparing this workbook, we were asked to consider modifying these procedures to account for the two-dimensional character of some accident blast waves. Although we have generated some graphs for the prediction of two-dimensional blast wave properties in Chapter II, these are not extensive enough to allow modification of the previous procedures. We suggest that at present the reader simply use the procedures in the previous workbook.

In certain fixed ground installations having a high potential for accidental explosion, or limited real estate, barricades may be built in an attempt to attenuate blast waves and to reduce fragment hazards. The barricades may be earth berms, retaining

walls backed by earth fill, or built-up walls of reinforced concrete, timber, or steel construction. Unless structures to be protected are located very close to the barricades, they are almost totally ineffective in attentuating blast waves. The waves simply diffract over the barricades and reform. Barricades are, however, quite effective in arresting fragments and may be worth constructing for that purpose alone. We will give some prediction graphs for blast attentuation for barricades of several forms located close to protected structures. No data or proven prediction methods exist for effects of barricades on non-ideal blast waves, so the predictions will be limited to attentuations for condensed high explosives.

5-2 Penetration Effects of Massive Missiles

Some prediction methods of penetrating effects of massive missiles can be added to the methods in Baker, et al (1975). The "targets" for these missiles are primarily reinforced concrete or steel plate panels or walls.

Concrete Panels

Concrete containment walls are very likely to be struck by fragments generated by an accidental explosion. Unfortunately, analytical prediction of penetration phenomena is in many ways more difficult for concrete than for homogeneous materials. This is due to the inhomogeneity of the panels and to the different construction techniques in use today--prestressing and post-tensioning, for example. In addition, since concrete targets are so expensive to fabricate, the amount of extant test data is limited.

Figure 5-1 shows schematically three different mechanisms of missile impact damage. At low velocities, the missile strikes the panel and rebounds without causing any local damage. As the velocity increases, pieces of concrete are spalled (ejected) off of the front or impacted face of the target. This spalling forms a spall crater that extends over a substantially greater area than the cross-sectional area of the striking missile. As the velocity continues to increase, the missile will penetrate the target to depths beyond the depth of the spall crater, forming a cylindrical penetration hole with a diameter only slightly greater than the missile diameter. As the penetration depth increases, the missile will stick to the concrete target rather than rebounding. At this stage the impact meets the criterion of a "plastic" impact. However, even at lesser penetration depths the impact can be approximately treated as a plastic impact when determining the energy absorbed by the impacted target. Further increases in velocity produce cracking of the concrete on the back surface followed by scabbing (ejection) of concrete from this rear surface. The zone of scabbing will generally be much wider, but not as deep as the front face spall crater. One scabbing begins, the

depth of penetration will increase rapidly. For low barrier thickness to missile diameter ratios (less than 5), the pieces of scabbed concrete can be large in size and have substantial velocities. As the missile velocity increases further, perforation of the target will occur as the penetration hole extends through to the scabbing crater. Still higher velocities will cause the missile to exit from the rear face of the target.

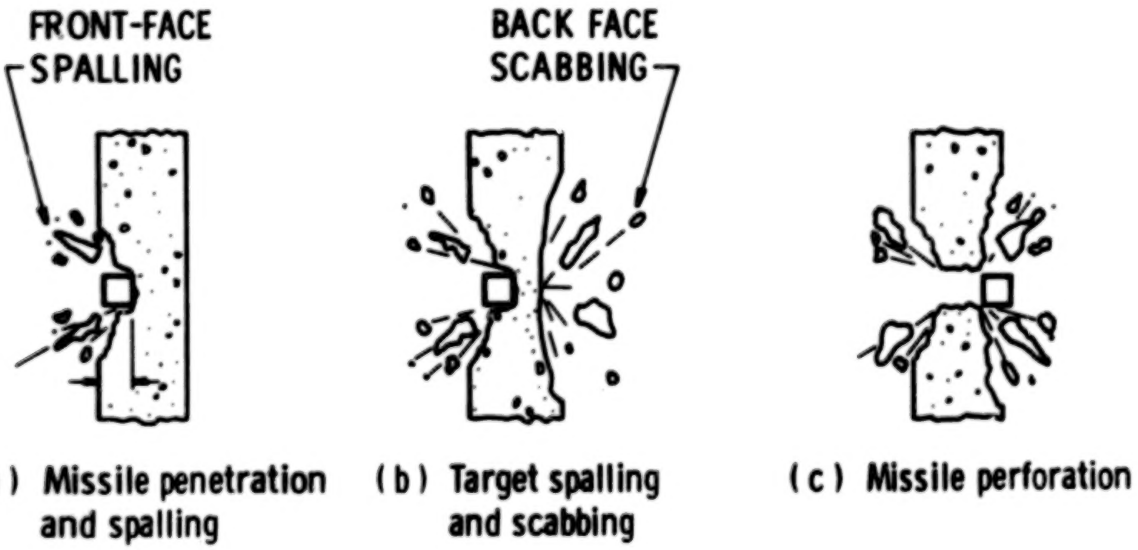

Figure 5-1. Missile Impact Damage [Kennedy (1976)]

Upon plastic impact, portions of the total kinetic energy of the impacting missile are converted to strain energy associated with deformability of the missile, and energy losses associated with target penetration. The remainder of the energy is absorbed or inputted to the impact target. This absorbed energy results in overall target response that includes flexural deformation of the target barrier and deformation of its supporting structure.

Currently depth of penetration, perforation and scabbing thickness are being predicted using one of several empirical formulas. These equations are based on experiments conducted prior to 1946 for concrete slabs perforated by projectiles and bombs. The most commonly used formulas are the modified Petry, Army Corps of Engineers, modified NRDC, the Amman and Whitney, and the BRL. [These formulas and their limitations and limits of applicability are summarized by Kennedy (1976)]. All of these formulas were derived for a nondeformable projectile (often made from armor-piercing steel) impacting normal to the target face.

In 1946 the National Defense Research Committee proposed a theory of penetration for a short, nondeforming projectile pene-

trating a massive concrete target which offered a good approximation of the experimental results. This theory of penetration enables one to not only calculate the total depth of penetration, but also to calculate the impact force-time history and penetration-depth time history. Based upon this theory of penetration, the National Defense Research Committee (NDRC) proposed that the penetration depth x be obtained from

$$G_{(x/d)} = KNd^{0.20}D\ (V_S/304.7)^{1.80} \qquad (5\text{-}1)$$

where

$$G_{(x/d)} = \begin{cases} (x/2d)^2, & \text{for } x/d \leq 2.0 \\ [(x/d) - 1], & \text{for } x/d \geq 2.0 \end{cases} \qquad (5\text{-}2)$$

and

K = Concrete penetrability factor (measures the resistance of concrete to penetration) ($m^{2.8}/kg$).

N = Projectile nose shape factor: 0.72 for flat nose shapes, 0.84 for blunt bodies, 1.0 for average bullet nose, and 1.14 for very sharp nose.

d = Projectile diameter (m). The equations presented herein are based entirely on cylindrical projectiles. For arbitrary shaped fragments, d is the diameter of an equivalent cylindrical projectile with the same contact surface area as the actual missile.

D = M/d^3 = caliber density of the projectile (kg/m^3)

V_S = Missile striking velocity (m/s).

x = Total penetration depth (m); the depth a missile will penetrate into an infinitely thick target. This neglects all rear face boundary effects and therefore applies only when target thickness is sufficient to prevent scabbing at the rear face.

The primary advantage of this formula is that, since it is based on a theory of penetration, it can be extrapolated beyond the range of available test data with greater confidence than is true with the other equations. Unfortunately, because of the reduction of interest in projectile penetration of concrete after 1946, the NRDC effort was aborted before the factor K was completely defined.

According to the NDRC report, K should lie between 2 and 5 (in English units), depending upon the concrete strength, to fit the available test data. Based upon both theoretical and experi-

mental considerations, it was suggested in 1966 that the concrete penetrability factor K is proportional to the reciprocal of the ultimate concrete tensile strength, which in turn was taken to be proportional to the square root of the ultimate concrete compressive strength f'_c. By fitting this relationship to the experimental data available for the larger missile diameters, the following relationship for K was obtained:

$$K = 1.134/(f'_c)^{1/2} \quad (m^{2.8}/kg) \tag{5-3}$$

The combination of Equations 5-2 and 5-3 is defined herein as the modified NDRC formula for penetration.

For slab thickness to projectile diameter ratios greater than three, Equation 5-1 can be used in conjunction with Equations 5-4 and 5-5 for predicting perforation and scabbing thicknesses.

$$e/d = 1.32 + 1.24\ (x/d), \text{ for } (3 \leq e/d < 18) \tag{5-4}$$

$$s/d = 2.12 + 1.36\ (x/d), \text{ for } (3 \leq s/d \leq 18) \tag{5-5}$$

where

e = perforation thickness (m); the maximum thickness of concrete which will be completely penetrated by missile at a given velocity.

and

s = scabbing thickness (m); thickness of a target required to prevent scabbing of material from the backface for a missile with a given velocity.

However, for many impact problems, the slab thickness to projectile diameter is substantially less than three. Beth (1945) gives a curved-fit extrapolation of these equations for slab thickness to projectile diameter ratios less than three so that the equation would pass through the origin. Parabolic fits which both pass through the origin and have the same slope as Equations 5-4 and 5-5 at a slab thickness to projectile diameter ratio of three have been proposed [Kennedy (1976)]. This parabolic fit leads to

$$\frac{e}{d} = 3.19\left(\frac{x}{d}\right) - 0.718\left(\frac{x}{d}\right)^2, \text{ for } x/d \leq 1.35, \tag{5-6}$$

$$\frac{s}{d} = 7.91\left(\frac{x}{d}\right) - 5.06\left(\frac{x}{d}\right)^2 - \text{ for } x/d \leq 0.65, \tag{5-7}$$

whereas for larger x/d ratios, Equations 5-4 and 5-5 are to be used. These modifications, when used together with Equations 5-2 and 5-3, are known as the modified NDRC formulae for perforation and scabbing. Their primary advantage over the other formulae is that they can be extrapolated to slab thickness to projectile diameter ratios less than three without leading to unreasonable results.

All of the formulas for concrete penetration are based on a limited range of parameter variation. Unless otherwise noted, these formulas are valid only for the following ranges:

$$
\begin{aligned}
& t/d \geq 3 \\
& d \leq 0.4 \text{ m} \\
& 5.5 \times 10^3 \text{ kg/m}^3 \leq D \leq 2.20 \times 10^4 \text{ kg/m}^3 \\
& 500 \text{ m/s} \leq V \leq 3000 \text{ m/s} \\
& 3 \leq e/d \leq 18 \\
& 3 \leq s/d \leq 18
\end{aligned}
\qquad (5\text{-}8)
$$

For long rods impacting concrete panels, recent model and full-scale testing of simulated tornado-borne missiles also gives prediction methods for scabbing thresholds for reinforced concrete panels. Sources for the basic data are discussed, and the curves generated, by Baker, Hokanson, et al (1976).

Figure 5-2 gives scabbing thresholds for steel pipes impacting normally on lightly reinforced concrete panels, with rebar percentages <1%. In this figure, KE is impact kinetic energy, h is concrete panel thickness, d is pipe outside diameter, and t_w is pipe wall thickness. Length-to-diameter ratios are variable, but all are greater than 5:1. Each curve gives the scabbing threshold for a particular wall thickness ratio.

Curves for scabbing caused by normal impact of solid rods, of material strong compared to the concrete, are given in Figure 5-3. The thresholds are quite different for slabs which are reinforced heavily enough for the rebar spacing to be significantly closer than the rod diameter (heavy reinforcing) and for spacing open enough that a rod can pass through without striking a rebar (light reinforcing). Rods were of ℓ/d ratios ranging from 1.75-40. A number of long wooden missiles were also fired against reinforced concrete panels, but these missiles were invariably defeated by the panels, with negligible damage to the panels themselves.

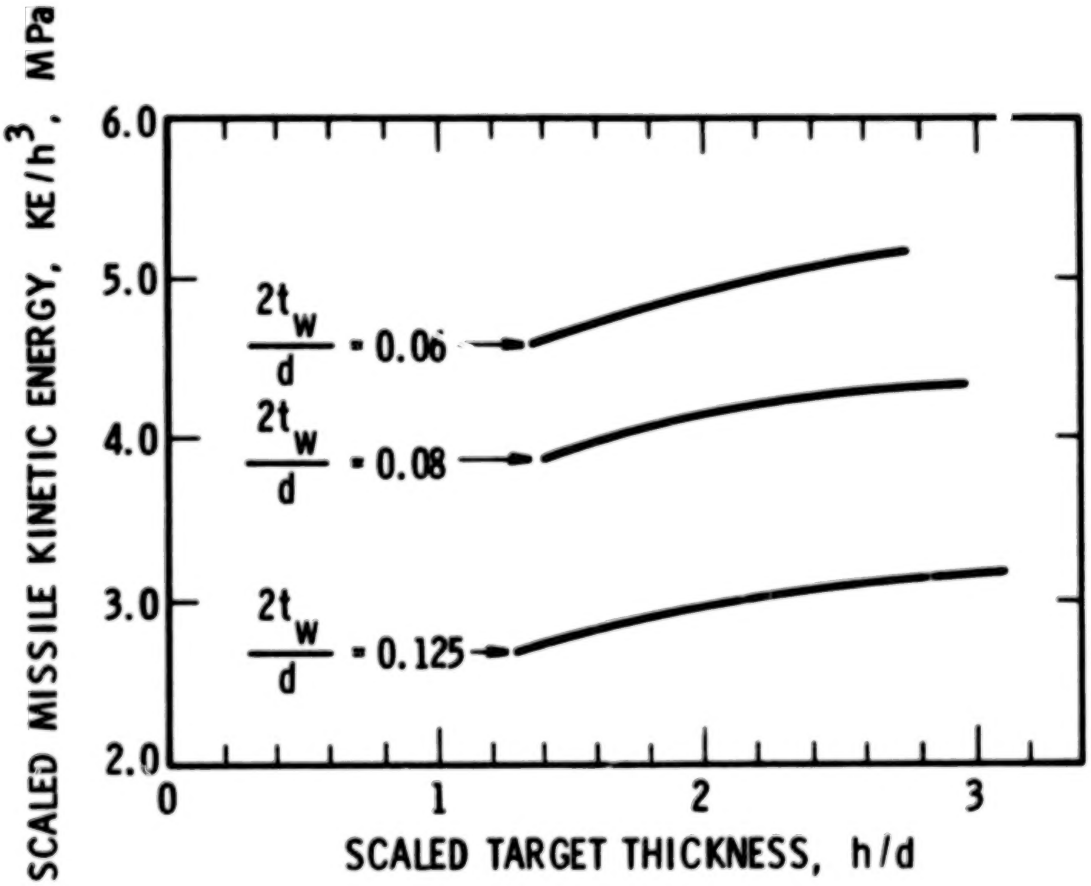

FIGURE 5-2. SCABBING THRESHOLD FOR MILD STEEL PIPES IMPACTING REINFORCED CONCRETE PANELS

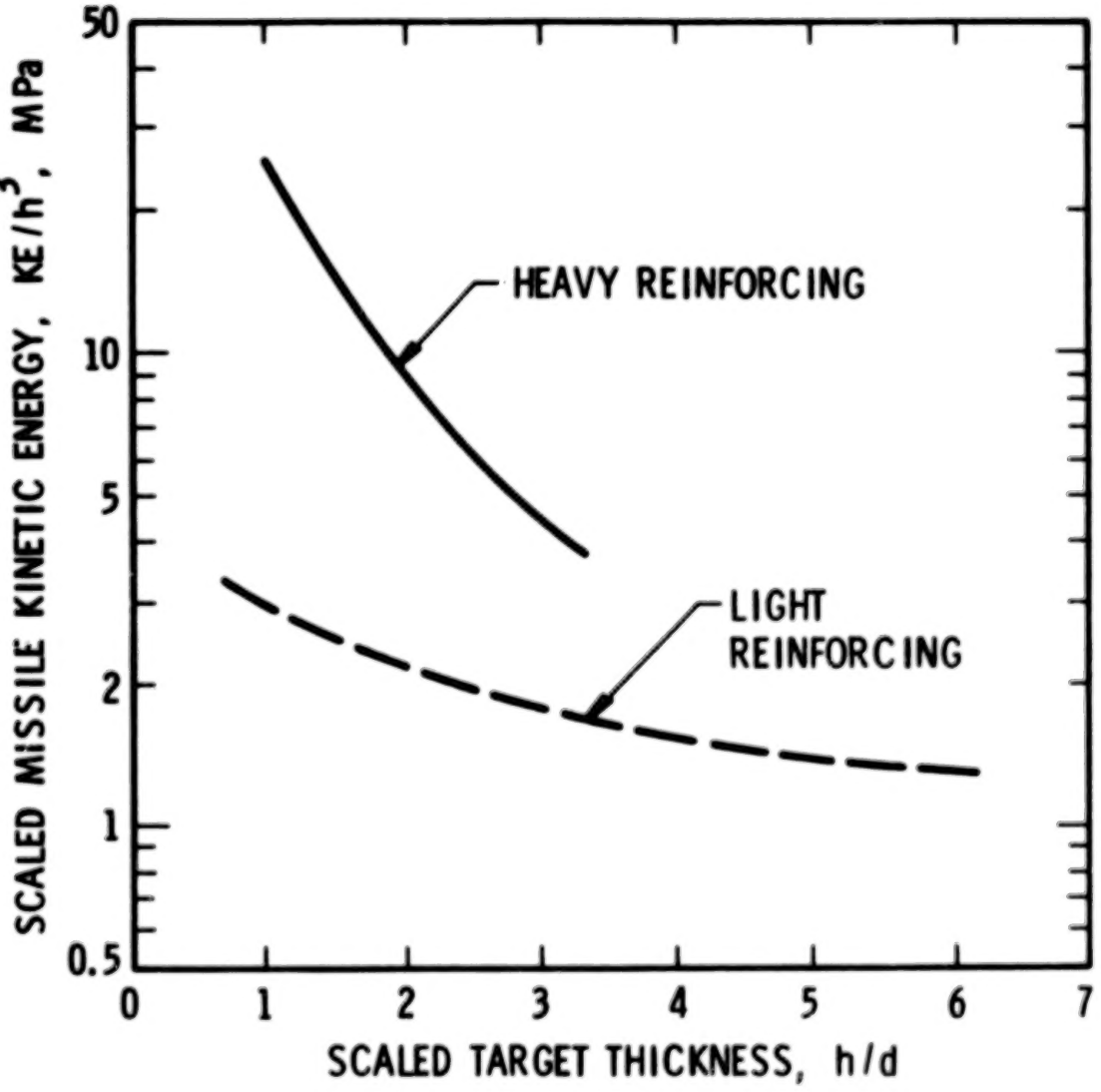

FIGURE 5-3. SCABBING THRESHOLDS FOR SOLID ROD MISSILES IMPACTING REINFORCED CONCRETE PANELS

Steel Panels

In Baker, et al (1975), prediction curves have already been given for perforation thresholds for thin metal impacted by chunky fragments of essentially nondeforming material. Long, deforming missiles, such as wood poles, can also perforate steel plate panels. Baker, Hokanson et al (1976) fit a penetration threshold curve for wooden missiles impacting large steel panels normally. This curve is reproduced here as Figure 5-4, and the empirically-fitted equation is given by

$$\frac{\rho_p V_s^2}{\sigma_t} = 1.751 \left(\frac{h}{d}\right)\left(\frac{\ell}{d}\right)^{-1} + 144.2 \left(\frac{h}{d}\right)^2 \left(\frac{\ell}{d}\right)^{-1} \qquad (5\text{-}9)$$

Here, ρ_p is density of projectile material, V_s is striking velocity, and σ_t is yield strength of the steel plate material. Figure 5-4 applies for the test length-to-diameter ratio, ℓ/d = 31.1.

In using the empirically-fitted curves in Figures 5-2, 5-3 and 5-4, the reader is cautioned to avoid extrapolation. Equation 5-9 should also be limited to the ranges:

$$5 \leq \ell/d \leq 40$$
$$0.042 \leq h/d \leq 0.1 \qquad (5\text{-}10)$$

Example 1:

A flat-ended cylindrical steel rod, with a mass M of 8 kg and diameter d of 75 mm impacts a thick concrete wall with compressive strength f'_c = 26 MPa at a striking velocity V_s = 600 m/s. What is the penetration depth x, perforation thickness e, and scabbing thickness s?

Step 1. Calculate K from Equation 5-3.

$$K = 1.134/(26 \times 10^6)^{1/2} = 2.224 \times 10^{-4}\ m^{2.8}\ kg$$

Step 2. Chose projectile nose shape factor N. This is 0.72 for the flat nose shape.

Step 3. Calculate caliber density D from its definition.

$$D = M/d^3 = 8/(0.075)^3 = 1.896 \times 10^4\ kg/m^3$$

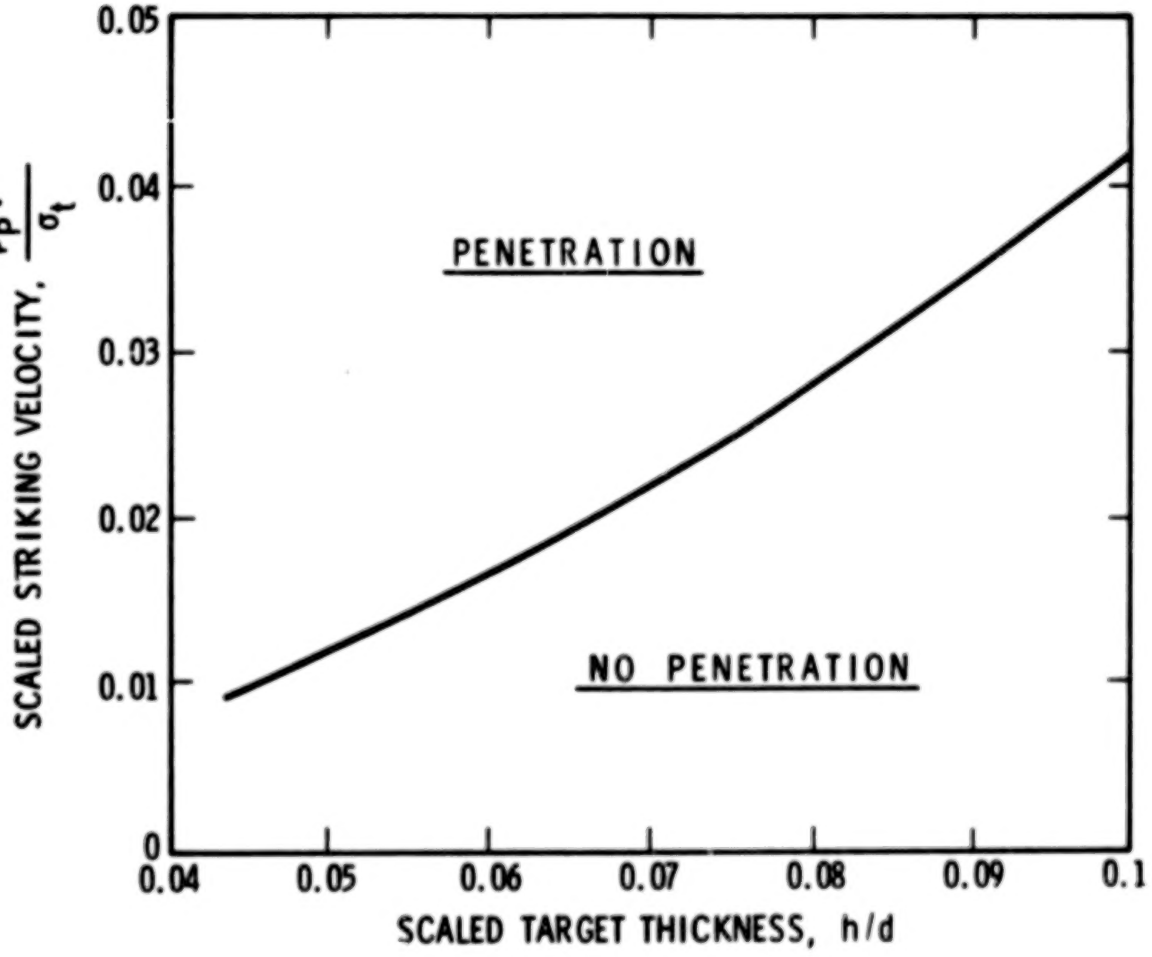

FIGURE 5-4. PREDICTION OF PENETRATION THRESHOLD FOR STEEL PANELS IMPACTED BY WOODEN PROJECTILES WITH $\ell/d = 31.1$

Step 4. Substitute in Equation (5-1) and calculate G.

$$G = 2.224 \times 10^{-4} \times 0.72 \times 0.075^{0.2} \times 1.896 \times 10^{4} \left(\frac{600}{304.7}\right)^{1.8}$$

$$G = \underline{6.124}$$

Step 5. Use Equation (5-2) to calculate penetration x. Assume that (x/2d) > 2.0. Then, (x/d) = 1 + G = 1 + 6.124 = 7.124.

$$x = 7.124\ d = 7.124 \times 75 = \underline{534\ mm} = \underline{0.534\ m}$$

Step 6. Use Equation (5-4) to calculate e.

$$e = 75\ [1.32 + 1.24 \times \frac{534}{75}] = \underline{762\ mm} = \underline{0.762\ m}$$

Step 7. Use Equation (5-5) to calculate s.

$$S = 75\ [2.12 + 1.36 \times \frac{534}{75}] = \underline{886\ mm} = \underline{0.886\ m}$$

Example 2:

A steel rod of diameter d = 25 mm with a mass M = 10 kg impacts a heavily reinforced concrete wall which has a thickness h = 100 mm with an impact velocity v = 60 m/s. Will the wall scab?

Step 1. Calculate impact kinetic energy.

$$KE = (\frac{1}{2})MV^2 = \frac{1}{2} \times 10 \times 60^2 = 18kJ$$

Step 2. Calculate scaled kinetic energy.

$$\frac{KE}{h^3} = \frac{18 \times 10^3}{0.1^3} = 18\ MPa$$

and scaled target thickness

$$\frac{h}{d} = \frac{100}{25} = 4$$

Step 3. Enter Figure 5-3, and plot intercept from Step 2. This lies well <u>above</u> the threshold curve for heavy reinforcing, so scabbing <u>should</u> occur.

Example 3:

A long steel pipe with d = 75 mm, t_w = 3.0 mm impacts a 100 mm reinforced concrete panel at 20 m/s. It has a mass of 10 kg. Will it cause scabbing?

Step 1. Calculate impact kinetic energy.

$$KE = \frac{1}{2} \times 10 \times 20^2 = 2 \text{ kJ}$$

Step 2. Calculate scaled kinetic energy, and scaled target thickness, scaled wall thickness

$$\frac{KE}{h^3} = \frac{2 \times 10^3}{0.1^3} = 2 \text{ MPa}$$

$$\frac{h}{d} = \frac{75}{100} = 0.750$$

$$\frac{2t_w}{d} = \frac{2 \times 3}{75} = 0.08$$

Step 3. Enter Figure 5-2. In this case, our intercept lies along the bottom line and somewhat to the left of the curves. We wish to compare to the middle curve, for which scaled wall thickness is 0.08. We cannot say unequivocally whether scabbing will or will not occur, because we are beyond the range of the fitted curves.

Example 4:

A wooden post is hurled against a steel curtain wall at 100 m/s. The post has a diameter d = 150 mm, a length ℓ = 4.5 m, and a density ρ_p = 650 kg/m^3. The steel curtain wall is 6 mm thick and has a yield strength σ_t = 240 MPa. Will the post penetrate?

Step 1. Calculate scaled quantities to enter Equation (5-9).

$$\frac{h}{d} = \frac{6}{150} = 0.04$$

$$\frac{\ell}{d} = \frac{4500}{150} = 30$$

Step 2. Calculate scaled striking velocity from Equation (5-9) for incipient penetration.

$$\frac{\rho_p V_s^2}{\sigma_t} = \frac{1.751 \times 0.040}{30} + \frac{144.2 \times 0.04^2}{30}$$

$$\frac{\rho_p V_s^2}{\sigma_t} = \underline{\underline{1.00 \times 10^{-2}}}$$

Step 3. Calculate scaled striking velocity from input parameters, and compare to threshold value.

$$\frac{\rho_p V_s^2}{\sigma_t} = \frac{650 \times 100^2}{240 \times 10^6} = \underline{\underline{2.71 \times 10^{-2}}}$$

This value is more than double the threshold for penetration, so the wood post goes through the steel curtain wall like a knife through hot butter.

5-3 Effects of Barricades on Blast Waves

Barricades are constructed either near potential explosion sources or near structures and facilities located in the vicinity of potential explosion sources. As noted earlier, they are intended as protective devices to arrest fragments or attenuate blast waves.

The two most common types of barricades are earthworks (mounds), and earthworks behind retaining walls (single-revetted barricades). The definitions of these types of barricades, taken from Department of Defense explosive safety regulations, follow:

> Mound. An elevation of earth having a crest at least 3 feet wide, with the earth at the natural slope on each side and with such elevation that any straight line drawn from the top of the side wall of a magazine or operating building or the top of a stack containing explosives to any part of a magazine, operating building or stack to be protected will pass through the mound. The toe of the mound shall be located as near the magazine, operating building, or stack as practicable.
>
> Single-Revetted Barricade. A mound which has been modified by a retaining wall, preferably of concrete, of such slope and thickness as to hold firmly in place the 3-feet width of earth required for the top, with

the earth at the natural angle on one side. All other requirements of a mound shall be applicable to the single-revetted barricades.

Most of the useful data on attenuation of blast effects behind barricades appear in a single reference, Wenzel and Bessey (1969). Scaled tests for both mound and single-revetted barricades, with spherical Pentolite explosion sources generating the blast waves, were conducted for the explosion sources near the barricades (near field) and near the protected structure (far field). Specific configurations tested are shown in Figure 5-5. All explosive spheres were located at scaled height $\bar{H} = 0.036$ above an armor plate reflecting surface to eliminate cratering effects, at the scaled distances $\bar{R}$ shown in Figure 5-5.* The barricade dimensions were scaled to represent full-size barricades with heights h of about 3 m and 6 m.

The principal conclusions reached by Wenzel and Bessey (1969) as a result of their tests were:

1) Barricades do reduce the peak pressures and impulses immediately behind the barricades.

2) Single-revetted barricades are more efficient in reducing peak pressures and impulses than mound barricades.

3) Values of peak pressure and impulse are greatly influenced by the gage height relative to the ground, the location of the barricade, and the barricade dimensions and configurations.

4) In the near field case for single-revetted barricade configurations, a significant reduction of pressure and impulse was observed out to scaled distances of $\bar{R} = 1$. Beyond that distance, the peak pressures tend to approach those of the free field case very rapidly, and the impulses also tend to approach those of the free field case but not as rapidly as the peak pressures. The times of arrival in specific locations are greater than those of the free field case up to scaled distances of $\bar{R} = 1.6$. At scaled distances greater than $\bar{R} = 1.6$ they approach rapidly those of the free field case.

---

*Definitions for scaled distance are given in Chapter II.

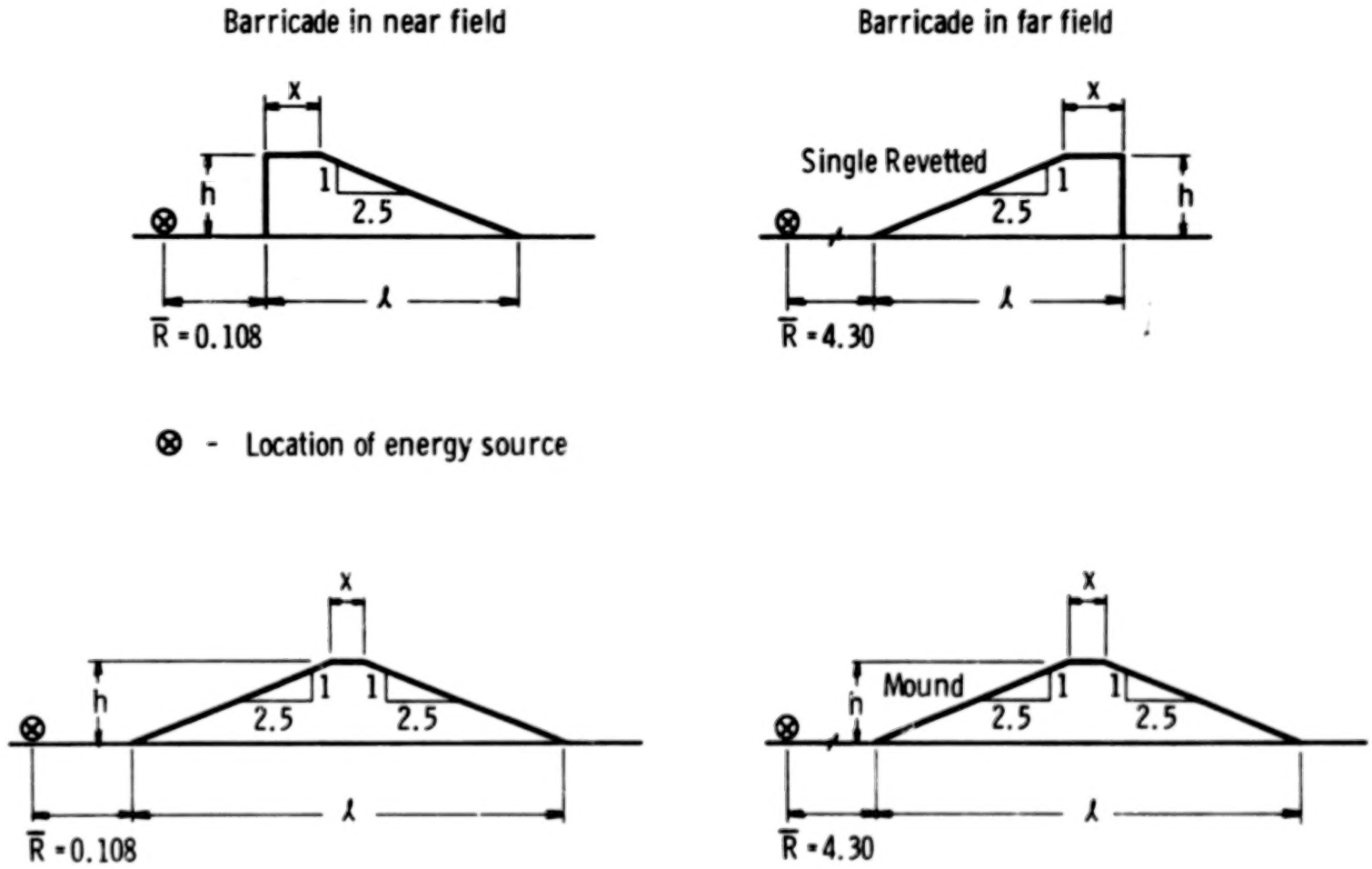

FIGURE 5-5. BARRICADE CONFIGURATIONS STUDIED BY WENZEL & BESSEY (1969)

5) In the near field case, mound configuration, the peak pressures and impulses are not greatly reduced, and actually are increased over the free field case at a scaled gage height of $\bar{H}_g = 0.02$ and a scaled distance of $\bar{R} = 0.43$. However, the pressure and impulse observed at the scaled gage height of $\bar{H}_g = 0.05$ at $\bar{R} = 0.32$ are both less than the free field values. There was a considerable decrease in pressure and impulse for the gage located at $\bar{R} = 4.84$ and scaled height of $\bar{H}_g = 0.016$, respectively. The times of arrival were the same as those observed in the free field case for all scaled distances and scaled heights.

6) For the far field case, single-revetted barricade configuration, the peak pressures and impulses were significantly reduced immediately behind the barricade; however, their individual values varied as a function of gage height. The times of shock arrival were the same as those observed in the free field case for all stations measured.

7) For the far field case, mound configuration, the same observations as those made for the single-revetted case can be made here except that the effect of the barricades is considerably less than for the single-revetted configurations.

The blast attenuation caused by mound barricades, although measurable in the experiments cited above, is small enough to be essentially negligible, for the purposes of this workbook. Similarly, the attenuation for single-revetted barricades in the far-field case is so localized and directional that no general predictions can be made. But, for the single-revetted barricades in the near field, we can give scaled curves for blast wave properties which are attenuated from surface burst explosion waves without barricades. Figure 5-6 shows variation of scaled side-on overpressure $\bar{P}_s$ with scaled distance $\bar{R}$ for this configuration, for surface burst explosive charges without barricade and with single-revetted barricade. Similarly Figure 5-7 gives variation of scaled side-on pressures $\bar{I}_s$ versus $\bar{R}$ for this situation.

These curves should only be used to predict blast attenuations over the ranges of scaled distances shown, i.e., $0.35 \leq \bar{R} \leq 9.0$. They should also be applied with caution for blast sources other than condensed explosives because there are no extant data for effects of barricades on the non-ideal blast waves from accidental explosions. Data scatter for the peak overpressure curves is about $\pm 5\%$, and for the impulse curves, about $\pm 10\%$.

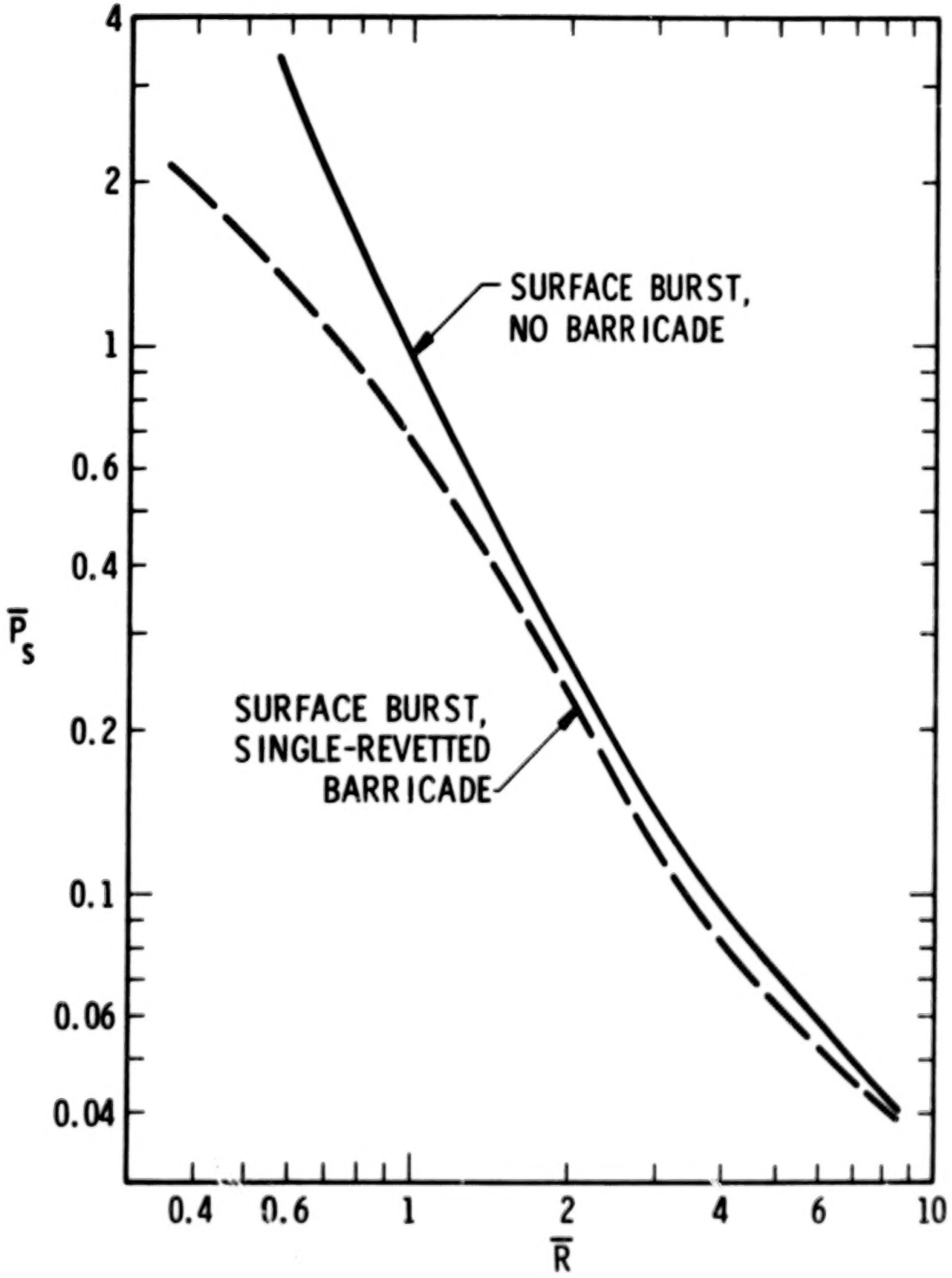

FIGURE 5-6. EFFECT OF NEAR-FIELD, SINGLE-REVETTED BARRICADE ON PEAK OVERPRESSURE

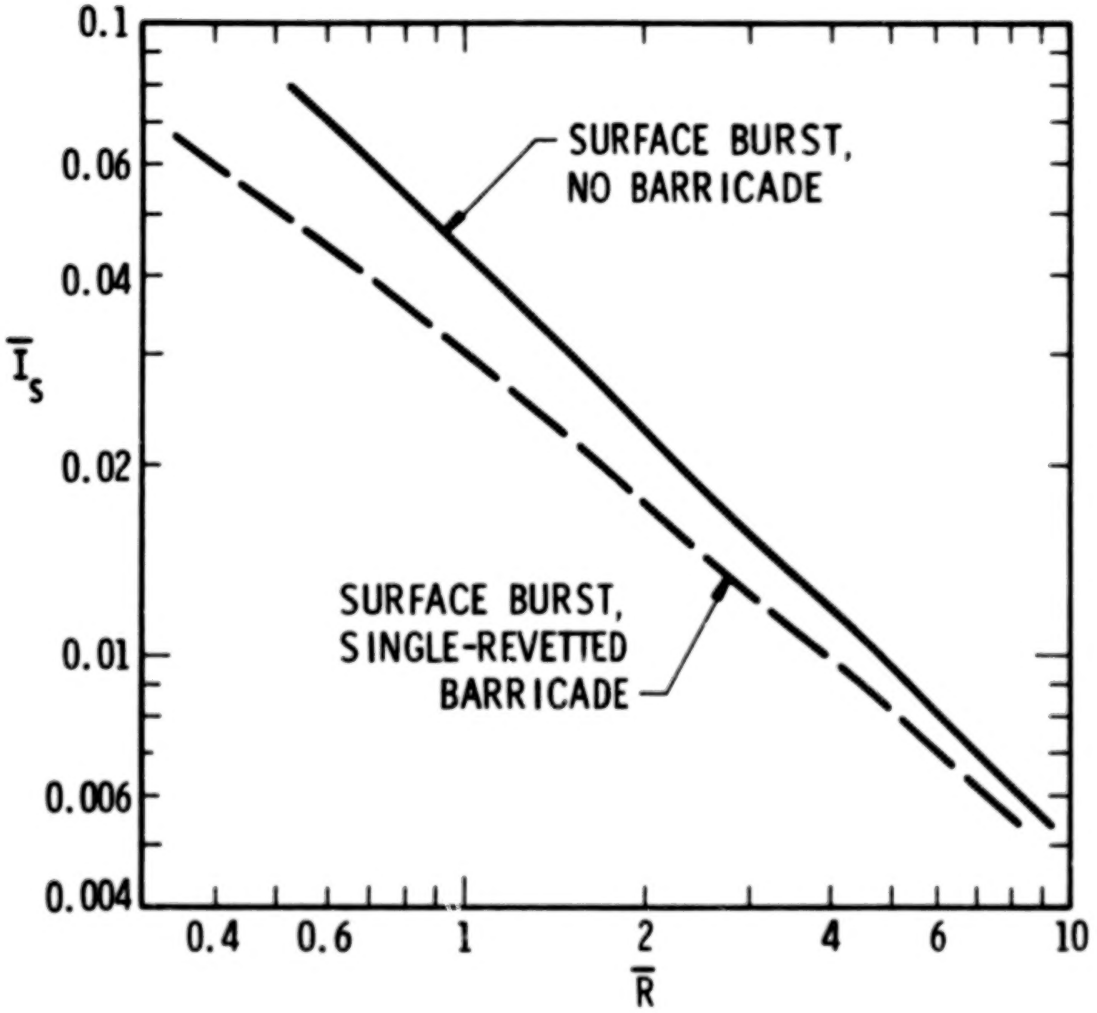

FIGURE 5-7. EFFECT OF NEAR-FIELD, SINGLE-REVETTED BARRICADE ON SIDE-ON IMPULSE

Example Problem

A single-revetted barricade is located close to a propellant storage source with potential blast energy E = 1000MJ, calculated by methods given in Chapter I. If the source explodes, what are the incident blast wave parameters at a distance of 100 m? The site is located near sea level, with $p_o = 1.01 \times 10^5$ Pa and a_o = 340 m/s.

Step 1. Calculate scaled distance $\bar{R}$. It is defined as (see Chapter II).

$$\bar{R} = R\, p_o^{1/3}/E^{1/3}$$

$$\bar{R} = \frac{100 \times (1.01 \times 10^5)^{1/3}}{(10^9)^{1/3}} = \underline{4.66}$$

Step 2. Enter Figures 5-6 and 5-7 to obtain scaled overpressure and impulse. From dashed curves,

$$\bar{P}_s = 0.070,\ \bar{I}_s = 0.0087$$

Step 3. "Unscale" to obtain blast parameters.

$$P_s = \bar{P}_s \times p_o = 0.070 \times 1.01 \times 10^5 = \underline{7.07\ \text{kPa}}$$

$$I_s = \frac{\bar{I}_s \times p_o^{2/3} \times E^{1/3}}{a_o} = \frac{0.0087 \times (1.01 \times 10^5)^{2/3} \times (10^9)^{1/3}}{340}$$

$$I_s = \underline{55.5\ \text{Pa}\cdot\text{s}}$$

REFERENCES, CHAPTER V

1. Baker, W. E., Hokanson, J. C. and Cervantes, R. A., (1976) "Model Tests of Industrial Missiles", Final Report, SwRI Project No. 02-9153-001, Southwest Research Institute, San Antonio, Texas, May 1976.

2. Baker, W. E., Kulesz, J. J., Ricker, R. E., Bessey, R. L., Westine, P. S., Parr, V. B., and Oldham, G. A., (1975) "Workbook for Predicting Pressure Wave and Fragment Effects of Exploding Propellant Tanks and Gas Storage Vessels", NASA CR-134906, Contract NAS3-19231, November 1975 (reprinted 1977).

3. Beth, R. A. , (1945) "Concrete Penetration", OSRD-4856, National Defense Research Committee Report, A-319, March 1945.

4. Degen, P., Furrer, H., and Jemielewski, J., (1976) "Structural Analysis and Design of a Nuclear Power Plant Building for Aircraft Crash Effects", Nuclear Engineering and Design, 37, 1976, pp. 249-268.

5. Drittler, K. and Gruner, P., (1976a) "Calculations of the Total Force Acting Upon a Rigid Wall by Projectiles", Nuclear Engineering and Design, 37, 1976, pp. 231-244.

6. Drittler, K. and Gruner, P., (1976b) "The Force Resulting from Impact of Fast-Flying Military Aircraft Upon a Rigid Wall", Nuclear Engineering and Design, 37, 1976, pp. 245-248.

7. Hammel, J., (1976) "Aircraft Impact on a Spherical Shell", Nuclear Engineering and Design, 37, 1976, pp. 205-223.

8. Kennedy, R. P., (1976) "A Review of Procedures for the Analysis of Design of Concrete Structures to Resist Missile Impact Effects", Nuclear Engineering and Design, 37, 1976, p. 183-203.

9. Peterson, R. E., Editor, (1976), Proceedings of the Symposium on Tornadoes. Assessment of Knowledge and Implications for Man, Texas Technological University, Lubbock, Texas, June 22-24, 1976.

10. Wenzel, A. B. and Bessey, R. L., (1969) "Barricaded and Unbarricaded Blast Measurements", Final Report Contract No. DAHC04-69-C-0028, Subcontract 1-OU-431, Southwest Research Institute, San Antonio, Texas, October 1969.

CHAPTER VI

DISCUSSION AND RECOMMENDATIONS

We believe that this workbook should be a definite aid to designers and safety engineers in predicting damage and hazards from accidental explosions in ground handling systems. It should prove to be a useful adjunct to our earlier workbook for predicting explosion hazards in flight systems, NASA CR-134906. For the convenience of the reader, microfiche copies of the earlier work are attached to each copy of this report.

Parts of this work should have wider application than indicated by the title. The additional methods for rapid structural damage prediction can be used for any blast source, provided the peak overpressures and positive impulses can be predicted. The computer programs and methods for prediction of velocities and trajectories of lifting fragments and thrusting burst vessels can be effectively applied to transportation accidents with tank cars and tank trucks containing many types of pressurized fluids, in addition to rocket propellants. The methods for estimating explosive energy release for flash-evaporating fluids can be used to predict severity of boiler explosions, or severity of blast for any type of liquid and gas mixture stored under high pressure. The data and prediction methods for effects of impact of massive fragments or missiles are not limited to fragments generated by accidental explosions in ground handling systems, and indeed were taken from other related studies.

A number of prediction waves are given in this work for the characteristics of blast waves from bursting gas pressure vessels, and some for bursting vapor spheres. These waves exhibit some characteristics which are distinctly different from blasts from condensed explosives such as TNT, including pronounced negative phases and pronounced second shocks. Most structural response or damage analyses account only for pressures and impulses in the first positive phase, and we therefore recommend further study of responses to waves with characteristics such as in Figure 2-8. It would also be very desirable to conduct more scaled experiments with bursting, pressurized vessels, to generate additional blast prediction curves. These should probably include:

1) Tests with light gases such as helium.

2) Tests of bursting spheres filled with vapors of higher saturation pressure such as Freon-22, Freon-13, or sulfur hexafluoride (SF_6) to better determine the effect of sphere pressure on the overpressures measured.

3) Tests using the same fluids as above but in liquid form just above saturation pressure at room temperature.

4) Tests using flash-evaporating fluids in liquid form at a high-pressure heated above room temperature to just below the saturation temperature.

Concurrent with the continuation of study of the character of blast waves from accidental explosions, one should also review, and alter if necessary, the prediction methods for structural response and damage in this workbook, in NASA CR-134906, and related references which assume that the wave can be described as a simple, single pulse. The basic analytic tools to do this are readily available, but application to as complex a loading pulse as Figure 2-8 will require careful application of these techniques, and almost invariably, some increase in complexity of response prediction.

For reasons of economy, this workbook, unlike NASA CR-134906, contains no assessment of accident scenarios for typical situations which have occurred or could occur in ground transport or storage of liquid propellants and compressed gases. A supplement containing evaluations and predictions of blast and fragment effects for a number of cases, should prove useful and instructive to safety engineers.

Several related and potential problems with potentially explosive ground storage and transport systems could perhaps be addressed in following studies. One question concerns planning of in-service testing of pressure storage vessels to avoid or prevent accidental explosions. Many new and effective nondestructive testing methods and equipment have been developed in recent years, and applied in industries such as the nuclear power industry. For storage vessels of large volume and/or high pressure, where the hazards are great in the event of vessel failure, the frequency or thoroughness of such testing might be increased.

This workbook includes a number of prediction methods for fragment and missile impact conditions and locations near explosions, and some relatively new data and prediction curves for effects of impacts of relatively massive missiles. There is still a serious lack of data on massive missile impact effects. Scale model techniques have proven to be efficient in gathering enough data rapidly and relatively inexpensively to generate impact effects curves (see Figures 5-2 through 5-4), but most of the classes of missiles expected in accidental explosions have not been tested against industrial or residential "targets". We would certainly recommend a carefully planned model test program to fill this gap.

Looking into the future, we can perhaps anticipate an increasing shift to a hydrogen fuel economy. If this occurs, large volumes of hydrogen must be stored either as a compressed gas or as a cryogenic liquid near distribution points. As an aircraft fuel, the hydrogen would most probably be used as a cryogenic liquid, which would necessitate large volume storage near airports. Can this be done safely? A thorough safety study would have to precede any serious plans for such a change, with workbooks like this report providing part of the input to assess the hazards.

APPENDIX A

Calculations of Blast Wave Properties for Pressure Vessel Bursts

The method for predicting the overpressure and specific impulse from the burst of a thick-walled pressure vessel is the result of the following analysis.

TUTTI [Gentry, et al (1966)],a two dimensional finite difference computer program for compressible fluids, was used to calculate the axisymmetric flowfield surrounding a quadrant of a bursting pressure vessel. The geometry is shown in Figure A-1. During the calculation, the quadrant of the vessel moves along the axis of symmetry at a prescribed velocity. The velocity and position of the vessel are calculated by a computer program called FRAG [see Baker, et al (1975)]. These are supplied to TUTTI. (TUTTI was modified to allow a moving solid boundary.)

Six sets of initial conditions were used (Table A-1), with $T_1/T_a = 1$ for all of them. The radius of the sphere is 0.19 m. Increments $\Delta r = 0.0375$ m, and $\Delta z = 0.0300$ m were chosen for the flowfield. The rather large Δr and Δz cause the shocks to be spread out, and some accuracy is lost, but this is necessary for economy.

$\bar{P}_s$ vs. $\bar{R}$ is plotted for these computer runs in Figure A-2. $\bar{I}$ vs. $\bar{R}$ is plotted in Figure A-3.

Figure A-2 was used to derive the overpressure prediction method in the text. The point at the end of the dashed line is $(\bar{P}_{so}, \bar{R}_o)$, where $\bar{P}_{so}$* is defined in the text and $\bar{R}_o$ is $\bar{R}$ corresponding to the edge of the sphere. The solid lines show the overpressure behavior after a shock has formed. On the dashed portion of the curves, a shock has not formed yet. Connecting the points of transition to a shock in Figure A-2 gives Curve A in Figure 2-5. It is observed that, for these bursts, the overpressure on curve A, $\bar{P}_a$, is related to $\bar{P}_{so}$ by $\bar{P}_a = 0.21\ \bar{P}_{so}$. This permits the location of a starting point for $\bar{P}_s$ vs. $\bar{R}$ behavior. A family of $\bar{P}_s$ vs. $\bar{R}$ curves has been drawn on Figure 2-5. Once the starting point has been found, the nearest curve(s) can be followed.

As was true for the one-dimensional study in Baker, et al (1975), the $\bar{I}$ vs. $\bar{R}$ behavior is not clear, and the pentolite curve

---

*$\bar{P}_{so}$ is calculated by assuming constant pressure across the contact surface between the stored gas and the atmosphere immediately after the vessel burst. See Baker, et al (1975).

has been extrapolated to small $\bar{R}$ to provide a conservative estimate for $\bar{I}$.

The computer outputs from TUTTI also show the highly directional nature of the blast field close to the bursting sphere. Figs. A-4 and A-5 are indicative of this directionality. The printed output also gives some indication of variation of overpressure along other radial lines from the center in addition to along the plane of symmetry; in particular, along the lines $\theta = 30°$ and $\theta = 60°$. But, the limitations of cell size and computer capability precluded complete mapping along these lines.

TABLE A-1. INITIAL CONDITIONS FOR PRESSURE VESSEL BURSTS

Run Number	Gas	$\frac{P_1}{P_a}$	γ_1
1	air	987.2	1.4
2	H_2	987.2	1.4
3	He	987.2	1.667
5	CO_2	987.2	1.225
7	air	98.72	1.4
9	CO_2	14.81	1.225

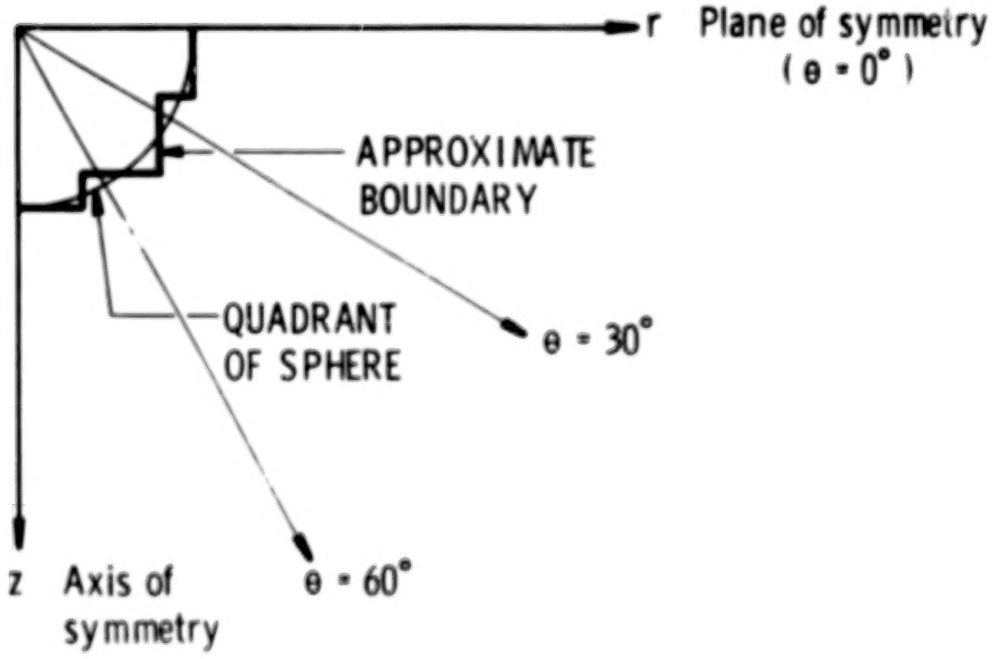

FIGURE A-1. QUADRANT OF FLOWFIELD FOR BURSTING PRESSURE VESSEL

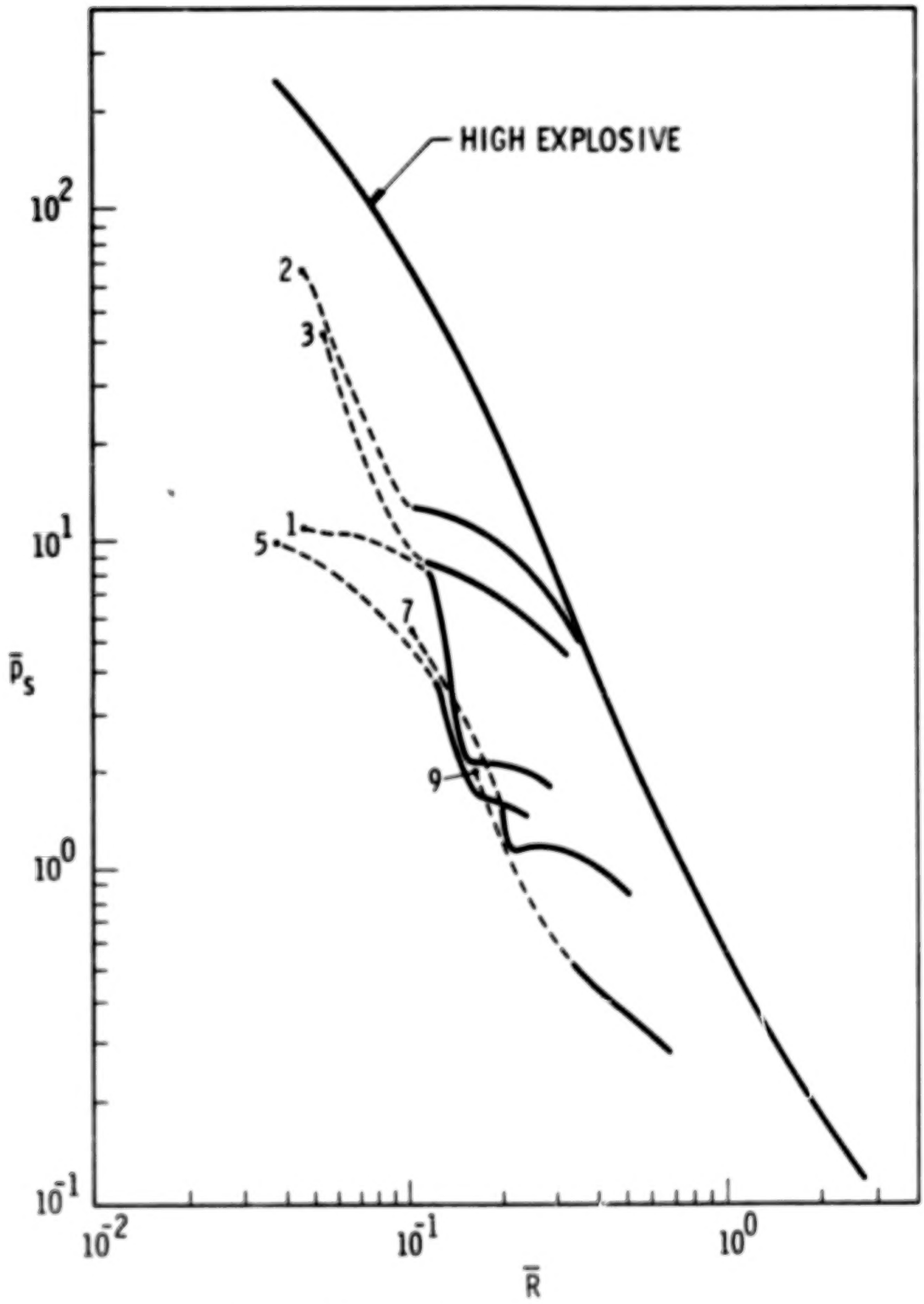

FIGURE A-2. $\bar{P}_s$ VS $\bar{R}$ FOR BURSTING PRESSURE VESSELS ALONG PLANE OF SYMMETRY

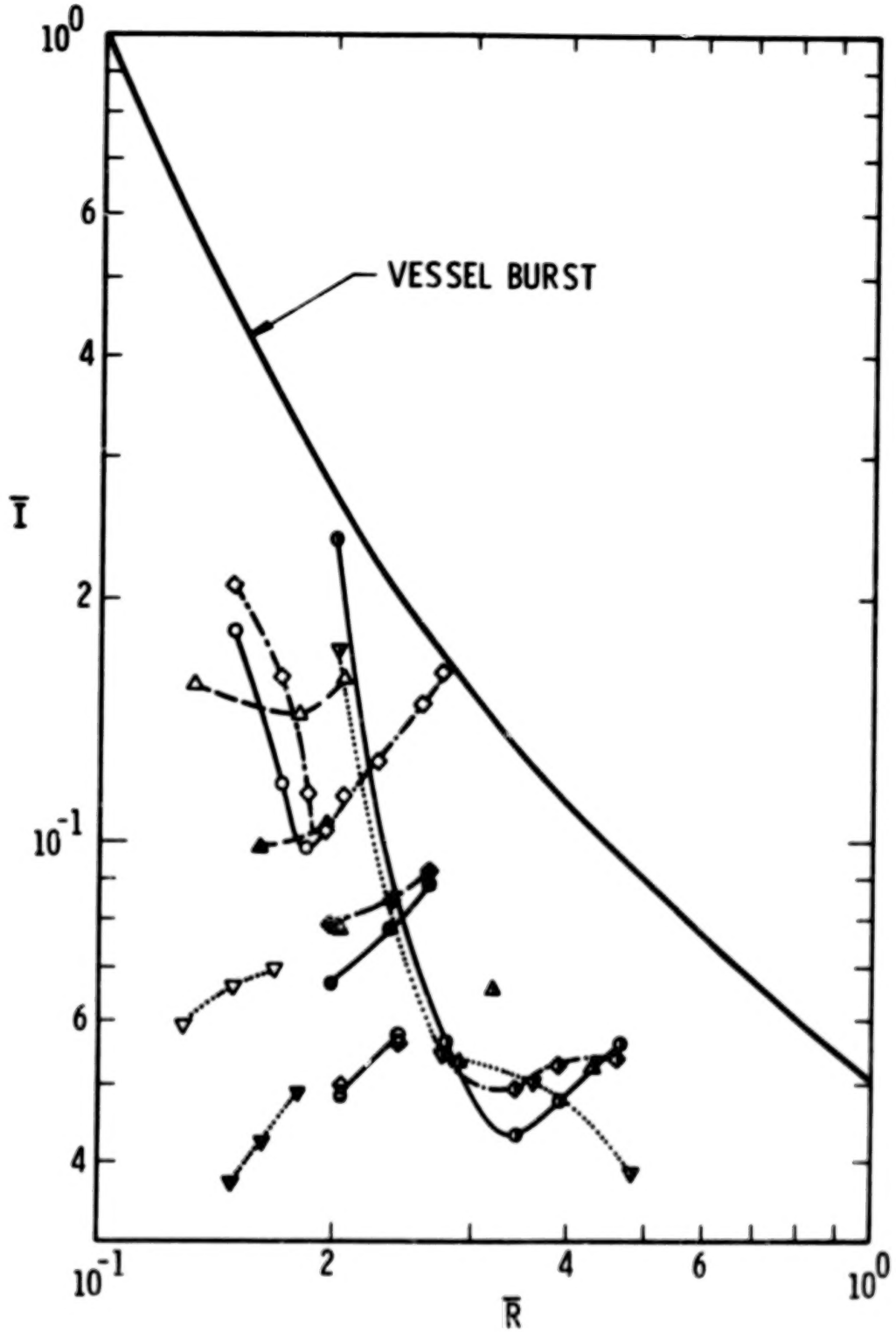

FIGURE A-3. $\bar{I}$ VS $\bar{R}$ FOR BURSTING PRESSURE VESSELS

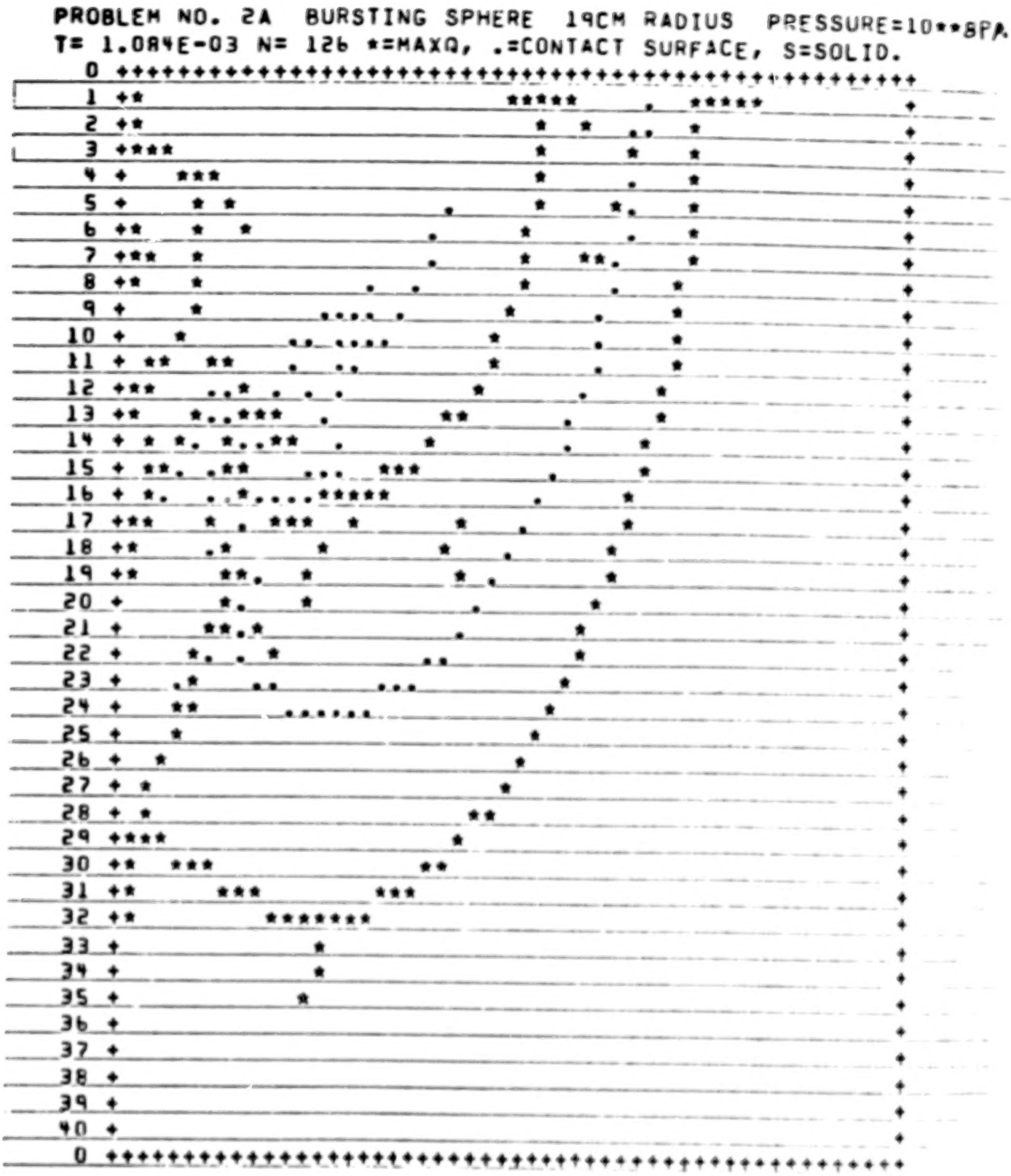

FIGURE A-4. SAMPLE PLOT FROM TUTTI FOR SPHERE BURSTING AS TWO HEMISPHERES

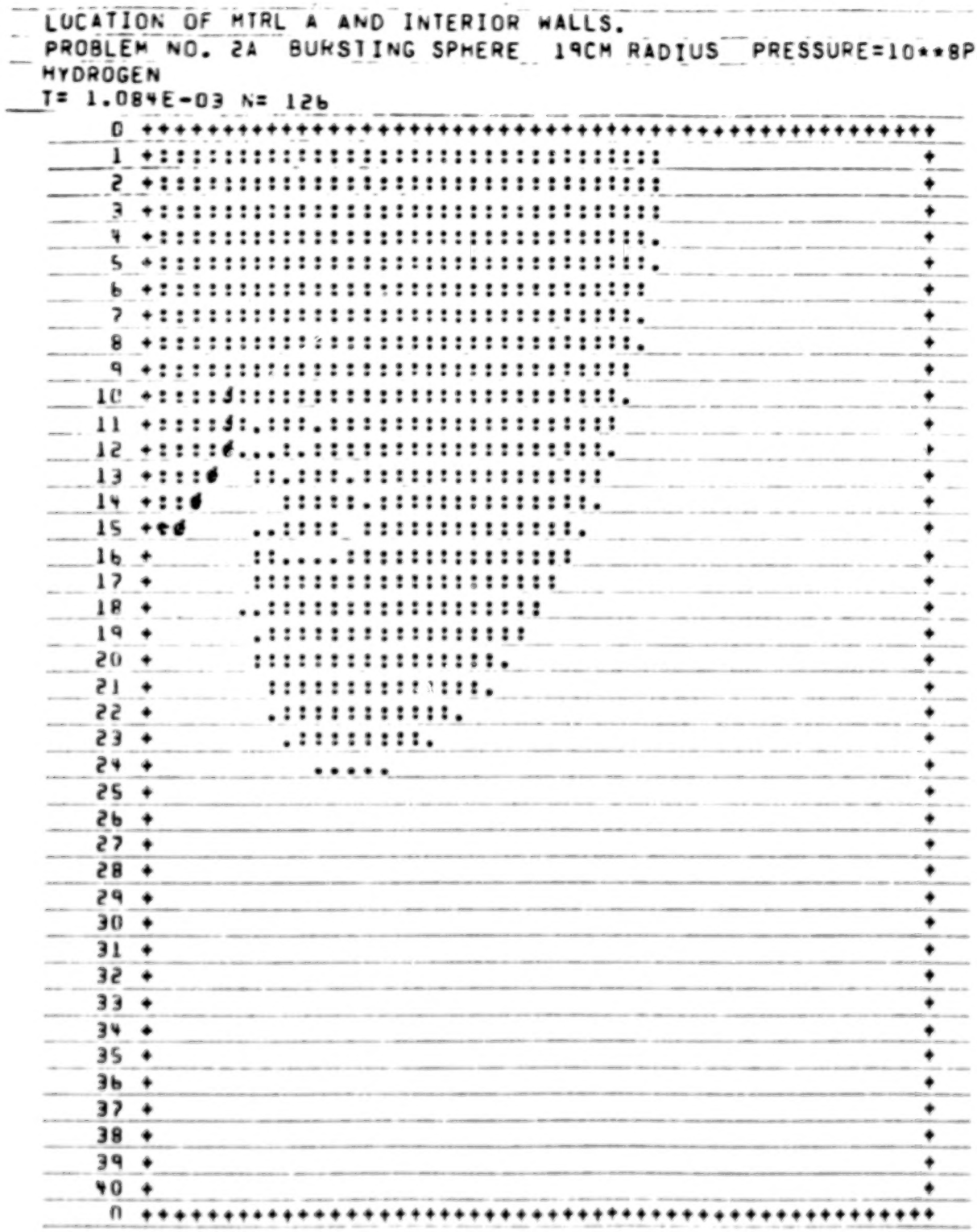

FIGURE A-5. SAMPLE PLOT FROM TUTTI FOR SPHERE BURSTING AS TWO HEMISPHERES

APPENDIX B

Development of Additional Prediction Methods for Structural Response to Blast Wave Loading

The elastic and elastic-plastic beam solutions which are presented in Figures 3-1 and 3-2 were derived using conservation of energy principles. To illustrate how these relationships can be derived, we will compute Figure 3-2 for an elastic, simply-supported beam. A deformed shape must be assumed in beam and plate like structures. Assuming a deformed shape which corresponds to the static deformed shape for a beam undergoing uniform loads gives:

$$Y = \frac{16}{5} w_o \left[\frac{x}{\ell} - 2\left(\frac{x}{\ell}\right)^3 + \left(\frac{x}{\ell}\right)^4\right] \qquad \text{(B-1)}$$

This deformed shape is then differentiated twice with respect to x so that the elastic bending moment M can be obtained from $M = -EI\frac{d^2y}{dx^2}$. This procedure gives for the bending moment

$$M = \frac{192}{5} \frac{EIw_o}{2} \left[\left(\frac{w}{\ell}\right) - \left(\frac{w}{\ell}\right)^2\right] \qquad \text{(B-2)}$$

The strain energy S.E. stored in a deformed beam can then be determined by substitution into $S.E. = \int_o^\ell \frac{M^2 dx}{2EI}$. Substitution gives:

$$SE = \frac{(192)^2 EIw_o^2}{(50)\ell^4} \int_o^\ell \left[\left(\frac{x}{\ell}\right)^2 - 2\left(\frac{x}{\ell}\right)^3 + \left(\frac{x}{\ell}\right)^4\right] dx \qquad \text{(B-3)}$$

Or after completing the integration

$$SE = 24.576 \frac{EIw_o^2}{\ell^3} \qquad \text{(B-4)}$$

The asymptote which is impulse dependent is determined by equating the kinetic energy KE to the strain energy. The kinetic energy is given by:

$$KE = (1/2)m V_o^2 = \frac{I^2}{2m} \qquad \text{(B-5)}$$

Substituting $\rho A\ell$ for m and $ib\ell$ for I gives:

$$KE = \frac{i^2 b^2 \ell}{2\rho A} \tag{B-6}$$

Equating U to KE gives the impulsive loading realm asymptote

$$\frac{i^2 b^2 \ell}{2\rho A} = 24.576 \frac{EI\, w_o^2}{\ell^3} \tag{B-7}$$

Equation (B-7) relates applied impulse to deformation. To relate impulse to bending stress we must use the moment-curvature relationships. The maximum moment as given by Equation (B-2) occurs at $x/\ell = 1/2$. The maximum moment is then given by:

$$M_{max} = \frac{192}{20} \frac{EI\, w_o}{\ell^2} \tag{B-8}$$

Substituting $\sigma_{max} = \frac{M_{max}\, H/2}{I}$ and solving for $\frac{w_o}{\ell}$ gives:

$$\frac{w_o}{\ell} = \frac{5}{24} \frac{\sigma_{max}\, \ell}{E\, H} \tag{B-9}$$

Finally, taking the square root of Equation (B-7) and substituting Equation (B-9) into Equation (B-7) to eliminate w_o gives the asymptote for the impulsive loading realm in terms of the maximum bending stress.

$$\frac{ibH}{\sqrt{\rho EIA}} = 1.461 \frac{\sigma_{max}}{E} \tag{B-10}$$

Equation (B-10) is the impulsive loading realm asymptote plotted in Figure 3-2. The numerical coefficient 1.461 in Equation (B-10) is the α_i coefficient for a simply-supported beam. In Equation (B-9), the number 5/24 is the C_w coefficient in Figure 3-2 to relate stress to deformations in a simply-supported beam.

The quasi-static asymptote in Figure 3-2 is computed by calculating the maximum possible work WK and equating this quantity to the strain energy. This quantity equals:

$$Wk = \int_0^{\ell} pb(dx)Y \tag{B-11}$$

After substituting Equation (B-1) for Y:

$$Wk = \frac{16}{5} pbw_o \int_o^{\ell} \left[\frac{x}{\ell} - 2\left(\frac{x}{\ell}\right)^3 + \left(\frac{x}{\ell}\right)^4\right] dx \qquad (B\text{-}12)$$

Or after integrating:

$$Wk = \frac{16}{25} pb\ell\ w_o$$

The strain energy has already been calculated as Equation (B-4). Equating S.E. to Wk gives the quasi-static loading realm asymptote.

$$\frac{16}{25} pb\ell\ w_o = 24.576 \frac{EI\ w_o^2}{\ell^3} \qquad (B\text{-}13)$$

Equation (B-13) relates applied pressure to deformation. To relate pressure to bending stress, we substitute Equation (B-9) for w_o and algebraically rearrange terms to obtain:

$$\frac{pbH\ell^2}{EI} = 8.0\ (\sigma/E) \qquad (B\text{-}14)$$

Equation (B-14) is the quasi-static loading realm asymptote plotted in Figure 3-2. The numerical coefficient 8.0 in Equation (B-14) is the α_p coefficient for a simply-supported beam. The coefficient C_v relating maximum bending stress to the maximum shear force is obtained by differentiating the moment equation, Equation (B-2), with respect to x to obtain the shear force V with respect to deformation w_o.

$$V = \frac{dM}{dx} = \frac{192}{5} \frac{EI\ w_o}{\ell^3} \left[1 - \frac{2x}{\ell}\right] \qquad (B\text{-}15)$$

The maximum shear occurs at x = 0 or x = ℓ. Setting x = 0 and substituting Equation (B-9) for w_o gives:

$$V_{max} = 8.0 \frac{\sigma_{max}\ I}{\ell H} \qquad (B\text{-}16)$$

Equation (B-16) is the shear equation presented in Figure 3-2. The numerical value of 8.0 in Equation (B-16) is the C_v coefficient for a simply-supported beam.

The intermediate transition was faired in using a hyperbolic tangent squared relationship which from our practical experience seems to fit quite well. Note that for small values

$$SE = Wk \tanh^2 \left[\frac{KE}{Wk}\right]^{1/2} \qquad \text{(B-17)}$$

of the argument, the tanh equals its argument and we obtain the impulsive loading realm asymptote from SE = KE. For large arguments the tanh equals 1.0, and we obtain the quasi-static loading realm asymptote from SE = Wk.

This approach, within the bounds of a Bernoulli-Euler, small deformation, beam solution, gives exact answers for both strain and deformation in the quasi-static loading realm. These "exact" answers occur because the deformed shape is correct in this domain. In the impulsive loading realm only approximate answers are given because the deformed shape is not quite right; however, the results are sufficiently accurate, especially when one realizes the uncertainties associated with the load. More accurate answers are obtained if a more accurate deformed shape is assumed. Actually the interrelationship of one variable with another remains the same irrespective of the assumed deformed shape. The only effect of using other deformed shapes is to slightly modify the numerical coefficients α_i, α_p, C_v, and C_w.

To compute the p-i diagram for cantilever, clamped-clamped, clamped-pinned, or beams with any other boundary condition, the same procedure can be followed. If the assumed deformed shape corresponds even approximately to a beam with the correct boundary conditions, then fairly accurate answers will result. The only difference in the solutions of beams with different boundary conditions is that different numerical values arise in the α_i, α_p, C_v, and C_w coefficients.

At this stage we will not compute the p-i diagram for the elastic-plastic beams as complex integrations are involved which must be performed on a computer. Response of a rigid-plastic beam can, however, be determined using hand calculations. The only differences are that after an assumed deformed shape is assumed and the curvature is obtained by differentiation, the strain energy is determined by integrating the plastic yield moment times the curvature over the entire span of the beam. The procedure of then equating strain energy to kinetic energy to obtain the impulsive-loading realm asymptote, and strain energy to work for the quasi-static asymptote remains the same. The deformations obtained from such a rigid-plastic analysis are residual permanent deformations and strains. In the elastic analysis, maximum deformations and strains are estimated.

Several observations should be noted from these numerical calculations. In the impulsive loading realm, maximum bending stress is independent of span ℓ. This conclusion is mathematically correct. It is caused by span entering the strain energy

and kinetic energy expressions to the same power, so that it cancels. In the impulsive loading realm, the response depends only on the impulse or area under the applied pressure time history. In the quasi-static loading realm, response is independent of beam density and duration of the loading.

To derive the graphical solution presented in Figure 3-3, a deformed shape was assumed to be given by:

$$y = w_o \sin \frac{\pi x}{\ell} \tag{B-18}$$

The extensional strain for small deformations is approximated by $1/2\left(\frac{dy}{dx}\right)^2$. Differentiating Equation (B-18) and substituting gives:

$$\varepsilon = \frac{\pi^2 w_o^2}{2\ell^2} \cos^2\left(\frac{\pi x}{\ell}\right) \tag{B-19}$$

The maximum strain occurs when the cosine equals 1.0 or:

$$\varepsilon_{max} = \frac{\pi^2 w_o^2}{2\ell^2} \tag{B-20}$$

This equation is the relationship relating strains to deformation in Figure 3-3. If this solution is to be an elastic-plastic one, we need an elastic-plastic constitutive relationship. Equation (B-21) is assumed to be this relationship because it lets stress equal $E\varepsilon$ for values of $E\varepsilon/\sigma_y$ less than 0.5, and lets stress equal σ_y for values of $E\varepsilon/\sigma_y$ greater than 2.0.

$$\sigma = \sigma_y \tanh\left(\frac{E\varepsilon}{\sigma_y}\right) \tag{B-21}$$

The strain energy per unit volume in an elastic-plastic system is the area under the stress strain curve. Equation (B-22) gives for the strain energy per unit volume

$$\text{SE/Vol.} = \int_0^{\varepsilon} \sigma_y \tanh\left(\frac{E\varepsilon}{\sigma_y}\right) d\varepsilon \tag{B-22}$$

Or:

$$\text{SE/Vol.} = \frac{\sigma_y^2}{E} \log \cosh\left(\frac{E\varepsilon}{\sigma_y}\right) \tag{B-23}$$

Substituting Equation (B-19) for ϵ in Equation (B-23) and multiplying by the differential volume A, dx gives as an integral for the strain energy:

$$SE = \frac{\sigma_y^2 A}{E} \int_0^{\ell} \log \cosh \left[\frac{\pi^2 E w_o^2}{2\sigma_y \ell^2} \cos^2 \left(\frac{\pi x}{\ell} \right) \right] dx \qquad \text{(B-24)}$$

Substituting in a dimensionless variable Z equal to $\pi x/\ell$ and substituting in ϵ_{max} for $\frac{\pi^2 w_o^2}{2\ell^2}$ (Equation B-20) finally gives an integral for the strain energy:

$$SE = \frac{\sigma_y^2 A \ell}{\pi E} \int_0^{\pi} \log \cosh \left[\frac{E\epsilon_{max}}{\sigma_y} \cos^2 Z \right] dZ \qquad \text{(B-25)}$$

The asymptotes can now be calculated as before. The impulsive loading realm asymptote is obtained by equating kinetic energy KE to strain energy. The kinetic energy is given by:

$$KE = \frac{I^2}{2m} = \frac{i^2 b^2 \ell}{2\rho A} \qquad \text{(B-26)}$$

Equating Equations (B-26) and (B-24) plus rearranging terms gives:

$$\left[\frac{ibE^{1/2}}{\rho^{1/2} \sigma_y A} \right]^2 = \frac{2}{\pi} \int_0^{\pi} \log \cosh \left[\left(\frac{E\epsilon_{max}}{\sigma_y} \right) \cos^2 Z \right] dZ \qquad \text{(B-27)}$$

A computer is needed to numerically integrate Equation (B-27) for various constant values of scaled strain $\frac{E\epsilon_{max}}{\sigma_y}$. Equation (B-27) does show that the impulsive loading realm asymptote in functional format can be given by:

$$\frac{ibE^{1/2}}{\rho^{1/2} \sigma_y A} = \Psi \left(\frac{E \epsilon_{max}}{\sigma_y} \right) \quad \text{(Impulsive Realm)} \qquad \text{(B-28)}$$

Equation (B-28) is plotted as the asymptotes to the impulsive loading realm in Figure 3-3.

To obtain the quasi-static loading realm asymptote, we calculate the work Wk.

$$Wk = pbw_o \int_o^{\ell} \sin \frac{\pi x}{\ell} \, dx \qquad \text{(B-29)}$$

Or

$$Wk = \frac{2pb\ell w_o}{\pi} \qquad \text{(B-30)}$$

Substituting Equation (B-20) for w_o in Equation (B-30), equating (B-30) to Equation (B-29), and rearranging terms gives an equation for the quasi-static aysmptote.

$$\frac{pb\ell E^{1/2}}{\sigma_y^{3/2} A} = \frac{(\pi/2)^{3/2}}{\left(\frac{E\epsilon_{max}}{\sigma_y}\right)^{1/2}} \int_o^{\pi} \log \cosh \left[\left(\frac{E\epsilon_{max}}{\sigma_y}\right) \cos^2 z\right] dz \qquad \text{(B-31)}$$

A computer is also needed to numerically integrate Equation (B-31) for constant values of $\frac{E\epsilon_{max}}{y}$. Equation (B-31) shows that the quasi-static loading realm asymptote is functionally given by:

$$\frac{pb\ell E^{1/2}}{\rho^{1/2} \sigma_y A} = \Psi\left(\frac{E\epsilon_{max}}{\sigma_y}\right) \text{ (Quasi-Static Realm)} \qquad \text{(B-32)}$$

Equation (B-32) with the proper functional format is plotted as the asymptotes to the quasi-static loading realm in Figure 3-3. An approximation still had to be made to establish a transition between the impulsive and quasi-static loading realms. The same hyperbolic tangent squared relationship, Equation (B-17), was used for this string solution as had been used in the beam solutions.

To derive the solution for buckling of a column, we must assume a deformed shape. If the column is simply-supported without side-sway, a sine wave as in Equation (B-33) is a good assumption

$$Y = w_o \sin \frac{\pi x}{\ell} \qquad \text{(B-33)}$$

Differentiating Equation (B-33) twice and substituting into $M = -EI\frac{d^2y}{dx^2}$ gives the moment

$$M = \frac{\pi^2 EIw_o}{\ell^2} \sin \frac{\pi x}{\ell} \qquad \text{(B-34)}$$

The strain energy is the integral $\int_o^\ell \frac{M^2 dx}{2EI}$ or:

$$SE = 2 \int_o^{\ell/2} \frac{\pi^4 EIw_o^2}{2\ell^4} \sin^2 \left(\frac{\pi x}{\ell}\right) dx \qquad \text{(B-35)}$$

Which, upon completion, gives:

$$SE = \frac{\pi^4 EIw_o^2}{4\ell^3} \qquad \text{(B-36)}$$

The load on the column will act through a deflection δ equal to S-ℓ, where ℓ is the original length of the column. The differential length ds is given by:

$$ds = dx\sqrt{1 + \left(\frac{dy}{dx}\right)^2} \qquad \text{(B-37)}$$

Upon expanding with the binomial theorem and integrating this gives:

$$\delta = \int_o^\ell \left[1 + (1/2)\left(\frac{dy}{dx}\right)^2 + \ldots\ldots\ldots\right] \qquad \text{(B-38)}$$

Completing this integration and substracting ℓ from s to obtain δ gives as a first approximation:

$$\delta = (1/2)\int_o^\ell \left(\frac{dy}{dx}\right)^2 dx \qquad \text{(B-39)}$$

We can now proceed to solve for the work:

$$Wk = pA\,\delta = \frac{pA}{2} \int_o^\ell \left(\frac{dy}{dx}\right)^2 dx \qquad \text{(B-40)}$$

Substituting in the first derivative of Equation (B-33) to integrate gives:

$$Wk = \frac{\pi^2 pAw_o^2}{2\ell} \int_0^{\ell} \cos^2\left(\frac{\pi x}{\ell}\right) dx \qquad \text{(B-41)}$$

Or upon completion:

$$Wk = \frac{\pi^2 pAw_o^2}{4\ell} \qquad \text{(B-42)}$$

The quasi-static asymptote is obtained when the strain energy is equated to the work:

$$\frac{\pi^4 EIw_o^2}{4\ell^3} = \frac{\pi^2 pAw_o^2}{4\ell} \qquad \text{(B-43)}$$

Or:

$$\frac{pA\ell^2}{EI} = \pi^2 \quad \begin{matrix}\text{(quasi-static asymptote} \\ \text{S.S. beam-no side sway)}\end{matrix} \qquad \text{(B-44)}$$

Equation (B-44) should look familiar. It is the Euler beam buckling solution. The dynamic load factor equals 1.0 instead of 2.0. Because the vertical load pA is independent of w_o, we have the classical small deformation Euler column instability. The factor α_p in Figure 3-4 is equal to π^2 for this pinned-pinned column without side-sway. The concept of effective column length with ℓ being the distance between points of inflection can be applied in analysis. A review of α_p for a pinned-pinned column with side-sway shows a column with only one quarter the strength because the effective length of the column is twice as long. Similarly α_p for a clamped-clamped column without side-sway is four times stronger than the simply-supported column because the effective length of the column is halved.

To compute buckling in the impulsive loading realm, we need the kinetic energy imparted to the overlying mass. This kinetic energy equals:

$$KE = (1/2)\, mV_o^2 = (1/2)m\left(\frac{iA}{m}\right)^2 \qquad \text{(B-45)}$$

Or

$$KE = \frac{i^2A^2}{2m} \qquad \text{(B-46)}$$

Equating KE to SE gives the impulsive loading realm asymptote.

$$\frac{(iA)^2}{2m} = \frac{\pi^4 EIw_o^2}{4\ell^3} \qquad \text{(B-47)}$$

Notice that, unlike the quasi-static loading realm result, the deformation w_o does not cancel out of Equation (B-47). This result means that "stable buckling" occurs in the impulsive loading realm. A certain quantity of kinetic energy is being put into the column, which strain energy can dissipate until the deformations are large enough to cause yielding. This observation means that we must use Equation (B-34) to obtain the maximum moment, sin $\pi x/\ell$ equal 1.0, and substitute into a $\sigma = MH/2I$ to relate the maximum bending stress to be limited by σ_y) to the deformation w_o. This substitution gives:

$$\sigma_y = \frac{\pi^2 EHw_o}{2\ell^2} \qquad \text{(B-48)}$$

Substituting Equation (B-48) into Equation (B-47), rearranging terms algebraically, and taking the square root of the result finally gives:

$$\frac{(iA)H\sqrt{E}}{\sigma_y\sqrt{m\,\ell\,I}} = \sqrt{2.0} \quad \begin{matrix}\text{(impulse asymptote} \\ \text{s.s. beam, no side-sway)}\end{matrix} \qquad \text{(B-49)}$$

The numerical coefficient $\sqrt{2.0}$ is the α_i coefficient in Figure 3-4. Other α_i coefficients must be computed independently. The static concept of effective length no longer applies in the impulsive loading realm; hence, it should not be used. We have already mentioned that in the impulsive loading realm, it is a "stable buckling" or actually bending phenomenon that occurs. Permanent deformation does not occur until the column yields. The same Equation (B-17) was used to estimate a transition between the quasi-static and impulsive loading realms as has been used to approximate this transition in all earlier analysis.

APPENDIX C

Model Analysis for Bursting Containment Vessels

The model analysis used here is patterned after the techniques explained by Baker, Westine, and Dodge (1973). The purpose of the model analysis is to devise a method of consolidating the results of the computer runs made to predict velocities of fragments from pressurized spheres and cylinders. Such a consolidation will result in the need for fewer graphs and tables, will be of a more general nature, and will be easier to use.

To conduct the model analysis, it is necessary to list all of the physical parameters which are indigenous to the problem. A listing of these parameters is contained in Table C-1 which includes vessel characteristics, gas characteristics, and a response term. Since only spheres and cylinders with hemispherical endcaps and with an L/D ratio of 10.0 (includes the endcaps) are being considered, one needs to include the vessel's diameter d, thickness h, length ℓ, volume V, mass M_c, the yield strength σ_y of the material of the vessel's walls, and the number of fragments n that the vessel breaks into. It is assumed that the vessel breaks into n equal fragments. Cylinders break into either two equal fragments along a plane perpendicular to the axis of symmetry or n equal strip fragments along the cylindrical wall (endcaps are ignored). The relevant gas parameters are the ratio of specific heats γ, the ideal gas constant R_M which is adjusted for molecular weight, the speed of sound a_o of the gas, the pressure P_o of the gas at burst, the temperature T_o of the contained gas at burst, the energy E of the gas, and atmospheric pressure p_a. The response term is the velocity u of the fragment.

There are 11 pi terms or nondimensional ratios which can be created from the above 15 parameters. Table C-2 presents one possible list of these 11 pi terms. This list of 11 pi terms can be reduced to a smaller number of pi terms by examining some interrelationships among variables. Summaries of the various relationships appear in Table C-2 and will be expanded here. There are only two values for ℓ/d (π_2) being considered, spheres with an ℓ/d of 1.0 and cylinders with hemispherical endcaps and an ℓ/d of 10.0. Since there are so few values of ℓ/d, one might consider putting several curves on one graph. Pi terms π_7 and π_8 are directly related through the relationship

$$a_o = \sqrt{\gamma R_m T_o} \qquad \text{(C-1)}$$

For the sake of simplicity, pi term π_8 will be eliminated.

The thickness of the vessel is related to its diameter and the yield strength of the vessel material. Consider a sphere as shown in Figure C-1a. For the simplest design where the design thickness is much smaller than the diameter of the vessel,

TABLE C-1. PERTINENT PARAMETERS FOR BURSTING SPHERICAL AND CYLINDRICAL CONTAINMENT VESSELS

Symbol	Description	Dimensions*
d	diameter	L
h	thickness	L
ℓ	length	L
V	volume	L^3
M_c	mass of container	FT^2/L
σ_y	yield strength of material	F/L^2
n	number of fragments	--
γ	ratio of specific heats	--
R_M	ideal gas constant (adjusted for molecular weight)	$L^2/T^2\theta$
a_o	speed of sound in gas	L/T
P_o	burst pressure	F/L^2
T_o	initial temperature of gas	θ
E	energy of gas	FL
P_a	atmospheric pressure	F/L^2
u	velocity of fragment	L/T

* L = length
F = force
T = time
θ = temperature

TABLE C-2. LIST OF Pi TERMS FOR BURSTING CONTAINMENT VESSELS

π_1	$\frac{h}{d}$	proportional to $(P_o - p_a)\sigma_y$
π_2	$\frac{\ell}{d}$	constant (equals 1.0 or 10.0)
π_3	$\frac{V_o}{d^3}$	
π_4	$\frac{M_c a_o^2}{pad^3}$	
π_5	$\frac{\sigma_y}{p_a}$	constant
π_6	n	
π_7	γ	$a_o = \sqrt{\gamma R_M T_o}$ (see π_4 and π_{11})
π_8	$\frac{R_M T_o}{a_o^2}$	
π_9	$\frac{P_o}{p_a}$	
π_{10}	$\frac{E}{p_a h d^2}$	$E = \frac{(P_o - p_a)V_o}{(\gamma - 1)}$ (see π_3, π_7 and π_9)
π_{11}	$\frac{u}{a_o}$	

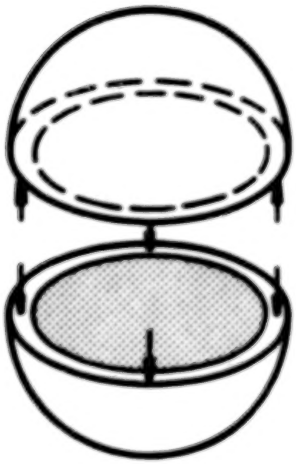

(a) Sphere

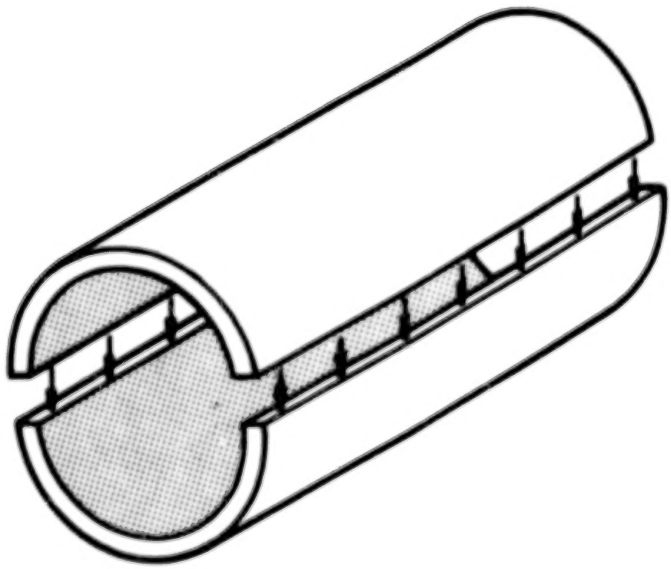

(b) Cylinder

FIGURE C-1. DETERMINATION OF VESSEL THICKNESS

the vessel will burst when the force exerted on the vessel walls by the internal pressure equals the force required to break the vessel. If one considers that the vessel (sphere) bursts in half, one has

$$(P_o - p_a)\ \frac{\pi d^2}{4} = \sigma_y \pi dh \qquad \text{(C-2)}$$

or

$$\frac{h}{d} = \frac{P_o - p_a}{4\sigma_y} \qquad \text{(C-3)}$$

Cylinders must have thicker walls than spheres to contain equal amounts of internal pressures. A simplified design for a cylinder can be based on Figure C-1b which shows a cylinder without hemispherical endcaps.

The most likely plane of fracture of a cylinder made of a homogeneous material is along the longitudinal axis as shown in Figure C-1b. For vessels whose thickness is much smaller than its diameter, the vessel will burst when the force exerted on the vessel walls by the internal pressure equals the force required to break the vessel. If one considers that the vessel (cylinder) bursts into two pieces as shown in Figure C-1b, one has

$$(P_o - p_a)\ d\ell = \sigma_y 2\ell h \qquad \text{(C-4)}$$

or

$$\frac{h}{d} = \frac{(P_o - p_a)}{2\sigma_y} \qquad \text{(C-5)}$$

Equations C-3 and C-5 indicate that (h/d) is proportional to $(P_o - p_a)/\sigma_y$ and thus pi term π_1 can be eliminated. If one assumes that only one material with one yield strength will be used in constructing the vessel, then pi term π_5 can also be eliminated.

Energy E in the gas is defined as

$$E = \frac{(P_o - p_a)V_o}{(\gamma - 1)} \qquad \text{(C-6)}$$

Pi term π_9 contains p_o and p_a, π_3 contains V_o, and π_7 contains γ. Therefore, the energy of the gas is completely defined by these other pi terms and pi term π_{10} can be eliminated.

Variables in π_7 and π_8 appear in π_4 and π_{11}. It seems logical that the problem has been overdefined and that π_7 and π_8 can be eliminated from the analysis.

Since π_3, π_4 and π_9 have some terms in common, it appeared beneficial to combine them. Thus, one has

$$\frac{\pi_9 \times \pi_3}{\pi_4} = \frac{\frac{p_o}{p_a} \times \frac{V_o}{d^3}}{\frac{M_c}{p_a d^3} \frac{a_o^2}{}} \qquad \text{(C-7)}$$

Rearranging Equation C-7 and substituting Equation C-1 for a_o, one has

$$\pi_9' = \frac{P_o V_o}{M_c \gamma R_m T_o} \qquad \text{(C-8)}$$

Substituting $(P_o - p_a)$ for P_o in order to emphasize the importance of the differential in pressure between the inside and outside of the vessel walls, one obtains the abscissa of Figure 4-2. Plotting π_{11} with equation C-1 substituted for a_o, versus the modified version of Equation C-8 yields the desired result. Figure 4-2 in the text consolidates the presentation of the analysis by allowing one to plot several curves for different L/D ratios and numbers of fragments n on one curve and still maintain accurate estimation of fragment velocity u. Several computer checks have shown that the curves presented in Figure 4-2 can be used for materials of different densities and yield strengths, provided that the thickness of the vessel is less than 1/3 of the diameter of the vessel. For cylinders bursting into three or more "strip" fragments as explained in Baker, Kulesz, et al (1975), the hemispherical endcaps were ignored.

Some cases were run for cylinders with hemispherical endcaps and an L/D ratio of 10.0 which burst into two unequal segments perpendicular to the cylindrical axis of symmetry. It seemed reasonable that the velocity of each fragment would be related to the velocity of the fragments from cylinders bursting in half by some constant k which depends on the unequal fragment's fraction of the total mass of the container. Figure 4-4 in the text was

plotted from an average of several computer runs for unequal fragments which showed amazing consistency. Note that for equal fragments k equals 1.0. For unequal fragments from bursting cylinders (two fragments total), one must determine the fragment's fraction of the total mass and find k in Figure 4-4. Once k is known, Figure 4-2 can be used to calculate the velocity of the fragment.

APPENDIX D

Estimate of Initial Velocities of Fragments from Spheres and Cylinders Bursting Into Two Unequal Fragments

The method developed by Taylor and Price (1971) and modified by Baker, et al (1975) for calculating velocities of fragments from bursting spherical and cylindrical gas reservoirs was further adapted to provide velocity calculations for unequal fragments from cylindrical gas vessels. To compute the velocity of fragments from bursting cylinders which contain gas under pressure, the following assumptions were made:

(1) The vessel with gas under pressure breaks into two unequal fragments along a plane perpendicular to the cylindrical axis, and the two container fragments are driven in opposite directions.

(2) Gas within the vessel obeys the ideal gas law.

(3) Originally contained gas escapes from the vessel through the opening between the fragments into a surrounding vacuum. The escaping gas travels perpendicular to the direction of motion of the fragments with local sonic velocity.

(4) Energy necessary to break the vessel walls is negligible compared to the total energy of the system.

(5) Drag and lift forces are ignored since the distance the fragment travels before it attains its maximum velocity are too short for drag and lift forces to have a significant effect.

A schematic depicting the essential characteristics of the modified solution for bursting cylinders is shown in Figure (D-1). Before accelerating into an exterior vacuum, the cylinder has internal volume V_{oo} and contains a perfect gas of adiabatic exponent (ratio of specific heats) γ and gas constant R_M with initial pressure P_{oo} and temperature T_{oo} (Figure D-1a). At a time $T = 0$, rupture occurs along a perimeter Π, and the two fragments are propelled in opposite directions due to forces applied against the area F which is perpendicular to the axis of motion of the fragments (Figure D-1b). The masses of the fragments, M_1 and M_2, are considered large relative to the mass of the remaining gas at elevated pressure (Figure D-1c).

Figure D-2 contains the geometric parameters associated with cylindrical vessels. The generalized fragment velocity solution and subsequent computer program allow for computation of the velocities of both segments of the cylinder. The vessel is assumed

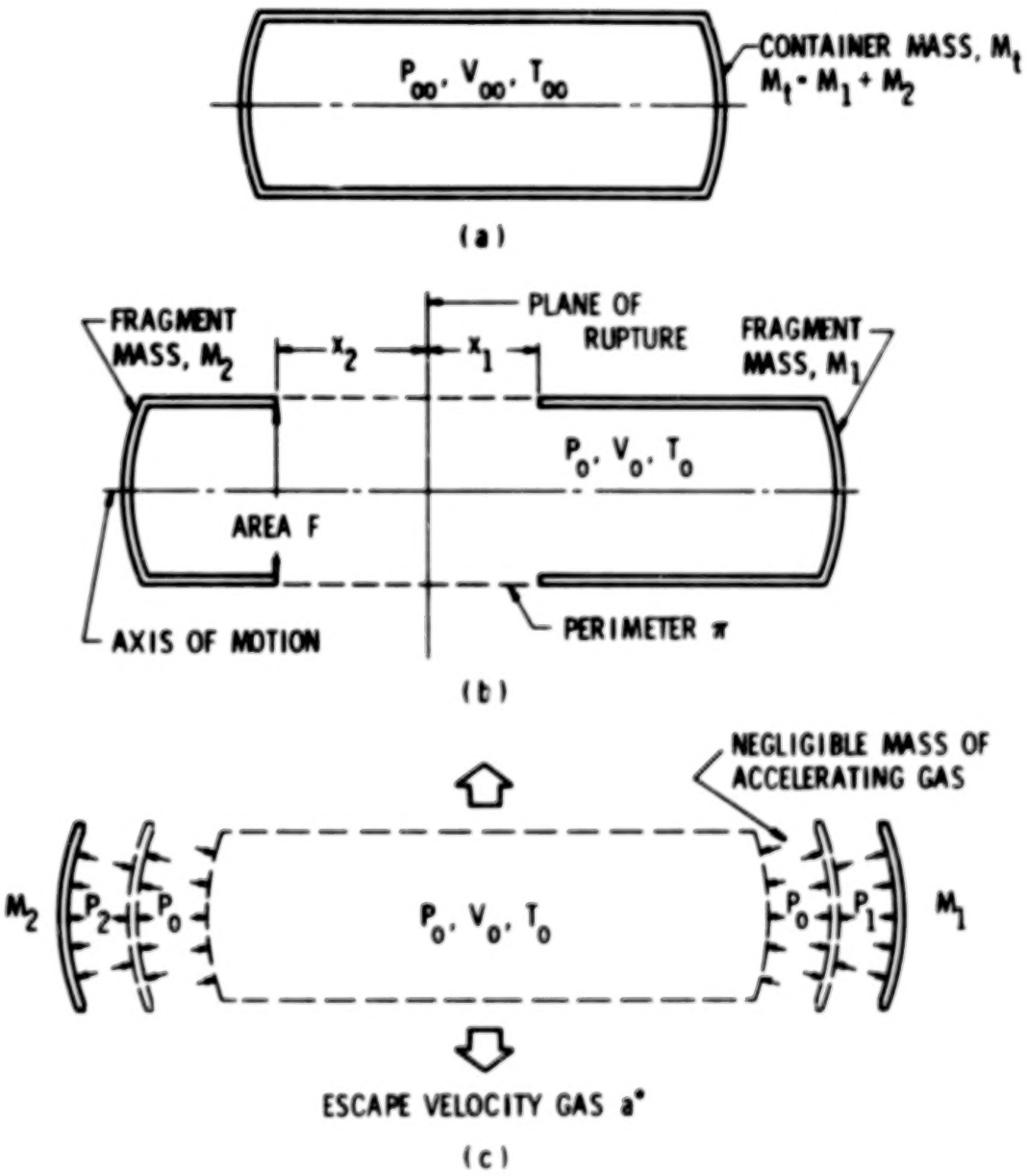

FIGURE D-1. PARAMETERS FOR CYLINDER BURSTING INTO TWO UNEQUAL SEGMENTS

to break into two unequal segments along a plane perpendicular to its cylindrical axis. The cylinder can have spherical segment end caps or can have flat faces. The vessel has cylindrical radius r, cylindrical thickness C_t, end cap thickness E_t, cylindrical length C_ℓ, and end cap length E_ℓ beyond the cylindrical portion.

The Taylor and Price (1971) solution, generalized to allow for cylindrical vessels bursting into unequal fragments, follows. The equations of motion and initial conditions of the two fragments are

$$M_1 \frac{d^2X_1(\tau)}{d\tau^2} = FP_1(\tau), \text{ with } X_1(0) = 0, \frac{dX_1(0)}{d\tau} = 0 \qquad \text{(D-1)}$$

$$M_2 \frac{d^2X_2(\tau)}{d\tau^2} = FP_2(\tau) \text{ with } X_2(0) = 0, \frac{dX_2(0)}{d\tau} = 0 \qquad \text{(D-2)}$$

where subscripts refer to each fragment and X_1 is a displacement distance taken along the axis of motion. To allow for cylindrical containment vessels, the cross sectional area F over which the force is applied becomes

$$F = \pi (r - C_t)^2 \qquad \text{(D-3)}$$

The equation of state for the unaccelerated gas remaining within the confinement of the container fragments is

$$P_o(\tau)\, V_o(\tau) = C(\tau)\, RT_o(\tau) \qquad \text{(D-4)}$$

where subscript "o" denotes reservoir conditions immediately after failure, R is the gas constant, P is pressure, V is volume, T is temperature and $C(\tau)$ is the mass of gas confined at high pressure as a function of time. The rate of change of the confined mass is

$$\frac{d\,C(\tau)}{d(\tau)} = k\, \Pi\, X\, \rho_* a_* \qquad \text{(D-5)}$$

where

$$X = X_1 + X_2, \qquad \text{(D-6)}$$

K is the coefficient of discharge of the area between the fragments and ρ_* is the gas density at critical gas velocity a_*. The expression for perimeter Π is

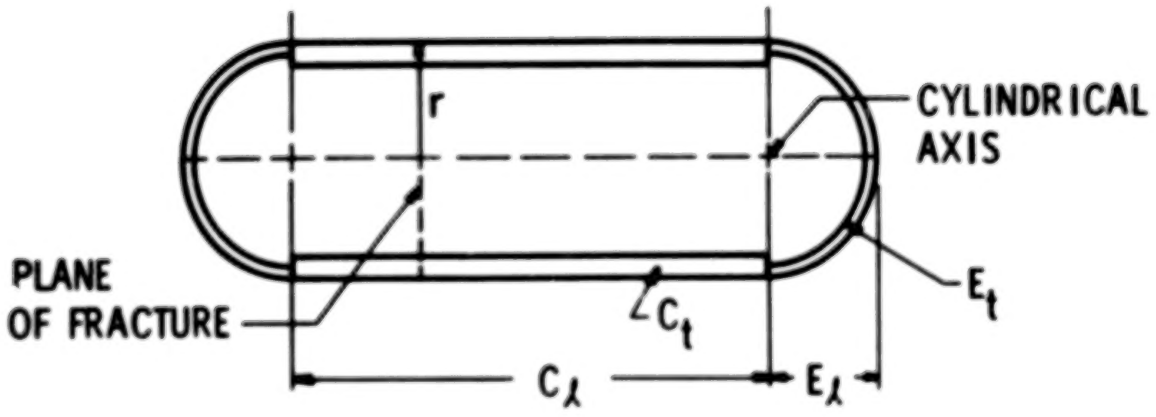

FIGURE D-2. GEOMETRY OF CYLINDRICAL VESSELS

$$\Pi = 2\pi r \tag{D-7}$$

Gas density ρ_* and a_* are standard expressions

$$\rho_* = \rho_o(\tau)\left(\frac{2}{\gamma + 1}\right)^{1/(\gamma-1)}$$
$$a_* = a_o(\tau)\left(\frac{2}{\gamma + 1}\right)^{1/2} \tag{D-8}$$

where γ is the adiabatic exponent (ratio of specific heats) for an ideal gas. The volume is assumed to be variable and can be described by

$$V_o(\tau) = V_{oo} + Fx \tag{D-9}$$

where $x = x_1 + x_2$.

Nearly all of the gas is assumed to be accelerated with the fragments, with gas immediately adjacent to the fragments being accelerated to the velocity of the fragments. From simple one-dimensional flow relationships,

$$P_1(\tau) = P_o(\tau)\left(1 - \left\{\frac{\gamma - 1}{2[a_o(\tau)]^2}\right\}\left[\frac{dx_1(\tau)}{d\tau}\right]^2\right)^{\gamma/(\gamma-1)}$$
$$P_2(\tau) = P_o(\tau)\left(1 - \left\{\frac{\gamma - 1}{2[a_o(\tau)^2}\right\}\left[\frac{dx_2(\tau)}{d\tau}\right]^2\right)^{\gamma/(\gamma-1)} \tag{D-10}$$

To generalize the solution, one can use the following nondimensional forms of the variables:

Dimension: $x(\tau) = Xg(\zeta)$, $x_1(\tau) = Xg_1(\zeta)$, $x_2(\tau) = Xg_2(\zeta)$

Time: $\tau = \theta\zeta$ (D-11)

Pressure: $P_o(\tau) = P_{oo}P_*(\zeta)$

From appropriate solutions and initial conditions:

$$\frac{dx_1(\tau)}{d(\tau)} = \frac{X}{\theta}\, g_1'(\zeta)\ ,\ \frac{dx_2(\tau)}{d\tau} = \frac{X}{\theta}\, g_2'(\zeta)$$

$$\frac{d^2x_1(\tau)}{d\tau^2} = \frac{X}{\theta^2} g_1''(\zeta) \quad , \quad \frac{d^2x_2(\tau)}{d\tau^2} = \frac{X}{\theta^2} g_2''(\zeta)$$

$$\frac{dP_o(\tau)}{d\tau^2} = \frac{P_{oo}}{\theta} P_*' \qquad \text{(D-12)}$$

Initial conditions:

$$x_1(0) = x_2(0) = \frac{dx_1(0)}{d\tau} = \frac{dx_2(0)}{d\tau} = g_1(0) =$$

$$g_2(0) = g_1'(0) = g_2'(0) = 0$$

$$P_*(0) = 1$$

where primes denote differentiation with respect to ζ. The pair of characteristic values for dimension X and time θ chosen by Taylor and Price are:

$$X = \frac{M_t a_{oo}^2}{F P_{oo}} \left(\frac{2}{\gamma - 1}\right)$$

$$\theta = \frac{M_t a_{oo}}{F P_{oo}} \left(\frac{2}{\gamma - 1}\right)^{1/2} \qquad \text{(D-13)}$$

The final derived equations contain two dimensionless groups which define the nature of the solutions, these are

$$\alpha = \frac{P_{oo} V_{oo}}{M_t a_{oo}^2}$$

$$\beta = k\left(\frac{2}{\gamma + 1}\right)^{\frac{\gamma+1}{2(\gamma-1)}} \left(\frac{2}{\gamma - 1}\right)^{1/2} \frac{\Pi V_{oo}}{F^2} \qquad \text{(D-14)}$$

Differences between the Taylor and Price solution for spheres and our solution for cylinders, with spherical caps being a special case of cylinders, occur in the determination of area F given by Equation (D-3) and perimeter Π given in Equation (D-7) where r is cylindrical radius instead of spherical radius. A difference also exists in the calculation of initial volume of the gas which, for the cylindrical case with spherical segment endcaps with one base, becomes

$$V_{oo} = \pi\left\{(r - C_t)^2 C_\ell + (E_\ell - E_t)\left[(r - E_t)^2 + \frac{(E_\ell - E_t)^2}{3}\right]\right\} \quad \text{(D-15)}$$

for the adiabatic case,

$$\frac{P_o(\tau)}{P_{oo}} = \left[\frac{\rho_o(\tau)}{\rho_{oo}}\right]^{\gamma} = \left[\frac{T_o(\tau)}{T_{oo}}\right]^{\frac{\gamma}{\gamma-1}} = \left[\frac{a_o(\tau)}{a_{oo}}\right]^{\frac{2\gamma}{\gamma-1}} \quad \text{(D-16)}$$

Substitution of Equations (D-10), (D-12) through (D-14), and (D-16) into Equations (D-1) and (D-2) gives

$$\frac{M_1}{M_t} g_1'' = P_* \left[1 - \left(\frac{g_1'^2}{P_*^{(\gamma-1)/\gamma}}\right)\right]^{\gamma/(\gamma-1)} \quad \text{(D-17a)}$$

by analogy,

$$\frac{M_2}{M_t} g_2'' = P_* \left[1 - \left(\frac{g_2'^2}{P_*^{(\gamma-1)/\gamma}}\right)\right]^{\gamma/(\gamma-1)} \quad \text{(D-17b)}$$

Differentiation of Equation (D-4) and substitution of Equations (D-5) through (D-9), (D-11) and (D-12) yields

$$\left[\left(\frac{\gamma - 1}{2}\right)a + g\right]\frac{P_*'}{P_*} = -\frac{\beta\gamma}{a} g P_*^{(\gamma-1)/2\gamma} - \gamma g' \quad \text{(D-18)}$$

In the solution for equal fragments, the fragment masses are equal, and the equations for the motion of the two fragments become identical. However, since the fragment masses in the new solution are unequal, the equations of motion become

$$g_1'' = \frac{M_t}{M_1} P_* \left[1 - \left(\frac{g_1'^2}{P_*^{(\gamma-1)/\gamma}}\right)\right]^{\gamma/(\gamma-1)}$$

$$g_2'' = \frac{M_t}{M_2} P_* \left[1 - \left(\frac{g_2'^2}{P_*^{(\gamma-1)/\gamma}}\right)\right]^{\gamma/(\gamma-1)} \quad \text{(D-19)}$$

Rearranging terms in Equation (D-18) produces

$$P_*' = \frac{\frac{\beta\gamma}{\alpha}(g_1 + g_2) P_*^{(3\gamma-1)/2\gamma} - \gamma(g_1' + g_2')P_*}{\left[\left(\frac{\gamma - 1}{2}\right)\alpha + (g_1 + g_2)\right]} \qquad \text{(D-20)}$$

For initial conditions, $g_1(0) = 0$, $g_2(0) = 0$, $g_1'(0) = 0$, $g_2'(0) = 0$, and $P_*(0) = 1$, nondimensional values of distance, velocity, accerlation and pressure as a function of time can be calculated by solving Equations (D-19) and (D-20) simultaneously using the Runge-Kutta method of numerical iteration. Dimensional values can then be calculated from

$$\tau = \theta\,\zeta,\ x_1(\tau) = Xg_1(\zeta),\ x_2(\tau) = Xg_2(\zeta),$$

$$x_1'(\tau) = \frac{X}{\theta} g_1'(\zeta),\ X_2'(\tau) = \frac{X}{\theta} g_2'(\zeta), \qquad \text{(D-21)}$$

$$x_1''(\tau) = \frac{X}{\theta^2} g_1''(\zeta),\ X_2''(\tau) = \frac{X}{\theta^2} g_2''(\zeta),\ P_o(\tau) = P_{oo}P_*(\zeta)$$

The computer program entitled /UNQL/ was written in BASIC and was exercised on a Tektronix 4051 microprocessor. The computer program requires input in English units and gives output in both English and SI units. Rigorous English measure input is not used for length and mass measurements. Instead, inches are used for length measurements and pounds-force(weight measure) are used for mass measurements in both input and output stages of the program since these units are commonly used in these types of measurements. The ratio of specific heats (γ), speed of sound (a_{oo}), initial pressure (P_{oo}), external radius of the cylinder of sphere, and the discharge coefficient are input parameters. The user has a choice of inputting cylinder length, end length, cylinder thickness, end thickness, and wall density; or volume, mass of the reservoir, and cylinder thickness (see Figure D-2). The program also requires that a step size and limit be added to allow for the iterative process to begin and end. Nondimensional times are inputted for this purpose. The user has a choice of displaying nondimensional distance, velocity, acceleration, and pressure as a function of nondimensional time and/or displaying dimensional distance, velocity, acceleration and pressure as a function of dimensional time. In all cases, final dimensional times, distance, velocity, acceleration, and pressure are printed.

An explanation of the Runge-Kutta subroutine can be found in Baker, et al (1975). This is a standard computer library function which has nine arguments. A list of the program variables, a listing of the program, and sample input and output follow in Table D-1.

In summary, the solution of the case with two unequal fragments differs from that with equal halves in Equations (D-19) through (D-21) because the masses of the two segments are not identical. The program which follows has been adjusted to account for these differences.

Table D-1. Computer Program Entitled /UNQL/ in Basic

Function: This program computes the velocity of a fragment from a bursting sphere or cylinder, with or without spherical segment end caps with one base, which contains gas under pressure. It is assumed that the vessel breaks into two unequal fragments along a plane perpendicular to the cylindrical axis. Distance, acceleration and residual pressure as a function of time are also computed.

Input-Output Considerations: The program accepts input in English units only and prints output in SI and English units making any conversions needed internally. The program considers SI units of mass in kilograms, length in meters and time in seconds. The program considers English units of mass in pounds of force (weight measure used for convenience), length in inches and time in seconds. Input data are:

(A) Gas characteristics:

(CØ) Adiabatic exponent (ratio of specific heats) for gas in the containment vessel

(AØ) Speed of sound in gas of vessel

(PØ) Initial pressure of gas in vessel

(B) Vessel characteristics:

(RØ) Cylinder radius

choice of

(Z1) = 1:
- (A) Cylinder length
- (B) Length of end cap
- (C) Cylinder thickness
- (D) Thickness of end cap
- (E) Wall density

(Z1) = 2:
- (A) Volume of containment vessel
- (B) Mass of reservoir
- (C) Cylinder thickness

(C) Dynamic variables:

(KØ) Discharge coefficient

(X8) Nondimensional time increment for calculations

(X9) Maximum nondimensional time calculation

(D) Input/Output format:

(F9) Fraction of total cylinder length (or mass) for first fragment

(F1) Display nondimensional dynamic variance
1. = Yes
2. = No

(F2) Display dimensional dynamic variance
1. = Yes
2. = No

Variables: The definition and units of variables in this program follow.

Program Variable	Variable	Definition	Units SI	Units English
F2	--	if-1., program displays normal time, distance, velocity, accelerations and pressure	--	--
C1	C_ℓ	cylinder length	m	in
E1	E_ℓ	end length	m	in
C2	C_t	cylinder thickness	m	in
E2	E_t	end thickness	m	in
DØ	--	wall density	kg/m^3	lb-f/in^3*
VØ	--	outside volume of vessel	m^3	in^3
V1	V_{oo}	internal volume of vessel	m^3	in^3
V2	--	wall volume of vessel	m^3	in^3
MØ	M_t	total mass of reservoir	kg	lb-f*
V5	--	outside volume of frag #1	m^3	in^3

*lb-f indicates English weight measurement of pounds of force. Sea level gravitation is assumed.

Program Variable	Variable	Definition	Units SI	Units English
V6	--	internal volume of frag #1	m^3	in^3
V7	--	wall volume of frag #1	m^3	in^3
M7	M_1	mass of frag #1	kg	lb-f*
M8	M_2	mass of frag #2	kg	lb-f*
CØ	γ	adiabatic exponent	--	--
AØ	a_{oo}	sound speed	m/s	in/sec
PØ	P_{oo}	initial pressure	Pa	psi
RØ	r	cylinder radius	m	in
Z1	--	if = 1., input is if = 2., input is	-- --	-- --
KØ	--	gas discharge coefficient	--	--
X8	--	dimensionless time interval of iteration	--	--
X9	--	maximum dimensionless time of iteration	--	--
F9	--	fraction of total cylinder length (or mass) for frag #1	--	--
F1	--	if = 1., program displays	--	--
F2	--	if = 1., program displays	--	--
P5	Π	perimeter(calculated)	m	in
F5	F	area of cross-section to which force is applied(calculated)	m^2	in^2
X2	X	characteristic dimension(calculated)	m^2	in^2

Program Variable	Variable	Definition	Units SI	Units English
O	θ	characteristic time (calculated)	s	sec
C7	--	quantity $(\gamma/(\gamma-1)$	--	--
C8	--	quantity $(3\gamma-1)/2\gamma$	--	--
C9	--	quantity $(\gamma+1)/2(\gamma-1)$	--	--
Q1	α	dimensionless parameter	--	--
B1	β	dimensionless geometry parameter	--	--
X	--	normalized time	--	--
Y(1)	--	normalized initial displacement of frag #1	--	--
Y(2), F(1)*	--	normalized velocity of frag #1	--	--
Y(3)	--	normalized pressure	--	--
Y(4)	--	normalized initial displacement of frag #2	--	--
Y(5), F(4)*	--	normalized velocity of frag #2	--	--
F(2)*	--	normalized acceleration of frag #1	--	--
F(3)*	--	normalized rate of change of pressure	--	--
F(5)*	--	normalized acceleration of frag #2	--	--
Q2	--	quantity $[(\gamma-1)/2]\alpha + (g_1 + g_2)$		
U	g'	$(g_1' + g_2')$ quantity	--	--
T9	--	normalized time(output)	--	--

*indicates differential equations solved.

Program Variable	Variable	Definition	Units SI	Units English
G	G_1	normalized distance of frag #1 (output)	--	--
G1	g_1'	normalized velocity of frag #1 (output)	--	--
G2	g_1''	normalized acceleration frag #1 (output)	--	--
P9	P_*	normalized pressure (output)	--	--
G3	g_2	normalized distance of frag #2 (output)	--	--
G4	g_2'	normalized velocity of frag #2 (output)	--	--
G5	g_2''	normalized acceleration of frag #2 (output)	--	--
T1, E5	--	time (output)	s	sec
H1, E6	--	distance of frag #1 (output)	m	in
H2, E7	--	velocity of frag #1 (output)	m/s	in/sec
H3, E8	--	acceleration of frag #1 (output)	m/s^2	in/sec^2
H4, E9	--	pressure (output)	Pa	psi
H5, S6	--	distance of frag #2 (output)	m	in
H6, S7	--	velocity of frag #2 (output)	m/s	in/sec
H7, S8	--	acceleration of frag #2 (output)	m/s^2	in/sec^2

BLANK PAGE

SAMPLE INPUT AND OUTPUT

```
100 INIT
110 PAGE
120 REM
130 REM----------------------------------------------------------------
140 REM /UNQL/--VELOCITY OF FRAGMENTS FROM CYLINDRICAL
150 REM PRESSURE VESSELS BURSTING INTO TWO UNEQUAL SEGMENTS
160 REM PERPENDICULAR TO AXIS OF SYMMETRY
170 REM ENGLISH INPUT UNITS ONLY (IN,LBF,PSI)
180 REM----------------------------------------------------------------
190 REM
200 DIM F(5),Y(5),W1(5),W2(5),P9(50),T9(50),G(50),G1(50),G2(50)
210 DIM G3(50),G4(50),G5(50)
220 PRINT "GAMMA, SOUND SPEED, INITIAL PRESSURE? ";
230 INPUT C0,P0,P8
240 PRINT
250 PRINT "CYLINDER RADIUS? ";
260 INPUT R0
270 PRINT
280 PRINT "IF PARAMETERS ARE:"
290 PRINT "CYL LEN, END LEN, CYL THICK, END THICK, WALL DENS--ENTER 1"
300 PRINT "VOLUME, MASS OF RESERVOIR, CYL THICK--ENTER 2--------------";
310 INPUT Z1
320 PRINT
330 PRINT "READ IN VALUES ";
340 INPUT A,B,C,D,E
350 PRINT
360 PRINT "FRACTION OF TOTAL CYLINDER LENGTH(OR MASS) FOR FRAG#1? ";
370 INPUT F9
380 PRINT
390 PRINT "DISCHARGE COEF.? ";
400 INPUT K0
410 PRINT
420 PRINT "TIME INTERVAL, MAXIMUM TIME? ";
430 INPUT X0,X9
```

```
440 PRINT
450 PRINT "DISPLAY NONDIMENSIONAL DYNAMIC VAR.? YES=1 NO=2--";
460 INPUT F1
470 PRINT
480 PRINT "DISPLAY DIMENSIONAL DYNAMIC VAR.? YES=1 NO=2--";
490 INPUT F2
500 A$="ITEM"
510 B$="ENGLISH UNITS"
520 D$="GAMMA"
530 E$="SOUND SPEED"
540 F$="PRESSURE"
550 G$="RADIUS"
560 H$="CYL. LENGTH"
570 I$="END LENGTH"
580 J$="CYL. THICK."
590 K$="END THICK."
600 L$="WALL DENSITY"
610 M$="RESERVOIR MASS"
620 O$="IN"
630 P$="VOLUME"
640 PAGE
650 PRINT "DATE ";
660 INPUT Z$
670 PRINT "PAGE NO. ";
680 INPUT J9
690 PRINT
700 IF Z1=2 THEN 1100
710 C1=A
720 E1=B
730 C2=C
740 E2=D
750 D0=E
760 V0=PI*(R0*R0*C1+E1*R0*R0+E1*E1*E1/3)
770 V1=PI*((R0-C2)↑2*C1+(E1-E2)*((R0-E2)↑2+(E1-E2)↑2/3))
780 V2=V0-V1
```

```
790 M0=D0*V2
800 REM CALCULATE MASS OF FRAG #1(M7) AND FRAG #2(M8)
810 V5=PI*(R0*R0*F9*C1+E1*R0*R0/2+E1*E1*E1/6)
820 V6=PI*((R0-C2)↑2*F9*C1+(E1-E2)*((R0-E2)↑2/2+(E1-E2)↑2/6))
830 V7=V5-V6
840 M7=D0*V7
850 M8=M0-M7
860 PRINT "FRACTION OF TOTAL CYL. LENGTH(LESS END CAPS) FOR FRAG#1 IS ";
870 PRINT USING 880:F9
880 IMAGE 1D.4D
890 PRINT USING 900:"ENGLISH INPUT/ENGLISH OUTPUT",A$,B$,D$,C0
900 IMAGE /,28A,2/,4A,13X,13A,/,5A,11X,3E
910 PRINT USING 920:E$,A0,"IN/SEC",F$,P0,"PSI",G$,R0,O$
920 IMAGE 11A,5X,3E,1X,6A,/,8A,8X,3E,1X,3A,/,6A,10X,3E,1X,2A
930 PRINT USING 940:H$,C0,O$,I$,E1,O$,J$,C2,O$
940 IMAGE 11A,5X,3E,1X,2A,/,10A,6X,3E,1X,2A,/,11A,5X,3E,1X,2A
950 PRINT USING 960:K$,E2,O$,L$,D0,"LBF/CU IN",P$,V1,"CU IN"
960 IMAGE 11A,5X,3E,1X,2A,/,12A,4X,3E,1X,3A,/,6A,10X,3E,1X,5A
970 PRINT USING 980:M$,M0,"LBF"
980 IMAGE 14A,2X,3E,1X,3A
990 PRINT USING 1000:"FRAG#1 CYL L",F9*C1,O$
1000 IMAGE 12A,4X,3E,1X,2A
1010 PRINT USING 1020:"FRAG#1 MASS",M7,"LBF"
1020 IMAGE 11A,5X,3E,1X,3A
1030 PRINT USING 1000:"FRAG#2 CYL L",(1-F9)*C1,O$
1040 PRINT USING 1020:"FRAG#2 MASS",M8,"LBF"
1050 D0=D0/386.0886
1060 M0=M0/386.0886
1070 M7=M7/386.0886
1080 M8=M8/386.0886
1090 GO TO 1350
1100 V1=A
1110 M0=B
1120 M7=F9*M0
1130 M8=M0-M7
```

TABLE OF CONTENTS

```
1140 C2=C
1150 PRINT "FRACTION OF TOTAL VESSEL MASS FOR FRAG#1 IS "1
1160 PRINT USING 1170:F9
1170 IMAGE 1D.4D
1180 PRINT USING 1190:"ENGLISH INPUT/ENGLISH OUTPUT",A$,B$,D$,C0
1190 IMAGE /,28A,2/,4A,13X,13A,/,5A,11X,3E
1200 PRINT USING 1210:E$,A0,"IN/SEC",F$,P0,"PSI",G$,R0,O$
1210 IMAGE 11A,5X,3E,1X,6A,/,8A,8X,3E,1X,3A,/,6A,10X,3E,1X,2A
1220 PRINT USING 1230:P$,V1,"CU IN",M$,M0,"LBF",J$,C2,O$
1230 IMAGE 6A,15X,3E,1X,5A,/,14A,2X,3E,1X,3A,/,11A,5X,3E,1X,2A
1240 PRINT USING 1250:"FRAG#1 MASS",M7,"LBF"
1250 IMAGE 11A,5X,3E,1X,3A
1260 PRINT USING 1250:"FRAG#2 MASS",M8,"LBF"
1270 M0=M0/386.0886
1280 M7=M7/386.0886
1290 M8=M8/386.0886
1300 REM
1310 REM-----------------------------------------------------------------
1320 REM BEGIN VELOCITY CALCULATIONS
1330 REM-----------------------------------------------------------------
1340 REM
1350 J1=0
1360 P5=2*PI*R0
1370 F5=PI*(R0-C2)↑2
1380 X2=M0*A0*A0*(2/(C0-1))/(F5*P0)
1390 O=M0*A0*(2/(C0-1))↑0.5/(F5*P0)
1400 C7=C0/(C0-1)
1410 C8=(3*C0-1)/(2*C0)
1420 C9=(C0+1)/(2*(C0-1))
1430 Q1=P0*V1/(M0*A0*A0)
1440 B1=K0*(2/(C0+1))↑C9*(2/(C0-1))↑0.5*P5*V1/(F5*F5)
1450 REM
1460 REM-----------------------------------------------------------------
1470 REM          X=T-NORM
1480 REM       Y(1)=G#1
```

```
1490 REM Y(2)=F(1)=G'01
1500 REM      Y(3)=P-NORM
1510 REM      F(2)=G''01
1520 REM      F(3)=P-NORM PRIME
1530 REM
1540 REM      Y(4)=G02
1550 REM Y(5)=F(4)=G'02
1560 REM      F(5)=G''02
1570 REM-----------------------------------------------------------------
1580 REM
1590 X=0
1600 Y(1)=0
1610 Y(2)=0
1620 Y(3)=1
1630 Y(4)=0
1640 Y(5)=0
1650 PRINT
1660 PRINT "INITIAL CONDITIONS"
1670 PRINT USING 1680:"X(0)=",X,"G1(0)=",Y(1),"G1'(0)=",Y(2)
1680 IMAGE 5A,2D,/,6A,2D,/,7A,2D
1690 PRINT USING 1700:"G2(0)=",Y(4),"G2'(0)=",Y(5),"P-NORM=",Y(3)
1700 IMAGE 6A,2D,/,7A,2D,/,7A,2D
1710 N=5
1720 F(1)=Y(2)
1730 F(2)=M0/M7*Y(3)*(1-Y(2)*Y(2)/Y(3)↑(1/C7))↑C7
1740 Q2=(C0-1)/2*Q1+Y(1)+Y(4)
1750 F(3)=(-B1*C0/Q1*(Y(1)+Y(4))*Y(3)↑C8-C0*(Y(2)+Y(5))*Y(3))/Q2
1760 F(4)=Y(5)
1770 F(5)=M0/M8*Y(3)*(1-Y(5)*Y(5)/Y(3)↑(1/C7))↑C7
1780 STOP
1790 PAGE
1800 PRINT "CHARACTERISTICS OF MOTION OF FRAGMENTS (NORMALIZED)"
1810 PRINT "     T-NORM          G              G'             G''          P-NORM"
1820 U=1000
1830 N2=0
```

```
1840 GOSUB 2990
1850 F(1)=Y(2)
1860 F(2)=M0/M7*Y(3)*(1-Y(2)*Y(2)/Y(3)↑(1/C7))↑C7
1870 Q2=(C0-1)/2*Q1+Y(1)+Y(4)
1880 F(3)=(-B1*C0/Q1*(Y(1)+Y(4))*Y(3)↑C8-C0*(Y(2)+Y(5))*Y(3))/Q2
1890 F(4)=Y(5)
1900 F(5)=M0/M8*Y(3)*(1-Y(5)*Y(5)/Y(3)↑(1/C7))↑C7
1910 IF S=1 THEN 1840
1920 PRINT
1930 PRINT USING 1940:"1",X,Y(1),Y(2),F(2),Y(3)
1940 IMAGE 1A,1X,3E,4(1X,3E)
1950 PRINT USING 1960:"2",X,Y(4),Y(5),F(5)
1960 IMAGE 1A,1X,3E,3(1X,3E)
1970 J1=J1+1
1980 T9(J1)=X
1990 G(J1)=Y(1)
2000 G1(J1)=Y(2)
2010 G2(J1)=F(2)
2020 P9(J1)=Y(3)
2030 G3(J1)=Y(4)
2040 G4(J1)=Y(5)
2050 G5(J1)=F(5)
2060 IF X=>X9 THEN 2100
2070 IF ABS(LOG(U)-LOG(Y(2)+Y(5)))<=3.0E-5 THEN 2100
2080 U=Y(2)+Y(5)
2090 GO TO 1830
2100 STOP
2110 PAGE
2120 IF F1=2 THEN 2400
2130 I=0
2140 K=I+1
2150 IF K>J1 THEN 2350
2160 PRINT USING 2170:"DATE ",Z$
2170 IMAGE 5A,1XA
2180 PRINT USING 2190:"PAGE NO. ",J9+1
```

```
2190 IMAGE 90,3D
2200 J9=J9+1
2210 PRINT
2220 PRINT "CHARACTERISTICS OF MOTION OF FRAGMENTS (NORMALIZED)"
2230 PRINT "      T-NORM          G              G'             G''          P-NORM"
2240 FOR I=K TO J1
2250 PRINT
2260 PRINT USING 2270:"1",T9(I),G(I),G1(I),G2(I),P9(I)
2270 IMAGE 1A,1X,3E,4(1X,3E)
2280 PRINT USING 2290:"2",T9(I),G3(I),G4(I),G5(I)
2290 IMAGE 1A,1X,3E,3(1X,3E)
2300 IF I=1C THEN 2140
2310 IF I/2=1A THEN 2140
2320 IF I/3=1A THEN 2140
2330 IF I/4=1A THEN 2140
2340 NEXT I
2350 STOP
2360 PAGE
2370 I=0
2380 K=I+1
2390 IF K>J1 THEN 2680
2400 PRINT USING 2410:"DATE ",Z$
2410 IMAGE 5A,1A
2420 PRINT USING 2430:"PAGE NO. ",J9+1
2430 IMAGE 9A,3D
2440 J9=J9+1
2450 IF F2=2 THEN 2680
2460 PRINT
2470 PRINT "CHARACTERISTICS OF MOTION OF FRAGMENTS (ENGLISH UNITS)"
2480 PRINT "      TIME          DIST.          VEL.          ACCEL.    PRESSURE"
2490 FOR I=K TO J1
2500 T1=0*T9(I)
2510 H1=X2*G(I)
2520 H2=X2/0*G1(I)
2530 H3=X2/(2*0)*G2(I)
```

```
2540 H4=P0*P9(I)
2550 H5=X2*G3(I)
2560 H6=X2/0*G4(I)
2570 H7=X2/(0*0)*G5(I)
2580 PRINT
2590 PRINT USING 2600:"1",T1,H1,H2,H3,H4
2600 IMAGE 1A,1X,5(3E)
2610 PRINT USING 2620:"2",T1,H5,H6,H7
2620 IMAGE 1A,1X,4(3E)
2630 IF I=10 THEN 2380
2640 IF I/2=10 THEN 2380
2650 IF I/3=10 THEN 2380
2660 IF I/4=10 THEN 2380
2670 NEXT I
2680 E5=0*X
2690 E6=X2*Y(1)
2700 E7=X2/0*Y(2)
2710 E8=X2/(0*0)*F(2)
2720 E9=P0*Y(3)
2730 S6=X2*Y(4)
2740 S7=X2/0*Y(5)
2750 S8=X2/(0*0)*F(5)
2755 IF F2=2 THEN 2820
2760 STOP
2770 PAGE
2780 PRINT USING 2790:"DATE ",Z$
2790 IMAGE 5A,10A
2800 PRINT USING 2810:"PAGE NO. ",J9+1
2810 IMAGE 9A,3D
2820 PRINT
2830 PRINT USING 2840:"FINAL VALUES","TIME= ",E5," SEC"
2840 IMAGE 12A,/,6A,3E,4A
2850 PRINT USING 2860:"DISTANCE #1= ",E6," IN (",E6*0.0254," METERS)"
2860 IMAGE 13A,3E,5A,3E,8A
2870 PRINT USING 2880:"VELOCITY #1= ",E7," IN/SEC (",E7*0.0254," M/SEC)"
```

```
2880 IMAGE 13A,3E,9A,3E,7A
2890 PRI USI 2900:"ACCEL. A1= ",E8," IN/SQ-SEC (",E8*0.0254," M/SQ-SEC)"
2900 IMAGE 11A,3E,12A,3E,10A
2910 PRINT USING 2920:"PRESSURE= ",E9," PSI (",E9*6894.757," PASCALS)"
2920 IMAGE 10A,3E,6A,3E,9A
2930 PRINT
2940 PRINT USING 2860:"DISTANCE A2= ",S6," IN (",S6*0.0254," METERS)"
2950 PRINT USING 2880:"VELOCITY A2= ",S7," IN/SEC (",S7*0.0254," M/SEC)"
2960 PRI USI 2900:"ACCEL. A2= ",S8," IN/SQ-SEC (",S8*0.0254," M/SQ-SEC)"
2970 REM
2980 REM-----------------------------------------------------------------
2990 REM SUBROUTINE RUNGE-KUTTA
3000 REM-----------------------------------------------------------------
3010 REM
3020 DIM Q(5)
3030 N2=N2+1
3040 IF N2=1 THEN 3080
3050 IF N2=2 THEN 3140
3060 IF N2=3 THEN 3160
3070 IF N2=4 THEN 3190
3080 FOR J=1 TO N
3090 Q(J)=0
3100 NEXT J
3110 A=0.5
3120 X=X+X8/2
3130 GO TO 3250
3140 A=0.29289321881
3150 GO TO 3250
3160 A=1.7071067812
3170 X=X+X8/2
3180 GO TO 3250
3190 FOR I=1 TO N
3200 Y(I)=Y(I)+X8*F(I)/6-Q(I)/3
3210 NEXT I
3220 N2=0
```

```
3230 S=2
3240 GO TO 3300
3250 FOR L=1 TO N
3260 Y(L)=Y(L)+Q*(X8*F(L)-Q(L))
3270 Q(L)=2*A*X8*F(L)+(1-3*A)*Q(L)
3280 NEXT L
3290 S=1
3300 RETURN
3310 END
```

APPENDIX E

MODEL ANALYSIS FOR FRAGMENT TRAJECTORIES

In order to generalize the analysis for determining the range of a flying fragment from a bursting spherical or cylindrical container, a model analysis was performed. The analysis for calculating the fragment range and the subsequent computer program (FRISB) are presented in detail in Baker, et al (1975). However, for the sake of clarity, a brief discussion of this analysis is presented below.

The equations for calculating the horizontal and vertical (X and Y) accelerations of a fragment are as follows:

$$\ddot{Y} = -g - \frac{A_D C_D \rho_o (\dot{X}^2 + \dot{Y}^2) \sin \alpha}{2M} + \frac{A_L C_L \rho_o (\dot{X}^2 + \dot{Y}^2) \cos \alpha}{M} \qquad \text{(E-1)}$$

$$\ddot{X} = \frac{-A_D C_D \rho_o (\dot{X}^2 + \dot{Y}^2) \cos \alpha}{2M} - \frac{A_L C_L \rho_o (\dot{X}^2 + \dot{Y}^2) \sin \alpha}{M} \qquad \text{(E-2)}$$

where

X	=	range, m
Y	=	altitude, m
$\dot{X}$	=	horizontal velocity
$\dot{Y}$	=	vertical velocity
$\ddot{X}$	=	horizontal acceleration
$\ddot{Y}$	=	vertical acceleration
C_D	=	drag coefficient
A_D	=	drag area
C_L	=	lift coefficient
A_L	=	lift area
ρ_o	=	density of air, kg/m^3
M	=	mass, kg
α	=	trajectory angle, rad
α_i	=	initial trajectory angle, rad
g	=	acceleration of gravity

at t = 0

$$\dot{X} = V_i \cos \alpha_i \tag{E-3}$$

$$\dot{Y} = V_i \sin \alpha_i \tag{E-4}$$

By solving the two second-order differential equations simultaneously, one can obtain velocity, and by numerically integrating the velocities, one can obtain the displacement, i.e., fragment range.

The first step in performing the model analysis was to list all of the pertinent physical parameters in the analysis, i.e., drag coefficient, drag area, lift coefficient, lift area, mass, etc., together with their fundamental dimensions, in a mass, length, and time (M, L, T) system. This list is presented in Table E-1. It should be noted that since the coefficient of lift, the lift area, and the density of air are interrelated as are the coefficient of drag, the drag area, and the density of air, they were combined as shown in Table E-1. These dimensional parameters were than combined into a lesser number of dimensionless groups (pi terms) by the methods of dimensional analysis as outlined in Baker, et al (1973). Table E-2 presents the dimensionless parameters in pi terms. It should be noted that this set of pi terms is not a unique set and that other combinations of pi terms are possible. It should also be noted that the number of pi terms equals the number of original dimensional parameter minus the number of fundamental dimensions.

For the special case of the fragment whose geometry is such that there are no lift forces acting on it, the fourth pi term listed on Table E-2 drops out of the model analysis.

TABLE E-1

LIST OF DIMENSIONAL PARAMETERS

Parameter	Dimension
$C_D A_D \rho_o$	M/L
$C_L A_L \rho_o$	M/L
V	L/T
M	M
g	L/T^2
R	L
α	-

TABLE E-2

DIMENSIONLESS PARAMETERS (PI TERMS)

π_1	α
π_2	$\frac{\rho_o C_D A_D V^2}{Mg}$
π_3	$\frac{\rho_o C_D A_D R}{M}$
π_4	$\frac{C_L A_L}{C_D A_D}$

APPENDIX F

ROCKETING OF STORAGE AND TRANSPORTATION VESSELS

In an accident involving propellant (propane, butane, etc.) storage systems, fragments are often generated and propelled by the force of an explosion. The fragments generated in an explosion which travel large distances typically are of much smaller mass than that of the storage vessel. However, in some instances, a large portion or portions of the vessel (greater than one-fourth) will break free intact and will travel larger distances than would be possible solely from the force of the explosion. These large fragments exhibit a rocketing behavior (see Appendix H) which results from the changing of the liquid propellant into a gas when the external pressure is released during the fracturing of the vessel. The gas escapes from the opening in the vessel in a manner similar to gas exiting a rocket motor and propels the, somewhat stabilized, fragment to great distances.

Figure F-1 schematically demonstrates the fragment rocketing process. After a portion of the vessel breaks off, the remaining portion of the tank emits gas out of its open end as the fluid in the tank vaporizes. This mass flows out of the aft end of the tank and produces a force F(t) in the direction opposite to the mass flow which varies as a function of time t, and the tank accelerates along a trajectory angle θ with respect to the horizontal axis (ground). The force of gravity Mg also acts on the vessel inhibiting its vertical ascent. Since every action has an equal and opposite reaction, the vertical and horizontal inertial forces $M\ddot{y}$ and $M\ddot{x}$, respectively, complete the simplified free-body diagram in Figure F-1. Note that for the purposes of this analysis, drag and lift forces are assumed to be much smaller than the thrust and gravitational forces and are ignored. It is also assumed that the "rocket" never changes its angle of attack θ during its flight.

The equations of motion for this simplified rocketing problem are then

$$M(t)g + M(t)\ddot{y} - F(t)\sin\theta = 0 \qquad \text{(F-1)}$$

and

$$M(T)\ddot{x} - F(t)\cos\theta = 0 \qquad \text{(F-2)}$$

Note that the mass (mass of the fragment and its contents) as well as the force, changes with time. From basic rocketry, the thrust F is

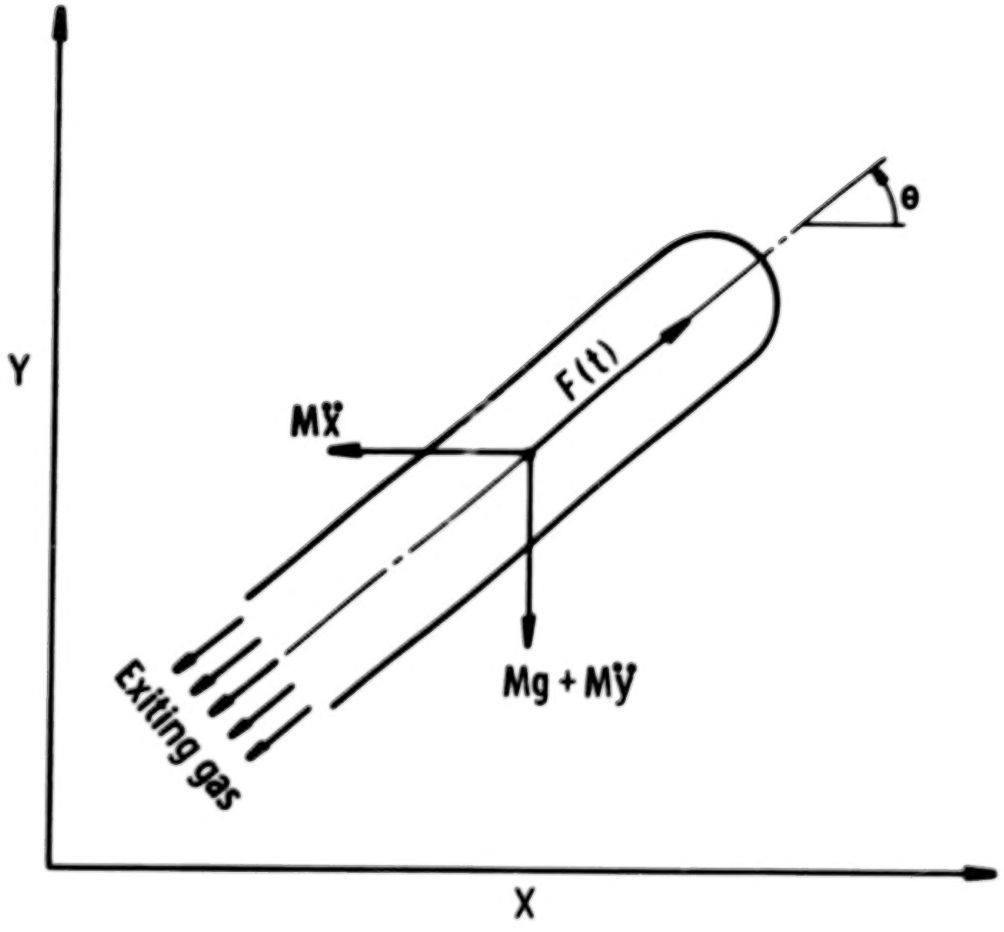

FIGURE F-1. ROCKETING FRAGMENT

$$F = A_e \left(\frac{U_e^2}{v_e g} + p_e - p_o \right) \qquad \text{(F-3)}$$

where

A_e = exit area
U_e = exit velocity
v_e = specific volume of the gas
g = gravity constant
p_e = exit pressure
p_o = atmospheric pressure

Balancing the energy in the system, one has

$$h_i + q = h_e + \frac{U_e^2}{2g} \qquad \text{(F-4)}$$

where

h_i = enthalpy of the gas at time t_i
q = energy expended in heating the gas
h_e = enthalpy of the gas at the nozzle (exit)

If the gas expansion is isentropic, $q = 0$, and Equation (F-4) reduces to

$$\frac{V_e^2}{2g} = h_i - h_e \qquad \text{(F-5)}$$

Flow continuity gives

$$\dot{w}v = AU \qquad \text{(F-6)}$$

where $\dot{w}$ is the mass flow rate.

To determine the fragment's trajectory, one starts with a wet vapor in a tank having known initial state conditions of pressure p_i, specific volume v_i, entropy s_i, and enthalpy h_i which can be determined from tables of thermodynamic properties. One next assumes isentropic expansion through the nozzle, That is,

$$s_{i+1} = s_e = s_i \qquad \text{(F-7)}$$

where s_e is the entropy of the gas at the nozzle (exit) and s_{i+1} is the entropy at time t_{i+1}.

When the backpressure p_o is less than the critical pressure p_c given by

$$p_c = 0.58\ p_i \tag{F-8}$$

the flow will be sonic and p_e in Equation (F-3) equals p_c. When the backpressure p_o is greater than the critical pressure p_c, then p_e equals p_o in Equation (F-3). Also, the pressure in the vessel at time t_{i+1} is given by

$$p_{i+1} = p_e \tag{F-9}$$

Equations (F-7) and (F-9) allow one to obtain the value for h_2, the enthalpy at time t_{i+1}, from the table of thermodynamic properties once one knows the values of s_e and p_e. Equation (F-5) gives U_e, and the thrust obtained by substitution into Equation (F-3). At the exit, Equation (F-6) gives

$$\dot{w}v_e = A_e U_e \tag{F-10}$$

where v_e is also obtained from the thermodynamic tables. In reality, the state variables of the gas within the tank change continuously, but, for computational purposes, we will assume quasi-steady flow. From Equation (F-10), one can obtain the mass flow rate $\dot{w}$ and calculate a new total mass of the fluid after a small time Δt from

$$M_{i+1} = M_i - \frac{\dot{w}}{g}\,\Delta t \tag{F-11}$$

After this time, a new specific volume can be determined from

$$v_{i+1} = \frac{V}{gM_{i+1}} \tag{F-12}$$

where V is the total volume of the fragment. Knowing v_{i+1} one can then obtain p_{i+1} from the table of thermodynamic properties of the gas and start a second iteration.

The above iteration process continues until backpressure p_o is greater than the critical pressure in Equation (F-8). Then the flow becomes subsonic and Equation (F-3) reduces to

$$F = A_e \frac{U_e^2}{v_e g} \tag{F-13}$$

Some thrusting will continue until the internal pressure p_n equals p_o, and the state of the gas in the vessel after n iterations lies on the p_o isobar.

To complete the process of calculating tank acceleration, velocity, and position one must solve Equations (F-1) and (F-2) during each iteration. The acceleration in the y and x directions is given by

$$\ddot{y}_i = \frac{F_i \sin\theta}{M_i} - g \tag{F-14}$$

and

$$\ddot{x}_i = \frac{F_i \cos\theta}{M_i} \tag{F-15}$$

Assuming the thrust F_i and mass of the vessel and enclosed substance M_i to be constant during the time step Δt, one can obtain velocity for time t_{i+1} by integrating Equations (F-14) and (F-15) obtaining

$$\dot{y}_{i+1} = \Delta t \left(\frac{F_i \sin\theta}{M_i} - g \right) + \dot{y}_i \tag{F-16}$$

and

$$\dot{x}_{i+1} = \Delta t \left(\frac{F_i \cos\theta}{M_i} \right) + \dot{x}_i \tag{F-17}$$

where

$$\dot{y}(o) = \dot{x}(o) = 0$$

Integrating Equations (F-16) and (F-17), one can obtain displacement from

$$y_{i+1} = \frac{\Delta t^2}{2}\left(\frac{F_i \sin\theta}{M_i} - g\right) + \dot{y}_i\,\Delta t + y_i \qquad \text{(F-18)}$$

and

$$x_{i+1} = \frac{\Delta t^2}{2}\left(\frac{F_i \cos\theta}{M_i}\right) + \dot{x}_i\,\Delta t + x_i \qquad \text{(F-19)}$$

where $y(o) = x(o) = 0$.

The thermodynamic processes followed by the expanding fluids are shown on the pressure-volume (p - v) plane and temperature-entropy (T - s) plane in Figures 1-1 and 1-2, respectively.

A computer program entitled "THRUST" was written to perform computations for determining acceleration, velocity, and position of a thrusting fragment as a function of time, as explained. The program was written in BASIC and was run on a Tektronix 4051 microprocessor. The program was exercised using the state properties of propane gas to compare with measurements made after propane/butane accidents (Appendix H). The program was written with enough flexibility to allow for rocketing calculations of large portions of vessels containing other types of gases. To change the contained gas, one merely inputs the state variables of the appropriate gas at the beginning of the program. Linear interpolation was used to estimate values of the state variables between those acquired from the thermodynamic properties tables [Din (1962)]. Table F-1 contains a list of the program variables, a listing of the program, and sample input and output.

TABLE F-1

COMPUTER PROGRAM ENTITLED "THRUST" IN BASIC

FUNCTION: This program computes the acceleration, velocity, and displacement of a fragment containing a vaporizing liquid. It is assumed that a large portion of a vessel containing a liquid/gas mixture in equilibrium at greater than atmospheric pressure separates from the rest of the storage vessel. As the liquid underpressure converts to a gas when exposed to atmospheric pressure, thrust is produced causing the fragment to "rocket".

INPUT-OUTPUT CONSIDERATIONS: This program is written in BASIC computer language and is compatible in its existing form with a Tektronix 4051 microprocessor. Thermodynamic properties of the gas to be considered are stored in arrays on files using the program for storing data arrays contained in Table F-2. Input data follow.

A. Thermodynamic properties of the liquid/vapor:

1) entropy (S) in cal/mole, °K
2) enthalpy (H) in cal/mole
3) specific volume (V) in cm^3/mole

B. Vessel characteristics:

1) launch angle (A1) in degrees
2) volume of the vessel (V0) in cubic meters
3) volume of the fragment enclosure (V1) in cubic meters
4) exit area (A) in square meters
5) mass of the fragment (M) in kilograms

C. Initial conditions of the liquid/vapor:

1) initial pressure (P1) in Pascals
2) volume of the liquid (V8) in the vessel in cubic meters
3) volume of the vapor (V9) in the vessel in cubic meters

D. Dynamic variable:

1) time step (T) in seconds

BLANK PAGE

VARIABLES

The program variable, identifying variable in the derivation above, definition, and units of variables in this program follow.

PROGRAM VARIABLE	VARIABLE	DEFINITION	UNITS
S	s	Array of entropy liquid/vapor values for propane	cal/mole, °K
H	h	Array of enthalpy liquid/vapor values for propane	cal/mole
V	v	Array of specific volume liquid/vapor values for propane	cm^3/mole
A1	--	Array for storing launch angles to be tested	degrees
P1	p1	Initial pressure	Pa
VØ		Volume of the container	m^3
V1		Volume of fragment enclosure	m^3
V8		Volume of liquid in the container	m^3
V9		Volume of vapor in the container	m^3
A		Exit area	m^2
M		Mass of fragment	kg
T		Time step	s
BØ	θ	Current launch angle	degrees
J	--	Counter used once to determine mass of gas and specific volume of frag portion immediately after breakup	--
PØ	P_o	Atmospheric pressure	Pa
E1		Horizontal velocity at current time	m/s
E1		Vertical velocity at current time	m/s
T1		Current time	s
N	--	Unit conversion constant for interpolations in specific volume	J · mole/cal · kg
NI	--	Unit conversion constant for interpolations in entropy or enthalpy	m^3 · mole/cm^3 · kg
P8		Nondimensional internal pressure	--
V3		Interpolated liquid specific volume	m^3/kg
V4		Interpolated vapor specific volume	m^3/kg
M1		Initial mass of gas/liquid	kg
V2		Initial specific volume	m^3/kg
Q1		Initial quality (based on specific volume)	--

PROGRAM VARIABLE	VARIABLE	DEFINITION	UNITS
P3		Pressure at nozzle	Pa
Q8		Quality after pressure release (based on specific volume)	--
Q9		Quality after pressure release (based on entropy)	--
D1		Stabilization time (no more thrust)	s
D2		Stabilization distance (no more thrust)	m
D3		Stabilization height (no more thrust)	m
T2		Time from stabilization until maximum height is reached	l
H1		Maximum height reached by fragment	m
Y3		Final vertical velocity	m/s
T3		Time from point of maximum height to the end of flight	s
T4		Total time fragment is in air	s
D		Total range of the thrusting fragment	m
X9		Horizontal (X) position of fragment at maximum height	m

PROGRAM VARIABLE	VARIABLE	DEFINITION	UNITS
M2		Mass of gas/liquid in thrusting portion of tank	kg
S3		Interpolated liquid entropy	J/kg
S4		Interpolated vapor entropy	J/kg
S5		Calculated entropy	J/kg
H3		Interpolated liquid enthalpy	J/kg
H4		Interpolated vapor enthalpy	J/kg
H5		Calculated enthalpy	J/kg
C		Constant (1/0.58)	--
P9		Nondimensional exit pressure	--
S6		Interpolated liquid entropy at nozzle (exit)	J/kg
S7		Interpolated vapor entropy at nozzle (exit)	J/kg
Q2		Quality at nozzle (exit)	--
H6		Interpolated liquid enthalpy at nozzle (exit)	J/kg
H7		Interpolated vapor enthalpy at nozzle (exit)	J/kg
H9		Calculated enthalpy at nozzle (exit)	J/kg
V6		Interpolated liquid specific volume at nozzle	m^3/kg
V7		Interpolated vapor specific volume at nozzle	m^3/kg
V5		Calculated specific volume at nozzle	m^3/kg
U		Exit velocity	m/s
F		Thrust	N
W		Mass flow rate	kg/s
X2		Horizontal acceleration	m/s^2
Y2		Vertical acceleration	m/s^2
X1		New horizontal velocity	m/s
Y1		New vertical velocity	m/s
X		Horizontal distance (range)	m
Y		Vertical distance (height)	m
P2		Pressure in container	Pa

COMPUTER PROGRAM LISTING AND SAMPLE OUTPUT

```
100 REM PROGRAM FOR STORING DATA ARRAYS--------------------
110 PAGE
120 INIT
130 DIM A(18,4)
140 FOR I=1 TO 18
150 FOR J=1 TO 4
160 PRINT "A(";I;",";J;")=?";
170 INPUT A(I,J)
180 NEXT J
190 NEXT I
200 PAGE
210 FOR I=1 TO 18
220 PRINT USING 230:A(I,1),A(I,2),A(I,3),A(I,4)
230 IMAGE 4(6D.2D,1X)
240 NEXT I
250 STOP
260 REM MAKE CORRECTIONS ABOVE OR STORE DATA BELOW----------
270 PRINT "DATA STORAGE FILE?";
280 INPUT F
290 FIND F
295 FOR I=1 TO 18
300 PRINT @33:A(I,1),A(I,2),A(I,3),A(I,4)
301 NEXT I
305 CLOSE
310 STOP
320 REM CHECK STORED DATA FILE IN REST OF PROGRAM----------
330 PAGE
340 INIT
350 PRINT "FILE NO.?";
360 INPUT G
370 FIND G
375 FOR I=1 TO 18
380 INPUT @33:A(I,1),A(I,2),A(I,3),A(I,4)
385 NEXT I
390 GO TO 210
400 END
```

```
100 REM THRUST--THIS PROGRAM CALCULATES THE ACCELERATION,VELOCITY,AND
110 REM       DISTANCE TRAVELED BY A THRUSTING LIQUID
120 REM       HYDROCARBON STORAGE TANK
130 REM
140 PAGE
150 INIT
160 SET DEGREES
170 REM INPUT ENTROPY(S),ENTHALPY(H), AND SPECIFIC VOLUME(V) LIQUID/
180 REM         VAPOR VALUES
190 DIM S(18,4),H(18,4),V(18,4),A1(5)
200 FIND 5
210 INPUT @33:S
220 FIND 6
230 INPUT @33:H
240 FIND 7
250 INPUT @33:V
260 REM INPUT INITIAL CONDITIONS
261 DATA 5,10,15,30,45
262 READ A1(1),A1(2),A1(3),A1(4),A1(5)
270 PRINT "INITIAL PRESSURE (PA) = ";
280 INPUT P1
290 PRINT "VOLUME OF CONTAINER (CU M) = ";
300 INPUT V0
310 PRINT "VOLUME OF FRAG ENCLOSURE (CU M) = ";
320 INPUT V1
330 PRINT "VOLUME OF LIQUID (CU M) = ";
340 INPUT V8
350 PRINT "VOLUME OF VAPOR (CU M) = ";
360 INPUT V9
370 PRINT "EXIT AREA (SQ M) = ";
380 INPUT A
390 PRINT "MASS OF FRAG (KG) = ";
400 INPUT M
401 A$="DATE "
```

```
402 B$="PAGE NO. "
403 PRINT "INPUT DATE";
404 INPUT Z$
430 PRINT "TIME STEP (SEC) = ";
440 INPUT T
450 FOR J1=1 TO 5
460 B0=A1(J1)
470 Z=J1
705 J=0
710 X=0
720 Y=0
730 P0=101353
740 E1=0
750 E2=0
760 T1=0
860 N=94.96
870 N1=44094
880 P8=P1/P0
890 FOR I=1 TO 18
900 IF V(I,1)=>P8 THEN 920
910 NEXT I
920 V3=(V(I-1,3)+(P8-V(I-1,1))/(V(I,1)-V(I-1,1))*(V(I,3)-V(I-1,3)))/N1
930 V4=(V(I-1,4)+(P8-V(I-1,1))/(V(I,1)-V(I-1,1))*(V(I,4)-V(I-1,4)))/N1
940 REM
950 REM DETERMINE INITIAL MASS-F,GAS,SPECIFIC VOLUME,QUALITY,AND
960 REM             MASS OF GAS WITH FRAG
970 REM
980 M1=V8/V3+V9/V4
990 V2=V0/M1
1000 Q1=(V2-V3)/(V4-V3)
1010 M2=V1/V2
1020 REM
1030 REM DETERMINE ENTROPY
1040 REM
1070 S3=(S(I-1,3)+(P8-S(I-1,1))/(S(I,1)-S(I-1,1))*(S(I,3)-S(I-1,3)))*N
```

BLANK PAGE

BLANK PAGE

```
1080 S4=(S(I-1,4)+(P8-S(I-1,1))/(S(I,1)-S(I-1,1))*(S(I,4)-S(I-1,4)))*N
1090 S5=S3+Q1*(S4-S3)
1100 IF P8<1 THEN 1582
1110 IF E1=0 THEN 1210
1120 FOR I=1 TO 18
1130 IF V(I,1)=>P8 THEN 1150
1140 NEXT I
1150 V3=(V(I-1,3)+(P8-V(I-1,1))/(V(I,1)-V(I-1,1))*(V(I,3)-V(I-1,3)))/N1
1160 V4=(V(I-1,4)+(P8-V(I-1,1))/(V(I,1)-V(I-1,1))*(V(I,4)-V(I-1,4)))/N1
1170 Q1=(V2-V3)/(V4-V3)
1180 REM
1190 REM DETERMINE INITIAL ENTHALPY
1200 REM
1210 H3=(H(I-1,3)+(P8-H(I-1,1))/(H(I,1)-H(I-1,1))*(H(I,3)-H(I-1,3)))*N
1220 H4=(H(I-1,4)+(P8-H(I-1,1))/(H(I,1)-H(I-1,1))*(H(I,4)-H(I-1,4)))*N
1230 H5=H3+Q1*(H4-H3)
1240 C=1/0.58
1250 IF P8<=C THEN 1280
1260 P9=0.58*P8
1270 GO TO 1290
1280 P9=1
1290 FOR I=1 TO 18
1300 IF S(I,1)=>P9 THEN 1356
1310 NEXT I
1320 REM
1330 REM DETERMINE QUALITY AT NOZZLE (EXIT)
1340 REM
1350 S6=(S(I-1,3)+(P9-S(I-1,1))/(S(I,1)-S(I-1,1))*(S(I,3)-S(I-1,3)))*N
1360 S7=(S(I-1,4)+(P9-S(I-1,1))/(S(I,1)-S(I-1,1))*(S(I,4)-S(I-1,4)))*N
1370 Q2=(S5-S6)/(S7-S6)
1380 REM
1390 REM DETERMINE ENTHALPY AT NOZZLE (EXIT)
1400 REM
1410 H6=(H(I-1,3)+(P9-H(I-1,1))/(H(I,1)-H(I-1,1))*(H(I,3)-H(I-1,3)))*N
1420 H7=(H(I-1,4)+(P9-H(I-1,1))/(H(I,1)-H(I-1,1))*(H(I,4)-H(I-1,4)))*N
```

```
1430 H9=H6+Q2*(H7-H6)
1440 REM
1450 REM DETERMINE SPECIFIC VOLUME AT NOZZLE (EXIT)
1460 REM
1470 V6=(V(I-1,3)+(P9-V(I-1,1))/(V(I,1)-V(I-1,1))*(V(I,3)-V(I-1,3)))/N1
1480 V7=(V(I-1,4)+(P9-V(I-1,1))/(V(I,1)-V(I-1,1))*(V(I,4)-V(I-1,4)))/N1
1490 V5=V6+Q2*(V7-V6)
1500 REM DETERMINE EXIT VELOCITY,THRUST,AND MASS FLOW RATE
1510 REM
1520 U=SQR(2*(H5-HS))
1530 F=A*(U*U/V5+(P9*P0-P0))
1540 W=A*U/V5
1550 M2=M2-W*T
1560 REM
1570 REM DETERMINE ACCELERATION
1580 REM
1581 IF P8>1 THEN 1590
1582 P8=1
1583 F=0
1590 X2=F*COS(B0)/(M+M2)
1600 Y2=F*SIN(B0)/(M+M2)-9.80665
1610 REM
1620 REM DETERMINE VELOCITY
1630 REM
1640 X1=F*COS(B0)/(M+M2)*T+E1
1650 Y1=(F*SIN(B0)/(M+M2)-9.80665)*T+E2
1660 REM
1670 REM DETERMINE POSITION
1680 REM
1690 X=F*COS(B0)/(M+M2)*T*T/2+E1*T+X
1700 Y=(F*SIN(B0)/(M+M2)-9.80665)*T*T/2+E2*T+Y
1710 P2=P8*P0
1720 P3=P9*P0
1730 T1=T1+T
1771 E1=X1
```

```
1772 E2=Y1
1775 IF F=0 THEN 2091
1780 REM
1790 REM DETERMINE NEW MASS OF GAS AND SPECIFIC VOLUME OF FRAG PORTION
1800 REM
1810 IF Y<=0 THEN 2091
1811 IF P8=1 THEN 1590
1820 V2=V1/M2
1825 IF J>0 THEN 1910
1830 FOR J=1 TO 18
1840 IF V(J,1)=>P8 THEN 1910
1850 NEXT J
1860 REM
1870 REM DETERMINE PRESSURE AT WHICH QUALITIES Q8(SPECIFIC VOLUME) AND
1880 REM             Q9(ENTROPY) ARE EQUAL--THIS IS THE NEW INTERNAL
1890 REM             PRESSURE.
1900 REM
1910 Q8=(V2-V(J,3))/(V(J,4)-V(J,3))
1920 Q9=(S5-S(J,3))/(S(J,4)-S(J,3))
1930 IF V(J,1)<=0.5 THEN 1950
1940 GO TO 1960
1950 P8=1
1951 GO TO 1100
1960 IF X>0 THEN 1970
1961 P8=V(J,1)
1970 IF ABS(Q9-Q8)<=1.0E-3 THEN 1100
1971 IF P8=>2 THEN 1980
1972 P8=P8-T*0.1
1973 GO TO 1990
1980 P8=P8-T
1990 IF P8>V(J-1,1) THEN 2020
2000 J=J-1
2010 GO TO 1910
2020 V6=(V(J,3)-(V(J,1)-P8)/(V(J,1)-V(J-1,1))*(V(J,3)-V(J-1,3)))/44094
2030 V7=(V(J,4)-(V(J,1)-P8)/(V(J,1)-V(J-1,1))*(V(J,4)-V(J-1,4)))/44094
```

```
2040 Q8=(V2-V6)/(V7-V6)
2050 S6=(S(J,3)-(S(J,1)-P8)/(S(J,1)-S(J-1,1))*(S(J,3)-S(J-1,3)))*94.96
2060 S7=(S(J,4)-(S(J,1)-P8)/(S(J,1)-S(J-1,1))*(S(J,4)-S(J-1,4)))*94.96
2070 Q9=(S5-S6)/(S7-S6)
2080 IF ABS(Q9-Q8)<=1.0E-3 THEN 1100
2090 GO TO 1971
2091 D1=T1
2092 D2=X
2093 D3=Y
2100 PAGE
2140 PRINT A$;Z$;
2150 PRINT
2160 PRINT B$;Z;
2180 PRINT
2190 PRINT "INITIAL CONDITIONS"
2200 PRINT
2210 PRINT USING 2220:"INITIAL PRESSURE",P1,"PASCALS"
2220 IMAGE 16A,8X,4E,1X,7A
2230 PRINT USING 2240:"VOLUME OF CONTAINER",V0,"CU M"
2240 IMAGE 19A,5X,4E,1X,4A
2250 PRINT USING 2260:"VOLUME OF FRAG ENCLOSURE",V1,"CU M"
2260 IMAGE 24A,4E,1X,4A
2270 PRINT USING 2280:"VOLUME OF LIQUID",V8,"CU M"
2280 IMAGE 16A,8X,4E,1X,4A
2290 PRINT USING 2300:"VOLUME OF VAPOR",V9,"CU M"
2300 IMAGE 15A,9X,4E,1X,4A
2310 PRINT USING 2320:"EXIT AREA",A,"SQ M"
2320 IMAGE 9A,15X,4E,1X,4A
2330 PRINT USING 2340:"MASS OF FRAG",M,"KG"
2340 IMAGE 12A,12X,4E,1X,4A
2350 PRINT USING 2360:"LAUNCH ANGLE",B0,"DEGREES"
2360 IMAGE 12A,12X,4E,1X,7A
2361 PRINT USING 2362:"TIME STEP",T,"SEC"
2362 IMAGE 9A,15X,4E,1X,3A
2370 T2=E2/9.80665
```

```
2380 H1=Y+0.5*E2*T2
2390 Y3=SQR(2*9.80665*H1)
2400 T3=Y3/9.80665
2410 T4=T1+T2+T3
2420 D=X+E1*(T2+T3)
2425 X9=D-E1*T3
2430 PRINT
2440 PRINT "FINAL VALUES";
2450 PRINT
2451 PRINT USING 2452:"STABILIZATION X-VEL.",E1,"M/SEC"
2452 IMAGE 20A,4X,4E,1X,5A
2453 PRINT USING 2452:"STABILIZATION Y-VEL.",E2,"M/SEC"
2454 PRINT USING 2455:"STABILIZATION TIME",D1,"SEC"
2455 IMAGE 18A,6X,4E,1X,3A
2456 PRINT USING 2457:"STABILIZATION DISTANCE",D2,"M"
2457 IMAGE 22A,2X,4E,1X,1A
2458 PRINT USING 2459:"STABILIZATION HEIGHT",D3,"M"
2459 IMAGE 20A,4X,4E,1X,1A
2460 PRINT USING 2470:"TOTAL RANGE",D,"M"
2470 IMAGE 11A,13X,4E,1X,1A
2480 PRINT USING 2490:"FINAL VERT. VELOCITY",Y3,"M/SEC"
2490 IMAGE 20A,4X,4E,1X,5A
2500 PRINT USING 2490:"FINAL HORZ. VELOCITY",E1,"M/SEC"
2510 PRINT USING 2520:"TOTAL TIME",T4,"SEC"
2520 IMAGE 10A,14X,4E,1X,3A
2530 PRINT USING 2540:"MAXIMUM HEIGHT",H1,"M"
2540 IMAGE 14A,10X,4E,1X,1A
2541 PRINT USING 2542:"X POSITION AT MAX.HT.",X9,"M"
2542 IMAGE 21A,3X,4E,1X,1A
2543 PRINT USING 2544:"TIME AT MAX.HT.",T1+T2,"SEC"
2544 IMAGE 15A,9X,4E,1X,3A
2545 PRINT USING 2546:"INTERNAL PRESSURE",P2,"PASCALS"
2546 IMAGE 17A,7X,4E,1X,7A
2550 COPY
2560 NEXT J1
2570 END
```

DATE 9/30/77
PAGE NO. 1
INITIAL CONDITIONS

INITIAL PRESSURE	7.0120E+005	PASCALS
VOLUME OF CONTAINER	3.8020E+001	CU M
VOLUME OF FRAG ENCLOSURE	2.8230E+001	CU M
VOLUME OF LIQUID	3.3100E+001	CU M
VOLUME OF VAPOR	4.9160E+000	CU M
EXIT AREA	3.7500E+000	SQ M
MASS OF FRAG	3.8850E+003	KG
LAUNCH ANGLE	5.0000E+000	DEGREES
TIME STEP	5.0000E-003	SEC

FINAL VALUES

STABILIZATION X-VEL.	1.9383E+002	M/SEC
STABILIZATION Y-VEL.	6.0238E+000	M/SEC
STABILIZATION TIME	1.1150E+000	SEC
STABILIZATION DISTANCE	1.0779E+002	M
STABILIZATION HEIGHT	3.3347E+000	M
TOTAL RANGE	4.2617E+002	M = 1398 ft
FINAL VERT. VELOCITY	1.0084E+001	M/SEC
FINAL HORZ. VELOCITY	1.9383E+002	M/SEC
TOTAL TIME	2.7576E+000	SEC
MAXIMUM HEIGHT	5.1848E+000	M = 17.01 ft
X POSITION AT MAX.HT.	2.2686E+002	M
TIME AT MAX.HT.	1.7293E+000	SEC
INTERNAL PRESSURE	1.0135E+005	PASCALS

actual range = 1029 ft = before first hitting ground

TABLE F-2

PROGRAM FOR STORING DATA ARRAYS

Function: This program stores data arrays in files on tape. The program is written in BASIC and is compatible with a Tektronix 4051 microprocessor.

BLANK PAGE

BLANK PAGE

```
100 REM PROGRAM FOR STORING DATA ARRAYS--------------------
110 PAGE
120 INIT
130 DIM A(18,4)
140 FOR I=1 TO 18
150 FOR J=1 TO 4
160 PRINT "A(";I;",";J;")=?";
170 INPUT A(I,J)
180 NEXT J
190 NEXT I
200 PAGE
210 FOR I=1 TO 18
220 PRINT USING 230:A(I,1),A(I,2),A(I,3),A(I,4)
230 IMAGE 4(6D.2D,1X)
240 NEXT I
250 STOP
260 REM MAKE CORRECTIONS ABOVE OR STORE DATA BELOW----------
270 PRINT "DATA STORAGE FILE?";
280 INPUT F
290 FIND F
295 FOR I=1 TO 18
300 PRINT @33:A(I,1),A(I,2),A(I,3),A(I,4)
301 NEXT I
305 CLOSE
310 STOP
320 REM CHECK STORED DATA FILE IN REST OF PROGRAM----------
330 PAGE
340 INIT
350 PRINT "FILE N0.?";
360 INPUT G
370 FIND G
375 FOR I=1 TO 18
380 INPUT @33:A(I,1),A(I,2),A(I,3),A(I,4)
385 NEXT I
```

APPENDIX G

MODEL ANALYSIS FOR ROCKETING OF STORAGE AND TRANSPORTATION VESSELS

The model analysis used here is patterned after the techniques explained in Baker, Westine and Dodge (1973). The purpose of the model analysis is to devise a method of consolidating the results of the computer runs made to predict the ranges of fragments which exhibit "rocketing" behavior as explained in Appendix F.

To conduct the model analysis, it is necessary to list all of the physical parameters which are indigenous to the problem. It is better to overdefine the important parameters initially than to leave out potentially pertinent items. Unnecessary parameters or parameters which weakly affect the results can be eliminated after the nondimensional pi terms are ascertained. A listing of these parameters is contained in Table G-1 which includes vessel characteristics, gas characteristics, and response parameters. Since we will ignore drag and lift forces (see Appendix F), the pertinent vessel characteristics can be limited to the internal volume V of the fragment, the exit area A, the mass M of the fragment, and the initial launch angle α. Relevant gas parameters are the ratio of specific heats γ of the gas, the ideal gas constant R_M, the temperature T of the liquid/vapor at rupture, the volume of vapor to volume of liquid ratio V_v/V_l, the pressure P of the gas at rupture, and the atmospheric pressure p_a. The acceleration g due to gravity is also important since it affects the vertical travel of the thrusting fragment. Pertinent response terms are the velocity u of the fragment and the distance X traveled by the fragment.

There are nine pi terms or nondimensional ratios which can be created from the above 13 parameters. Table G-2 presents one possible list of these nine pi terms. This list of nine pi terms can be reduced by making some simplifying assumptions. Since we were unable to readily locate the thermodynamic properties of butane and since most of the accidents examined involved propane for which we did have the thermodynamic properties, only rocketing due to the expansion of propane was considered. Since the ratio of specific heats γ in this case is constant, π_1 can be eliminated. Since the gas is constant, R_M is constant. The acceleration g due to gravity is nearly constant on earth and is also contained in π_6, temperature T is proportional to pressure P [illegible] V which are contained in π_5, π_6, π_7, and π_8. Thus π_2 can be [illegible]minated. If one assumes that atmospheric pressure p_a is con[illegible]nt and one observes that internal pressure P is contained in π_6, π_8 can also be disregarded. Finally, we are not concerned with the velocity u of the fragment, a response term, and the volume V of the fragment is contained in π_6. Thus π_7 can also be eliminated. No other simplifications are readily discernible.

TABLE G-1

Pertinent Parameters for Rocketing Fragments

Symbol	Description	Dimensions*
V	internal volume of the fragment	L^3
A	exit area	L^2
M	mass of the fragment	FT^2/L
α	launch angle	--
γ	ratio of specific heats of the gas	--
R_M	ideal gas constant (adjusted for molecular weight	$L^2/T^2\theta$
T	temperature of the liquid/vapor at rupture	θ
V_v/V_l	volume of vapor to volume of liquid ratio	--
P	pressure of the gas at rupture	F/L^2
P_a	atmospheric pressure	F/L^2
g	acceleration due to gravity	L/T^2
u	velocity of the fragment	L/T
X	distance traveled by the fragment	L

* L = length

F = force

T = time

θ = temperature

TABLE G-2

LIST OF PI TERMS FOR ROCKETING FRAGMENT

π_1	γ
π_2	$\frac{R_M T}{g V^{1/3}}$
π_3	V_v / V_l
π_4	α
π_5	$\frac{A}{V^{2/3}}$
π_6	$\frac{Mg}{PV^{2/3}}$
π_7	$\frac{u}{g^{1/2} V^{1/6}}$
π_8	$\frac{P}{P_a}$
π_9	$\frac{X}{V^{1/3}}$

Therefore, one finds that the distance traveled by a fragment experiencing rocketing due to the expansion of a single gas (propane in this case), depends upon the relative volumes of the vapor and liquid at fracture (V_v/V_l), the launch angle (α), a vent area to fragment volume ($A/V^{2/3}$), and a ratio of inertial force to the force of the gas inside the vessel ($Mg/PV^{2/3}$). Representing these observations in equation form, one has

$$\frac{X}{V^{1/3}} = f\left(\frac{V_v}{V_l},\ \alpha,\ \frac{A}{V^{2/3}},\ \frac{Mg}{PV^{2/3}}\right) \qquad \text{(G-1)}$$

Several computer runs were made to simulate actual accidents recorded in accident reports Because these accidents were not experimental tests, some parameters such as launch angle and internal pressure of the tank at rupture had to be assumed. In spite of these obvious obstacles, the predicted values for distance traveled by the fragments, in most instances, correlated well with accident report observations. A summary of these comparative computer runs is contained in Table G-3. When one observes the sensitivity of fragment range to launch angle in this table and in Table 4-2 and keeps in mind the limitations on predicting launch angle from the accident reports, one can readily appreciate the apparent accuracy of the computer program.

Due to the complexity of the thrusting process (explained in greater detail in Appendix F) and limitations on the number of computer runs performed, no reduction of the five parameter space described by Equation (G-1) was readily apparent. Until further analysis can be performed for propane and other gases, it is recommended that the reader use the results contained in Table G-3 and Table 4-2 where appropriate or actually exercise the computer program.

TABLE G-3. COMPARISON OF COMPUTER PREDICTED RANGES AND REPORTED RANGES FOR ACCIDENTS INVOLVING ROCKETING FRAGMENTS

EXAMPLE NUMBER	SOURCE OF ACTUAL DATA	INITIAL PRESSURE (P_o)	VOLUME OF CONTAINER (m^3)	VOLUME OF FRAGMENT ENCLOSURE (m^3)	VOLUME OF LIQUID BEFORE RUPTURE (m^3)	VOLUME OF VAPOR BEFORE RUPTURE (m^3)	EXIT AREA (m^2)	MASS OF FRAGMENT (kg)	LAUNCH ANGLE (degrees)	CALCULATED IMPACT VELOCITY (m/s)	CALCULATED RANGE (m)	ACTUAL RANGE (m)	PERCENT DIFFERENCE IN RANGE (%)	BEST ESTIMATE FOR LAUNCH ANGLE (degrees)
1	NTSB-HAR-76-4 4/29/75	701,197	38.02	28.23	33.10	4.916	3.75	3885	5	194	4[illegible]6	314	36	5
2	NTSB-HAR-73-4 9/21/72	1,034,214	37.85	30.32	27.29	10.56	3.41	5087		189	471	398	18	5
3	NTSB-HAR-73-4 9/21/72	1,034,214	37.85	1.28	27.29	10.56	3.41	652	5	94	154	165	-6.7	5
4a	Propane Tank Explosion in San Antonio	1,378,951	1.8927	0.5513	1.586	0.3067	2.336	171	5	159	450	123	266	5-10
4b	Propane Tank Explosion in San Antonio	1,378,951	1.8927	0.5513	1.586	0.3067	2.336	171	10	154	8[illegible]	123	-588	5-10
4c	Propane Tank Explosion in San Antonio	1,378,951	1.8927	0.2002	1.586	0.3067	0.6567	171	5	72	90	123	-27	5-10
4d	Propane Tank Explosion in San Antonio	1,378,951	1.8927	0.2002	1.586	0.3067	0.6567	171	10	71	179	123	46	5-10

APPENDIX H

Accident Data and Statistical Fitting to Fragment Data

A literature search was conducted in which accident reports and other available, related data sources were reviewed for information on characteristics of fragments and pressure waves of bursting thick-wall, compressed fluid storage and transportation vessels. Fluids and gases considered in the survey were propane, anhydrous ammonia, oxygen, argon, air and propylene. Organizations and contractors contributing sources included the National Transportation Safety Board, Naval Surface Weapons Center, NASA Langley Research Center, Department of Transportation, National Technical Information Service and Ballistic Research Laboratory. Also, an incident which occurred in San Antonio, Texas during the accumulation of data, in which a propane storage tank exploded, was personally investigated by two staff members, W. E. Baker and L. M. Vargas, for information on energy release. The missile map developed as a result of this investigation proved very useful in determining effects of fragment impact. Data obtained from this literature were organized in a logical manner for the subsequent analysis. Records of the data include the reference and date of the explosion; the quantity of the explosion source; the estimated energy release; the shape, volume, mass, material and dimensions of the container vessel; the number of fragments; the masses, ranges, trajectory elevations (if given), drag coefficients and shapes of the fragments; and any additional pertinent information. Each vessel is assigned an identifying number. Twenty-five vessel explosions form the data base. These data are given in Tables H-1 and H-2.

In order to uncover any trends in terms of different variables which affect the chracteristics and effects of fragment impact and pressure waves, all the data were tabulated in terms of absolute numbers, percentiles, means, standard deviations and variations in information. The tabulations and analyses of different combinations of variables follow. A bibliography of sources utilized is also included.

Derivation of Fragment Range Distributions

(Figures 4-6 and 4-7)

The fragment range data for each of the six event groups (see Table 4-3) were sorted in ascending order. For event groups 1, 2, 3, 4 and 6, the values for the range for the 10th to the 90th percentile in 10% steps were identified. For event group 5, the values from the 14.3 percentile to the 85.7 percentile in 14.3% steps were identified. Table H-3 is a listing of these values.

TABLE H-1. LISTING OF EXPLOSION EVENT SOURCE AND VESSEL DATA

I.D. NUMBER	REFERENCE	EXPLOSION SOURCE				VESSEL				
		MATERIAL	QUANTITY (M^3 OR KG)	OTHER DATA	ESTIMATED ENERGY (JOULES)	SHAPE	DIMENSIONS	VOLUME (M^3)	MASS (KG)	MATERIAL
1	NTSB-RAB-	Propane	62,700	Temp:	$5.417 \times 10^{}$	Railroad Tank	Inside	32.07m	115,000 kg	A 212Gr B Steel
	72-2		kg =	83°F	Joules	Car #27 with	diameter			
	Train		31,300 m^3	Specific		Hemispherical	2.44m & 1.2m			
	Derailment			Gravity:		heads	Surface			
	6-21-70			0.507			Area:			
							181.1 m^2			
							Thickness			
							sheets 1.91			
							0.02m			
							Outage			
							0.1m			
							Length: 21m			
2	NTSB	Propane	66,900 kg	Temp: 66°F	3.934×10^{5}	Tank car #28	Inside	20.71 m^3	142,000 kg	TC128Gr B Steel
	RAB-72-2		= 32,400 m^3	Specific	Joules	with	Diameter:			
	Train			Gravity:		Hemispherical	2.44m			
	Derailment			0.507		heads	Surface			
	6-21-70						Area:			
							181.1 m^2			
							Thickness			
							sheets			
							0.01m			
							O.D. =			
							Outage 0.8m			
							Length:			
							19.4m			

TABLE H-1. LISTING OF EXPLOSION EVENT SOURCE AND VESSEL DATA (CONT.)

I.D. NUMBER	REFERENCE	EXPLOSION SOURCE				VESSEL				
		MATERIAL	QUANTITY (M^3 OR KG)	OTHER DATA	ESTIMATED ENERGY (JOULES)	SHAPE	DIMENSIONS	VOLUME (M^3)	MASS (KG)	MATERIAL
3	NTSB-RAR-72-2 Train Derailment 6-21-70	Propane	64,800 kg = 32,300m^3	Temp = 78°F Specific Gravity: 0.507	1.272×10^5 Joules	Tank Car #30 with Hemispherical heads	Inside Diameter: 3.01m Surface Area: 182.18m^2 Thickness sheets: 0.019m, 0.02m Outage: 0.38m Length:19.3m	4.19m^3	37,800 kg	TC128B steel
4	NTSB-RAR-72-2 Train Derailment 6-21-70	Propane	64,600 kg = 32,200m^3	Temp: 80°F Specific Gravity: 0.507	3.030×10^5 Joules	Tank Car #32 with hemispherical heads	Inside Diameter: 2.66m-2.96m Surface Area: 618.13m^2 Outage: 0.36m Length:?m	12.21m^3	95,600 kg	A212Gr B steel

BLANK PAGE

BLANK PAGE

TABLE H-1. LISTING OF EXPLOSION EVENT SOURCE AND VESSEL DATA (CONT.)

		EXPLOSION SOURCE				VESSEL				
I.D. NUMBER	REFERENCE	MATERIAL	QUANTITY (M^3 OR KG)	OTHER DATA	ESTIMATED ENERGY (JOULES)	SHAPE	DIMENSIONS	VOLUME (M^3)	MASS (KG)	MATERIAL
5	NTSB	Propane	65,400	Temp: 80° F	1.288×10^6	Tank Car #33	Inside	10.73m^3	83,900 kg	TC128GrB Steel
	RAR-72-2		kg =	Specific	Joules	with hemispheri-	Diameter:			
	Train		32.600m^3	Gravity:		cal heads	2.997m			
	Derailment			0.507			Surface			
	6-21-70						Area:			
							604.42m^2			
							Thickness			
							Sheets			
							0.016m,0.013m			
							Outage:			
							0.36m			
							Length: 64.3m			
5	NTSB	LPG	114m^3	Specific	3814	Section of Tank	About 19.29m	3.253m^3	25,400kg	ASTMA212
	1-25-69			Gravity:	Joules	car (POTX car	long	(estimated from		Grade B or
	Train			0.505		261) with		BRL report)		AAR TC128
	Derailment			Temp: 157°F		hemispherical				Grade B steel
	(wheel					heads				
	fracture)									
7	NTSB	LPG	114m^3	Specific	3814	Section of tank	About 19.29m	3.253m^3	25,400 kg	ASTMA212
	1-25-69			Gravity:	Joules	car with hemis-	long	Xestimated		Grade B or
	Train			0.505		pherical heads		from BRL re-		AAR TC128
	Derailment			Temp: 157°F		(POTX 260)		port)		Grade B steel
	(wheel									
	fracture)									

TABLE H-1. LISTING OF EXPLOSION EVENT SOURCE AND VESSEL DATA (CONT.)

I.D. NUMBER	REFERENCE	EXPLOSION SOURCE				VESSEL				
		MATERIAL	QUANTITY (M^3 OR KG)	OTHER DATA	ESTIMATED ENERGY (JOULES)	SHAPE	DIMENSIONS	VOLUME (M^3)	MASS (KG)	MATERIAL
8	NTSB	LPG	$114m^3$	Specific	3814	Section of tank	About	$3.253m^3$	25,400 kg	ASTM A212
	1-25-69			Gravity:	Joules	car with hemis-	18.29m	(estimated		Grade B or
	Train			0.505		pherical heads	long	from BRL re-		AAR TC128
	Derailment			Temp: 157°F		(GALX car 557)		port)		Grade B steel
	(wheel									
	fracture)									
9	NTSB	LPG	$114m^3$	Specific	3814	Section of Tank	About	$3.253m^3$	25,400 kg	ASTM A212
	1-25-69			Gravity:	Joules	car with hemis-	18.29m	(estimated		Grade B or
	Train			0.505		pherical heads	long	from BRL		AAR TC128
	Derailment			Temp: 157°F		(POTX 162)		report)		Grade B Steel
	(wheel									
	Fracture)									
10	NTSB	LPG	$114m^3$	Specific	3814	Section of tank	About 18.29m	$3.253m^3$	25,400 kg	ASTM A212
	1-25-69			Gravity:	Joules	car with hemis-	long	(estimated		Grade B or
	Train			0.505		pherical heads		from BRL re-		AARTC 128
	Derailment			Temp: 157°F		(GATX 89971)		port)		Grade B steel
	(wheel									
	fracture)									

TABLE H-1. LISTING OF EXPLOSION EVENT SOURCE AND VESSEL DATA (CONT.)

I.D. NUMBER	REFERENCE	EXPLOSION SOURCE				VESSEL				
		MATERIAL	QUANTITY (M^3 OR KG)	OTHER DATA	ESTIMATED ENERGY (JOULES)	SHAPE	DIMENSIONS	VOLUME (M^3)	MASS (KG)	MATERIAL
11	NTSB PAR-75-3 Pipeline Accident 3-15-74	Natural gas		Pressure: 3.427 x 10^6 Pa Temp: 40°F-50°F		Cylindrical pipe	Diameter: 0.3048m Thickness: 0.0025m (corroded from 0.005m) Length"			Steel (pipe was not cathodically protected)
12	NTSB-PAR-76-2 Pipeline Accident 4-22-74	AIR (Tank partially filled with water)		Pressure: 1.2066 x 10^6 Pa		Cylindrical tank; concave bottom, convex top; designed to operate at maximum pressure of 75 psig	1.524m high Diameter: 0.61m Length:"	0.43m^3	3520 kg	Steel
13	NTSB-PAR-76-8 9-1-75	LPG	125m^3	Pressure: 2.41 x 10^6 Pa Temp: 157° F (estimated from BRL report)	3920 Joules	Cylindrical tank car #27 with hemispherical heads (NATX34071)	None given	3.253m^3 (estimated from BRL report)	25,400kg	DOT 112A340W & DOT 114A340W Tank cars steel

TABLE H-1. LISTING OF EXPLOSION EVENT SOURCE AND VESSEL DATA (CONT.)

		EXPLOSION SOURCE				VESSEL				
I.D. NUMBER	REFERENCE	MATERIAL	QUANTITY (M^3 OR KG)	OTHER DATA	ESTIMATED ENERGY (JOULES)	SHAPE	DIMENSIONS	VOLUME (M^3)	MASS (KG)	MATERIAL
14	NTSB-RAR-76-8 9-1-75	LPG	125m^3 (estimated from BRL report)	Tank Pressure: 2.41 x 10^6 Pa Temp: 157° F	3920 Joules	Cylindrical tank car #32 with hemispherical heads (GATX 83347)	None given	3.253m^3 (estimated from BRL report)	25,400kg	DOT 112A340W & DOT 114A340W tank cars steel
15	NTSB-RAR-76-8 9-1-75	LPG	125m^3 (estimated from BRL report)	Tank Pressure: 2.41 x 10^6 Pa Temp: 157°F	3920 Joules	Cylindrical tank car #33 with hemispherical heads (GATX 83340)	None given	3.253m^3 (estimated from BRL report)	25,400kg	DOT 112A340W & DOT 114A340W Tank cars steel
16	NTSB-RAR-71-6 3-30-70	Liquified Oxygen (LOX)	8.21m^3	Pressure in tank: at time of delivery 68,948Pa-82,737Pa Temp: was refrigerated in tank at 290°F Purity in tank: 99.71%	?	Cargo tank assembly with hemispherical heads	None given	8.97m^3	70,200kg	Tank surrounded by about 0.15m of powdered inert insulating material contained in a steel jacket

TABLE H-1. LISTING OF EXPLOSION EVENT SOURCE AND VESSEL DATA (CONT.)

		EXPLOSION SOURCE				VESSEL				
I.D. NUMBER	REFERENCE	MATERIAL	QUANTITY (M^3 OR KG)	OTHER DATA	ESTIMATED ENERGY (JOULES)	SHAPE	DIMENSIONS	VOLUME (M^3)	MASS (KG)	MATERIAL
17	Report of	AIR	92,900 kg =	Pressure:	5.196 x 10^{11}	Air system	Three 2.-m	18.6 m^3	145,800 kg	USS T-1
	Accident		71,900 m^3	2.99 x 10^6	Joules	manifolds;	in diameter			Carilloy steel
	Investigation			Pa		Composed of	spheres			
	Board to NASA			Outside		series of cylin-	(0.032m			
	Langley Re-			temp:		drical pipes	thick) con-			
	search Center			72°F-75°F		and spheres	nected by			
	9-30-71						1.22m dia-			
							meter pip-			
							ing (0.013m			
							thick) -dis-			
							tribute air			
							to 6 of 12			
							large stor-			
							age bottles			
							thru 0.9m			
							diameter man-			
							ifolding			
							(0.009m			
							thick)			

TABLE H-1. LISTING OF EXPLOSION EVENT SOURCE AND VESSEL DATA (CONT.)

		EXPLOSION SOURCE				VESSEL				
I.D. NUMBER	REFERENCE	MATERIAL	QUANTITY (M^3 OR KG)	OTHER DATA	ESTIMATED ENERGY (JOULES)	SHAPE	DIMENSIONS	VOLUME (M^3)	MASS (KG)	MATERIAL
18	NTSB-RAR-71-2 Train Derailment & Collision 2-18-69	Anhydrous ammonia	72,400 kg = 93,800m^3	Temp: 4°F (ambient temp) Pressure: 1.37×10^5	1.487×10^9 Joules	Cylindrical Tank car with hemispherical heads struck when another train derailed; released gas to form ammonia cloud	18.2m long tank 3.02m inside diameter shell thickness; 0.01m tank head thickness: 0.017m car length: 19.28m wheels = 0.91m 100 ton trucks 15.9m apart - other train was travelling about 52 mph at time of derailment(but speed at that section of track was 30 mph)	3.26m^3	25,500 kg	Steel plate

TABLE H-1. LISTING OF EXPLOSION EVENT SOURCE AND VESSEL DATA (CONT.)

		EXPLOSION SOURCE				VESSEL				
I.D. NUMBER	REFERENCE	MATERIAL	QUANTITY (M^3 OR KG)	OTHER DATA	ESTIMATED ENERGY (JOULES)	SHAPE	DIMENSIONS	VOLUME (M^3)	MASS (KG)	MATERIAL
19	BRL R 1935	LPG	About 125m^3	Pressure:	3920	Cylindrical	18.3m long	3.253m^3	25,400 kg	TC-128 steel
	September	(97.9% Pro-		9.63×10^5	Joules	tank car with	3.05m in			
	1926	pane)		Pa		ellipsoidal	diameter			
				Temp: 70°F		heads (RAR	shell			
				tank pres-		201)	thickness			
				sure at			0.019m			
				rupture:			Avg. tank			
				2.41×10^5 Pa			temp: 137°F			
20	MTTB-	Propylene	27.29m^3	Vapor		Cylindrical	Cylinder	1.001m^3	7840 kg	Quenched-and-
	BAR-72-4	LPG		Pressure:		cargo tank	wall thick-			tempered steel
	Multiple-			1.03×10^6		semitrailer	ness:			
	vehicle			Pa		with hemis-	0.011m			
	collision			Temp: 65°F		pherical heads	head thick-			
	9-21-72			Weight:			ness:			
				14,217.7			0.0063m			
				kg			tank length			
							11.57m			
							semitrailer			
							length 11.8m			
							tank diam-			
							eter: 2.11m			
							(outside)			

TABLE H-1. LISTING OF EXPLOSION EVENT SOURCE AND VESSEL DATA (CONT.)

		EXPLOSION SOURCE				VESSEL				
I.D. NUMBER	REFERENCE	MATERIAL	QUANTITY (M^3 OR KG)	OTHER DATA	ESTIMATED ENERGY (JOULES)	SHAPE	DIMENSIONS	VOLUME (M^3)	MASS (KG)	MATERIAL
21	NSWC/	Argon	28.2 kg =	Pressure:	2.438×10^9	Spherical	Internal	$0.0283 m^3$	46.2 kg	T-1 steel
	WOL/TR		$15.8 m^3$	1.034×10^8	Joules		radius:0.19m	(internal)		
	75-87			Pa			Shell			
	2-9-76			Temp: 17°C			thickness:			
							0.012m			
							External			
							Radius 0.203m			
22	NSWC/	Argon	35.2 kg =	Pressure:	6.078×10^9	Spherical	Internal	$0.0283 m^3$	136 kg	T-1 steel
	WOL/TR		$19.7 m^3$	2.068×10^8 Pa	Joules		radius:0.19m	(internal)		
	75-87			Temp:17°C			Shell			
	2-9-76						thickness:			
							0.025m			
							External			
							radius:			
							0.216m			
23	NSWC/	Argon	39.3 kg =	Pressure:	1.133×10^{10}	Spherical	Internal	$0.0283 m^3$	187 kg	T-1 steel
	WOL/TR		$22.0 m^3$	3.447×10^8 Pa	Joules		radius:0.19m	(internal)		
	75-87			Temp:17°C			Shell			
	2-9-76						thickness:			
							0.044m			
							External			
							radius:			
							0.23m			

TABLE H-1. LISTING OF EXPLOSION EVENT SOURCE AND VESSEL DATA (CONT.)

I.D. NUMBER	REFERENCE	EXPLOSION SOURCE				VESSEL				
		MATERIAL	QUANTITY (M^3 OR KG)	OTHER DATA	ESTIMATED ENERGY (JOULES)	SHAPE	DIMENSIONS	VOLUME (M^3)	MASS (KG)	MATERIAL
24	NTSB-	LPG	33.11m^3	Temp:	549.6	Cylindrical	Tank length:	0.810m^3	8340 kg	U.S. Steel T-1
	HAR-76-6	(Half propane		80°F	Joules	cargo tank on	10.87m			
	4-29-75	half butane)				semitrailer	Inside			
						with hemis-	diameter:			
						pherical heads	2.18m			
						attached to	Thickness:			
						tractor	0.0096m(min)			
							Tank head			
							thickness:			
							0.0064m			
							Design			
							Pressure:			
							1.724×10^6 Pa			
							at 150°F			
							Actual inter-			
							nal pressure:			
							5.998×10^5 Pa			
25	Propane tank	Propane	1.586m^3	Relief	24.72	Cylindrical	External	0.0654m^3	512 kg	Steel
	Explosion			valve trig-	Joules	tank with	diameter			
	8-9-77			gers at 200		hemispherical	.955 m			
				psi, wide		heads	Thickness:			
				at 225 psi			0.0794m			
							Head thick-			
							ness: .00508m			
							Tank length:			
							3.089m Cyl.			
							length: 2.13m			

TABLE H-2. LISTING OF EXPLOSION EVENT FRAGMENT DATA

I.D. NUMBER	TOTAL NUMBER FRAGMENTS	FRAGMENTS					
		MASSES (KG)	RANGE (M)	APPARENT TRAJECTORY ELEVATION	DRAG COEFFICIENT C_D	SHAPES OR OTHER DESCRIPTION	REMARKS
1	4		182m		1.20	East end hurled-	First in a series of ex
						eastward	plosions-dug a crater
							in track structure
			91.4m		1.20	West end hurled-	Struck & collapsed roof
						southwestward	of a gas station
			182m		0.82	Large Portion - (0.762m wide)	hurled southwesterly
			228m		0.82	large portion -	Hurled southwesterly.
							The force caused the
							next car (#28) to ro-
							tate with the north end
							elevated 10 ft higher
							than south end.
2	2		61.0m		0.82	South end -	hurled southward; en-
							tered a brick apartment
			487m		0.82	north end -	hurled northwest over
							several houses & landed
							in a field & continued
							to roll

TABLE H-2. LISTING OF EXPLOSION EVENT FRAGMENT DATA (CONT.)

I.D. NUMBER	TOTAL NUMBER FRAGMENTS	FRAGMENTS					
		MASSES (KG)	RANGE (M)	APPARENT TRAJECTORY ELEVATION	DRAG COEFFICIENT C_D	SHAPES OR OTHER DESCRIPTION	REMARKS
3	2		182m		0.82	about 1/2 of the	destroyed 2 buildings
						tank (north end)	after going through
							them & came to a stop
							in a third one
			20.0m			other end -	remained in general
							derailment area
							The remaining cars of
							the train were rear-
							ranged with this ex-
							plosion
4	2		0.0m	--		car split	both fragments re-
						longitudinally	mained stationary;
			0.0m	--			did not separate into
							hurling pieces
5	2		5.0m			west end -	did not travel beyond
							general area; struck
							next car
			15.24m		1.20	other end -	piece bounced off #39
							& ignited propane in
							#35

TABLE H-2. LISTING OF EXPLOSION EVENT FRAGMENT DATA (CONT.)

I.D. NUMBER	TOTAL NUMBER FRAGMENTS	FRAGMENTS					
		MASSES (KG)	RANGE (M)	APPARENT TRAJECTORY ELEVATION	DRAG COEFFICIENT C_D	SHAPES OR OTHER DESCRIPTION	REMARKS
6	2	3/4 of total tank	487m	low	0.82	11.2m long section	First fragment bounced at 304.8m, then again at 396.24m, coming to rest at 487.68m on top of a house. Smaller section was not carried as far
		1/4 of tank	30.5m	low	0.82		
7	3	3/4 of tank	335m		0.82	11.28m long - section	struck a roof of a mill at 243.24m from the track, then it bounced at 274.32m, 304.8m, and landed at 335.28m
		1/4 of tank	15.24m		1.17		
			30.51m		1.17		
8	1		213m		1.20		none of these rose much in the air; largest one traveled the farthest & destroyed a building
			182m		1.20		
			161m		1.17		

TABLE H-2. LISTING OF EXPLOSION EVENT FRAGMENT DATA (CONT.)

I.D. NUMBER	TOTAL NUMBER FRAGMENTS	FRAGMENTS					
		MASSES (KG)	RANGE (M)	APPARENT TRAJECTORY ELEVATION	DRAG COEFFICIENT C_D	SHAPES OR OTHER DESCRIPTION	REMARKS
9	2		30.5m		0.82		car ruptured
					1.20		circumferentially
			30.5m				without prior puncture
							damage
10	2		22.9m		1.20		fragments were ap-
							proximately equal
			30.5m		1.20		in size; car ruptured
							without prior damage
							by puncturing
11	2	23.2kg	29.9m		1.20	2.44m long -	fragment dug a crater
						section split	12.19m long, 3.18m
		23.2kg	--			in 2 places	wide, and 3.048m
							deep - 91.44m
							diameter area was
							charred; 2 people
							killed 10.06m from
							the fragment; one
							victim was almost 20m
							away

TABLE H-2. LISTING OF EXPLOSION EVENT FRAGMENT DATA (CONT.)

I.D. NUMBER	TOTAL NUMBER FRAGMENTS	FRAGMENTS					
		MASSES (KG)	RANGE (M)	APPARENT TRAJECTORY ELEVATION	DRAG COEFFICIENT C_D	SHAPES OR OTHER DESCRIPTION	REMARKS
12	1			90°	1.20		bottom blew out of the tank, rocketing it upward to strike a 0.152m gas service line above it
13	2		0.0m		1.20	16.15m long piece	found next to track, split open on top, upright
			22.6m		1.20	6.09m long piece	
14	3		4.57m		1.98	main section -	tank shell flattened into a sheet
			19.8m		1.20	end piece (about 7.04m long)	found upright
			19.8m		1.20	other end (about 3.04m long	located 39.62m from first end piece

TABLE OF CONTENTS

TABLE H-2. LISTING OF EXPLOSION EVENT FRAGMENT DATA (CONT.)

I.D. NUMBER	TOTAL NUMBER FRAGMENTS	FRAGMENTS					
		MASSES (KG)	RANGE (M)	APPARENT TRAJECTORY ELEVATION	DRAG COEFFICIENT C_D	SHAPES OR OTHER DESCRIPTION	REMARKS
15	2		65.23m		0.82	13.41m long	
						piece	
			60.96m		1.17	2.74m by	
						1.524m piece	
16	3				1.20	①section of -	reduction in thickness:
						cargo tank wall	about 63kg of metal mis-
							sing from inner wall
					1.20	②spray	
						header fragment	
			4.1m		1.17	③baffle plate	
17	35	①1703kg	191m		1.20	①Cylindrical pipe	soars over a building,
						Diameter:0.61m	struck the sidewalk,
						Thickness:0.0095m	broke, & destroyed 2
						Length:11.95m	cars totally
		②470kg	206m		1.20	② Pipe	
						Thickness;0.0095m	
						Length:3.302m	
		③2.22kg	233m		1.20	③0.61m diameter	see diagrams
						pipe	
						Thickness:0.0095m	
						Length:0.57m	

TABLE H-2. LISTING OF EXPLOSION EVENT FRAGMENT DATA (CONT.)

I.D. NUMBER	TOTAL NUMBER FRAGMENTS	FRAGMENTS					
		MASSES (KG)	RANGE (M)	APPARENT TRAJECTORY ELEVATION	DRAG COEFFICIENT C_D	SHAPES OR OTHER DESCRIPTION	REMARKS
17	35	④ 1930kg	208m		0.82	⑭ 0.91m diameter	see diagram
Cont'						cylindrical pipe	
						Thickness:	
						0.0095m	
						Length:	
		⑤	146m		1.17	⑮ Very small piece	" "
						of 0.91m in dia-	
						meter pipe	
		⑥	185m		1.17	⑯ Very small piece	" "
						of 0.91m in dia-	
						meter cylindri-	
						cal pipe	
		⑦ 1340kg	40.0m		0.82	⑰ 0.91m in diame-	" "
						ter cylindrical	
						pipe; thickness	
						0.0093m; Length	
						6.33m	
		⑧ 1440kg	44.0m		1.20	⑱ long piece of	" "
						0.91m in diame-	
						ter pipe;thick-	
						ness:0.0095m	
						Length:6.77m	
		⑨ 1627kg	54.2m		1.20	⑲ long piece of	" "
						0.91m in diame-	
						ter pipe; thick	
						ness: 0.0095m	
						Length:7.65m	

TABLE H-2. LISTING OF EXPLOSION EVENT FRAGMENT DATA (CONT.)

I.D. NUMBER	TOTAL NUMBER FRAGMENTS	FRAGMENTS					
		MASSES (KG)	RANGE (M)	APPARENT TRAJECTORY ELEVATION	DRAG COEFFICIENT C_D	SHAPES OR OTHER DESCRIPTION	REMARKS
17	35	(10) 1082kg	63.00m		1.20	(11) 0.91m in diameter	See Diagram
cont'd.						cylindrical pipe;	
						Thickness:0.0095m	
						Length:5.089m	
		(11) 1039kg	66.4m		0.47	(12) 2.44m in diameter	" "
						sphere;thickness	
						= 0.032m	
		(12) 2020kg	73.1m		1.20	(13) long piece at	" "
						0.91m diameter	
						cylindrical pipe;	
						Thickness:0.0095m	
						Length:9.5m	
		(13)	67.7m		1.17	(14) very small piece	" "
						of 0.91m in dia-	
						meter cylindrical	
						pipe, 0.0095m	
						thick	
		(14) 93.6kg	63.7m		1.17	(15) small piece of	" "
						0.91m diameter	
						pipe; 0.0095m	
						thick	
						Length:0.44m	
		(15) 2007kg	68.4m		1.20	(16) 0.91m diameter	" "
						cylindrical pipe	
						0.0095m thick	
						Length: 9.44m	

TABLE H-2. LISTING OF EXPLOSION EVENT FRAGMENT DATA (CONT.)

I.D. NUMBER	TOTAL NUMBER FRAGMENTS	FRAGMENTS					
		MASSES (KG)	RANGE (M)	APPARENT TRAJECTORY ELEVATION	DRAG COEFFICIENT C_D	SHAPES OR OTHER DESCRIPTION	REMARKS
17	35	(16) 2220kg	75.9m		1.20	(17) 0.91m in diameter	See Diagrame
Cont'd.						cylindrical pipe;	
						0.0095m thick	
						Length: 10.45m	
		(17)	67.1m		1.17	(18) Very small piece	" "
						Of 0.91m diameter	
						pipe, 0.0095m	
						thick	
		(18)	88.0m		1.17	(19) Very small piece	" "
						of 0.91m diameter	
						pipe, 0.0095m	
						thick	
		(19) 1285kg	97.5m		0.82	(20) Connecting cy-	" "
						lindrical pipe,	
						1.22m diameter,	
						0.013m thick	
						Length: 3.29m	
		(20) 104.0kg	112m		0.47	(21) 2.44m diameter	" "
						sphere, 0.32m	
						thick	
		(21) 1130kg	110m		0.82	(22) 0.91m diameter -	badly crumpled; does
						cylindrical pipe,	not even look
						0.0095m thick;	cylindrical
						Length: 5.334m	

TABLE H-2. LISTING OF EXPLOSION EVENT FRAGMENT DATA (CONT.)

I.D. NUMBER	TOTAL NUMBER FRAGMENTS	FRAGMENTS					
		MASSES (KG)	RANGE (M)	APPARENT TRAJECTORY ELEVATION	DRAG COEFFICIENT C_D	SHAPES OR OTHER DESCRIPTION	REMARKS
17	35	(42) 2400kg	32.5m		0.82	(425) 11.28m long piece of 0.91m diameter cylindrical pipe, 0.009m thick	demolished several buildings while still connected to B12, then broke apart & destroyed a car in the parking lot
Cont'd.		(43)	22.4m		1.17	(426) very small piece of 0.91m diameter pipe, 0.009m thick	
		(45) 387kg	29.1m		1.20	(427) 0.91m diameter cylindrical pipe, 0.009m thick length: 1.83m	
		(47) 1080kg	65.7m		0.82	(428) 3.04m long piece of 0.91m diameter cylindrical pipe, 0.009m thick	
		(49) 903kg	69.8m		1.20	(429) 0.91m diameter cylindrical pipe, 0.005m thick length: 4.25m	

TABLE H-2. LISTING OF EXPLOSION EVENT FRAGMENT DATA (CONT.)

I.D. NUMBER	TOTAL NUMBER FRAGMENTS	FRAGMENTS					
		MASSES (KG)	RANGE (M)	APPARENT TRAJECTORY ELEVATION	DRAG COEFFICIENT C_D	SHAPES OR OTHER DESCRIPTION	REMARKS
17	35	(27) 399kg	5.42m		1.20	(27) 0.9m diameter	
Cont'd.						cylindrical pipe	
						0.009m thick	
						Length: 1.88m	
		(28) 242kg	292m		1.17	(28) small piece of	
						0.9m diameter	
						cylindrical pipe	
						0.009m thick	
						Length: 1.14m	
		(29) 238kg	116m		1.20	(29) 0.9m diameter	
						cylindrical pipe	
						0.009m thick	
						Length: 1.12m	
		(30)	110m		1.17	(30) very small frag-	does not appear on
						ment	reconstruction picture
		(31)	48.1m		0.82	(31) very small frag-	does not appear on
						ment	reconstruction picture
		(32)	40.6m		1.20	(32) very small frag-	does not appear on
						ment	reconstruction picture
		(33)	102.3m		0.82	(33) very small piece	
						of 0.9m diame-	
						ter cylindrical	
						pipe, 0.009m	
						thick	

TABLE H-2. LISTING OF EXPLOSION EVENT FRAGMENT DATA (CONT.)

I.D. NUMBER	TOTAL NUMBER FRAGMENTS	FRAGMENTS					
		MASSES (KG)	RANGE (M)	APPARENT TRAJECTORY ELEVATION	DRAG COEFFICIENT C_D	SHAPES OR OTHER DESCRIPTION	REMARKS
17	35	(64)	1.12m		0.82	very small piece	
Cont'd.						of 0.91m diameter	
						cylindrical pipe,	
						0.0095m thick	
		(65) 244kg	4.06m		0.82	small piece of	
						0.91m diameter	
						cylindrical pipe	
						0.0095 m thick,	
						Length: 1.06m	
18	7	10,800kg	0.0m		1.20	longer section of	remained intact; came
						tank, about	to rest north of the
						9.1m long	track siding
		4800kg	61.0m		0.82	top portion of -	landed in front yard
						shell, 4.88m long	of a residence
		1910	42.7m		1.05	bottom portion -	hurled northward
						of tank head	
			40m		1.05	other section -	hurled toward north
						of tank	side of track
			161m		1.05	other section -	hurled toward north
						of tank	side of track

TABLE H-2. LISTING OF EXPLOSION EVENT FRAGMENT DATA (CONT.)

I.D. NUMBER	TOTAL NUMBER FRAGMENTS	FRAGMENTS					
		MASSES (KG)	RANGE (M)	APPARENT TRAJECTORY ELEVATION	DRAG COEFFICIENT C_D	SHAPES OR OTHER DESCRIPTION	REMARKS
18	7		174m		1.05	other section -	hurled toward north
cont'd.							side of track
			183m		1.20	other section -	hurled toward north
							side of track
19	9	① 7470kg	15.4m		1.20	Item 76: portion	located in pit
	major ones					of tank car shell	
	(6) total of RAX	② 350kg	21.2m		1.17	Item 58: portion	located in pit
	201)					of ellipsoidal	
	(127 total of					head	
	entire test struc-	③ 94.8kg	19.9m			Item 114: Added	located in pit
	ture)					manway	
		④ 1150kg	104.2m		1.17	Item 15: Portion	located west of pit
						of ellipsoidal	
						head	
		⑤ 74.8kg	112.9m		1.20	Item 16: Portion	located west of pit
						of tank car	
						shell	
		⑥ 220.0kg	94.5m			Item 1: Standard	located southeast
						manway	of pit

TABLE H-2. LISTING OF EXPLOSION EVENT FRAGMENT DATA (CONT.)

I.D. NUMBER	TOTAL NUMBER FRAGMENTS	FRAGMENTS					
		MASSES (KG)	RANGE (M)	APPARENT TRAJECTORY ELEVATION	DRAG COEFFICIENT C_D	SHAPES OR OTHER DESCRIPTION	REMARKS
19	9	⑦ 12,200kg	133m		1.20	Item 4: Portion	located southeast of
cont'd.						of tank shell	pit
		⑧ 1180kg	146m		1.17	Item 7: Portion	located south of pit
						of ellipsoidal	
						head	
		⑨ 183kg	73.6m		1.17	Item 9: Portion	located south of
						of ellipsoidal	pit
						head	
20	6	① 5080kg	39m		0.82	front section of	northeast of
	main ones					tank shell:8.23m	explosion point
						in length(3/4 the	
						length of tank)	
		② 652kg	165m		1.17	rear head	southwest of
							explosion point
		③ 2060kg	85.0m		0.82	rear 1/4 of	southwest of
						cylindrical sec-	explosion point
						tion:3.34m long	
		⑩	15.2m		1.55	part of trailer-	found along eastern
						suspension	embankment of
							turnpike

TABLE H-2. LISTING OF EXPLOSION EVENT FRAGMENT DATA (CONT.)

I.D. NUMBER	TOTAL NUMBER FRAGMENTS	FRAGMENTS					
		MASSES (KG)	RANGE (M)	APPARENT TRAJECTORY ELEVATION	DRAG COEFFICIENT C_D	SHAPES OR OTHER DESCRIPTION	REMARKS
20	6	⑤	15.2m		1.98	the two axles -	found along eastern
cont'd.						(with the tires	embankment of turnpike
						burned off)	
		⑥	54.9m		1.17	front pair of -	southeast of
						trailer wheels	explosion point
		(Shot No.)					
21	2 each	(1a)	max. of 512.06m	54°	0.165	top half of sphere	never found
	from 3 different	(1b) 23.8kg	202.69m	54°	0.165	bottom half of	avg. measured velocity
	shots					sphere	96.93m/sec
		(2a)	max. of 423.37m	64°	0.165	top half -	never found
		(2b) 23.9kg	168.25m	64°	0.165	bottom half -	avg. velocity =
							98.76m/sec
		(6a) 23.2kg	0.0m		0.165	top -	impacted rear wall of
							steel
		(6b) 23.2kg	0.0m		0.165	bottom -	confining structure;
							both halves remained
							inside the arena
		(Shot No.)					
22	2 each	(3a) 69.2kg	max. of 346.25m	70°	0.165	top -	never found (probably
	for 2 shots						landed in wooded area)
		(3b) 66.9kg	0.0m		0.165	bottom -	found inside the arena;
							mean fragment velocity
							= 107.59m/sec

TABLE H-2. LISTING OF EXPLOSION EVENT FRAGMENT DATA (CONT.)

I.D. NUMBER	TOTAL NUMBER FRAGMENTS	FRAGMENTS: MASSES (KG)	RANGE (M)	APPARENT TRAJECTORY ELEVATION	DRAG COEFFICIENT C_D	SHAPES OR OTHER DESCRIPTION	REMARKS
		(Shot No.)					
22	2 each	(7a) 42.4kg	0.0m		0.165	top	both found inside the
cont'd.	for 2 shots	(7b) 49.0kg	0.0m		0.165	bottom	arena; average velocity
							for bottom section =
							83.52m/sec
		(Shot No.)					
23	2 each	(4a) 117kg	0.0m		0.165	large portion -	found inside arena; avg
	for 2 shots						velocity = 63.84m/sec
		(4b) 70.3kg	max. of 220.07m	78°	0.165	small portion -	never found
		(5a) 123kg	0.0m		0.165	large portion	both found inside
		(5b) 66.4kg	0.0m		0.165	small portion	the arena
24	25	(1)	304m			large forward -	struck on elevated sign
						section	first hit ground at
							313.64m, bounced up,
							touched again after
							84.73m and demolished
							a mobile home; bounced
							into the air & went
							another 105.77m over
							a second mobile home
							which caught fire &
							struck a third mobile
							home to stop 304.14m
							from explosion point

TABLE H-2. LISTING OF EXPLOSION EVENT FRAGMENT DATA (CONT.)

I.D. NUMBER	TOTAL NUMBER FRAGMENTS	FRAGMENTS					
		MASSES (KG)	RANGE (M)	APPARENT TRAJECTORY ELEVATION	DRAG COEFFICIENT C_D	SHAPES OR OTHER DESCRIPTION	REMARKS
24	25	②	244m			aft section	
cont'd.						(split in 3	
						parts actually)	
		③	39.9m			Tractor frame	
		④	39.9m			Tractor engine	
		⑤	51.5m			Tractor fuel tank	
		⑥	163m			Rear tank baffle	
		⑦	76.0m		1.17	Spare tire	
		⑧	85.0m			Trailer hose rack	
		⑨	57.3m			Fifth wheel	
						plate	
		⑩	66.1m			Tractor drive	
						shaft	
		⑪	137m			Trailer spare	
		⑫	373m			Trailer landing	
						gear assembly	
		⑬	60.0m			Left door of	
						trailer	
		⑭	32.0m			Tank vapor pipe	

TABLE H-2. LISTING OF EXPLOSION EVENT FRAGMENT DATA (CONT.)

I.D. NUMBER	TOTAL NUMBER FRAGMENTS	FRAGMENTS					
		MASSES (KG)	RANGE (M)	APPARENT TRAJECTORY ELEVATION	DRAG COEFFICIENT C_D	SHAPES OR OTHER DESCRIPTION	REMARKS
24	25	(15)	57.9m			Trailer rear	
cont'd.						bumber assembly	
		(16)	67.7m			Trailer relief	
						valve system	
		(17)	81.7m			Tractor radiator	
		(18)	89.0m			Right seat of	
						tractor	
		(19)	104m			Portion of bot-	
						tom tank shell	
		(20)	230m			Portion of bot-	
						tom tank shell	
		(21)	160m			Trailer front	
						tandem axle	
						wheels	
		(22)	169m			Trailer rear	
						tandem axle	
						wheels	
		(23)	255m			Portion of tank	
						shell (rear	
						head)	
		(24)	220m			Right door of	
						tractor	
		(25)	239m			Tractor	
						muffler	

TABLE H-2. LISTING OF EXPLOSION EVENT FRAGMENT DATA (CONT.)

I.D. NUMBER	TOTAL NUMBER FRAGMENTS	FRAGMENTS					
		MASSES (KG)	RANGE (M)	APPARENT TRAJECTORY ELEVATION	DRAG COEFFICIENT C_D	SHAPES OR OTHER DESCRIPTION	REMARKS
		(Fragment ID)					
25	11	(I) 104kg	31.4m to		0.47	hemispherical end	struck wall 2.8448m
	main ones		wall, then			cap; diameter =	above ground level;
			another 4.57m			.0144m, .00508m thick	impact on wall also included
		(II) 171.1kg	123m		1.20	main por-	one attached
						tion of cylinder;	end cap
						2.1336m long;	
						m circum-	
						ference; .07144m	
						thick	
		(III) 52.2kg	119m		0.47	section of	located in creek
						end cap (about	3.05m from the
						1/2)	main portion of the
							cylinder
		(1) 0.0341kg	31.4m		1.05	cubical section	tank was sitting on
						of cement block	these concrete blocks
		(2) 1.56kg	40.2m		1.55	fairly	
						rectangular	
						section of block	
		(3) 1.22kg	17.7m		2.05	pie-shaped	12.2m from a van
						piece of block	
		(4) 0.998kg	25.2m		1.55	Pie-shaped	
						piece of block	
		(5) 1.22kg	15.2m		0.80	sort of cubical	
						section of block	
		(6) 0.967kg	28.3m		2.05	rectangular	
						section of block	

TABLE H-2. LISTING OF EXPLOSION EVENT FRAGMENT DATA (CONT.)

I.D. NUMBER	TOTAL NUMBER FRAGMENTS	FRAGMENTS					
		MASSES (KG)	RANGE (M)	APPARENT TRAJECTORY ELEVATION	DRAG COEFFICIENT C_D	SHAPES OR OTHER DESCRIPTION	REMARKS
25	11	Ⓐ 9.3kg	58.8m		1.20	fence pipe;	found across the
cont'd.						5.77m long	street against the
							curb
		Ⓑ 1.00kg	41.8m		1.20	1.96m long	struck wall about
						fence pipe	1.96m above ground
							level

TABLE H-3. PERCENTILES FOR PLOTTING FRAGMENT RANGES OF THE SIX EVENT GROUPS

Percent	Event Group Numbers					
	1	2	3	4	5	6
10.0	20.00	15.24	22.35	32.00		15.24
14.3					168.27	
20.0	40.00	19.81	40.64	51.51		17.68
28.6					202.69	
30.0	60.96	27.43	54.19	60.65		25.20
40.0	91.44	30.48	66.38	76.02		28.35
42.9					220.07	
50.0	161.00	60.96	68.41	85.04		31.39
57.1					346.25	
60.0	182.88	94.50	88.05	136.86		41.76
70.0	182.88	133.40	109.73	164.59		58.83
71.4					423.37	
80.0	228.60	167.64	115.82	238.96		119.79
85.7					512.06	
90.0	487.68	335.28	206.59	373.73		122.83

Figures H-1 through H-6 are plots of the percentile points on log normal probability paper for each of the respective six events groups.

Table H-4 is a listing of the estimated means and standard deviations for the log normal (to the base e) distributions.

A "W" statistic [see Hahn and Shapiro (1967)] for goodness of fit was calculated for each of the distributions. The approximate probability of obtaining the calculated test statistic, given that the chosen distribution is correct, was then determined. The results are shown in Table H-5.

Deviation of Fragment Mass Distributions

(Figures 4-8 and 4-9)

Sufficient pertinent mass data were available only from event groups 2, 3 and 6. Table H-6 is a listing of the percentiles of these event groups.

Figures H-7 through H-9 are plots of the percentile points on log normal probability paper for each of the respective event groups.

Table H-7 is a listing of the estimated means and standard deviations for the log normal (to the base e) distributions.

The calculated "W" statistic along with the approximate probability of obtaining the calculated test statistic, given that the chosen distribution is correct are presented for each of the three event groups in Table H-8.

Correlation Analyses of Fragment Range and Fragment Mass Within Event Groups

(Figures 4-11 and 4-12)

For each of the three event groups (2, 3 and 6) with sufficient fragment range and mass data, three models were exercised to determine the degree of correlation between fragment range and mass. The three models and equivalent equations were:

1) Linear -

$$R = a + b\,M$$

2) Power Curve -

$$R = aM^{b}$$

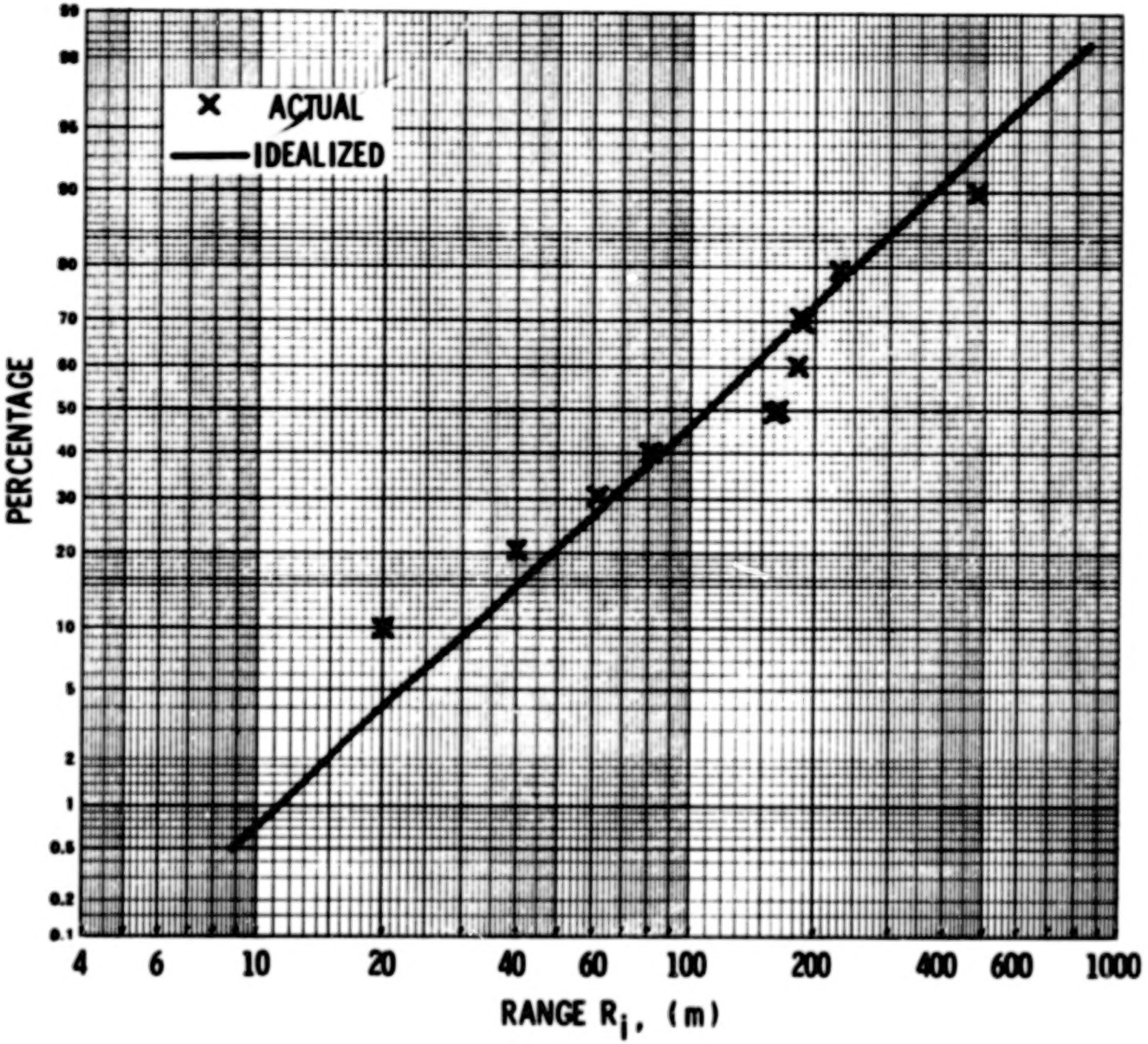

FIGURE H-1. EVENT GROUP 1 (EVENTS 1,2,3,18) PROBABILITY DISTRIBUTION RANGE

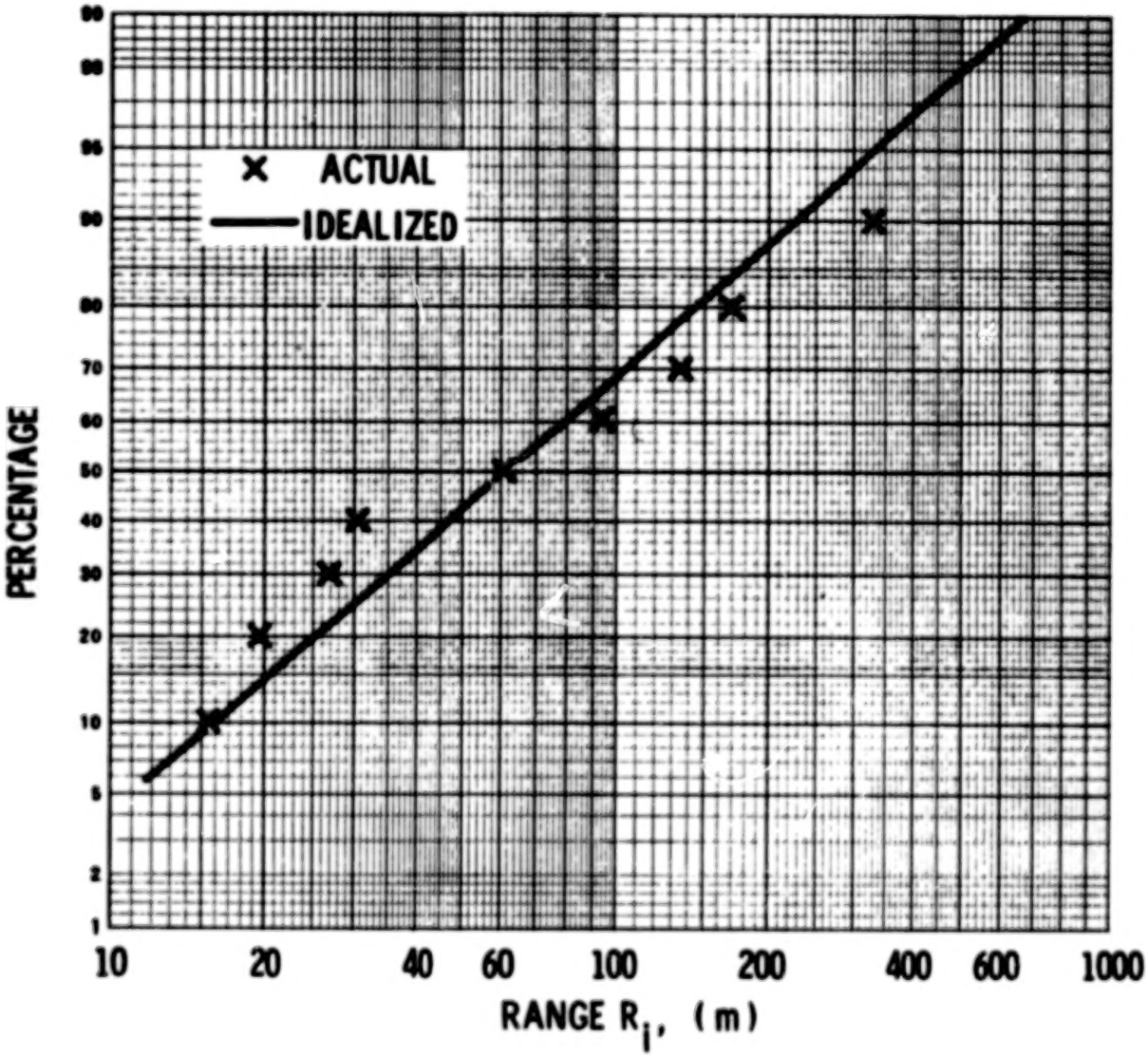

FIGURE H-2. EVENT GROUP 2 (EVENTS 6,7,8,9,10,13,14,15 and 19) PROBABILITY DISTRIBUTION, RANGE

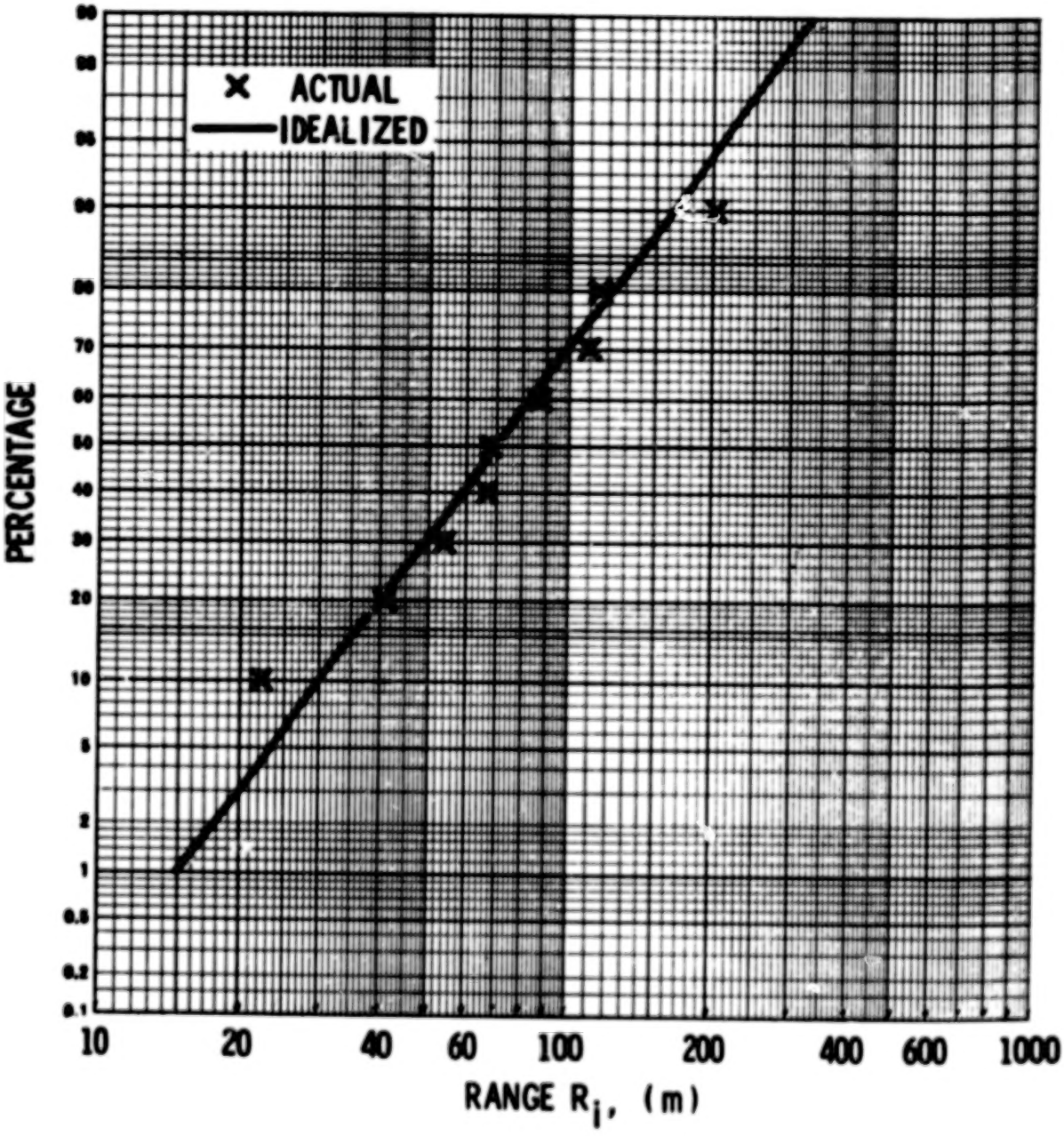

FIGURE H-3. EVENT GROUP 3 (EVENT 17) PROBABILITY DISTRIBUTION, RANGE

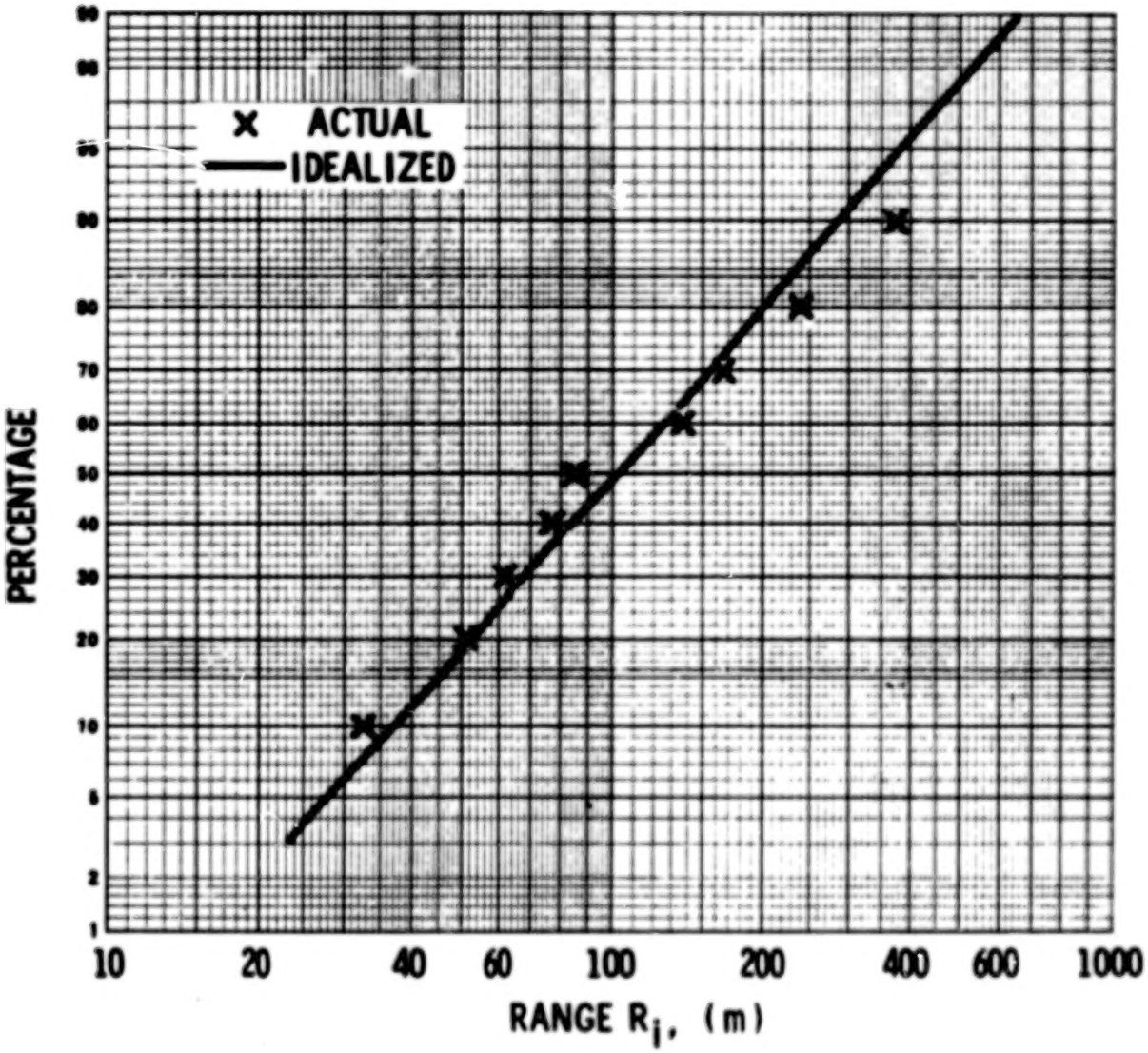

FIGURE H-4. EVENT GROUP 4 (EVENTS 20 and 24) PROBABILITY DISTRIBUTION, RANGE

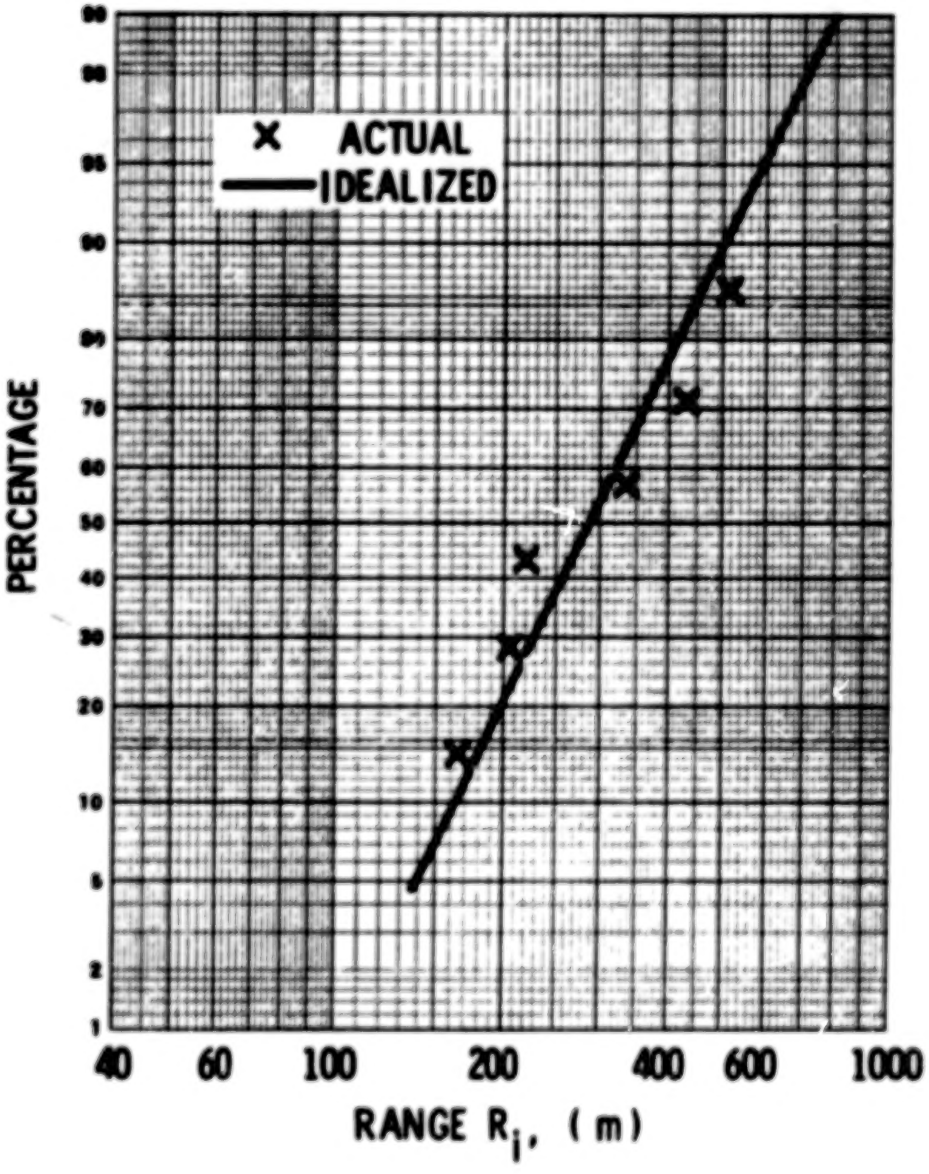

FIGURE H-5. EVENT GROUP 5 (EVENTS 21, 22, 23)
PROBABILITY DISTRIBUTION, RANGE

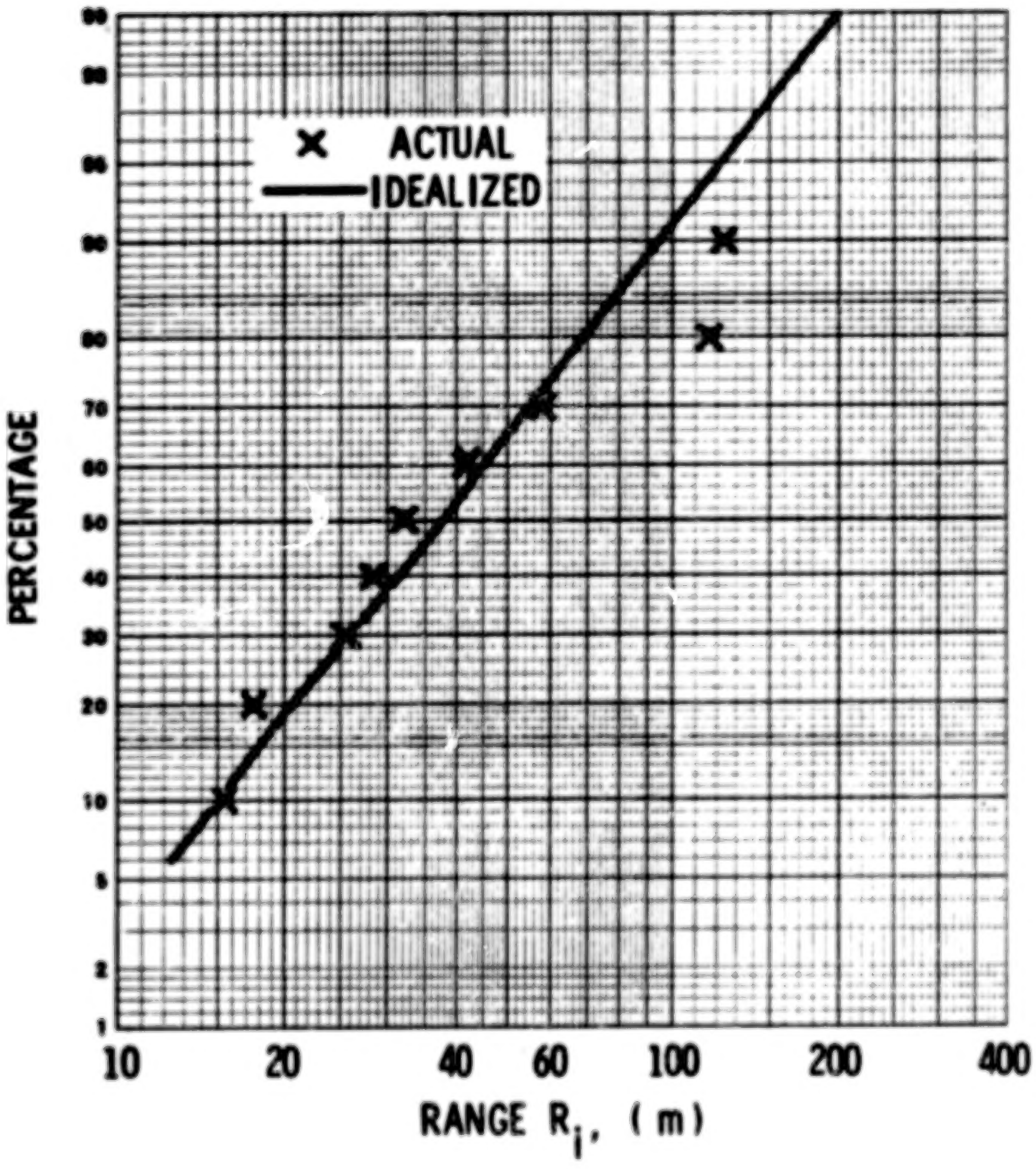

FIGURE H-6. EVENT GROUP 6 (EVENT 25) PROBABILITY DISTRIBUTION, RANGE

TABLE H-4. LISTING OF ESTIMATED MEANS AND STANDARD DEVIATIONS FOR LOG-NORMAL RANGE DISTRIBUTIONS (TO THE BASE e) FOR THE SIX EVENT GROUPS

Event Group No.	Estimated Mean	Estimated Standard Deviation
1	4.569939	0.906041
2	4.103086	1.062895
3	4.275966	0.646206
4	4.633257	0.785540
5	5.660840	0.446785
6	3.668606	0.758061

TABLE H-5. SUMMARY OF "W" TEST ON NORMALITY FOR FRAGMENT RANGE DISTRIBUTIONS FOR EVENT GROUPS 1 THROUGH 6

Event Group No.	"W"	Probability
1	.964	.82
2	.951	.68
3	.986	.98
4	.980	.95
5	.936	.57
6	.917	.2?

As it is customary to consider values exceeding 2 to 10% as adequate grounds for not rejecting the hypothesis that the data belong to the chosen distribution, the fits for the six event groups are more than adequate.

TABLE H-6. PERCENTILES FOR PLOTTING FRAGMENT MASSES OF EVENT GROUPS 2, 3 AND 6

Percent	Event Group Numbers		
	2	3	6
10	74.8	93.61	.0341
20	94.8	241.98	.967
30	220.0	399.28	.998
40	350.0	1,039.52	1.00
50	1.180.0	1.080.29	1.22
60	3,183.0	1,281.78	9.30
70	7,470.0	1,439.81	52.23
80	12.200.0	1,935.88	104.46
90	19,098.0	2,020.84	171.38

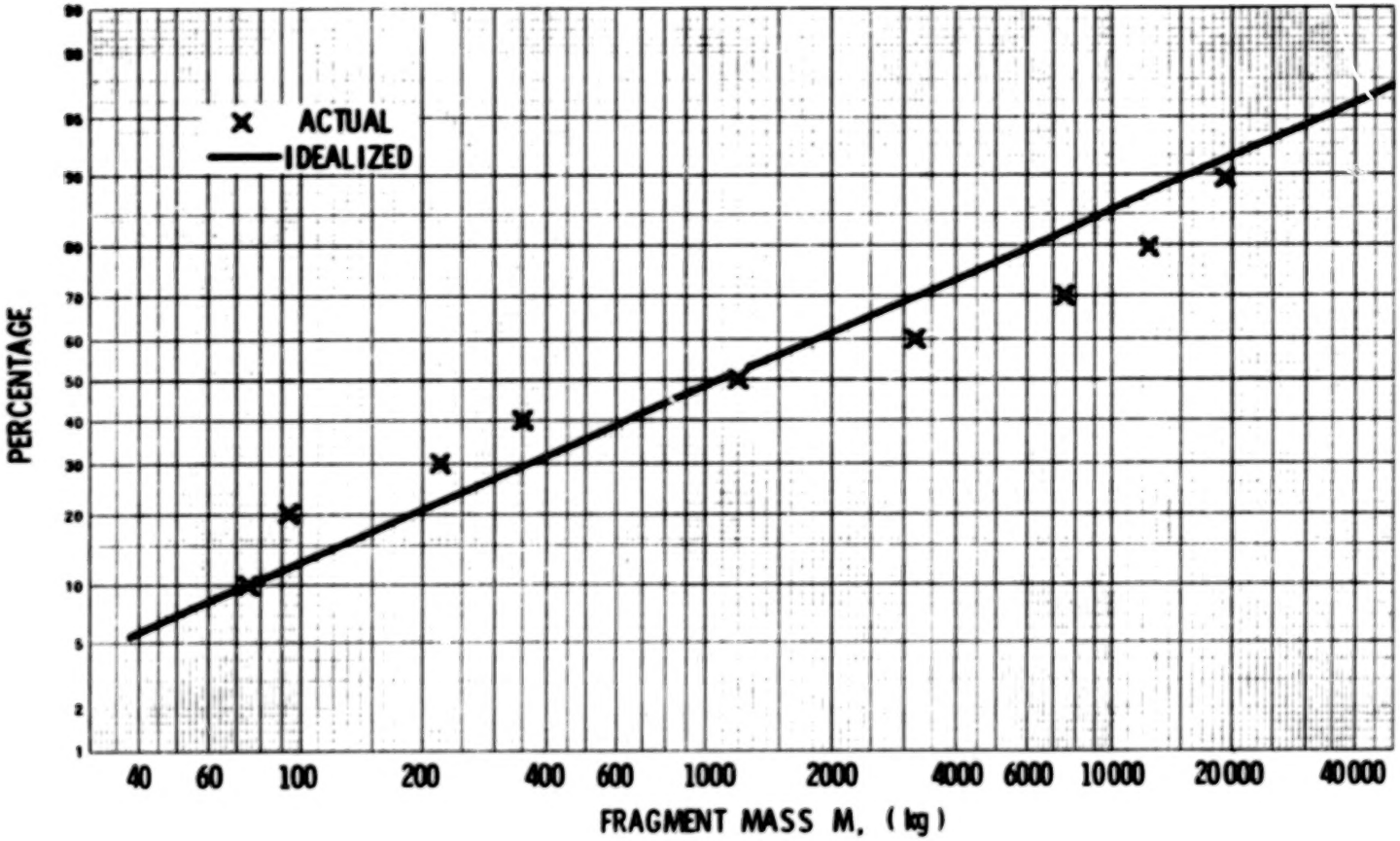

FIGURE H-7. EVENT GROUP 2 (EVENTS 6, 7, 8, 9, 10, 13, 14, 15, 19)
PROBABILITY DISTRIBUTION, MASS

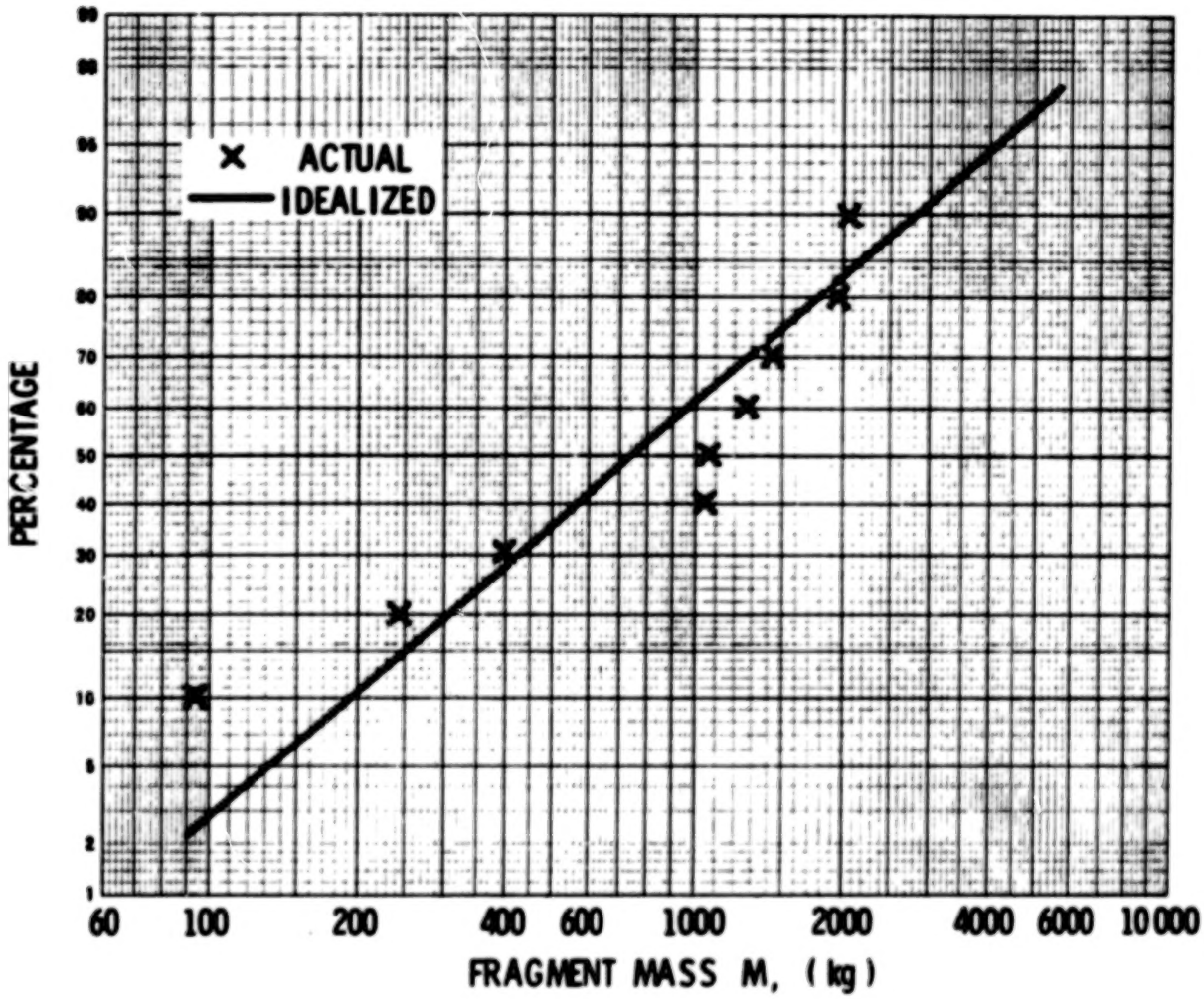

FIGURE H-8. EVENT GROUP 3 (EVENT 17) PROBABILITY DISTRIBUTION, MASS

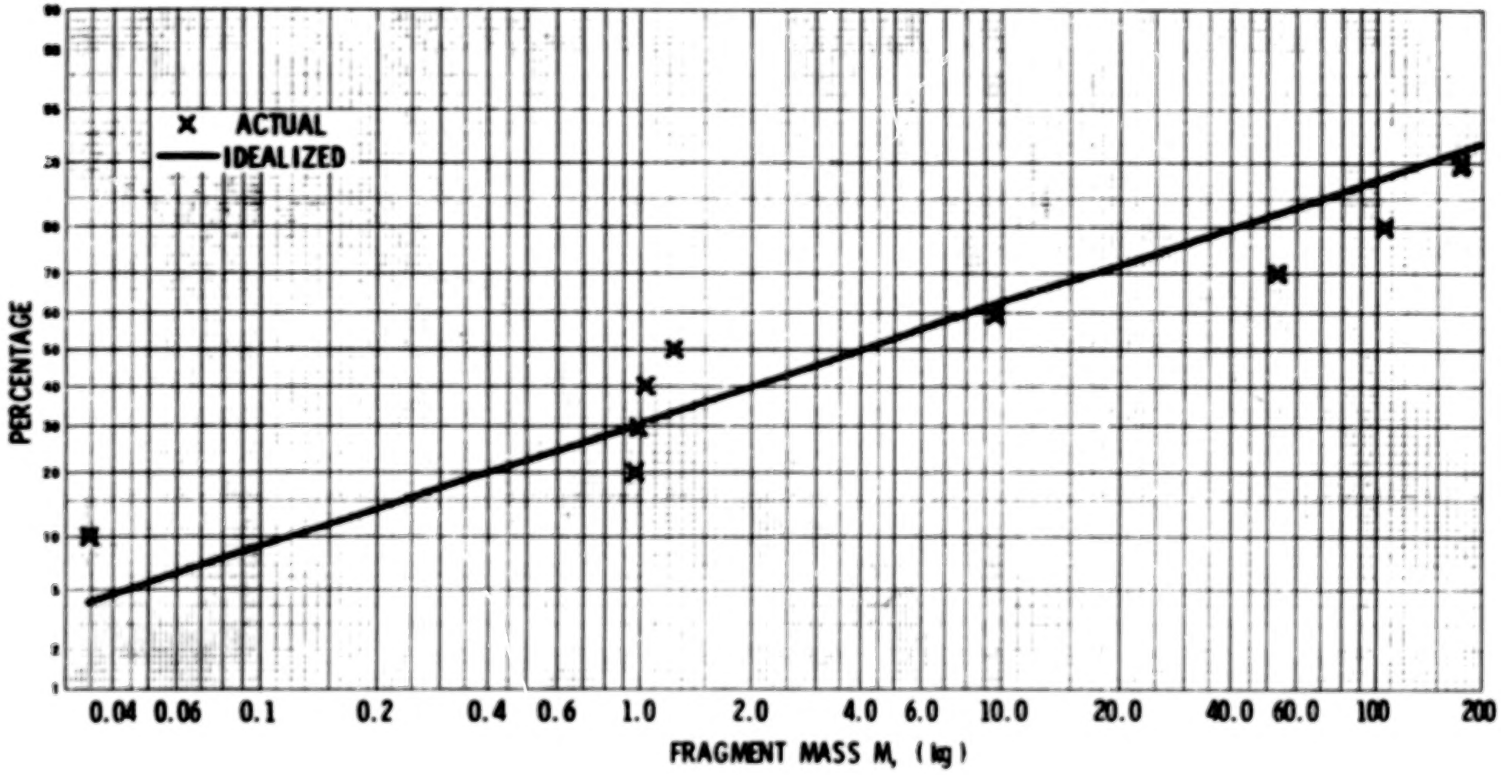

FIGURE H-9. EVENT GROUP 6 (EVENT 25) PROBABILITY DISTRIBUTION, MASS

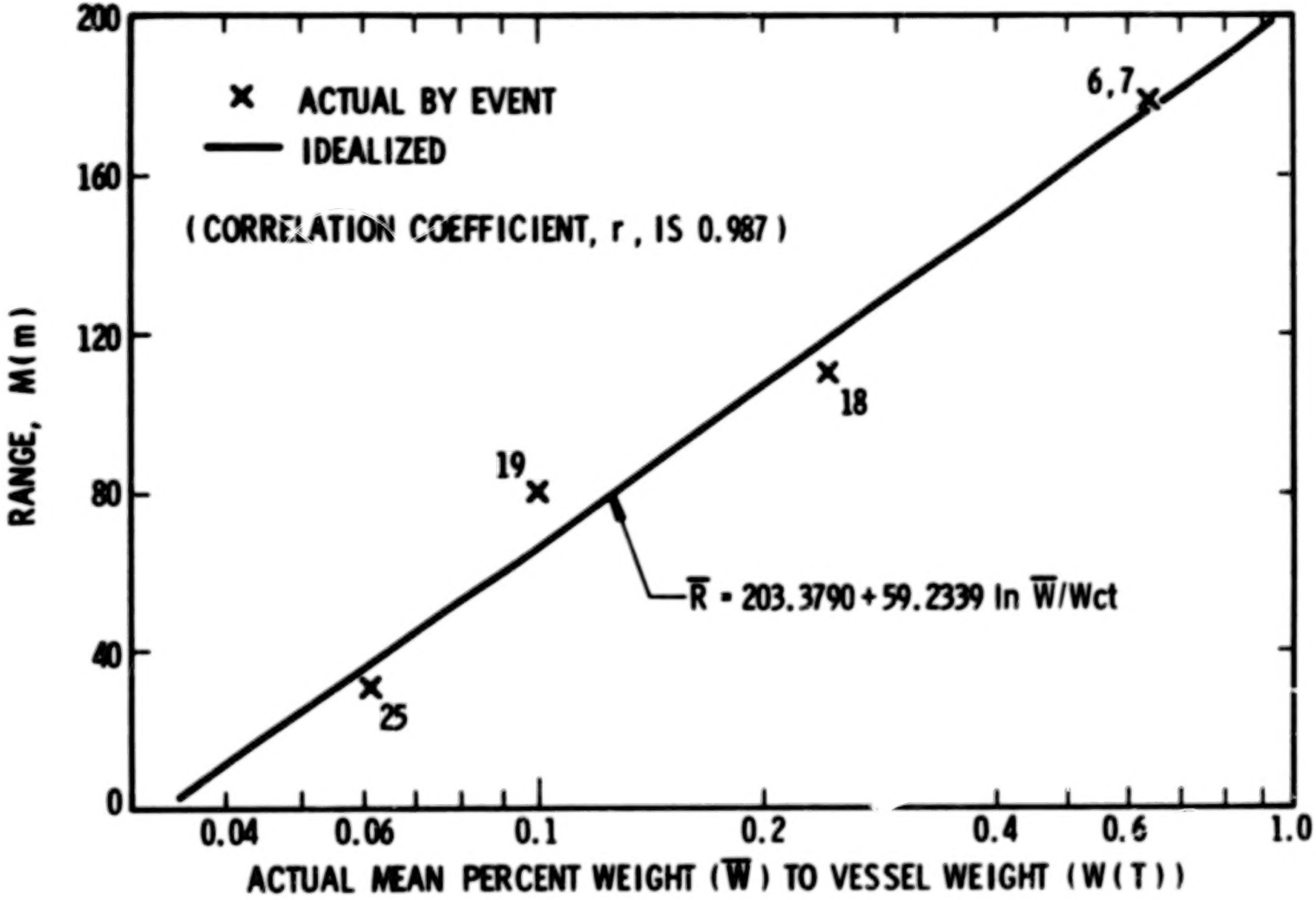

FIGURE H-10. RANGE VERSUS THE RATIO OF MEAN FRAGMENT WEIGHT TO TANK WEIGHT FOR CYLINDRICAL VESSELS (EVENTS 6 and 7, 18, 19, 25)

TABLE H-7. LISTING OF ESTIMATED MEANS AND STANDARD DEVIATIONS FOR LONG-NORMAL FRAGMENT MASS DISTRIBUTIONS (TO THE BASE e) FOR EVENT GROUPS 2, 3 AND 6

Event Group No.	Estimated Mean	Estimated Standard Deviation
2	7.049131	2.117124
3	6.617446	1.051264
6	1.418576	2.784658

TABLE H-8. SUMMARY OF "W" TEST ON NORMALITY FOR FRAGMENT MASS DISTRIBUTIONS FOR EVENT GROUP 2, 3 AND 6

Event Group No.	"W"	Probability
2	.920	.37
3	.860	.10
6	.914	.32

3) Logarithmic Curve -

$$R = a + b \ln M$$

Table H-9 is a listing of fragment range and mass for the three event groups. Table H-10 contains a listing of the estimated parameters and correlation coefficients for each model for each event group.

From Table H-10, the largest correlation coefficients over each of the three models are .79, .35, and .68 for the event groups 2, 3 and 6, respectively. These values of r can be transformed to a normal variate, Z, by the following formula [Arkin and Colton (1950)]:

$$Z = .5 \left[\ln (1 + r) - \ln (1 - r)\right] \qquad \text{(H-1)}$$

The standard error of Z, σ_Z, is:

$$\sigma_Z = 1/(N - 3) \qquad \text{(H-2)}$$

where N is the number of fragment range-mass pairs in Table H-9 an event group.

A 95% confidence limit (L_Z) on the range of sampling variation on Z can be set by:

$$L_Z = Z \pm 1.96\ \sigma_Z \qquad \text{(H-3)}$$

Then, the 95% confidence limit on r can be established by substituting the two values of L_Z (one at a time) into Equation (H-1) for Z, and solving for r.

The 95% confidence limits on r for the three event groups are:

1) Event group 2

$.70 < r < .85$

2) Event group 3

$.39 < r < .43$

3) Event group 6

$.61 < r < .74$

TABLE H-9. LISTING OF FRAGMENT RANGE AND MASS FOR EVENT GROUPS 2, 3 AND 6

Event Group 2		Event Group 3		Event Group 6	
Range	Mass	Range	Mass	Range	Mass
112.9	74.8	233.0	2.22	31.39	.0341
19.9	94.8	63.37	93.61	28.35	.0967
73.6	183.0	115.82	237.66	25.2	.998
94.5	220.0	4.064	224.70	41.76	1.00
21.2	350.0	292.61	241.98	15.24	1.22
104.2	1150.0	29.13	387.18	17.68	1.22
145.7	1180.0	5.42	399.28	40.23	1.56
15.24	3183.0	206.59	470.70	58.83	9.3
30.48	6366.0	69.77	903.18	119.79	52.23
15.4	7470.0	112.44	1039.52	31.39	104.46
133.4	12200.0	66.38	1039.52	122.83	171.38
487.68	19098.0	65.70	1080.29		
335.28	19098.0	63.00	1082.13		
		110.41	1134.30		
		97.54	1281.78		
		39.96	1345.72		
		44.03	1439.81		
		54.19	1627.08		
		191.69	1703.20		
		207.94	1935.88		
		64.41	2007.72		
		73.15	2020.84		
		75.86	2223.24		
		32.51	2399.70		

TABLE H-10. ESTIMATED PARAMETERS FOR REGRESSION MODELS FOR CORRELATION BETWEEN FRAGMENT RANGE AND MASS FOR EVENT GROUPS 2, 3 AND 6

Model*	Event Group								
	2			3			6		
	a	b	r	a	b	r	a	b	r
Linear	37.5572	.01558	.79	731.72	-0.5789	.18	34.2328	0.4534	.68
Power Curve	20.3775	.16782	.30	101.93	-0.0640	.09	31.3277	0.1692	.63
Logarithmic Curve	-9258.7	3472.05	.56	210.41	-17.4501	.35	32.9911	10.2442	.60

* a is the range axis intercept

b is the slope

r is the correlation coefficient

Since one can be 95% confident that the correlation coefficient for event group 3 is less than .43, there would be little benefit in using the corresponding prediction model for fragment mass given fragment range, or vice-versa. However, for event groups 2 and 6 a sufficient degree of correlation between fragment range and fragment mass is indicated to make the prediction models worthwhile. These models are shown on Figures 4-11 and 4-12.

Correlation Analysis of Fragment Range to the Ratio of Mean Fragment Weight to Vessel Weight For Cylindrical Tanks

Five events with cylindrical tanks contained sufficient fragment mass information to determine the degree of correlation of fragment range to the ratio of mean fragment weight to vessel weight. It was necessary to group events 6 and 7 to have a sufficient sample size.

Table H-11 presents the data by event number, the ratio of the arithmetic mean fragment weight ($\overline{W}$) to the vessel weight (W(T)), and the arithmetic mean fragment range ($\overline{R}$). Figure H-10 is a plot of the points in Table H-11 along with the prediction equation. The sample correlation coefficient is .987. Using the same techniques as described earlier, one can be 90% confident that the true population correlation coefficient is greater than .74.

TABLE H-11. MEAN RANGE AND RATIO OF MEAN FRAGMENT WEIGHT TO VESSEL WEIGHT FOR CYLINDRICAL TANKS

Event	$\bar{W}/W(T)$	$\bar{R}$
6,7	.644	179.83
18	.242	110.30
19	.100	80.08
25	.0612	39.20

LIST OF SYMBOLS

English Symbols

A	= cross-sectional area; loaded area; differential volume
A_a	= speed of sound in surrounding atmosphere
A_D	= drag area
A_e	= exit area
A_L	= lift area
a	= conditions in surrounding atmosphere; range axis intercept
a_*	= critical gas velocity
a gas	= sound speed of gas
a_o	= speed of sound
b	= loaded width, slope
C_D	= drag coefficient
C_L	= lift coefficient
$\frac{C_L A_L}{C_D A_D}$	= lift/drag ratio
C_ℓ	= cylindrical length
C_t	= cylindrical thickness
$C(T)$	= mass of gas confined at high pressure as a function of time
C_v	= coefficient relating maximum bending shear stress to the maximum
C_W	= coefficient to relate stress to deformations
$D = M/d^3$	= caliber density of the projectile
d	= coefficient; projectile diameter; pipe outside diameter
ds	= differential length

$\left(\frac{dv}{dx}\right)_{max}$ = maximum slope

E = blast yield (energy); elastic modulus

E' = blast yield (energy) for bursting pressure vessels

E_c = total heat of combustion

E_e = effective blast yield

E_K = kinetic energy of the fragment

E_ℓ = end cap length

E_o = energy of detonation of 1 gram of TNT

E_t = end cap thickness

e = specific energy; specific work; perforation thickness

F = thrust; cross-sectional area; force

f'_c = ultimate concrete compressive strength

subscript_f = fluid (saturated liquid)

g = acceleration of gravity; gravity constant

$\sqrt{g}$ = square root of the acceleration of gravity

subscript_g = gas (saturated vapor)

H = total depth

$\overline{H}$ = scaled height

$\overline{H}_g$ = scaled gage height

h = enthalpy; concrete panel thickness; height

h_e = enthalpy of gas at nozzle

h_i = enthalpy of gas

I = second moment of area

$\overline{I}$ = scaled (dimensionless) impulse

I_s = side-on specific impulse

$I_s(-)$ = negative phase impulse for first shock

$I_s(+)$ = positive phase impulse for first shock

$\bar{I}_s$ = scaled (dimensionless) side-on overpressure

i = impulse

i_r = reflected impulse

i_s = positive impulse

K = coefficient of discharge; constant; concrete penetrability factor

KE = impact kinetic energy

L/D = length-to-diameter ratio

L_Z = confidence limit

ℓ = length; span

M = total mass; mass of the overlying floor

M_C = mass of the container

Mg = force of gravity

M_i = enclosed substance

$M_{\dot{y}}$ = vertical inertial force

$M_{\dot{x}}$ = horizontal inertial force

(MW) = molecular weight

m = mass of the liquid in the vessel

N = number of fragment-mass pairs; projectile nose-shape factor

n = number of fragments

o = reservoir conditions immediately after failure

P = peak applied pressure; pressure; internal pressure

$\bar{P}$ = average burst pressure

P_a = atmospheric pressure

$\bar{P}_A$ = starting overpressure

P-i = nondimensionalized pressure impulse

P_{oo} = initial pressure

P_r = peak reflected overpressure

P_s = peak side-on overpressure

$\bar{P}_S$ = dimensionless overpressure

P_{s1} = first shock side-on overpressure

P_{s2} = second shock side-on overpressure

$\bar{P}V/E_o$ = normalized yield

p = absolute pressure

p_1 = initial absolute pressure in the vessel

p_1, V_1, S_1, U_1, h_1 = initial state variables

pA = vertical load

p_a = outside atmosphere absolute pressure; ambient pressure; atmospheric pressure

p_c = critical pressure

p_e = exit pressure

p_n = internal pressure

p_o = atmospheric pressure; back pressure

p-v = pressure-volume plane

q = energy expended in heating gas

R = range

$\bar{R}$ = dimensionless distance; scaled distance; mean fragment range

R_M = ideal gas constant

r = correlation coefficient; cylindrical radius; distance along the plane of symmetry from the center of tank

s = entropy, scabbing thickness

s_2 = final entropy

s_e = entropy of gas at the nozzle (exit)

T = absolute temperature

$\bar{T}$ = scaled (dimensionless) time

T_o = temperature of the gas

T_{oo} = temperature

T-s = temperature-entropy plane

$T_s(-)$ = duration of negative impulse for first shock

$T_s(+)$ = duration of positive impulse for first shock

t_w = pipe wall thickness

U = mean fragment velocity

U_e = exit velocity

u = internal energy; velocity

V = maximum shear force; shear force

V_l = vessel volume

V_o = internal volume

V_{oo} = internal volume

V_s = missile striking velocity

V_v/V_l = volume of vapor to volume of liquid ratio

v = specific volume

v_2, u_2, h_2 = thermodynamic parameters

v_e = specific volume

V_f = final volume occupied by the gas originally in the vessel

$\bar{W}$ = geometric mean fragment mass; mean fragment weight

WK = maximum possible work

W(T) = sphere weight, vessel weight

W_o = deformation

$\dot{w}$ = mass flow rate

w_o = maximum elastic deformation

x = distance traveled by the fragment

X_1 = displacement distance along the axis of motion

$\ddot{X}$ = horizontal acceleration

x = quality of the vapor; characteristic dimension; total penetration depth; the depth a missile will penetrate into an infinitely thick target

x_1 = initial quality

x_2 = final quality

$\dot{x}$ = horizontal velocity

Y = altitude

$\ddot{Y}$ = vertical acceleration

$\dot{Y}$ = vertical velocity

Z = normal variate, dimensionless variable

z = plastic section modulus

Greek Symbols

α = trajectory angle

α_i = initial trajectory angle, coefficient for simply-supported beam

α_p = numerical coefficient

γ = ratio of specific heats, adiabatic exponent

γ_1 = ratio of specific heat for gas in the vessel

Δt = small time

σ = deflection

ϵ_{max} = maximum strain

θ = trajectory angle, characteristic time, temperature

Π = perimeter

ρ = mass density

ρ_* = gas density

ρgA = weight per unit length quantity

ρ_o = density of air

σmax = scaled stress

σ_t = yield strength

σ_u = ultimate stress

σ_y = yield point

$\frac{\sigma_y}{E}$ = yield strain

$\frac{E\epsilon_{max}}{\sigma_y}$ = scaled strain

σ_Z = standard error of Z

τ = time

Ψ_{p,i,ϵ,w_o} = coefficients

BIBLIOGRAPHY OF DATA SOURCES FOR MISSILE MAPS

Anonymous, "Railroad Accident Report-Derailment of Toledo, Peoria and Western Railroad Company's Train No. 20 with Resultant Fire and Tank Car Ruptures, Crescent City, Illinois, June 21, 1970," Report No. NTSB-RAR-72-2, National Transportation Safety Board, Washington, D.C., March 29, 1972.

Anonymous, "Railroad Accident Report - Southern Railway Company Train 154 Derailment with Fire and Explosion, Laurel, Mississippi, January 25, 1969," National Transportation Safety Board, Washington, D.C., October 6, 1969.

Anonymous, "Pipeline Accident Report - Southern Union Gas Company, Transmission Pipeline Failure, Near Farmington, New Mexico, March 15, 1974," Report No. NTSB-PAR-75-3, National Transportation Safety Board, Washington, D.C., December 23, 1975.

Anonymous, "Pipeline Accident Report - Consolidated Edison Company, Explosion at 305 East 45th Street, New York, New York, April 22, 1974," Report No. NTSB-PAR-76-2, National Transportation Safety Board, Washington, D.C., February 19, 1976.

Anonymous, "Railroad Accident Report Derailment of Tank Cars With Subsequent Fire and Explosion on Chicago, Rock Island and Pacific Railroad Company, Near Des Moines, Iowa, September 1, 1975," Report No. NTSB-RAR-76-8, National Transportation Safety Board, Washington, D.C., June 30, 1976.

Anonymous, "Highway Accident Report - Liquified Oxygen Tank Truck Explosion Followed by Fires in Brooklyn, New York, May 30, 1970," Report No. NTSB-HAR-71-6, National Transportation Safety Board, Washington, D.C., May 12, 1971.

Wilson, H. A., Jr., Belles, F. E., Clark, H. K., Crockett, C. D., Caplan, D. F., Shaw, R. C., Swain, R. L., Vincke, C. J., McSmith, D., "Report of Accident Investigating Board, 9 x 6 Thermal Structures Tunnel (TST), 600 PSIA Air Supply System," Report to Director, NASA Langley Research Center, Hampton, Virginia, April 1972.

Anonymous, "Railroad Accident Report - Chicago, Burlington and Quincy Railroad Company, Train 64 and Train 824, Derailment and Collision with Tank Car Explosion, Crete, Nebraska, February 18, 1969." Report No. NTSB-RAR-71-2, National Transportation Safety Board, Washington, D.C., February 24, 1971.

Anonymous, "Highway Accident Report - Multiple-Vehicle Collision, Followed by Propylene Cargo-Tank Explosion, New Jersey Turnpike, Exit 8, September 21, 1972," Report No. NTSB-HAR-73-4, National Transportation Safety Board, Washington, D.C., October 17, 1973.

Anonymous, "Pipeline Accident Report - United Gas Pipe Line Company, 20-Inch Pipeline Rupture and Fire, Cartwright, Louisiana, August 9, 1976," Report No. NTSB-PAR-77-1, National Transportation Safety Board, Washington, D.C., April 26, 1977.

Anderson, C., Townsend, W., Zook, J. A., Cowgill, G., "The Effects of a Fire Environment on a Rail Tank Car Filled With LPG," BRL Report No. 1935, Aberdeen Proving Ground, Maryland, September 1976.

Pittman, J. F., "Blast and Fragments From Superpressure Vessel Rupture," Report No. NSWC/WOL/TR 75-87, Naval Surface Weapons Center, White Oak, Silver Spring, Maryland, February 1976.

CONVERSION FACTORS

The following table provides multiplying factors for converting numbers and miscellaneous units to corresponding new numbers and SI units.

The first two digits of each numerical entry represent a power of 10. An asterisk follows each number which expresses an exact definition. For example, the entry "--02 2.54*" expresses the fact that 1 inch = 2.54×10^{-2} meter, exactly, by definition. Most of the definitions are extracted from National Bureau of Standards documents. Numbers not followed by an asterisk are only approximate representations of definitions, or are the results of physical measurements. The accepted abbreviation in Système International (SI) is given in parentheses in the second column.

To convert from	to	multiply by
atmosphere	Pascal (Pa), Newton/meter^2	+05 1.013 25*
bar	Pascal (Pa), Newton/meter^2	+05 1.00*
British thermal unit (mean)	Joule (J)	+03 1.055 87
calorie (mean)	Joule (J)	+00 4.190 02
dyne	Newton (N)	-05 1.00*
erg	Joule (J)	-07 1.00*
Fahrenheit (temperature)	Celsius (C)	$t_c=(5/9)(t_F-32)$
foot	meter (m)	-01 3.048*
inch	meter (m)	-02 2.54*
lb_f (pound force, avoirdupois)	Newton (N)	+00 4.448 221 651 260 5*
lb_m (pound mass, avoirdupois)	kilogram (kg)	-01 4.535 923 7*
Pascal	Newton/meter^2 (N/m^2)	+00 1.00*
pound force (lb_f avoirdupois)	Newton (N)	+00 4.448 221 615 260 5*

To convert from	to	multiply by
pound mass (lb_m avoirdupois)	kilogram (kg)	-01 4.535 923 7*
poundal	Newton (N)	-01 1.382 549 543 76*
slug	kilogram (kg)	+01 1.459 390 29
foot/second^2	meter/second^2 (m/s^2)	-01 3.048*
inch/second^2	meter/second^2 (m/s^2)	-02 2.54*
gram/centimeter^3	kilogram/meter^3 (kg/m^3)	+03 1.00*
lb_m/inch^3	kilogram/meter^3 (kg/m^3)	+04 2.767 990 5
lb_m/foot^3	kilogram/meter^3 (kg/m^3)	+01 1.601 846 3
slug/foot^3	kilogram/meter^3 (kg/m^3)	+02 5.153 79
lb_f/foot^2	Pascal (Pa), Newton/meter^2	+01 4.788 025 8
lb_f/inch^2 (psi)	Pascal (Pa), Newton/meter^2	+03 6.894 757 2
foot/second	meter/second (m/s)	-01 3.048*
inch/second	meter/second (m/s)	-02 2.54
foot^3	meter^3 (m^3)	-02 2.831 684 659 2*
inch^3	meter^3 (m^3)	-05 1.638 706 4*

GLOSSARY OF TERMS

appurtenance - a piece of equipment or an object located near a source of an explosion, which can be accelerated by the blast wave from the explosion.

blast yield - energy released in an explosion inferred from measurements of the characteristics of blast waves generated by the explosion.

burst pressure - the pressure at which a gas storage vessel bursts or fails.

concrete penetrability factor - measures the resistance of concrete to impact penetration.

drag coefficient - ratio of drag force to dynamic force exerted by wind pressure on a reference area.

explosive yield - energy released in an explosion, often expressed as a percent or fraction of energy which would be released by the same mass of a standard high explosive such as TNT.

far field barricade - a barricade located near the protected structure.

FRAG - a computer program for predicting velocities of fragments from bursting cylindrical and spherical pressure vessels.

FRISB - a computer program for predicting trajectories of fragments with both lift and drag aerodynamic forces.

lift coefficient- ratio of lift force to dynamic force exerted by wind pressure on a reference area.

LPG - liquified petroleum gas, usually liquified propane.

mound - An elevation of earth having a crest at least 3 ft. wide with the earth at the natural slope on each side and with such elevation that any straight line drawn from the top of the side wall of a magazine or operating building or the top of a stack containing explosives to any part of a magazine, operating building or stack to be protected will pass through the mound. The toe of the mound shall be located as near the magazine, operating building or stack as practicable.

near field barricade - barricades located near an explosive source

overpressure - pressure in a blast wave above atmospheric pressure

perforation thickness - the maximum thickness of material which will be completely penetrated by a missile at a given velocity.

reflected impulse - integral of reflected pressure-time history.

risk assessment - the estimation of effects of some potentially dangerous operation or situation; but also the estimation of the probability that the event will occur and cause some level of damage.

rocketing - propulsion of large fragments from liquid propellant vessels resulting from the change of the liquid propellant into a gas when the external pressure is released during the fracturing of the vessel.

scabbing thickness - thickness of a target required to prevent scabbing of material from the backface for a missile with a given velocity.

side-on impulse - integral of time history of side-on overpressure.

side-on overpressure - blast wave overpressure in an undisturbed blast wave.

single-revetted barricade - a mound which has been modified by a retaining wall preferably of concrete of such slope and thickness as to hold firmly in place the 3 ft. width of earth required for the top, with the earth at the natural angle on one side. All other requirements of a mound shall be applicable to the single-revetted barricades.

spalling or scabbing - the process of projection of pieces of material from impacted plates or walls by stress wave reflection.

stable buckling - bending of a column under axial impulsive load.

starting overpressure - a curve on a graph of dimensionless overpressure versus dimensionless distance used as a starting point to compute the overpressure at a given distance from the center of the vessel.

THRUST - a computer program for predicting trajectories of large parts of pressure vessels containing flash-evaporating fluids.

total penetration depth - the depth a missile will penetrate into an infinitely thick target.

TUTTI - two dimensional finite difference computer program for compressible fluids.

unconfined vapor cloud explosion - a quantity of fuel released to the atmosphere as a vapor or aerosol, subsequently mixed with air and then exploded by some ignition source.

UNQL - a computer program for predicting velocities of two unequal fragments of a failed pressure vessel.

vapor density - the ratio of the density of the vapor to that of air at standard temperature and pressure.

vapor dome - the dome-shaped curve on a plot of thermodynamic properties of a fluid which represents the boundary between wet vapor and superheat.

BIBLIOGRAPHY

Adamczyk, A. A. and Strehlow, R. A., (1977), "Terminal Energy Distribution of Blast Waves from Bursting Spheres", NASA CR 2303, Grant NSG 3008, September 1977.

AISC Handbook, (1961), "Steel Construction", American Institute of Steel Construction, 5th Edition, New York, New York, 1961.

Anderson, C., Townsend, W., Zook, J. A., Cowgill, G., (1976), "The Effects of a Fire Environment on a Rail Tank Car Filled With LPG", BRL Report No. 1935, Aberdeen Proving Ground, Maryland, September 1976.

Anonymous, (1969), "Railroad Accident Report - Southern Railway Company Train 154 Derailment with Fire and Explosion, Laurel, Mississippi, January 25, 1969", National Transportation Safety Board, Washington, D.C., October 6, 1969.

Anonymous, (1971a), "Railroad Accident Report - Chicago, Burlington and Quincy Railroad Company, Train 64 and Train 824, Derailment and Collision with Tank Car Explosion, Crete, Nebraska, February 18, 1969", Report No. NTSB-RAR-71-2, National Transportation Safety Board, Washington, D.C., February 24, 1971.

Anonymous, (1971b), "Highway Accident Report - Liquified Oxygen Tank Truck Explosion Followed by Fires in Brooklyn, New York, May 30, 1970", Report No. NTSB-HAR-71-6, National Transportation Safety Board, Washington, D.C., May 12, 1971.

Anonymous, (1972), "Railroad Accident Report-Derailment of Toledo, Peoria and Western Railroad Company's Train No. 20 with Resultant Fire and Tank Car Ruptures, Crescent City, Illinois, June 21, 1970", Report No. NTSB-RAR-72-2, National Transportation Safety Board, Washington, D.C., March 29, 1972.

Anonymous, (1973), "Highway Accident Report - Multiple-Vehicle Collision, Followed by Propylene Cargo-Tank Explosion, New Jersey Turnpike, Exit 8, September 21, 1972", Report No. NTSB-HAR-73-4, National Transportation Safety Board, Washington, D.C., October 17, 1973.

Anonymous, (1975), "Pipeline Accident Report - Southern Union Gas Company, Transmission Pipeline Failure, Near Farmington, New Mexico, March 15, 1974", Report No. NTSB-PAR-75-3, National Transportation Safety Board, Washington, D.C., December 23, 1975.

Anonymous, (1976a), "Pipeline Accident Report - Consolidated Edison Company, Explosion at 305 East 45th Street, New York, New York, April 22, 1974", Report No. NTSB-PAR-76-2, National Transportation Safety Board, Washington, D.C., February 19, 1976.

Anonymous, (1976b), "Railroad Accident Report - Derailment of Tank Cars with Subsequent Fire and Explosion on Chicago, Rock Island and Pacific Railroad Company, Near Des Moines, Iowa, September 1, 1975", Report No. NTSB-RAR-76-8, National Transportation Safety Board, Washington, D.C., June 30, 1976.

Anonymous, (1977), "Pipeline Accident Report - United Gas Pipe Line Company, 20-Inch Pipeline Rupture and Fire, Cartwright, Louisiana, August 9, 1976", Report No. NTSB-PAR-77-1, National Transportation Safety Board, Washington, D.C., April 26, 1977.

Arkin, H. and Colton, R. R., (1950), Tables for Statisticians, Barnes & Noble, New York.

ASHRAE Handbook of Fundamentals, (1972), Am. Soc. of Heating, Refrigerating and Air Conditioning Engineers, Inc., New York.

Baker, W. E., (1973), Explosions in Air, University of Texas Press, Austin, Texas.

Baker, W. E., Esparza, E. D., Hokanson, J. C., Funnell, J. E., Moseley, P. K., and Deffenbaugh, D. M. (1978), "Initial Feasibility Study of Water Vessels for Arresting Lava Flow", AMSAA Contractor **Report to be published.**

Baker, W. E., Hokanson, J. C., and Cervantes, R. A., (1976), "Model Tests of Industrial Missiles", Final Report, SwRI Project No. 02-9153-001, Southwest Research Institute, San Antonio, Texas, May 1976.

Baker, W. E., Kulesz, J. J., Ricker, R. E., Bessey, R. L., Westine, P. S., Parr, V. B., and Oldham, G. A., (1975), "Workbook for Predicting Pressure Wave and Fragment Effects of Exploding Propellant Tanks and Gas Storage Vessels", NASA CR-134906, Contract NAS3-19231, November 1975 (reprinted September 1977).

Baker, W. E., Westine, P. S. and Dodge, F. T., (1973), Similarity Methods in Engineering Dynamics, Hayden Book Co., Rochelle Park, N.J.

Beth, R. A., (1945), "Concrete Penetration", OSRD-4856, National Defense Research Committee Report A-319, March 1945.

Boyer, W. D., Brode, H. L., Glass, I. I., and Hall, J. G. (1958), Blast From A Pressurized Sphere, UTIA Report No. 48, Institute of Aerophysics, University of Toronto, 1958.

Brinkley, S. R., (1969), "Determination of Explosive Yields", AIChE Loss Prevention, 3, 79-82.

Brode, H. L., (1959), "Blast Wave from a Spherical Charge", Physics of Fluids, 2, 217.

Brown, J. A., (1973), "A Study of the Growing Danger of Detonation in Unconfined Gas Cloud Explosions", Final Technical Report for Exxon Corp., December 1973.

Choromokos, J., (1972), "Detonable Gas Explosions - SLEDGE", Proceedings, 3rd International Symposium on Military Applications of Blast Simulators, Schwetzingen, Germany, September 1972, pp B4-1 through B4-10.

Degen, P., Furrer, H. and Jemielewski, J., (1976), "Structural Analysis and Design of a Nuclear Power Plant Building for Aircraft Crash Effects", Nuclear Engineering and Design, 37, 249-268.

Din, F., Editor, (1962), Thermodynamic Functions of Gases, Vol. 1 Ammonia, Carbon Monoxide, and Carbon Dioxide, Vol. 2, Air, Acetylene, Ethylene, Propane and Argon, Butterworths, London.

Drittler, K. and Gruner, P. (1976a), "Calculations of the Total Force Acting Upon a Rigid Wall by Projectiles", Nuclear Engineering and Design, 37, 231-224.

Drittler, K. and Gruner, P., (1976b), "The Force Resulting from Impact of Fast-Flying Military Aircraft Upon a Rigid Wall", Nuclear Engineering and Design, 37, 245-248.

Esparza, E. D., and Baker, W. E., (1977a), "Measurement of Blast Waves from Bursting Pressurized Frangible Spheres", NASA CR-2843, Grant NSG 3008, May 1977.

Esparza, E. D., and Baker, W. E., (1977b), "Measurements of Blas-Waves from Bursting Frangible Spheres Pressurized with Flash-Evaporating Vapor or Liquid", NASA CR-2811, National Aeronautics and Space Administration, Washington, D.C., November 1977.

Gentry, R. A., Martin, R. E., and Daly, B. J., (1966), "An Eulerian Differencing Method for Unsteady Compressible Flow Problems", Journal Comp. Physics, 1, 87-118.

Goodwin, R. D., (1974), "The Thermophysical Properties of Methane, from 90 to 500K of Pressures to 700 Bar", NBS Technical Note 653, U. S. Dept. of Commerce, National Bureau of Standards, April 1974.

Goodwin, R. D., Roder, H. M., and Straty, G. C., (1976), "Thermophysical Properties of Ethane, from 90 to 600 K of Pressures to 700 Bar", NBS Technical Note 684, National Bureau of Standards, August 1976.

Hahn, G. J. and Shapiro, S. S., (1967), Statistical Models in Engineering, John Wiley & Sons, Inc., N.Y.

Hammel, J., (1976), "Aircraft Impact on a Spherical Shell", Nuclear Engineering and Design, 37, 205-223.

Kennan, J. H., Keyes, F. G., Hill, P. G., and Moore, J. G., (1969), Steam Tables, John Wiley & Sons, Inc., N.Y.

Kennedy, R. P., (1976), "A Review of Procedures for the Analysis of Design of Concrete Structures to Resist Missile Impact Effects", Nuclear Engineering and Design, Vol, 37, 1976, pp 183-203.

Lee, J., Guirao, C., Chiu, K., and Bach, G., (1977), "Blast Effects from Vapor Cloud Explosions", Loss Precention, Vol. 11, American Institute of Chemical Engineering, N.Y.

National Defense Research Committee, (1946), Effects of Impact and Explosion, Summary Technical Report of Division II, NDRC, Volume I, AD-221-586.

Parker, R. J., Pope, J. A., Davidson, J. F., and Simpson, W. J., (1974), "The Flixborough Disaster, Report of the Court of Inquiry", Her Majesty's Stationery Office London, June 1974.

Peterson, R. E., Editor, (1976), Proceedings of the Symposium on Tornadoes, Assessment of Knowledge and Implications for Man, Texas Tech. University, Lubbock, Texas, June 22-24, 1976.

Pittman, J. F., (1976), "Blast and Fragments From Superpressure Vessel Rupture", Report No. NSWC/WOL/TR 75-87, Naval Surface Weapons Center, White Oak, Silver Spring, Maryland, February 1976.

Pittman, J. F., (1972), "Blast and Fragment Hazards From Bursting High Pressure Tanks NOLTR-12-102, U. S. Naval Ordnance Laboratory, Silver Spring, Maryland, May 1972.

Robinson, C. A., Jr., (1973), "Special Report: Fuel Air Explosives, Services Ready Joint Development Plan", Aviation Week and Space Technology, February 19, 1973, pp 42-46.

Strehlow, R. A., and Baker, W. E., (1975), "The Characterization and Evaluation of Accidental Explosions", NASA CR-134779, Grant NSG 3008, June 1975.

Strehlow, R. A., and Baker, W. E., (1976), "The Characterization and Evaluation of Accidental Explosions", Progress in Energy and Combustion Science, 2, 1, pp 27-60.

Strehlow, R. A., and Ricker, R. E., (1976), "The Blast Wave from a Bursting Sphere", Loss Prevention, Vol. 10, American Institute of Chemical Engineering, N.Y. pp 115-121.

Stull, D. R., (1977), Fundamentals of Fire and Explosion, AIChE Monograph No. 10, Vol. 73, American Institute of Chemical Engineering, N.Y.

Taylor, D. B., and Price, C. F., (1971), "Velocities of Fragments from Bursting Gas Reservoirs", ASME Transactions, Journal of Engineering for Industry, November 1971.

Tucker, D. M., (1975), "The Explosion and Fire at Nypro (UK) Ltd., Flixborough, on 1 June 1974", Building Research Establishment, Fire Research Station, Borehamwood, Hertfordshire, England, July 1975.

Wenzel, A. B and Bessey, R. L. (1969), "Barricaded and Unbarricaded Blast Measurements, Final Report, Contract No. DAHC04-69-C-0028, Subcontract 1-OU-431, Southwest Research Institute, San Antonio, Texas, October 1969.

Wilson, H. A., Jr., Belles, F. E., Clark, H. K., Crockett, C. D., Caplan, D. F., Shaw, R. C., Swain, R. L., Vincke, C. J., McSmith, D., (1972), "Report of Accident Investigating Board, 9 x 6 Thermal Structures Tunnel (TST), 600 PSIA Air Supply System", Report to Director, NASA Langley Research Center, Hampton, Virginia, April 1972.

Zabetakis, M. G., (1965), "Flammability Characteristics of Combustible Gases and Vapors", Bulletin 627, Bureau of Mines, U. S. Dept. of the Interior.

☆U.S. GOVERNMENT PRINTING OFFICE: 1976-735-076/24

1. Report No.	2. Government Accession No.	3. Recipient's Catalog No.
NASA CR-3023		

4. Title and Subtitle	5. Report Date
WORKBOOK FOR ESTIMATING EFFECTS OF ACCIDENTAL EXPLOSIONS IN PROPELLANT GROUND HANDLING AND TRANSPORT SYSTEMS	August 1978
	6. Performing Organization Code

7. Author(s)	8. Performing Organization Report No.
W. E. Baker, J. J. Kulesz, R. E. Ricker, P. S. Westine, V. B. Parr, L. M. Vargas, and P. K. Moseley	02-4778
	10. Work Unit No.

9. Performing Organization Name and Address	11. Contract or Grant No.
Southwest Research Institute P.O. Drawer 28510 San Antonio, Texas 78284	NAS3-20497
	13. Type of Report and Period Covered
12. Sponsoring Agency Name and Address	Contractor Report
National Aeronautics and Space Administration Washington, D.C. 20546	14. Sponsoring Agency Code

15. Supplementary Notes

Final report. Project Manager, Paul M. Ordin, Space Propulsion and Power Division, NASA Lewis Research Center, Cleveland, Ohio 44135.

16. Abstract

This workbook is a supplement to an earlier NASA publication, NASA CR-134906, which is intended to provide the designer and safety engineer with rapid methods for predicting damage and hazards from explosions of liquid propellant and compressed gas vessels used in ground storage, transport, and handling. As in the earlier workbook, information is presented in the form of graphs and tables to allow easy calculation, using only desk or handheld calculators. When complex methods have been used to develop simple prediction aids, they are fully described in appendices. Topics covered in various chapters are

(1) Estimates of explosive yield
(2) Characteristics of pressure waves
(3) Effects of pressure waves
(4) Characteristics of fragments
(5) Effects of fragments and related topics

A short concluding chapter gives a general discussion and some recommendations for further work.

Microfiche copies of the companion workbook, NASA CR-134906, are attached for the convenience of the reader.

17. Key Words (Suggested by Author(s))	18. Distribution Statement
Fragmentation; Chemical explosions; Fragments; Compressed gases; Range safety; Debris; Blast loads; Blast effects; Ballistics; Terminal ballistics	Unclassified - unlimited STAR category 28

19. Security Classif. (of this report)	20. Security Classif. (of this page)	21. No. of Pages	22. Price*
Unclassified	Unclassified	273	$10.75

* For sale by the National Technical Information Service, Springfield, Virginia 22161

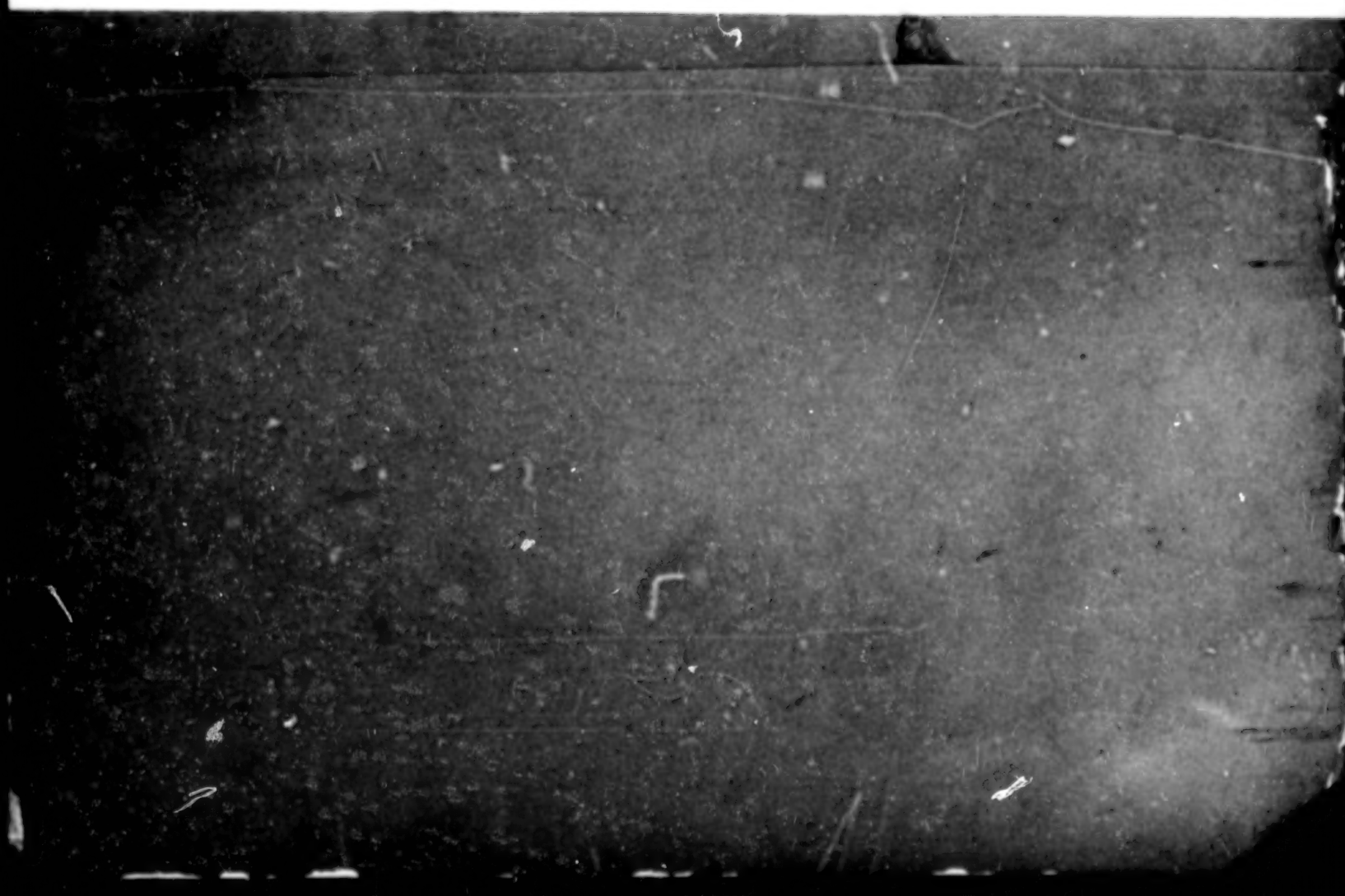

END

June 11, 1981